Morphometric Analysis to Characterize the Differentiation of Mesenchymal Stem Cells into Smooth Muscle Cells in Response to Biochemical and Mechanical Stimulation

by

Brandan Walters

A dissertation submitted in partial fulfillment
of the requirements for the degree of
Doctor of Philosophy
(Biomedical Engineering)
in The University of Michigan
2018

Doctoral Committee:

       Professor Jan P. Stegemann, Chair
       Associate Professor Lisa M. Larkin
       Professor Andrew J. Putnam
       Associate Professor Margaret V. Westfall

Brandan Walters

brandanw@umich.edu

ORCHID iD: 0000-0002-1364-8661

To my wife, my family, and my friends,

At the end of the day, when experiments are done, you make it all worthwhile.

ACKNOWLEDGEMENTS

"Nanos gigantum humeris insidentes" is metaphor in Latin meaning "dwarves standing on the shoulders of giants". The intention being that new discovery and knowledge is only possible because of those that came before us. I was only able to finish this work because of the support of my mentors, family, and friends, thank you for everything.

Dr. Jan Stegemann is the obvious choice to recognize first. I appreciate everything you've done and continue to do to help me become a better scientist. When many labs only care about the science, you have shown repeatedly that you care about the scientists. You always pushed me to learn more and you have set an example of how to pass what you know onto others. Thank you for being a "giant for me to stand on" and never giving up on me, even when I set optimistic deadlines that I can never meet.

To my committee, official and unofficial – Dr. Andrew Putnam, Dr. Lisa Larkin, Dr. Margaret Westfall, and Dr. Bernd Rolauffs – Thank you for your encouragement and always asking the right questions. They continue to improve my work and help to evolve as a scientist. I also appreciate all the time you've devoted and the different perspectives you've brought to my work over the past 4 years. It is clearer to me now, more than ever, that without your insights and expertise, I would not be the scientist or person that I am today.

I want to acknowledge my funding sources - the NIH Tissue Engineering and Regenerative Medicine Training Grant (TEAM), the Whitaker Fellowship, and the Rackham Predoctoral Fellowship. They have provided me invaluable experiences and have helped me become a better

I also want to thank lab members here and abroad who have helped me through this process. I have learned so much from you and appreciate your ceaseless support. Those who immediately come to mind are Dr. Ram Rao, Dr. Ethan Daley, Dr. Paul Turner, Dr. Ana Rioja, Dr. Adeline Hong, Dr. Ram Tiruvannamalai-Annamalai, Nick Schott, Nicole Friend, Eric Hobson, Dr. Biming Wu, Dr. Melanie Hart, Dr. Lewin Bartolic, Dr. Tatiana Uynuk-ool, and Dr. Miriam Rothdiener. There are countless other people I have met at the University of Michigan and the University of Tübingen who I owe a debt of gratitude that I will never be able to repay; thank you for walking down this crazy road of science with me

TABLE OF CONTENTS

LIST OF FIGURES

LIST OF APPENDICES

LIST OF ABBREVIATIONS

In order of appearance

Mesenchymal Stem Cells	MSCs
Bone Marrow Derived Stem Cells	bMSCs
Adipose Derived Mesenchymal Stem Cells	ASCs
Smooth Muscle Cells	SMCs
Cardiovascular disease	CVD
National Institute for Health and Care Excellence	NICE
Polytetrafluoroethylene	PTFE
Urinary Incontinence	UI
Embryonic Stem Cells	ESCs
Induced Pluripotent Stem Cells	iPSCs
Extracellular Matrix	ECM
Two Dimensional	2D
Three Dimensional	3D
Phosphate Buffered Saline	PBS
Good Manufacturing Practices	GMP
Dulbecco Modified Eagle Medium	DMEM
Fetal Bovine Serum	FBS
Real Time Polymerase Chain Reactions	RT-PCR
Smooth Muscle Acta 2	ACTA
Transgelin	TAGLN
Calponin	CNN

Peptidylprolyl Isomerase A	PPIA
Glyceraldehyde 3-phosphate dehydrogenase	GAPDH
Human Bladder Derived Smooth Muscle	hBdSMC
Smooth Muscle Actin	SMA
Analysis of Variance	ANOVA
Desmin	DES
Principle Component Analysis	PCA
Partial Least Squares Analysis	PLS Analysis
Alpha Modified Essential Medium	Alpha MEM
Penicillin and Streptomyocin	PS
Diamidino-2-phenylindole	DAPI
Bovine Serum Albumin	BSA
Transforming Growth Factor Beta	TGFβ
Platelet Derived Growth Factor	PDGF
Bone Morphogenic Protein 2	BMP2
Vasculogenic Endothelial Growth Factor	VEGF
Fibroblast Growth Factor	FGF
Microspheres	μspheres
Control	Con
Growth Factor in Media	GF
Growth Factor Loaded μSpheres	LS

ABSTRACT

The morphology and biochemical phenotype of cells are closely linked. This relationship is important in progenitor cell bioengineering, which generates functional, tissue-specific cells from uncommitted precursors. Advances in biofabrication have demonstrated that cell shape can regulate cell behavior and alter phenotype-specific functions. Establishing accessible and rigorous techniques for quantifying cell shape will therefore facilitate assessment of cellular responses to environmental stimuli, and will enable more comprehensive understanding of developmental, pathological, and regenerative processes. For progenitor cells being induced into specific lineages, this ability becomes a pertinent means for validating their degree of differentiation and may lead to novel strategies for controlling cell phenotype.

In our approach, we used the differentiation of adult human mesenchymal stem cells (MSCs) into smooth muscle cells (SMCs) as a model system to investigate the relationship between cell shape and phenotype. These cell types are responsive to mechanical and biochemical stimuli and the shape of SMCs is a recognized marker of differentiated state, providing a system in which morphological and biochemical phenotype are both understood and inducible. By applying exogenous stimuli, we changed cell shape and examined the corresponding cellular phenotype. In the first Aim, we applied stretch to MSCs on 2D collagen sheets to promote differentiation. Using mathematical shape factors, we quantified the morphological changes in response to defined stretch parameters. In the second Aim, we investigated the use of input energy

as a means of controlling cell shape and corresponding differentiation. We examined how combinations of stretch parameters that produce equal energy input impacted morphology, and postulated that cell shape is a function of energy input. In the third Aim, we translated our method of quantifying shape factors into 3D culture, and validated the method by investigating the differentiation of MSCs into SMCs by mechanical and growth factor stimulation. We used the shape factors to quantify morphological differences and compared these changes to biochemical markers.

Our results demonstrate that mechanical stretch influences multiple aspects of MSC phenotype, including cell morphology. Shape factors described these changes objectively and quantitatively, and enabled the identification of relationships between SMC shape and differentiated state. Similar morphological responses could be induced using different combinations of stretch parameters that resulted in equal energy input. Cell shape followed a linear relationship with energy input despite the variance introduced by using MSCs from different patients. Only one SMC gene marker directly exhibited this relationship; however, partial least squares regression analysis revealed that other genes were also associated with shape factors. Translation of the shape quantification method into 3D systems revealed that while the additional dimensionality hindered comparison of morphology between 2D and 3D samples, these shape factors were still applicable within 3D systems. Differences in cell morphology caused by growth factors and mechanical stretch in 3D constructs were elucidated by shape analysis, and these phenotypic changes were corroborated through biochemical assays. Taken together, these results validate the use of cell shape as means of characterizing phenotype and the process of progenitor cell differentiation. The automated method we developed generates a robust set of morphological parameters that provide a way to characterize the differentiation of MSCs into SMCs. This work

has implications in our understanding of the relationship between cell morphology and phenotype, and may lead to new ways to control and improve differentiation efficiency in a variety of cell and tissue systems.

CHAPTER 1

Introduction

1.1 - Cell Shape and its Relationship to Phenotype

The morphology of cells as a qualitative indication of overall cell health, viability, function, and phenotype is well recognized. Morphology has been associated with proliferation [1] and function [2,3], and has been recognized to respond to external stimuli [4–6]. Despite this acknowledgement, many studies that have examined these relationships have left them unquantified and unvalidated. For example, the use of specific growth factors has been suggested to produce a more "smooth muscle-like" morphology however these effects have not been quantified [7–11]. Others have found that stretching cells makes them longer and larger in area [4–6,12] or more "spindle-like" [5,6,13], but these findings have also not been confirmed quantitatively. When using stimuli to differentiate progenitor cells for potential clinical use, understanding these relationships would facilitate standards for recognizing the state of differentiation and could be exploited to induce progenitor cells into tissue-specific lineage.

To investigate the apparent relationship between shape and phenotype, a subfield of bioengineering has emerged to control the morphology of cells by directly altering their attachment to a surface. By printing specific patterns onto substrates and limiting where cells can adhere, tissue engineers have produced a means of controlling the size and curvature of the attached cells. This has led to significant discoveries regarding how cells differentiate and spread [14–18]. These studies have opened new avenues to explore regarding the role of morphology in differentiation

and cellular phenotype. While these fundamental studies have shown that directly controlling cell shape changes the phenotype, they have not shown that other means of stimulating differentiation can also induce changes in shape. In addition, while other studies have shown that environmental stimuli affect phenotype and *suggest* these stimuli also influence cell shape, they have not quantified these changes in shape to solidify this relationship. The gap connecting the induction of differentiation by stimuli, changes in phenotype, and corresponding changes in shape has yet to be bridged. It is a fundamental goal of our lab to quantify changes in cell shape that occur during exposure to external stimuli and relate these changes to a biochemical and functional phenotype.

The development of quantitative measurement tools requires modern advances in computational and image-analysis methods, particularly improved identification and tracking of cells [19]. Intensity thresholding is still the most commonly used method to distinguish cells from the background, but others use filters [20] or water-shedding [21] to distinguish cells from one another or their surroundings. These computational tools have continued to improve and allow the ability to objectively distinguish geometrical properties of cells and define them according to biological processes they are associated with. Our group has had success using manual intensity thresholds to segment cells and has used these data to collect information on cells' morphology. Particularly we examined cell roundness (normalized ratio of area to long axis squared which limits its values between 0-1), aspect ratio (ratio of long axis to short axis which limits its value to those greater than 1), circularity (normalized ratio of area to perimeter squared which limits its values between 0-1), and solidity (ratio of concave area to convex area which limits its values between 0-1). These could be used in multiple ways across many disciplines but we used them to analyze bMSCs and how they differentiate into SMCs [22]. The original panel of shape factors is described in Fig 1.1.

A

Shapes of Calcein-stained MSCs on Collagen I sheets (80mg/ml)

| Roundness | 0.133 | 0.299 | 0.330 | 0.350 | 0.364 | 0.400 | 0.470 | 0.490 | 0.510 | 0.550 | 0.554 | 0.566 | 0.612 |

B

C
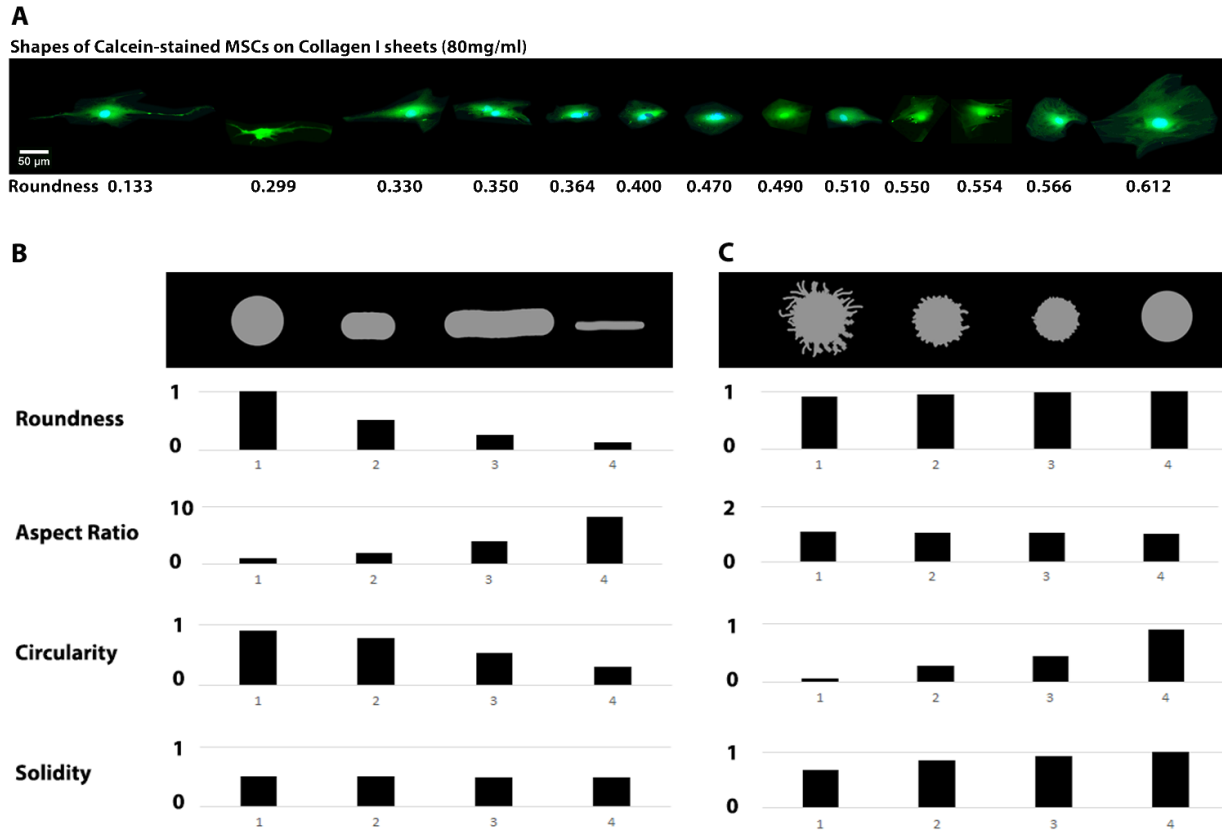
Figure 1.1: Range of observed MSC shapes and shapes drawn in silico to illustrate how cell morphology can be quantified using the four original shape descriptors. Representative images depicting bMSCs and their associated roundness to illustrate the range of shapes that was observed in this study (A). As examples, panel B illustrates how a circular shape morphing into an elongated shape is quantified with the descriptors roundness and aspect ratio. A high value for roundness indicates a round cell, and a high aspect ratio indicates an elongated cell (B). High values for both circularity and solidity indicate the absence of (cellular) protrusions. Circularity increases as protrusions decrease in size from left to right as the shape becomes more circular (C) Adapted from 22.

While the existence of a close relationship between cells shape and phenotype is well-documented, much remains to be learned about the causality of this phenomena and its possible implications in stem cell differentiation. While directly controlling shape has been shown to induce certain phenotypical changes, how exogenous stimuli induce differentiation and their effect on cell shape is less clear. With developments in computational power and increased capabilities through image analysis, it is becoming easier to understand the relationship between cell shape and differentiation. We discuss many of these relationships in later chapters as we explore the quantification of these relationships. By doing so, we will gain understanding of cell phenotype,

3

have better control over the process of differentiation, and be able to better characterize cells as they undergo physiological changes.

1.2 - Bone Marrow Derived Mesenchymal Stem Cells and Adipose Derived Stem Cells

Bone marrow-derived mesenchymal stem cells (bMSCs), a source specific subset of mesenchymal stem cells (MSCs), are stromal cells derived from patients through aspirates taken from cortical bone marrow. They are already being used in the clinic for transplant purposes and they have been shown to induce a minimal immunogenic response in vivo [23,24]. One of the most intriguing characteristics of these cells, from the perspective of regenerative medicine, is their multipotent potential. With the appropriate biochemical intervention, bMSCs have been shown to have a predisposition toward osteogenic [15,25–28], chondrogenic [16,29], and adipogenic [15,30] differentiation. Research has also demonstrated potential toward endothelial [31] and neurogenic lineages [32,33]. Our interest stemmed from their myogenic potential toward SMC-like lineages[16,34,35].

Another promising type of MSCs are adipose-derived stem cells (ASCs). These progenitor cells can be extracted from many fatty tissues making their extraction simpler and less invasive than bone marrow aspiration [36], and ASCs are already being used in the clinic [37]. Like bMSCs, ASCs have been shown to be immunoprivileged [36] and multipotent. They were first recognized by their ability to repair and regenerate adipose tissue [38], confirmed later by others [16,39–41], but were soon being recognized for their osteogenic [16,40–43], and chondrogenic [16,40,44,45] differentiation potential as well. More recently, their ability to differentiate into striated muscle [39,46] and smooth muscle lineages [16,47–50] has generated interest from other groups.

For certain desired clinical applications, differentiation of these MSCs into smooth muscle cells (SMCs) is desirable. Techniques to differentiate these progenitors into SMCs are well documented but vary by group. Research has shown that MSCs can be differentiated into smooth

muscle cells using induction from surrounding tissue [51] and multiple different growth factor combinations [7,8,35,52–56]. Among the main biochemical factors used for this differentiation process are TGFβ-1, TGFβ-3, PDGF, and BMP4. These factors have been added at varying doses and for various amounts of time with substantial success. Other groups have emulated the natural function of the smooth muscle to induce differentiation. One group found that electrical stimulation facilitated the differentiation of MSCs into SMCs [50] and many groups have found that cyclic mechanical stimulation induces an SMC phenotype from MSCs [13,34,47,55,57–59].

In general, MSCs are well recognized for their clinical potential and ability to differentiate into multiple lineages. Many of these applications call for differentiation into SMCs and to this end, multiple techniques for promoting their differentiation have been developed. To validate and better understand these processes, quantifying the changes in shape that MSCs go through during differentiation would maximize our ability to both understand and achieve better SMCs.

1.3 - Collagen and its Uses in Tissue Engineering

To culture MSCs, many groups use hydrogels composed of natural and synthetic proteins. A common matrix protein used for such purposes is collagen. The collagens comprise a superfamily of proteins that includes over 20 members of varying abundance, functionality, and distributions within tissues. Collagen Type I, one of the most common structural elements in a variety of tissues is a widely used protein in the field of biomaterials. Its unique properties and relative abundance in living tissue have made it an appropriate choice in a variety of restorative applications throughout medical history, and more recently it has been a key material in tissue engineering and regenerative medicine.

An important characteristic of collagen type I is its well-understood hierarchical structure from the nanoscale to the macroscale, shown schematically in Fig. 1.2. Cells internally synthesize,

5

modify and assemble the alpha chains into a procollagen form, which is secreted to the extracellular space and then partially cleaved by specific enzymes to form the tropocollagen molecule. These nanoscale subunits (typically '"1.5 nm in diameter and 300 nm in length) further self-assemble into fibrils consisting of multiple tropocollagen molecules, which can be tens to hundreds of nanometers in diameter and on the order of microns in length. The tropocollagen molecules are covalently bound to each other in a staggered manner, giving collagen fibrils a distinctive banded pattern when viewed at high magnification. Fibrils can then assemble into larger and longer fibers and fiber bundles on the order of microns to centimeters in scale, and such fibers are major structural components of many tissues. The intricate and highly organized architecture of collagen materials, from the level of alpha helices to fiber bundles, results in a stable extracellular matrix (ECM) protein with high tensile strength.
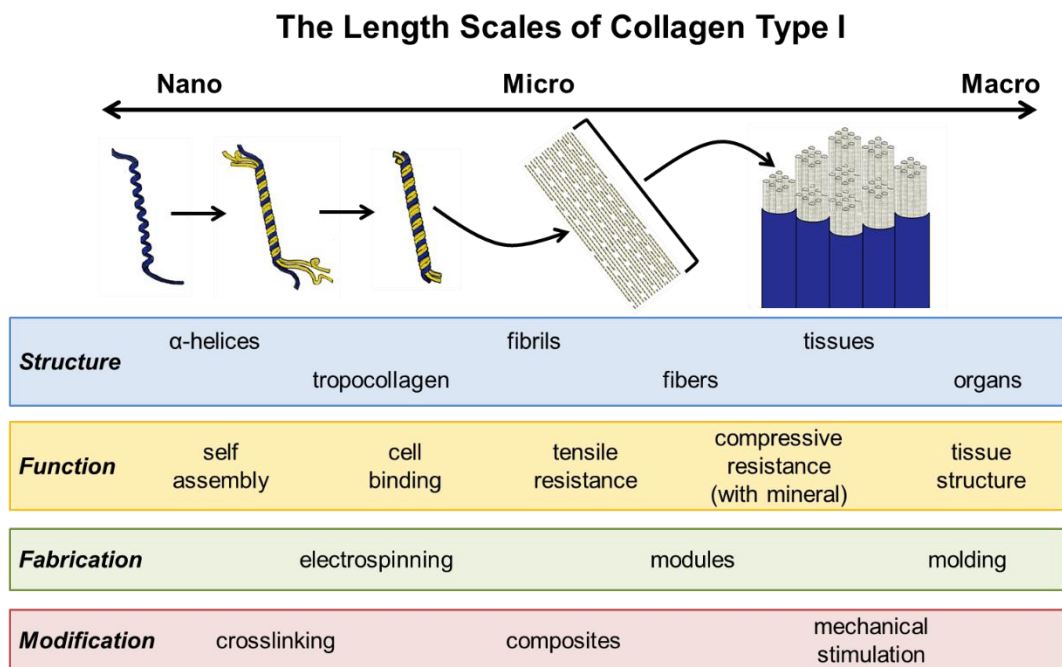
Figure 1.2: Structure of Collagen. The hierarchical structure of collagen type I leads to specific biological functions and characteristics across length scales. Fabrication of collagen hydrogel materials produces specific architectures, which can further be modified for particular applications.

Collagen is isolated from many fibrous tissues and while it can vary between tissue type and species [60–62] the protein is released from the tissue by dissolution with either enzymes and/or acid. The general process for reconstituting dissolved collagen and thereby creating collagen hydrogel constructs has been used widely since the 1970s. Solubilized collagen is maintained at low pH and low temperature to prevent annealing of the dissolved peptide fragments. Raising the pH and temperature allows aggregation and covalent bonding of the collagen fragments to re-form fibrils and create a hydrogel structure. Typically, solubilized collagen is poured into a mold and then exposed to a neutralizing agent, such as exposure to ammonia vapor, to initiate fibrillogenesis [63]. More recently, sodium hydroxide solutions have been used for this purpose, and can be directly mixed with cold collagen solutions immediately prior to introduction into a mold. Importantly, while still unpolymerized, culture medium, serum, other protein constituents, and cells can be incorporated into the hydrogels to promote subsequent behavior from embedded cells.

Cells that are embedded in 3D collagen not only attach to the collagen fibers, they respond to and remodel them according to other stimuli. A variety of mechanically active cells produce contractile forces to compact the hydrogels pulling the fibers together [64,65]. This process can reduce the volume of the gels to as low as 10% of their original volume and expel fluid components into the surrounding space. Cells can also remodel the matrix through tight regulation of enzymes called matrix metalloproteinases [66–69] which degrade the fibers of the extracellular matrix (ECM)

A useful application of hydrogel molding is creating collagen constructs in geometries that facilitate application of mechanical forces and/or measurement of mechanical properties. For example, hydrogel constructs can be molded between to two anchors [70–72] or into rings [73–75] that

can be stretched afterward. In addition, geometries conducive to compressive testing are also easily fabricated, and usually are in the form of disks or cylindrical samples.

The fabrication and control of collagen allows for numerous combinations of processes to be used. Composites can be easily created through incorporation of additional materials before the gel sets. Materials like elastin [76–80], hyaluronan [81–83], fibronectin [84], and other isoforms of collagen [85] are also sometimes used to change the properties of the hydrogel. Our lab focuses on combining collagen with fibrin, the primary protein responsible for blood clotting and initiating wound healing [74,86–90] and chitosan, a polysaccharide typically found in crustaceans [91,92]. When added together, these hydrogels retain properties of their constituents and can be optimized to emulate native tissue ECM. In addition, during fabrication, collagen can be crosslinked to slow degradation and increase mechanical properties [93–102]. Collagen can also be electrospun into sheets of fibers [103,104] of made into modular constructs [87,90–92,105,106].

Our group has found substantial evidence that culturing bMSCs on 2D collagen sheets enhances expression of SMC genes and protein over culture on tissue culture plastic. Additionally, these sheets can be cyclically strained which further increases the expression of SMC markers in the embedded cells [107]. Because of its versatility in fabrication, its ability to be functionally altered, its biocompatibility, and its inductive properties for differentiation, we continue to use collagen substrates for MSC differentiation into SMCs.

1.4 - Clinical Motivation

Cardiovascular disease (CVD) includes all pathologies related to decreased function of the circulatory system and currently accounts for 31% of deaths globally [108]. By 2030, worldwide mortality due to CVD is expected to increase to over 23 million people a year [109]. To combat this devastating epidemic most effectively, patients are recommended to modify their lifestyle and

improvements to diet [108,110,111]. Pharmaceutical intervention can be taken in combination with these changes in lifestyle. Statins [108], antibody therapies [112] and anti-platelet can be used in later stages of the disease [113]. If the disease continues to progress, surgical intervention is often needed to replace the diseased vasculature. Angioplasty, inserting a stent, or removal of the obstructed vessel are typically considered but vascular grafts are still a gold standard to maintain the highest patency [114]. Around 400,000 coronary artery grafts are used each year in the United States [115] but these surgeries are typically done with an autograft and can cause complications [116]. While the use of synthetic materials like polytetrafluoroethylene (PTFE) offer alternative options for graft material, their patency is around 2/3 that of the saphenous vein after a year and drops to 1/3 after 2 years [117]. Efforts to improve patency utilize cells seeded on the surface of the grafts but these are incapable of performing at the same level of autografts [118].

Fully tissue engineered grafts offer an alternative solution but several aspects must be considered before their use becomes commonplace. Scaffold materials must maintain mechanical properties while being able to grow and remodel with the patient, they must respond to the cyclic pressure of blood flow, and a proper cell source to seed the vessels must be established. Regardless of whether a decellularized matrix or a fully cell derived matrix is used, and whether that material has the mechanical properties to function correctly, a source of functional smooth muscle cells to populate the matrix must be established.

Urinary incontinence (UI) is a second pathology that must be addressed with an aging population. With up to 30% of the elderly population experiencing problems with continence [119], it is increasing problems with anxiety and depression [120]. Aging, childbirth, and obesity can increase the risk of UI [121] and something as minimal as a sneeze, coughing, or simply standing up and increase pressure and initiate involuntary urination [120]. While nerve damage can be a cause,

9

weakening of the urethral sphincter muscle around the ureter is usually the cause of UI. This tissue is made up of portions of both striated and smooth muscle and degeneration of either can lead to loss of function [122]. Again, the preferred method of treatment by physicians is changing lifestyle. Changes in weight loss, fluid management, and pelvic floor training are suggested [123]. If these approaches fail, the next step of intervention can involve electrical stimulation of the muscle [124]or bulking agents [125]. As a last resort, a sling can be surgically implanted to correct the positioning of the urethra but many people still experience issues after this intervention [126].

Cell-based therapy offers a promising alternative to treat this urological pathology. By implanting mature, functional smooth muscle cells, it may be possible to recover bladder control. And, while the scaffold material and the mechanical integrity of tissue engineered blood vessels is paramount, the source of the smooth muscle cells to be used in these therapies must be carefully considered. Using autologous smooth muscle cells for therapeutics has shown clinical promise [127,128] and it seems practical to use functional cells to regenerate dysfunctional tissue but using adult cells comes with its own challenges. Taking a biopsy from one part of the body to harvest cells can cause secondary sites of morbidity and these cells can lack the proliferative capacity to obtain the number of cells necessary for the selected use [122]. Expansion of autologous cells, if even possible, is slow and expensive. Pluripotent stem like embryonic stem cells (ESCs) or induced pluripotent stem cells (iPSCs) cells offer promising alternative sources, however maintenance of these lines is also expensive and efficient differentiation still needs to be developed (Reviewed in [129], [130]). Alternative sources of SMCs are needed if clinical therapies and engineering of smooth muscle is to become a reality.

In an aging global population, CVD and UI will continue to be significant clinical problems. To combat these epidemics, changes in routine and pharmaceutical intervention are

being employed, but deteriorating states still often require surgical intervention and demand tissue replacement. An abundant source of SMCs is necessary to use for these clinical purposes. While autogenic cell sources are available, they have substantial limitations, especially donor site morbidity in a population already experiencing slower healing. MSCs from bone and fat offer a potential source that can be easily expanded and manipulated into SMCs.

Before this can be clinically relevant, an effective and reproducible means of converting the cells must be developed. The clinical value of stem cell-derived smooth muscle cells will depend on the ability to produce fully functional and differentiated cells. One of the first and most common indications of a cell moving toward an SMC-like state is the expression of ACTA and its analogous protein, smooth muscle alpha actin (SMA) [131]. This protein is involved in force generation of smooth muscle cells [132] and is expressed transiently throughout development [133]. The calponin (CNN) and transgelin (TAGLN) genes code for calponin and SM-22 proteins which indicate intermediate differentiation and influence contraction of functional smooth muscle cells [133]. Desmin (DES) and smooth muscle myosin heavy chain (MHC) are late markers of differentiation and code for sarcomere and force production proteins, respectively [134]. Caldesmon is the last gene we actively measure in this study and it is an intermediate marker gene for smooth muscle differentiation that codes protein for calcium regulation and subsequent contraction [135]. Expression of these markers indicates a contractile phenotype as opposed to a synthetic phenotype. This contractile SMC phenotype is qualitatively associated with a long spindle like morphology and is necessary for functional tissue. Using MSCs, it might be possible to produce large numbers of contractile cells, given the correct culture conditions. Using cell shape, the quality of these MSC-derived SMCs may be better regulated and possibility even promoted.

1.5 - Objective

The relationship between cell shape and phenotype needs to be quantified and validated. The effects of environmental stimuli that result in functionally appropriate differentiation of progenitor cells needs to be understood and optimized. To these ends we propose the three specific Aims in the section below, represent them visually in Fig 1.3, and summarize them as follows.

We aim to show that changes in cell shape in response to environmental stimuli can be quantifiably characterized using a rich set of objective shape parameters and that these changes are indicative of cellular phenotype.

1.6 - Specific Aims

Aim 1: Quantify MSC Morphology After Stretch Using a Panel of Shape Factors

We seeded bMSCs on collagen sheets and applied cyclic stretch to the constructs. After using different stretch regimens, the shape of cells was measured with a semi-automated method of calculating four shape factors to examine morphology. These changes were compared to other indications of phenotype changes. The goal was to show that cell shape changes after mechanical stimulation, that we could quantify these differences, and that they corresponded to other accepted measurements of cell phenotype.

Aim 2: Apply Shape Factors to Determine the Effects of Energy Input and Assess Potential of Mechanical Stimulation as a Means of Controlling Cell Shape

We mechanically stimulated bMSCs on collagen sheets using cyclic uniaxial stretch. However, instead of comparing the effects of maximum strain or the duration of stimulation, these parameters were investigated in terms of their amount of relative input energy. The shapes of the

resulting cells were measured, but in this Aim this process was fully automated and completely consistent. The goal was to establish a relationship between the mechanical input energy and the resulting phenotype of stretched cells. This relationship provided a means to manipulate cell shape with more understanding and control.

Aim 3: Translate Shape Analysis from 2D into 3D Constructs and Use Shape to Compare Effects of Culture Conditions on ASC Differentiation into SMC

We seeded ASCs on collagen gels or embedded them inside gels. This aim switched the cell source from bMSCs to ASCs for multiple scientific and pragmatic reasons discussed in detail later. In addition, a range of concentrations of collagen were used to investigate the effect of concentration on ASC phenotype. We used the image analysis techniques from Aim 2 to compare the shape of cells in each "dimensionality" and compared their resulting phenotype using established SMC biochemical markers. The goal was to determine if the shape of cells in 3D could be analyzed, how their shape compared to those in 2D, and if the effects of different culture dimensions influenced the phenotype of the cells. ASCs were then embedded in collagen gels and exposed to growth factors known to induce SMC differentiation. The growth factors were delivered through the media or through gelatin microcarriers embedded in the gels. In addition, a subset of these gels was cyclically strained to mechanically stimulate the embedded ASCs. At time points before and after stretch, the shape of the cells was analyzed, and biochemical markers of SMC differentiation were used to assess ASC phenotype. The goal of this aim was to evaluate the influence of growth factors, their method of delivery, and application of mechanical stretch on the shape of ASCs as they differentiate into SMCs.
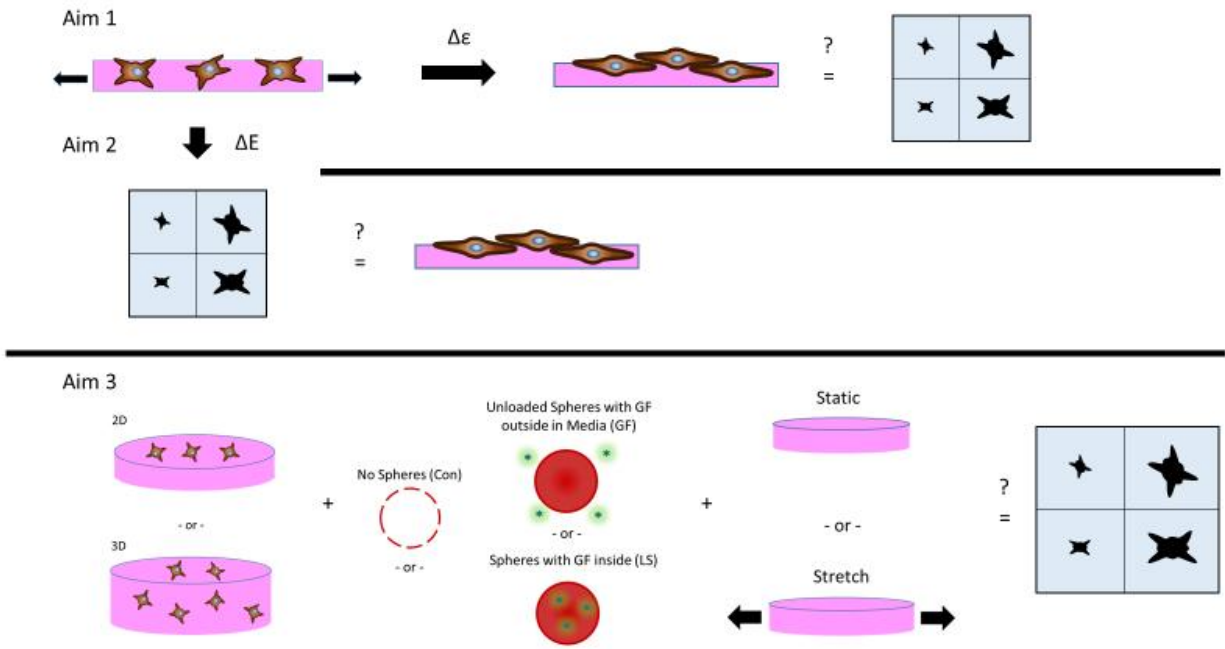
Figure 1.3: Specific Aims. Aim 1 stretched cells to induce differentiation toward SMCs and quantified the shape of MSCs in response to stretch. Aim 2 used energy to control cell shape and examined how the amount of energy and shape correlate with phenotype. Aim 3 translated the technique into 3D and use cell shape to demonstrate differentiation toward SMCs induced by grow factor delivery and stretch.

1.7 - Preview of Thesis

Chapter 2 introduces the concept of shape factors for morphological analysis and explains, and then applies them to examine how bMSCs change shape after being cyclically stretched (Aim 1). To better understand the effects of stretch, specific stretching regimen parameters are used to adjust how much and how long the cells are strained. The analysis specifically focuses on cell length and how this characteristic is necessary but not sufficient to describe the phenotype shift as bMSCs begin to differentiate into SMCs after mechanical stimulation. The main purpose of this Aim is to support and validate the use of cell shape as an indication of phenotype.

Chapter 3 extends the idea of using stretch to influence cell shape and cell phenotype by considering earlier stretch parameters as factors determining input energy and examining cell

phenotype in response to input energy. It compares cell shape using an expanded set of shape factors and asks which parameters of stretch are more important when differentiating bMSCs into an SMC phenotype (Aim 2). This Aim compares these findings on shape to other makers associated with SMC differentiation.

In Chapter 4, the idea of cell shape is applied to images of ASCs on a 2D surface as well as to projections of ASCs suspended in 3D matrices. It switches focus to ASCs from bMSCs for multiple reasons including less invasive and easier extraction (resulting in faster recovery), increased proliferation of ASCs, and the chance to apply these shape parameters on a new cell source. In addition, this study asks if the "dimensionality" (i.e. 2D or 3D) of the culture construct impacts the ability of our methods to measure the shape of cells, and how differences in culture dimensionality impact the shape and of the cell as well as other aspects of phenotype (Aim 3).

Chapter 5 uses shape as a diagnostic in combination with other biochemical and functional measures to the extent to which specific stimuli induce differentiation of ASCs into SMCs (Aim 3). It applies growth factors and mechanical stimulation to induce differentiation and investigates if shape and traditional measures of phenotype change capture the process.

The results and major findings of Chapters 1-5 are summarized in Chapter 6. The impact and contributions of these results to the field are then discussed. Conclusions from each Aim are made and finally, additional applications and experiments to further these findings are described in the Future Directions.

1.8 - References

1.   Singhvi R, Kumar A, Lopez GP, et al. Engineering Cell Shape and Function. 1994;264(5159):696-698.

2.   MANASEK F. Myocardial cell shape change as a mechanism of embryonic heart

looping*1. *Dev Biol*. 1972;29(4):349-371. http://linkinghub.elsevier.com/retrieve/pii/0012160672900772%5Cnpapers2://publication/doi/10.1016/0012-1606(72)90077-2.

3.   Folkman JJ, Moscona A. Role of cell shape in growth control. *Nature*. 1978;273(5661):345-349. doi:10.1038/273345a0.

4.   Liu B, Qu M-J, Qin K-R, et al. Role of cyclic strain frequency in regulating the alignment of vascular smooth muscle cells in vitro. *Biophys J*. 2008;94(4):1497-1507. doi:10.1529/biophysj.106.098574.

5.   Wanjare M, Agarwal N, Gerecht S. Biomechanical strain induces elastin and collagen production in human pluripotent stem cell-derived vascular smooth muscle cells. *Am J Physiol - Cell Physiol*. 2015;309(4):C271-C281. doi:10.1152/ajpcell.00366.2014.

6.   Song B, Jiang W, Alraies A, et al. Bladder Smooth Muscle Cells Differentiation from Dental Pulp Stem Cells: Future Potential for Bladder Tissue Engineering. *Stem Cells Int*. 2016;2016. doi:10.1155/2016/6979368.

7.   Wang C, Yin S, Cen L, et al. Differentiation of Adipose-Derived Stem Cells into Contractile Smooth Muscle Cells Induced by Transforming Growth Factor-β1 and Bone Morphogenetic Protein-4. *Tissue Eng Part A*. 2010;16(4):1201-1213. doi:10.1089/ten.tea.2009.0303.

8.   Williams C, Xie AW, Emani S, et al. A Comparison of Human Smooth Muscle and Mesenchymal Stem Cells as Potential Cell Sources for Tissue-Engineered Vascular Patches. *Tissue Eng Part A*. 2012;18(9-10):986-998. doi:10.1089/ten.tea.2011.0172.

9.   Feng C, Hu J, Liu C, et al. Association of 17-β estradiol with adipose-derived stem cells: New strategy to produce functional myogenic differentiated cells with a nano-scaffold for tissue engineering. *PLoS One*. 2016;11(10):1-18. doi:10.1371/journal.pone.0164918.

10.   Floren M, Bonani W, Dharmarajan A, Motta A, Migliaresi C, Tan W. Human mesenchymal stem cells cultured on silk hydrogels with variable stiffness and growth factor differentiate into mature smooth muscle cell phenotype. *Acta Biomater*. 2016;31:156-166. doi:10.1016/j.actbio.2015.11.051.

11.   Zhao Z, Yu H, Fan C, Kong Q, Liu D, Meng L. Differentiate into urothelium and smooth muscle cells from adipose tissue-derived stem cells for ureter reconstruction in a rabbit model. 2016;8(9):3757-3768.

12.   Girão-Silva T, Bassaneze V, Campos LCG, et al. Short-term mechanical stretch fails to differentiate human adipose-derived stem cells into cardiovascular cell phenotypes. *Biomed Eng Online*. 2014;13(1):1-15. doi:10.1186/1475-925X-13-54.

13.   Rabbani M, Tafazzoli-Shadpour M, Shokrgozar MA, Janmaleki M, Teymoori M. Cyclic Stretch Effects on Adipose-Derived Stem Cell Stiffness, Morphology and Smooth Muscle Cell Gene Expression. *Tissue Eng Regen Med*. 2017;14(3):279-286. doi:10.1007/s13770-017-0033-6.

14.   McBeath R, Pirone DM, Nelson CM, Bhadriraju K, Chen CS. Cell shape, cytoskeletal

tension, and RhoA regulate stem cell lineage commitment. *Dev Cell*. 2004;6(4):483-495. http://www.ncbi.nlm.nih.gov/pubmed/15068789.

15. Kilian K a, Bugarija B, Lahn BT, Mrksich M. Geometric cues for directing the differentiation of mesenchymal stem cells. *Proc Natl Acad Sci U S A*. 2010;107:4872-4877. doi:10.1073/pnas.0903269107.

16. Gao L, Mcbeath R, Chen CS. Stem Cell Shape Regulates a Chondrogenic versus Myogenic Fate through Rac1 and N-cadherin. *Stem Cells*. 2010;28(3):564-572. doi:10.1002/stem.308.Stem.

17. Lee J, Abdeen AA, Zhang D, Kilian KA. Directing stem cell fate on hydrogel substrates by controlling cell geometry, matrix mechanics and adhesion ligand composition. *Biomaterials*. 2013;34(33):8140-8148. doi:10.1016/j.biomaterials.2013.07.074.

18. Zhang D, Sun MB, Lee J, Abdeen AA, Kilian KA. Cell shape and the presentation of adhesion ligands guide smooth muscle myogenesis. *J Biomed Mater Res - Part A*. 2016;104(5):1212-1220. doi:10.1002/jbm.a.35661.

19. Meijering E, Dzyubachyk O, Smal I, van Cappellen WA. Tracking in cell and developmental biology. *Semin Cell Dev Biol*. 2009;20(8):894-902. doi:10.1016/j.semcdb.2009.07.004.

20. Jirapatnakul AC, Fotin S V., Reeves AP, Biancardi AM, Yankelevitz DF, Henschke CI. Automated nodule location and size estimation using a multi-scale laplacian of Gaussian filtering approach. *Proc 31st Annu Int Conf IEEE Eng Med Biol Soc Eng Futur Biomed EMBC 2009*. 2009:1028-1031. doi:10.1109/IEMBS.2009.5334683.

21. Meijering E. Cell Segmentation: 50 Years Down the Road. *IEEE Signal Process Mag*. 2012;29(5):140-145. doi:10.1109/MSP.2012.2204190.

22. Uynuk-Ool T, Rothdiener M, Walters B, et al. The geometrical shape of mesenchymal stromal cells measured by quantitative shape descriptors is determined by the stiffness of the biomaterial and by cyclic tensile forces. *J Tissue Eng Regen Med*. 2017;11(12):3508-3522. doi:10.1002/term.2263.

23. Koç ON, Peters C, Aubourg P, et al. Bone marrow-derived mesenchymal stem cells remain host-derived despite successful hematopoietic engraftment after allogeneic transplantation in patients with lysosomal and peroxisomal storage diseases. *Exp Hematol*. 1999;27(11):1675-1681. doi:10.1016/S0301-472X(99)00101-0.

24. Koç ON, Lazarus HM. Mesenchymal stem cells: Heading into the clinic. *Bone Marrow Transplant*. 2001;27(3):235-239. doi:10.1038/sj.bmt.1702791.

25. Qi M, Zou S, Han L, Zhou H, Hu J. Expression of bone-related genes in bone marrow MSCs after cyclic mechanical strain: implications for distraction osteogenesis. *Int J Oral Sci*. 2009;1(3):143-150. doi:10.4248/IJOS.09021.

26. Dumas V, Ducharne B, Perrier A, et al. Extracellular matrix produced by osteoblasts cultured under low-magnitude, high-frequency stimulation is favourable to osteogenic

differentiation of mesenchymal stem cells. *Calcif Tissue Int*. 2010;87(4):351-364. doi:10.1007/s00223-010-9394-8.

27. Kavlock KD, Goldstein AS. Effect of Pulse Frequency on the Osteogenic Differentiation of Mesenchymal Stem Cells in a Pulsatile Perfusion Bioreactor. *J Biomech Eng*. 2011;133(9):091005. doi:10.1115/1.4004919.

28. Pilz GA, Ulrich C, Ruh M, et al. Human Term Placenta-Derived Mesenchymal Stromal Cells Are Less Prone to Osteogenic Differentiation Than Bone Marrow-Derived Mesenchymal Stromal Cells. *Stem Cells Dev*. 2011;20(4).

29. Jeong JY, Park SH, Shin JW, Kang YG, Han KH, Shin JW. Effects of intermittent hydrostatic pressure magnitude on the chondrogenesis of MSCs without biochemical agents under 3D co-culture. *J Mater Sci Mater Med*. 2012;23(11):2773-2781. doi:10.1007/s10856-012-4718-z.

30. Khayat G, Rosenzweig DH, Quinn TM. Low frequency mechanical stimulation inhibits adipogenic differentiation of C3H10T1/2 mesenchymal stem cells. *Differentiation*. 2012;83(4):179-184. doi:10.1016/j.diff.2011.12.004.

31. Reyes M, Dudek A, Jahagirdar B, Koodie L, Marker PH, Verfaillie CM. Origin of endothelial progenitors in human postnatal bone marrow. *J Clin Invest*. 2002;109(3):337-346. doi:10.1172/JCI200214327.

32. Sanchez-Ramos J, Song S, Cardozo-Pelaez F, et al. Adult bone marrow stromal cells differentiate into neural cells in vitro. *Exp Neurol*. 2000;164(2):247-256. doi:10.1006/exnr.2000.7389.

33. Song G, Ju Y, Shen X, Luo Q, Shi Y, Qin J. Mechanical stretch promotes proliferation of rat bone marrow mesenchymal stem cells. *Colloids Surfaces B Biointerfaces*. 2007;58(2):271-277. doi:10.1016/j.colsurfb.2007.04.001.

34. Ghazanfari S, Tafazzoli-Shadpour M, Shokrgozar MA. Effects of cyclic stretch on proliferation of mesenchymal stem cells and their differentiation to smooth muscle cells. *Biochem Biophys Res Commun*. 2009;388(3):601-605. doi:10.1016/j.bbrc.2009.08.072.

35. Brun J, Lutz KA, Neumayer KMH, et al. Smooth Muscle-Like Cells Generated from Human Mesenchymal Stromal Cells Display Marker Gene Expression and Electrophysiological Competence Comparable to Bladder Smooth Muscle Cells. *PLoS One*. 2015:1-21. doi:10.1371/journal.pone.0145153.

36. Lindroos B, Suuronen R, Miettinen S. The Potential of Adipose Stem Cells in Regenerative Medicine. *Stem Cell Rev Reports*. 2011;7(2):269-291. doi:10.1007/s12015-010-9193-7.

37. Dai R, Wang Z, Samanipour R, Koo K, Kim K. Adipose-Derived Stem Cells for Tissue Engineering and Regenerative Medicine Applications. *Stem Cells Int*. 2016;2016:1-19. doi:10.1155/2016/6737345.

38. Halvorsen YDC, Bond A, Sen A, et al. Thiazolidinediones and glucocorticoids synergistically induce differentiation of human adipose tissue stromal cells: Biochemical,

cellular, and molecular analysis. *Metabolism*. 2001;50(4):407-413. doi:10.1053/meta.2001.21690.

39. Choi YS, Matsuda K, Dusting GJ, Morrison WA, Dilley RJ. Engineering cardiac tissue in vivo from human adipose-derived stem cells. *Biomaterials*. 2010;31(8):2236-2242. doi:10.1016/j.biomaterials.2009.11.097.

40. Iyyanki T, Hubenak J, Liu J, Chang EI, Beahm EK, Zhang Q. Harvesting technique affects adipose-derived stem cell yield. *Aesthetic Surg J*. 2015;35(4):467-476. doi:10.1093/asj/sju055.

41. Furuhata Y, Yoshitomi T, Kikuchi Y, Sakao M, Yoshimoto K. Osteogenic Lineage Commitment of Adipose-Derived Stem Cells Is Predetermined by Three-Dimensional Cell Accumulation on Micropatterned Surface. *ACS Appl Mater Interfaces*. 2017;9(11):9339-9347. doi:10.1021/acsami.6b15688.

42. Helder MN, Knippenberg M, Klein-Nulend J, Wuisman PIJM. Stem Cells from Adipose Tissue Allow Challenging New Concepts for Regenerative Medicine. *Tissue Eng*. 2007;13(8):1799-1808. doi:10.1089/ten.2006.0165.

43. Lim S, Cho H, Lee E, et al. Osteogenic stimulation of human adipose-derived stem cells by pre-treatment with fibroblast growth factor 2. *Cell Tissue Res*. 2016;364(1):137-147. doi:10.1007/s00441-015-2311-8.

44. Estes BT, Wu AW, Guilak F. Potent induction of chondrocytic differentiation of human adipose-derived adult stem cells by bone morphogenetic protein 6. *Arthritis Rheum*. 2006;54(4):1222-1232. doi:10.1002/art.21779.

45. Kabiri A, Esfandiari E, Hashemibeni B, Kazemi M, Mardani M, Esmaeili A. Effects of FGF-2 on human adipose tissue derived adult stem cells morphology and chondrogenesis enhancement in Transwell culture. *Biochem Biophys Res Commun*. 2012;424(2):234-238. doi:10.1016/j.bbrc.2012.06.082.

46. Desiderio V, De Francesco F, Schiraldi C, et al. Human Ng2+ adipose stem cells loaded in vivo on a new crosslinked hyaluronic acid-lys scaffold fabricate a skeletal muscle tissue. *J Cell Physiol*. 2013;228(8):1762-1773. doi:10.1002/jcp.24336.

47. Lee W-CC, Maul TM, Vorp DA, Rubin JP, Marra KG. Effects of uniaxial cyclic strain on adipose-derived stem cell morphology, proliferation, and differentiation. *Biomech Model Mechanobiol*. 2007;6(4):265-273. doi:10.1007/s10237-006-0053-y.

48. Heydarkhan-Hagvall S, Schenke-Layland K, Yang JQ, et al. Human adipose stem cells: A potential cell source for cardiovascular tissue engineering. *Cells Tissues Organs*. 2008;187(4):263-274. doi:10.1159/000113407.

49. Harris LJ, Abdollahi H, Zhang P, McIlhenny S, Tulenko TN, DiMuzio PJ. Differentiation of adult stem cells into smooth muscle for vascular tissue engineering. *J Surg Res*. 2011;168(2):306-314. doi:10.1016/j.jss.2009.08.001.

50. Bjorninen M, Gilmore K, Pelto J, et al. Electrically Stimulated Adipose Stem Cells on

Polypyrrole-Coated Scaffolds for Smooth Muscle Tissue Engineering. *Ann Biomed Eng*. 2016;45(4):1-12. doi:10.1007/s10439-016-1755-7.

51. Gunetti M, Tomasi S, Giammò A, et al. Myogenic Potential of Whole Bone Marrow Mesenchymal Stem Cells In Vitro and In Vivo for Usage in Urinary Incontinence. *PLoS One*. 2012;7(9). doi:10.1371/journal.pone.0045538.

52. Jeon ES, Moon HJ, Lee MJ, et al. Sphingosylphosphorylcholine induces differentiation of human mesenchymal stem cells into smooth-muscle-like cells through a TGF- -dependent mechanism. *J Cell Sci*. 2006;119(23):4994-5005. doi:10.1242/jcs.03281.

53. Park WS, Heo SC, Jeon ES, et al. Functional expression of smooth muscle-specific ion channels in TGF- 1-treated human adipose-derived mesenchymal stem cells. *AJP Cell Physiol*. 2013;305(4):C377-C391. doi:10.1152/ajpcell.00404.2012.

54. Brun J, Abruzzese T, Rolauffs B, Aicher WK, Hart ML. Choice of xenogenic-free expansion media significantly influences the myogenic differentiation potential of human bone marrow-derived mesenchymal stromal cells. *Cytotherapy*. 2016;18(3):344-359. doi:10.1016/j.jcyt.2015.11.019.

55. Parvizi M, Bolhuis-Versteeg LAM, Poot AA, Harmsen MC. Efficient generation of smooth muscle cells from adipose-derived stromal cells by 3D mechanical stimulation can substitute the use of growth factors in vascular tissue engineering. *Biotechnol J*. 2016;11(7):932-944. doi:10.1002/biot.201500519.

56. Elçin AE, Parmaksiz M, Dogan A, et al. Differential gene expression profiling of human adipose stem cells differentiating into smooth muscle-like cells by TGFβ1/BMP4. *Exp Cell Res*. 2017;352(2):207-217. doi:10.1016/j.yexcr.2017.02.006.

57. Zhang L, Kahn CJF, Chen H-Q, Tran N, Wang X. Effect of uniaxial stretching on rat bone mesenchymal stem cell: orientation and expressions of collagen types I and III and tenascin-C. *Cell Biol Int*. 2008;32(3):344-352. doi:10.1016/j.cellbi.2007.12.018.

58. Maul TM, Chew DW, Nieponice A, Vorp D a. Mechanical stimuli differentially control stem cell behavior: morphology, proliferation, and differentiation. *Biomech Model Mechanobiol*. 2011;10(6):939-953. doi:10.1007/s10237-010-0285-8.

59. Kim T, Sun J, Lu S, Qi Y, Wang Y. Prolonged Mechanical Stretch Initiates Intracellular Calcium Oscillations in Human Mesenchymal Stem Cells. 2014;9(10):1-9. doi:10.1371/journal.pone.0109378.

60. Bornstein P, Piez K a. Biochemical Study of Human Skin Collagen and the Relation Between Intra- and Intermolecular Cross-Linking. *J Clin Invest*. 1964;43(9):1813-1823. doi:10.1172/JCI105055.

61. Francis G, Thomas J. Isolation and chemical characterization of collagen in bovine pulmonary tissues. *Biochem J*. 1975;145(2):287-297. doi:10.1042/bj1450287.

62. Cliche S, Amiot J, Avezard C, Gariépy C. Extraction and characterization of collagen with or without telopeptides from chicken skin. *Poult Sci*. 2003;82(3):503-509.

doi:10.1093/ps/82.3.503.

63. Simkovic D. Contribution to the Method of Cultivation of Cells on a Transparent Collagen Gel. *Exp Cell Res*. 1959;17(3):573-576.

64. Grinnell F, Lamke CR. Reorganization of hydrated collagen lattices by human skin fibroblasts. *J Cell Sci*. 1984;66:51-63. doi:10.1007/s00247-010-1783-7.

65. Ehrlich HP, Rajaratnam JBM. Cell locomotion forces versus cell contraction forces for collagen lattice contraction: An in vitro model of wound contraction. *Tissue Cell*. 1990;22(4):407-417. doi:10.1016/0040-8166(90)90070-P.

66. Davis GE, Pintar Allen K a, Salazar R, Maxwell S a. Matrix metalloproteinase-1 and -9 activation by plasmin regulates a novel endothelial cell-mediated mechanism of collagen gel contraction and capillary tube regression in three-dimensional collagen matrices. *J Cell Sci*. 2001;114(Pt 5):917-930. doi:10.1083/jcb.149.3.741.

67. Townley WA, Cambrey AD, Khaw PT, Grobbelaar AO. Matrix Metalloproteinase Inhibition Reduces Contraction by Dupuytren Fibroblasts. *J Hand Surg Am*. 2008;33(9):1608-1616. doi:10.1016/j.jhsa.2008.06.013.

68. Martin-Martin B, Tovell V, Dahlmann-Noor AH, Khaw PT, Bailly M. The effect of MMP inhibitor GM6001 on early fibroblast-mediated collagen matrix contraction is correlated to a decrease in cell protrusive activity. *Eur J Cell Biol*. 2011;90(1):26-36. doi:10.1016/j.ejcb.2010.09.008.

69. Tovell VE, Chau CY, Khaw PT, Bailly M. Rac1 inhibition prevents tissue contraction and MMP mediated matrix remodeling in the conjunctiva. *Investig Ophthalmol Vis Sci*. 2012;53(8):4682-4691. doi:10.1167/iovs.11-8577.

70. Bian W, Liau B, Badie N, Bursac N. Mesoscopic hydrogel molding to control the 3D geometry of bioartificial muscle tissues. *Nat Protoc*. 2009;4(10):1522-1534. doi:10.1038/nprot.2009.155.

71. Chan BK, Wippich CC, Wu CJ, Sivasankar PM, Schmidt G. Robust and Semi-Interpenetrating Hydrogels from Poly(ethylene glycol) and Collagen for Elastomeric Tissue Scaffolds. *Macromol Biosci*. 2012;12(11):1490-1501. doi:10.1002/mabi.201200234.

72. Khaing ZZ, Schmidt CE. Advances in natural biomaterials for nerve tissue repair. *Neurosci Lett*. 2012;519(2):103-114. doi:10.1016/j.neulet.2012.02.027.

73. Seliktar D, Black R a, Vito RP, Nerem RM. Dynamic mechanical conditioning of collagen-gel blood vessel constructs induces remodeling in vitro. *Ann Biomed Eng*. 2000;28(4):351-362. http://www.ncbi.nlm.nih.gov/pubmed/10870892.

74. Rowe SL, Stegemann JP. Interpenetrating collagen-fibrin composite matrices with varying protein contents and ratios. *Biomacromolecules*. 2006;7(11):2942-2948. doi:10.1021/bm0602233.

75. Stegemann JP, Kaszuba SN, Rowe SL. Review: Advances in Vascular Tissue Engineering

Using Protein-Based Biomaterials. *Tissue Eng*. 2007;13(11):2601-2613. doi:10.1089/ten.2007.0196.

76. Madhavan K, Belchenko D, Motta A, Tan W. Evaluation of composition and crosslinking effects on collagen-based composite constructs. *Acta Biomater*. 2010;6(4):1413-1422. doi:10.1016/j.actbio.2009.09.028.

77. Caves JM, Cui W, Wen J, Kumar VA, Haller CA, Chaikof EL. Elastin-like protein matrix reinforced with collagen microfibers for soft tissue repair. *Biomaterials*. 2011;32(23):5371-5379. doi:10.1016/j.biomaterials.2011.04.009.Elastin-like.

78. Amruthwar SS, Puckett AD, Janorkar A V. Preparation and characterization of novel elastin-like polypeptide-collagen composites. *J Biomed Mater Res - Part A*. 2013;101 A(8):2383-2391. doi:10.1002/jbm.a.34514.

79. Grover CN, Cameron RE, Best SM. Investigating the morphological, mechanical and degradation properties of scaffolds comprising collagen, gelatin and elastin for use in soft tissue engineering. *J Mech Behav Biomed Mater*. 2012;10:62-74. doi:10.1016/j.jmbbm.2012.02.028.

80. Nguyen TU, Bashur CA, Kishore V. Impact of elastin incorporation into electrochemically aligned collagen fibers on mechanical properties and smooth muscle cell phenotype. *Biomed Mater*. 2016;11(2). doi:10.1088/1748-6041/11/2/025008.

81. Liao E, Yaszemski M, Krebsbach P, Hollister S. Tissue-Engineered Cartilage Constructs Using Composite Hyaluronic Acid/Collagen I Hydrogels and Designed Poly(Propylene Fumarate) Scaffolds. *Tissue Eng*. 2007;13(3):537-550. doi:10.1089/ten.2006.0117.

82. Xu B, Chow M-J, Zhang Y. Experimental and modeling study of collagen scaffolds with the effects of crosslinking and fiber alignment. *Int J Biomater*. 2011;2011:172389. doi:10.1155/2011/172389.

83. Franz S, Allenstein F, Kajahn J, et al. Artificial extracellular matrices composed of collagen i and high-sulfated hyaluronan promote phenotypic and functional modulation of human pro-inflammatory M1 macrophages. *Acta Biomater*. 2013;9(3):5621-5629. doi:10.1016/j.actbio.2012.11.016.

84. Deister C, Aljabari S, Schmidt CE. Effects of collagen 1, fibronectin, laminin and hyaluronic acid concentration in multi-component gels on neurite extension. *J Biomater Sci Polym Ed*. 2007;18(8):983-997. doi:10.1163/156856207781494377.

85. Hansen U, Bruckner P. Macromolecular specificity of collagen fibrillogenesis: Fibrils of collagens I and XI contain a heterotypic alloyed core and a collagen I sheath. *J Biol Chem*. 2003;278(39):37352-37359. doi:10.1074/jbc.M304325200.

86. Rowe SL, Lee S, Stegemann JP. Influence of thrombin concentration on the mechanical and morphological properties of cell-seeded fibrin hydrogels. *Acta Biomater*. 2007;3(1):59-67. doi:10.1016/j.actbio.2006.08.006.

87. Peterson AW, Caldwell DJ, Rioja AY, Rao RR, Putnam AJ, Stegemann JP. Vasculogenesis

and Angiogenesis in Modular Collagen-Fibrin Microtissues. *Biomater Sci*. 2014;2(10):1487-1508. doi:10.1002/ana.22528.Toll-like.

88.   Rao RR, Peterson AW, Ceccarelli J, Putnam AJ, Stegemann JP. Matrix composition regulates three-dimensional network formation by endothelial cells and mesenchymal stem cells in collagen/fibrin materials. *Angiogenesis*. 2012;15(2):253-264. doi:10.1007/s10456-012-9257-1.

89.   Rao RR, Vigen ML, Peterson AW, Caldwell DJ, Putnam AJ, Stegemann JP. Dual-Phase Osteogenic and Vasculogenic Engineered Tissue for Bone Formation. *Tissue Eng Part A*. 2015;21(3-4):530-540. doi:10.1089/ten.tea.2013.0740.

90.   Rioja AY, Tiruvannamalai Annamalai R, Paris S, Putnam AJ, Stegemann JP. Endothelial sprouting and network formation in collagen- and fibrin-based modular microbeads. *Acta Biomater*. 2016;29:33-41. doi:10.1016/j.actbio.2015.10.022.

91.   Wise JK, Alford AI, Goldstein SA, Stegemann JP. Comparison of Uncultured Marrow Mononuclear Cells and Culture-Expanded Mesenchymal Stem Cells in 3D Collagen-Chitosan Microbeads for Orthopedic Tissue Engineering. *Tissue Eng Part A*. 2014;20(1-2):210-224. doi:10.1089/ten.tea.2013.0151.

92.   Wise JK, Alford AI, Goldstein SA, Stegemann JP. Synergistic enhancement of ectopic bone formation by supplementation of freshly isolated marrow cells with purified MSC in collagen–chitosan hydrogel microbeads. *Connect Tissue Res*. 2016;57(6):516-525. doi:10.1016/j.antiviral.2015.06.014.Chronic.

93.   Girton TS, Oegema TR, Grassl ED, Isenberg BC, Tranquillo RT. Mechanisms of Stiffening and Strengthening in Media-. *J Biomech Eng*. 2000;122(June).

94.   Bedran-Russo AKB, Pereira PNR, Duarte WR, Drummond JL, Yamauchi M. Cytotoxicity of formaldehyde on human osteoblastic cells is related to intracellular glutathione levels. *J Biomed Mater Res B Appl Biomater*. 2007;83(2):268-272. doi:10.1002/jbmb.

95.   Wu X, Black L, Santacana-Laffitte G, Patrick CW. Preparation and assessment of glutaraldehyde-crosslinked collagen-chitosan hydrogels for adipose tissue engineering. *J Biomed Mater Res Part A*. 2007;81(1):59-65. doi:10.1002/jbm.a.

96.   Everaerts F, Torrianni M, Hendriks M, Feijen J. Biomechanical properties of carbodiimide crosslinked collagen: Influence of the formation of ester crosslinks. *J Biomed Mater Res - Part A*. 2008;85(2):547-555. doi:10.1002/jbm.a.31524.

97.   Francis-Sedlak ME, Uriel S, Larson JC, Greisler HP, Venerus DC, Brey EM. Characterization of type I collagen gels modified by glycation. *Biomaterials*. 2009;30(9):1851-1856. doi:10.1016/j.biomaterials.2008.12.014.

98.   Sundararaghavan HG, Monteiro GA, Firestein BL, Shreiber DI. Neurite growth in 3D collagen gels with gradients of mechanical properties. *Biotechnol Bioeng*. 2009;102(2):632-643. doi:10.1002/bit.22074.

99.   Yan LP, Wang YJ, Ren L, et al. Genipin-cross-linked collagen/chitosan biomimetic

scaffolds for articular cartilage tissue engineering applications. *J Biomed Mater Res - Part A*. 2010;95 A(2):465-475. doi:10.1002/jbm.a.32869.

100. Chandran PL, Paik DC, Holmes JW. Structural Mechanism for Alteration of Collagen. *Connect Tissue Res*. 2012;53(4). doi:10.3109/03008207.2011.640760.STRUCTURAL.

101. Walters VI, Kwansa AL, Freeman JW. Design and analysis of braid-twist collagen scaffolds. *Connect Tissue Res*. 2012;53(3):255-266. doi:10.3109/03008207.2011.634532.

102. Bou-Akl T, Banglmaier R, Miller R, Vandevord P. Effect of crosslinking on the mechanical properties of mineralized and non-mineralized collagen fibers. *J Biomed Mater Res - Part A*. 2013;101 A(9):2507-2514. doi:10.1002/jbm.a.34549.

103. Ekaputra AK, Zhou Y, Cool SM, Hutmacher DW. Composite electrospun scaffolds for engineering tubular bone grafts. *Tissue Eng Part A*. 2009;15(12).

104. McClure MJ, Sell SA, Simpson DG, Walpoth BH, Bowlin GL. A three-layered electrospun matrix to mimic native arterial architecture using polycaprolactone, elastin, and collagen: A preliminary study. *JOVE*. 2011;6(7). doi:10.1016/j.actbio.2009.12.029.

105. McGuigan AP, Bruzewicz DA, Glavan A, Butte M, Whitesides GM. Cell encapsulation in sub-mm sized gel modules using replica molding. *PLoS One*. 2008;3(5). doi:10.1371/journal.pone.0002258.

106. Leung BM, Sefton M V. A Modular Approach to Cardiac Tissue Engineering. *Tissue Eng Part A*. 2010;16(10):3207-3218. doi:10.1089/ten.tea.2009.0746.

107. Rothdiener M, Hegemann M, Uynuk-Ool T, et al. Stretching human mesenchymal stromal cells on stiffness-customized collagen type I generates a smooth muscle marker profile without growth factor addition. *Sci Rep*. 2016;6(October):35840. doi:10.1038/srep35840.

108. Stewart J, Manmathan G, Wilkinson P. Primary prevention of cardiovascular disease: A review of contemporary guidance and literature. *JRSM Cardiovasc Dis*. 2017;6:204800401668721. doi:10.1177/2048004016687211.

109. Mathers CD, Loncar D. Projections of global mortality and burden of disease from 2002 to 2030. *PLoS Med*. 2006;3(11):2011-2030. doi:10.1371/journal.pmed.0030442.

110. NICE. Cardio Cardiovascular disease: risk assessment vascular disease: risk assessment and reduction, including lipid and reduction, including lipid modification modification Y Your responsibility our responsibility. 2014;(July 2014). https://www.nice.org.uk/guidance/cg181/resources/cardiovascular-disease-risk-assessment-and-reduction-including-lipid-modification-pdf-35109807662293.

111. Piepoli MF, Hoes AW, Agewall S, et al. 2016 European Guidelines on cardiovascular disease prevention in clinical practice. *Eur Heart J*. 2016;37(29):2315-2381. doi:10.1093/eurheartj/ehw106.

112. Robinson JG, Farnier M, Krempf M, et al. Efficacy and Safety of Alirocumab in Reducing Lipids and Cardiovascular Events. *N Engl J Med*. 2015;372(16):1489-1499.

doi:10.1056/NEJMoa1501031.

113. Halvorsen S, Andreotti F, Ten Berg JM, et al. Aspirin therapy in primary cardiovascular disease prevention: A position paper of the european society of cardiology working group on thrombosis. *J Am Coll Cardiol*. 2014;64(3):319-327. doi:10.1016/j.jacc.2014.03.049.

114. Antoniou GA, Chalmers N, Georgiadis GS, et al. A meta-analysis of endovascular versus surgical reconstruction of femoropopliteal arterial disease. *J Vasc Surg*. 2013;57(1):242-253. doi:10.1016/j.jvs.2012.07.038.

115. Go AS, Mozaffarian D, Roger VL, et al. Heart disease and stroke statistics-2013 update: A Report from the American Heart Association. *Circulation*. 2013;127(1). doi:10.1161/CIR.0b013e31828124ad.

116. Harskamp RE, Lopes RD, Baisden CE, De Winter RJ, Alexander JH. Saphenous vein graft failure after coronary artery bypass surgery: Pathophysiology, management, and future directions. *Ann Surg*. 2013;257(5):824-833. doi:10.1097/SLA.0b013e318288c38d.

117. Pashneh-Tala S, MacNeil S, Claeyssens F. The Tissue-Engineered Vascular Graft—Past, Present, and Future. *Tissue Eng Part B Rev*. 2015;22(1):ten.teb.2015.0100. doi:10.1089/ten.teb.2015.0100.

118. Deutsch M, Meinhart J, Zilla P, et al. Long-term experience in autologous in vitro endothelialization of infrainguinal ePTFE grafts. *J Vasc Surg*. 2009;49(2):352-362. doi:10.1016/j.jvs.2008.08.101.

119. Klausner AP, Vapnek JM. Urinary incontinence in the geriatric population. *Mt Sinai J Med*. 2003;70(1):54-61.

120. Hart ML, Izeta A, Herrera-Imbroda B, Amend B, Brinchmann JE. Cell Therapy for Stress Urinary Incontinence. *Tissue Eng Part B Rev*. 2015;21(4):365-376. doi:10.1089/ten.TEB.2014.0627.

121. Stothers L, Friedman B. Risk factors for the development of stress urinary incontinence in women. *Curr Urol Rep*. 2011;12(5):363-369. doi:10.1007/s11934-011-0215-z.

122. Hart ML, Neumayer KMH, Vaegler M, et al. Cell-based therapy for the deficient urinary sphincter. *Curr Urol Rep*. 2013;14(5):476-487. doi:10.1007/s11934-013-0352-7.

123. Rovner ES, Wein AJ. Treatment options for stress urinary incontinence. *Rev Urol*. 2004;6 Suppl 3(Suppl 3):S29-47. doi:10.1002/nau.

124. Miller KL. Stress Urinary Incontinence in Women: Review and Update on Neurological Control. *J Women's Heal*. 2005;14(7):595-608. doi:10.1089/jwh.2005.14.595.

125. Kerr LA. Bulking agents in the treatment of stress urinary incontinence: history, outcomes, patient populations, and reimbursement profile. *Rev Urol*. 2005;7 Suppl 1:S3-S11. http://www.pubmedcentral.nih.gov/articlerender.fcgi?artid=1477593&tool=pmcentrez&rendertype=abstract.

126. Ashton-Miller JA, DeLancey JOL. Functional anatomy of the female pelvic floor. *Ann N Y Acad Sci*. 2007;1101:266-296. doi:10.1196/annals.1389.034.

127. Atala A, Bauer SB, Soker S, Yoo JJ, Retik AB. Tissue-engineered autologous bladders for patients needing cystoplasty. *Lancet*. 2006;367(9518):1241-1246. doi:10.1016/S0140-6736(06)68438-9.

128. Raghavan AM, Shenot PJ. Bladder augmentation using an autologous neo-bladder construct. *Kidney Int*. 2009;76(2):236. doi:10.1038/ki.2009.81.

129. Xie C, Ritchie RP, Huang H, Zhang J, Chen YE. Smooth muscle cell differentiation in vitro: Models and underlying molecular mechanisms. *Arter Thromb Vasc Bio*. 2011;31(7):1485-1494. doi:10.1161/ATVBAHA.110.221101.Smooth.

130. Dash BC, Jiang Z, Suh C, Qyang Y. Application, Induced Pluripotent Stem Cell-derived Vascular Smooth Muscle Cells: Methods and. *Biochem J*. 2015;465(2):185-194. doi:10.1042/BJ20141078.Induced.

131. Owens GK, Loeb a, Gordon D, Thompson MM. Expression of smooth muscle-specific alpha-isoactin in cultured vascular smooth muscle cells: relationship between growth and cytodifferentiation. *J Cell Biol*. 1986;102(2):343-352. doi:10.1083/jcb.102.2.343.

132. Kim HR, Gallant C, Leavis PC, Gunst SJ, Morgan KG. Cytoskeletal remodeling in differentiated vascular smooth muscle is actin isoform dependent and stimulus dependent. *Am J Physiol Cell Physiol*. 2008;295(3):C768-78. doi:10.1152/ajpcell.00174.2008.

133. Duband JL, Gimona M, Scatena M, Sartore S, Small JV. Calponin and SM22 as differentiation markers of smooth muscle: spatiotemporal distribution during avian embryonic development. *Differentiation*. 1993;55(1):1-11. doi:10.1111/j.1432-0436.1993.tb00027.x.

134. Babu GJ, Pyne GJ, Zhou Y, et al. Isoform switching from SM-B to SM-A myosin results in decreased contractility and altered expression of thin filament regulatory proteins. *AJP Cell Physiol*. 2004;287(3):C723-C729. doi:10.1152/ajpcell.00029.2004.

135. Morgan KG, Gangopadhyay SS. Signal Transduction in Smooth Muscle Invited Review: Cross-bridge regulation by thin filament-associated proteins. *J Appl Physiol*. 2001;91(4):953-962. doi:10.1152/japplphysiol.00017.2004.

CHAPTER 2

Engineering the Geometrical Shape of Mesenchymal Stromal Cells through Defined Cyclic Stretch Regimens

2.1 - Introduction

Mesenchymal stromal cells (MSCs) are well known for their ability to differentiate *in vitro* into a wide range of somatic cells including osteogenic, chondrogenic, adipogenic, myogenic, endothelial, and neurogenic lineages [1, 2, 3, 4, 5, 6, 7]. MSCs are recognized as adult, self-renewing, and multipotent stem cells with substantial potential for therapeutic use [8, 9]. They have been forecasted to substantially change disease outcomes and patient lives [10] and better understanding and controlling MSC properties could accelerate this goal substantially.

Cellular shape is a fundamental signal for proliferation [11], potently regulates cell growth and physiology, and is indicative of specific functions [12]. Membrane protrusions influence cell shape and are highly relevant for adhesion, migration, and rigidity sensing [13]. Moreover, specific MSC shapes accompany the differentiation into different cell lineages, as rounded MSC shapes are associated with adipogenic differentiation and elongated shapes with myogenesis [14, 15, 16, 17]. Utilizing this association of MSC shape with function, previous studies generated specific cell shapes for determining lineage commitment, using adhesive micro-patterned surfaces [18, 19] and multi-perforated polycarbonate membranes [17]. Other studies have used cyclic tensile forces for inducing myogenic differentiation, while generating dynamically elongated cell shapes [16, 20], based on the observation that elongated MSCs express markers of smooth muscle cells (SMCs) [17]. Thus,

27

MSC shape will likely play an important role in understanding and engineering tissue constructs for future applications.

Previously, we demonstrated that the geometrical shape of many bone marrow derived Mesenchymal Stem Cells (bMSCs) can be measured by quantitatively calculating mathematical shape descriptors with a semi-automated high-throughput method [21]. These shape descriptors describe different aspects of cell morphology (Fig. 1.1). Using this method and a system of competing cues for influencing bMSC shape (with dynamic effects on shape through cyclic stretch and static effects on shape through the stiffness-defined biomaterial), we discovered that stretching cells did not necessarily produce elongated bMSCs; instead, it produced bMSCs that were ultimately rounder than unstretched controls [21]. While this could have been interpreted as cells coming unattached, we were able to show that it was a reorganization of the entire cellular morphology to eventually elongate. In the present study we asked the fundamental question whether cyclic stretch regimens can be used for engineering a variety of defined cell morphologies, whether elongated bMSCs can be generated with this approach, and what the impact on smooth muscle cell (SMC) marker expression would be. These questions are important, as stem cells are continuously exposed to a dynamically changing mechanical environment [22], which acts as a key regulator of their fate [22, 23], and because producing a variety of shapes through biomechanical forces could theoretically be utilized *in vivo* for controlling bMSC function. Our general hypothesis was that varying parameters including maximum strain, stretch time, and the repetition of optimized stretch regimens (stretching the same specimen with the same parameters on two consecutive days) would generate significantly different bMSC morphologies, and that varying these parameters could be used for specifically producing an elongated bMSC shape. Consequently, we applied specific regimens of cyclic stretch to bMSCs seeded on compressed

28

collagen sheets (matched with nanoscale stiffness for myogenic differentiation [24]) and assessed the effects of this stimulus on cell phenotype. For assessing the impact of cell shape on phenotype, we investigated the expression of SMC markers as a function of stretch and respective morphology. Elongated bMSC morphologies have typically been associated with increased expression of SMC markers [16, 17], and because biomechanical forces increase bMSC differentiation towards a SMC phenotype [14, 15, 16], we expected these responses to correlate. Finally, because cyclic stretch is known to affect the alignment of cells relative to the stretch direction [14, 15, 16, 20, 25, 26, 27], we asked how cyclic stretch affects bMSC alignment and if these changes can be explained by cell morphology. Collectively, we aimed to introduce the novel concept of the targeted engineering of bMSC shape through defined cyclic stretch regimens; this would advance our understanding of cell differentiation and promises broad *in vitro* and *in vivo* applications in mechanobiology, tissue engineering, and clinical regenerative medicine.

Length (normalized)	1.0	1.0	2.0	1.0
Roundness	1.0	0.5	0.5	0.9
Circularity	1.0	0.8	0.8	0.4

Figure 2.1: Comparison of Shape Factors Using Hypothetical bMSCs. Figure 2.1 outlines the different features of cells that each shape factor defines. Cell length measures the "long axis" of each cell and has been used frequently in myogenic studies as cells undergoing differentiation become longer. Cell roundness is a ratio of "area" to "long axis" normalized to one. This quantitative measurement can be used to describe the rate of hypertrophy of cells with respect to both their short and long axes 55. Cells with different roundness values could plausibly have similar lengths or vice versa. Circularity describes a third biologically relevant feature as it mathematically measures the ratio of "area" to "perimeter", normalized to one. As cells spread or begin to migrate through their surroundings, they protrude out 13. This may or may not be captured by changes cell length or roundness but, according to our definition, can drastically decrease circularity.

2.2 - Materials and Methods

bMSC isolation and expansion

Bone Marrow aspirates were obtained from the proximal femurs of osteoarthritic patients (n=29, age 50 to 86) who underwent total hip replacement in the Department of Trauma and Restorative Surgery, BG Trauma Clinic, University of Tuebingen. Aspirates were taken with approval of the local research ethics committee of the Medical Faculty of the University of Tuebingen (623/2013BO2) and with informed consent from the patients. These cells were chosen as being sourced from similar demographics of patients requiring SMC cellular therapies as well. All methods were carried out in accordance with the guidelines of the local research ethics committee of the medical faculty of the University of Tuebingen. Human bone marrow bMSCs were isolated as described in [24]. Aspirates were washed with PBS, centrifuged at 150 g (10 minutes, room temperature), and the pellet was re-suspended in PBS, discarding the supernatant. The bMSC were then separated using a Ficoll density gradient fractionation (density 1.077 g/mL, GE Healthcare Life Sciences, Uppsala, Sweden, 400 g, 30 min, room temp). The mononuclear cell layer was removed, washed in PBS and seeded in T75 flasks. The separated bMSC were cultured and expanded at 37ºC and 5% CO_2 in good manufacturing practice (GMP)- compliant media made with DMEM low glucose (Sigma-Aldrich, Hamburg, Germany), 1000 IU heparin (Carl Roth, Karlsruhe, Germany), 25 mM hepes (Lonza, Basel, Switzerland), 5% human plasma (TCS Biosciences, Buckingham, UK), 5% human pooled platelet lysate (10^8 platelets/mL medium, ZKT Tuebingen, Germany), 2 mM L-glutamine (Lonza), and 1% penicillin-streptomycin solution (Life technologies, Darmstadt, Germany), according to [7, 51]. 24h after seeding, GMP expansion media was replaced and then changed twice a week. At near confluence, after around 7 days, cells were

removed with trypsin, counted, and re-plated (10^4 cells per flask) in GMP expansion media for further passaging.

Expression of cell surface antigens for bMSC identification and sorting

To distinguish and sort heterogenous populations from the marrow aspirates, the expression of CD90, CD14, CD11b (R&D Systems, Minneapolis, USA), CD105, CD73, CD45 and CD34 (BD Pharmingen, San Diego, USA) on MSC was analyzed by flow cytometry as we have shown previously [6, 52], and in accordance with [53]. bMSCs were detached gently using Accutase. Nonspecific binding of antibodies was blocked with Gamunex (Talecris Biotherapeutics, Frankfurt, Germany). The bMSC were washed twice with PFEA buffer (PBS, 2% FCS, 2mM EDTA, 0.01% sodium azide) and incubated for 20 min at 4°C with phycoerythrin (PE)-conjugated or allophycocyanin (APC)-conjugated monoclonal antibodies (mAB, BD Pharmingen, Heidelberg, Germany). Unbound antibodies were washed away twice with PFEA buffer, and MSCs were analyzed by flow cytometry (BD LSRII, San Diego, USA). Data were evaluated using the software FlowJo (Tree Star, Inc., Ashland, Oregon, USA).

bMSC seeding on compressed collagen sheets

Compressed rat collagen I sheets with a previously optimized collagen concentration of 80 mg/mL [21, 24] were generated (Amedrix, Esslingen, Germany) and cut into 4x1 cm sheets. This fabrication method is well established and commercialized and while bovine collagen meets more clinical standards, collagen is highly conserved across species. After passaging in GMP expansion media (DMEM with pooled plasma and platelet lysate as described [21, 24]), bMSCs (passages 3-5)

31

were seeded at 15,000 bMSC/cm^2 at day 0 onto collagen sheets. Sheets were cultured in high glucose DMEM (4g/L, Life Technologies, Darmstadt, Germany), 10% FBS (Biochrom), 2% penicillin-streptomycin (Gibco/Life Technologies), and 1% fungicide (Biochrom) at 37ºC and 5% CO_2 for 3 days before stretching on day 4.

Sinusoidal cyclic stretch of collagen sheets and adhering bMSCs

Collagen sheets seeded with bMSCs at passages 3-5 with 15,000 cells/cm^2 were cultured for 3 days and inserted on day 4 into the bioreactor chamber of an incubator-housed ElectroForce 5210 BioDynamic-Test-System (Bose, Minnesota, USA). Identical bioreactor chambers filled with 200 mL of control media were used for applying cyclic stretch and for incubating unstretched control sheets. Uniaxial displacement-controlled cyclic stretch was applied at 1 Hz with either 5% or 10% strain and for either 3 or 16 hours on day 4 only, or on days 4 and 5 before analysis. These parameters were chosen based on common strain parameters in literature and previous findings in our lab. Sheets stretched for a single regimen and their unstretched control sheets cultured for the same period of time were labeled "1x". One half of this set of sheets was analyzed, the other half of this set of sheets was incubated overnight and stretched again on day 5 with a second stretch regimen that was identical to day 4. This procedure was termed "repetition of a given stretch regimen" and these sheets and their respective unstretched controls were labeled "2x". After cyclic stretch, the sheets were cut in two equally sized halves. One half was processed for qRT-PCR and one was prepared for fluorescence microscopy.

bMSC seeding and stretching on silicone sheets

Non-reinforced vulcanized matt silicone sheets were obtained from Specialty Manufacturing (No. 70P001-200-030, 40durometer-Shore-A; Saginaw, Michigan, USA). Sheets were coated with fibronectin from bovine plasma (F1141; Sigma-Aldrich, Seinheim, Germany) diluted in PBS (12.5 μg/ml). Silicone sheets (2 × 1 cm) were covered with 700 μL coating substrate in 12-well culture plates for 24 h (room temperature), washed with 0.05% Tween 20 in 2 ml phosphate-buffered saline (PBS), and washed three times with 2 ml PBS. Silicone was seeded with MSCs at passages 3-5 with 15,000 cells/cm^2, was cultured for 3 days and inserted on day 4 into the bioreactor chamber of the same incubator-housed ElectroForce 5210 BioDynamic-Test-System (Bose, Minnesota, USA). Uniaxial displacement-controlled cyclic stretch was applied at 1 Hz with 10% strain for 16 hours, the sheet was allowed to recover for 8 hours and then stretched again for 16 hours before analysis. After the second cycle of stretch, the sheet was prepared for fluorescence microscopy.

bMSC seeding and stretching in collagen type I hydrogels

Solutions of human MSC (with a final concentration of 1.0 million cells/mL) combined with 5x concentrated DMEM, 10% fetal bovine serum, and acid-solubilized Type I bovine collagen (MP Biomedicals, Solon, OH) was brought to neutral pH with 0.1M NaOH. The final solution was pipetted into a bioreactor chamber designed and built by Tissue Growth Technologies (TGT LigaGenTM, Minnetonka, MN). The chambers were incubated at 37°C to permit gelation and an hour later 1x DMEM supplemented with 10% FBS (Lonza) and 1% Penstrep (Lonza) was added. The chambers were cultured for 3 days before the casting mold was removed, leaving the gel suspended. The next day the chamber was inserted in a bioreactor also designed by Tissue

Growth Technologies and proprietary software was used to stretch the gel at 10% strain over night before being relieved of stretch and then then stretched for a consecutive night. After the second cycle of stretch, the gel was prepared for fluorescence microscopy.

Fluorescence microscopy for cell shape

The bMSC-seeded sheets used for imaging were stained with Calcein and Hoechst Solution (Cell Viability Imaging Kit, Roche) based on the manufacturer's protocols and on our previous work [21]. bMSCs attached to the collagen sheets were imaged using a Zeiss LSM510 microscope with AxioVison4.8 and manual exposure correction. Calcein-stained bMSC morphology was visualized using the green filter and the nuclei were imaged using a blue filter. Using the MosaiX module, a mosaic of 10x10 images (with a size of 12,633 x 9,429px corresponding to 8,211.45 x 6,128.85 µm using a 10x objective) were stitched together for analysis. Using the stitched mosaic images, the individual shapes of large quantities of bMSCs were counted and measured simultaneously with an ImageJ macro, according to [21]. The following four mathematical shape descriptors were quantified for each bMSC: length (major axis), circularity (4*π(area/perimeter^2), roundness (4*area/(π*major axis length^2)), and cell angle (major axis angle relative to the direction of stretch/horizontal axis for controls). These measures were used to quantitatively compare the morphology of bMSC populations stretched with different regimens and examples are given in Fig. 2.1.

<u>Fluorescence microscopy for protein based analysis</u>

Samples were fixed with 4 % formaldehyde at 4° C for 10 min, washed three times with PBS, and permeabilized with Triton X100 for 20 min, washed three times with PBS, incubated for 1 h with 1:500 rabbit monoclonal anti-calponin (ab46794, Abcam) diluted in PBS containing 0.1 % BSA (Sigma-Aldrich), as described in [24]. After overnight incubation at 4°C, the samples were washed 3x with PBS, and incubated with secondary antibody (Goat anti-Rabbit IgG, sc-3739, Santa Cruz Biotechnology, dilution: 1:100) for 1 h at room temperature. Cells washed 3x with PBS, mounted with mounting medium (Dako Denmark A/S), and digitally recorded in a top-down view (Zeiss LSM 510, AxioVison 4.8, manual exposure correction). Thresholds were used to identify MSCs with pixel intensities above 80 (out of 255). These were termed bMSCs with a "strong" calponin signal, whereas bMSCs with pixel intensities below 80 were termed "weak". The bMSC locations of strong and weak bMSC signals were recorded to allow comparing their calculated shape descriptors (see above).

<u>Quantitative RT-PCR</u>

Compressed collagen sheets with cultured bMSCs were digested for 4 minutes at 55° C using Proteinase K (Fermentas/ThermoScientific). mRNA was isolated using the RNA-Extraction-RNeasy-Minikit (Qiagen, USA). cDNA was synthesized using the Advantage RT-for-PCR Kit (Clontech, USA). Quantitative RT-PCR was performed with the LightCycler 480 SybrGreen Master (catalog no. 04707516001, Roche) and LightCycler 480 Probes Master (no. 04707494001, Roche) using the LightCycler 480 system and Multiwell 96Plates (no. 04729692001, Roche). Gene expression levels of alpha smooth muscle actin (ACTA), transgelin (TAGLN), and calponin

(CNN) were examined as indications of early and late markers for smooth muscle differentiation according to MIQE guidelines [54]. Peptidylproplyl isomerase A (PPIA) and human glyceraldehyde-3-phosphate-dehydrogenase (GAPDH) were determined as house-keeping genes according to MIQE guidelines [54]. PPIA and GAPDH were used as reference genes. As positive controls and calibrator samples human bladder derived smooth muscle cells (HBdSMC, Promocell, Heidelberg, Germany) were used, as described in [24]. The oligonucleotide primers used in qRT-PCR assays were TTGCCTGATGGGCAAGTGAT (forward primer sequence) and TACATAGTGGTGCCCCCTGA (reverse primer sequence) for ACTA, AGATGGCATCATTCTTTGCGA and GCTGGTGCCAATTTTGGGTT for CNN, CTCTGCTCCTCCTGTTCG and ACGACCAAATCCGTTGACTC for GAPDH, and TTCATCTGCACTGCCAAGAC and TCGAGTTGTCCACAGTCAGC for PPIA. For TAGLN, the Quiagen assay Hs_TAGLN_2_SG (QT01678516) was used. For TAGLN and PPIA, SybrGreen (Roche) was used. For ACTA2, CNN, and GAPDH the Roche Universal Probe Library Probes N58 (ACTA, catalog no. 04688554001), N71 (CNN, no. 04688945001), and N60 (GAPDH, no. 04688589001) were used, as described in [21, 24].

Western blotting

bMSCs were harvested by scraping the cells from the surface the cells were lysed in 200 µl protein lysis buffer (40 mM Tris/HCl pH 7.4, 300 mM NaCl, 2 mM EDTA, 2% Triton-X-100) supplemented with proteinase inhibitor at 4˚C. Insoluble material was removed by centrifugation. The protein concentration in the supernatant was determined by Bradford protein assay. Protein samples (50 µg) were separated by 10% SDS-PAGE and transferred to a hydrophobic

polyvinylidene difluoride membrane (Immobilon-P; Merck KGaA, Darmstadt, Germany). After blocking with 5% powdered milk (Carl Roth, Karlsruhe, Germany) in TBS-T, membranes were incubated with primary antibodies (rabbit anti-α-smooth muscle actin (SMA), 1:1000 (Abcam), rabbit anti-calponin (CNN),1:1000 (Abcam), rabbit anti-SM22 alpha (SM22), 1:1500 (Santa Cruz), and rabbit anti-β-tubulin, 1:2000 (Cell Signaling, Danvers, MA, USA)) with gentle shaking overnight at 4˚C according to the manufacturer's protocols. Membranes were washed three times with TBS-T. Secondary antibody (horseradish peroxidase-conjugated anti-rabbit pAb, 1:20,000, Jackson Immuno Research) was added for 2 h at room temperature, and the membranes were washed another three times with TBS-T. Proteins were detected using ECL Western blotting substrate (Thermo Scientific) with membranes exposed to Amersham Hyperfilm ECL (GE Healthcare, Pittsburgh, PA, USA). A pre-stained protein ladder (PageRuler Plus; Thermo Scientific) was used for determination of molecular weights. For quantification, ImageJ (NIH) was used.

Statistical Analyses

Data are presented as mean ± standard error. All data was graphed and statistically analyzed in SigmaPlot (Systat, Chicago). Data were analyzed for normality. Normally distributed data were compared with a One-Way ANOVA test otherwise the data were analyzed with an ANOVA on Ranks test. If the ANOVA revealed significant differences, Dunn's Method was used for post-hoc analyses to compare individual groups to one another. Statistical differences were indicated with a bar but only when relevant in the presented context; for instance, when examining the effects of time, cells stretched for one vs. two stretch regimens were compared and resulting significant

differences related to time were indicated with a bar. In this example, significant differences between different stretch amplitudes (5% vs. 10%) were not indicated, as the analysis focused on the effect of time, not amplitude.

2.3 - Results

Shape Descriptor: Cell Length

Unstretched control bMSCs increased their cell length over time but the change was small. After applying one regimen of cyclic stretch, cell length of stretched cells was shorter than that of unstretched control bMSCs, regardless of the stretch parameters ($p<0.001$). Increased strain during the first stretch regimen decreased bMSC length (Fig. 2.2A: 1x 5% vs. 10%; $p<0.05$), and increased stretch time also decreased bMSC length (Fig. 2.2C: 1x 10% 3h vs. 16h; $p<0.05$). These trends were completely reversed after applying a repeated second regimen of cyclic stretch the following day. A second regimen of stretch the next day generated a longer cell length than one regimen for all stretch parameters including controls (Fig. 2.2B: 1x vs. 2x Control, 1x vs. 2x stretch with 5%, 1x vs. 2x stretch with 10% 16h; $p<0.05$). This effect was amplified with higher strains (Fig. 2.2B; $p<0.05$) and longer stretch time (Fig. 2.2C: compare 1x vs. 2x 10% for 3h to 1x vs. 2x 10% for 16h; $p<0.05$). Stretching the cells for longer durations has similar effects as stretching at different strains. After one regimen, increasing the duration of strain decreased cell length (Fig. 2.2C: 1x 10% 3h vs. 16h; $p<0.05$) but after a second regimen, longer durations produced longer cells (Fig. 2.2C: 2x 10% 3h vs. 16h; $p<0.05$). The shortest bMSCs were in populations that had been stretched at high strains for a single regimen and the highest bMSC length was observed after two regimens of 10% stretch for 16h. This was the highest strain applied for the longest period of time.

Shape Descriptor: Cell Roundness

Next, we analyzed the effect of stretch on cell roundness. With a single stretch regimen, bMSC roundness was either increased (Fig. 2.2D: 1x Control vs 5% for 16h; $p<0.05$) or was statistically the same as control populations (Fig. 2.2D: 1x Control vs 10% for 16h). After the first stretch regimen, increased strain decreased MSC roundness (Fig. 2.2D: 1x 5% vs. 10% for 16h; $p<0.05$) but increased stretch time had no effect on MSC roundness (Fig. 2.2F: 1x 10% for 3h vs. 16h). Generally, control cells were rounder than cells stretched for a repeated regimen the next day (Fig 2.2D; $p<0.05$) but this decrease in roundness was not strain-dependent (Fig. 2.2D: 2x 5% vs. 10% for 16h). While unstretched MSCs increased in roundness over time (Fig 2.2E: 1x vs. 2x Control; $p<0.05$) stretched MSC roundness values were lower than after one stretch regimen (Fig. 2.2E: 1x vs. 2x 5% for 16h and 1x vs. 2x 10% for 16h; $p<0.05$). Unlike with cell length, different responses were seen in roundness changes when using different strains and different durations. After one regimen, increasing the duration of stretch had no effect on cell roundness (Fig. 2.2F; 1x Control vs. 10% for 3h vs. 10% for 16h) but after a second, repeated regimen, increasing the duration decreased roundness (Fig. 2.2F: 2x 10% for 3h vs. 16h; $p<0.05$). Overall, the lowest MSC roundness was observed after two regimens of 5% and 10% stretch for 16h, which was the longest period of stretch time. The cells with the highest roundness were unstretched controls statically cultured throughout the time needed for two stretch regimens.
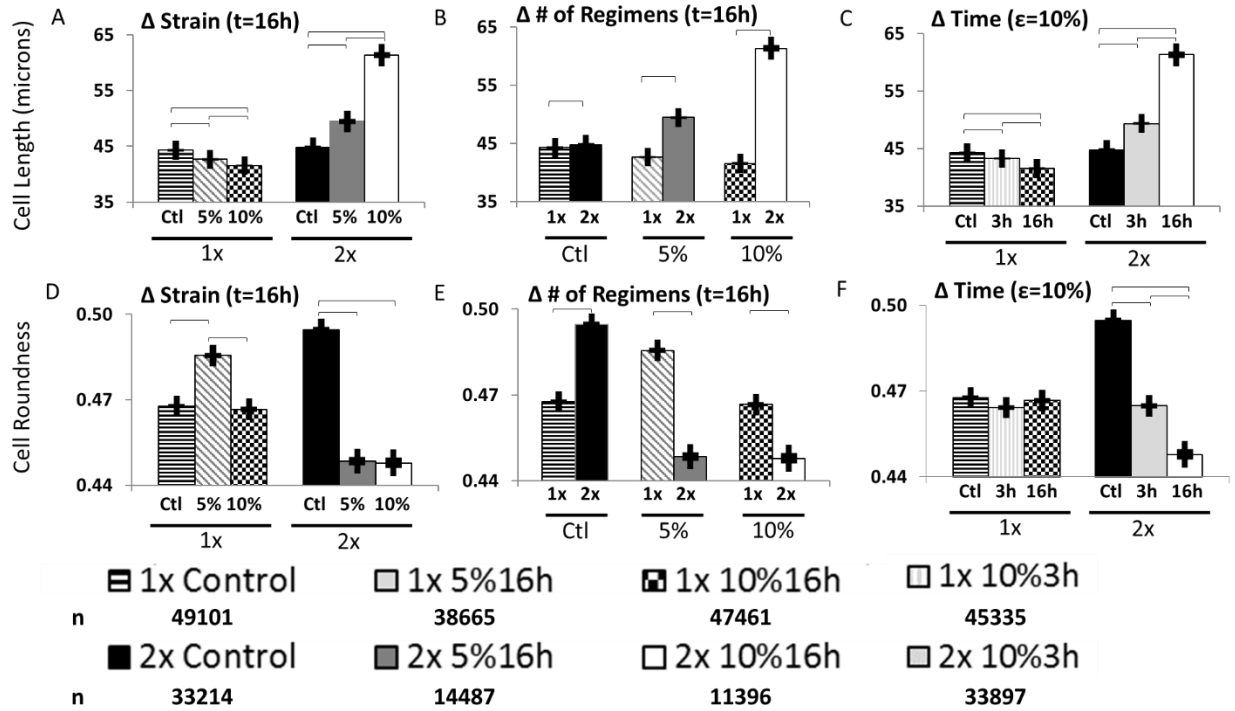
Figure 2.2: Effects of Stretch Parameters on Cell Length and Roundness. Stretching the cells at higher strains produces cells that are shorter after one regimen (p<0.05) but longer after two (A, p<0.05). Regardless of whether or not cells are stretched, they are longer when cultured for an additional regimen (B, p<0.05). After one stretch regimen, cells that are stretched longer periods of time are shorter (p<0.05), however after a second regimen of stretch, increased duration of stretch results in longer cells (C, p<0.05). Stretching the cells for one regimen produces round cells at low strains (p<0.05) but less round cells at high strain (D, p<0.05). Cells that are stretched for two regimens are much less round regardless of strain (D, p<0.05). If cells are left unstretched, they naturally round up but if they are stretched, additional regimens decrease roundness regardless of maximum strain (E, p<0.05). Stretching cells for longer durations has no effect on cell roundness after only one regimen but after a second regimen, longer durations of stretch produce less round cells (F, p<0.05). The number of cells from each condition are listed below the condition name in the legend.

Shape Descriptor: Cell Circularity

We analyzed bMSC circularity next. After a single stretch regimen, bMSC circularity was higher than controls (Fig. 2.3A: 1x Control vs. 5% for 16h; p<0.05) and this difference increased with strain (Fig. 2.3A: 1x 5% vs. 10% for 16h; p<0.05). After a second repeated stretch regimen the following day, stretched cells were less circular than controls but the amount of strain had no effect on cell circularity (Fig. 2.3A: 2x Control vs. 5% for 16h and 2x Control vs. 10% for 16h; p<0.05). Unstretched control bMSCs increased their circularity with time (Fig. 2.3B: 1x Control

40

vs. 2x Control; p<0.05) but stretching the cells inverted this response ubiquitously decreasing the cell circularity of cells stretched for two regimens compared one stretch regimen (Fig. 2.3B: 1x vs. 2x stretch with 5% for 16h and 1x vs. 2x stretch with 10% for 16h; p<0.05). After one regimen, increasing the length of time for each regimen also increased the resulting circularity, even over respective controls (Fig. 2.3C: 1x Control vs 10% for 3h and 1x 10% 3h vs 16h, p<0.05) before having overall lower circularity than controls after a second regimen (Fig. 2.3C: 2x Control vs 2x 10% 3h, 2x Control vs 2x 10% 16 h, p<0.05). Overall, the lowest circularities were observed in cells stretched for two regimens of stretch while the length of the stretch regimen and the strain had less significant impacts. The highest circularities were observed in cells left unstretched or cells stretched with high strain for a single regimen.

bMSC alignment relative to stretch

To assess the effects of cyclic stretch on cell alignment, we quantified the angle of the major cell axis relative to the direction of stretch or, in case of control bMSCs, relative to the horizontal axis of the image. Stretching generally increased alignment parallel to the direction of stretch (Fig. 2.3D-F, p<0.05). Stretching the bMSCs at higher strains (Fig. 2.3D: 2x 5% vs. 10% for 16h; p<0.05) or for longer durations (Fig. 2.3F: 2x 10% for 3h vs. 16h; p<0.05) resulted in more alignment from bMSCs. Even cells stretched the highest strain and longest duration had statistically similar angles as controls after a single regimen (Fig. 2.3E: 1x Control vs. 1x 10% for 16h). Regardless of the other parameters, it required a repeated stretch regimen on the next day to induce alignment and unstretched control bMSCs remained isotropic regardless of culture time (Fig. 2.3E). Thus, stretch consistently induced bMSC alignment and the degree of alignment

41

corresponded to the amount of stretch but interestingly, this effect was only visible after two regimens of stretch on day 4 and 5. The stretch-induced alignment is illustrated in Fig. 2.4A.
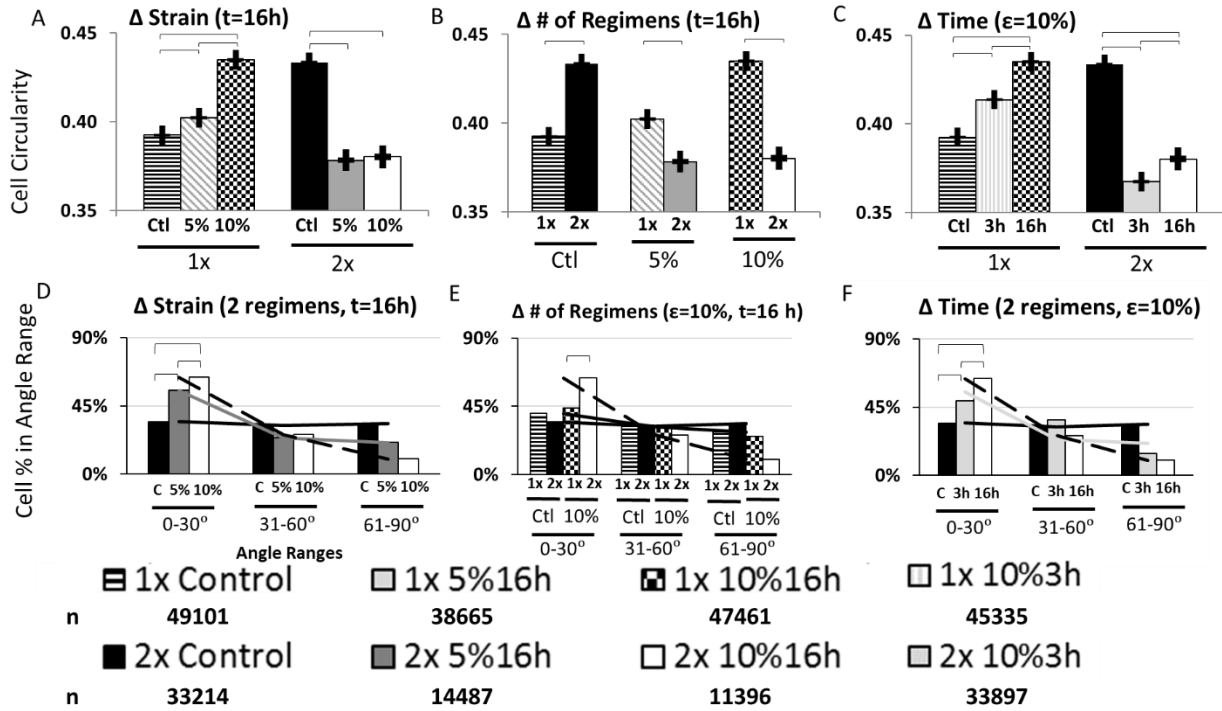
Figure 2.3: Effects of Stretch Parameters on Cell Circularity and Orientation. Cells stretched with 1 regimen have increased circularity and increasing the strain exaggerates this effect (A, $p<0.05$) but after a second regimen, cells that are stretched have lower circularity than controls ($p<0.05$) but strain has no effect (A). Control cells have significantly higher circularities with additional regimens ($p<0.05$) but cells that are stretched have lower circularity after a second stretch regimen (B, $p<0.05$). After one regimen, cells stretched for longer durations have higher circularity ($p<0.05$) but after a second regimen, they are much less circular than controls (C, $p<0.05$). Increasing the duration of stretch increases circularity after either one or two regimens of stretch (C, $p<0.05$). Stretching cells at higher strains produces cells that more aligned (D, $p<0.05$). Control cells are more aligned after additional culture time ($p<0.05$) and repeating a stretch regimen produces cells that are much more aligned (E, $p<0.05$). Increasing the length of time cells are stretched increases their alignment (F, $p<0.05$). The number of cells from each condition are listed below the condition name in the legend.

MSC Numbers

Stretched and unstretched control bMSCs were stained and counted. There were no statistical differences in the number of bMSCs analyzed between conditions (Fig. 2.4B).
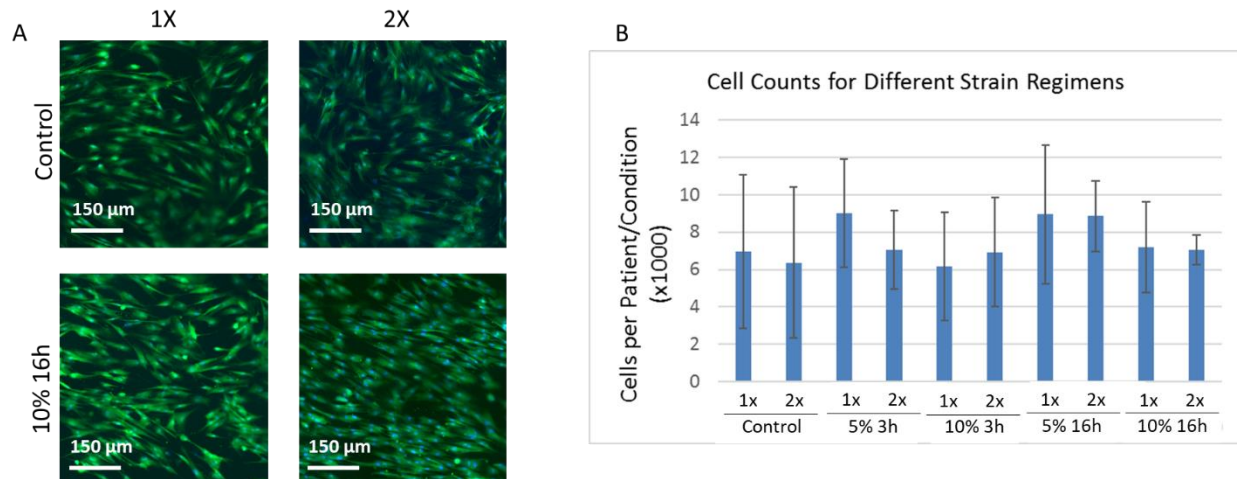
Figure 2.4: Shape and Cell Count of Stretched and Unstretched bMSCs. Stretched and unstretched bMSCs that adhered to the collagen type I sheets were stained with Calcein to illustrate bMSC shape (A). Cell nuclei stained with DAPI were counted to assess cell number per condition (B). The axis of stretch was along the horizontal direction. Clear differences in bMSC alignment can be seen in stretched vs. unstretched bMSCs, and alignment was more pronounced in 2x than 1x stretched bMSCs (A). More subtle differences in cell size and cell spreading were also present and quantified elsewhere. The number of bMSCs across the experimental conditions tested was not statistically different. Error bars indicate standard deviation.

bMSC mRNA Expression

As shape descriptors have been shown previously to correlate with the expression of specific smooth muscle markers [21], we asked if cell length had similar correlation and if these relationships were impacted by the stretch regimen. Using q-PCR and applying the above reported stretch regimens, we demonstrated that bMSC length correlated with smooth muscle ACTA regardless of stretch regimen (Fig. 2.5A: R=0.54; p<0.05) as did TGLN mRNA expression (Fig. 2.5B: R=0.59; p<0.05), which are respectively early and intermediate gene markers for smooth muscle differentiation [28]. Interestingly, bMSC length did not correlate with the expression of CNN, another intermediate marker for smooth muscle differentiation (Fig. 2.5C).

43
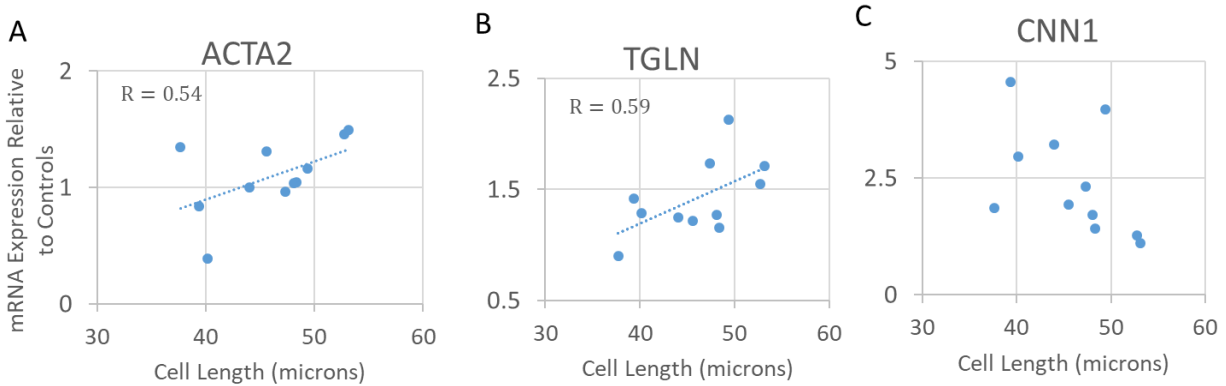
Figure 2.5: Correlation of Cell Length with Smooth Muscle Gene Expression. Cell length positively correlates significantly with ACTA mRNA expression of the population independently of stretch regimen (A, R=0.54, p<0.05). Cell length significantly and positively correlates with TGLN expression of the population regardless of stretch parameters (B, R=0.59, p<0.05). There is no significant correlation between cell length and CNN gene expression (C).

bMSC Protein Expression

While the expression of ACTA and TAGLN correlated well with bMSC length, we wanted to further examine if expression of protein related to bMSC length. This would allow us to confirm the relationship between ACTA and TAGLN with length and give us another measure to compare CNN and cell length. We chose the stretch regimen that generated the highest length (2x 10% for 16h) and compared the induced protein expression with their respective unstretched bMSC controls, asking whether bMSCs, whose length was generated through cyclic stretch, would generate more protein. Western Blots revealed that bMSCs stretched with 2x 10% for 16h expressed more SMA, the protein transcribed from ACTA (Fig. 2.6A, p<0.05), and SM22, the protein transcribed from TAGLN (Fig. 2.6B, p<0.05), than their respective controls. CNN protein expression did not exhibit a statistically significant relationship (Fig. 2.6C).

Because CNN mRNA expression and cell length did not correlate, and the CNN protein in western blots did not exhibit a statistically significant relationship to stretch, we investigated the expression of the protein through fluorescence microscopy. We noted that the fluorescence of CNN antibodies

of bMSCs stretched 2x 10% for 16h was not homogeneous. We asked whether CNN protein expression could be related to bMSC length on an individual cell basis. We fluorescently stained the cells for CNN and investigated how the length of bMSCs with a higher intensity (selected based on signals above a chosen threshold) differed from the length of bMSCs with a lower CNN fluorescent intensity (Fig. 2.6D and 2.6E). Stretched bMSCs did have a higher proportion of bMSCs with "high" CNN expression compared to unstretched controls (36.9% vs 17.6%). However, we demonstrated that stretched bMSCs expressing "high" CNN were statistically shorter (Fig. 2.6FD, $p<0.05$) and had similar lengths to controls. In unstretched populations, cells with higher expression and lower expression had similar lengths. Thus, while both the qRT-PCR and immunohistochemistry data suggested that stretch influenced the expression of CNN, increased expression seems to be unassociated with cells lengthening.
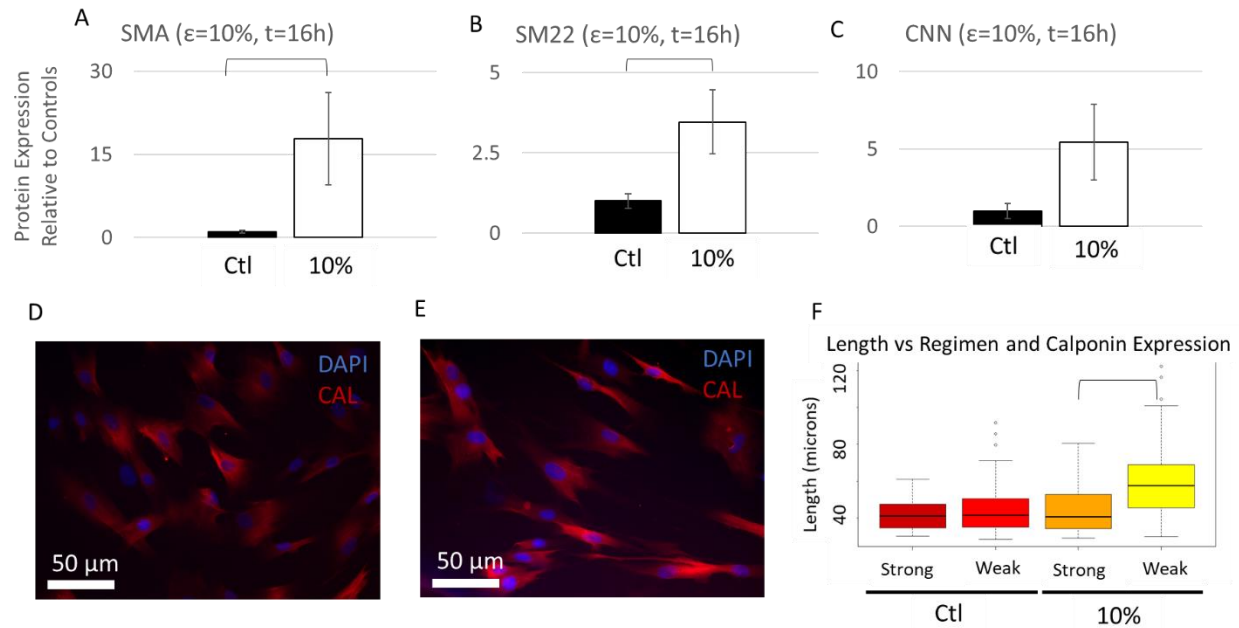
Figure 2.6: Effects of Stretch on Smooth Muscle Protein Expression. Western blots reveal that cells stretched to 10% for two 16 hour regimens expressed more SMA protein than controls (A, $p<0.05$). Cells stretched to 10% for two 16 hour regimens also expressed more SM22 protein (B, $p<0.05$). There was no statistical difference in CNN protein expression between cells stretched to 10% and their respective controls (C). Cells stretched at the maximum strain (10%) and duration (2x for 16 hours) as well as their respective control were stained with anti-calponin (D: controls; E: stretched bMSCs) and the length of cells with a bright signal (above a specific pixel intensity threshold) was compared to that of cells with a weaker signal (F). Visualizing the cell contours up close, the majority of cells with a strong Calponin signal appeared shorter than longer appearing bMSCs with a weaker Calponin signal. There was no statistical difference between the length of control cells expressing strong CNN signal or cells expressing weak amounts of protein. Stretched cells that exhibited weak expression of CNN were significantly longer than their strongly expressing counterparts ($p<0.05$).

Associations of bMSC shape and alignment

Based on these findings, we asked whether bMSC shape might be more dependent on alignment than stretch regimen. To investigate this, we examined the shape of cells aligned in specific directions after any given treatment. We compared bMSCs with an alignment parallel to the direction of stretch (0-30°) vs. bMSCs perpendicular to the direction of stretch (61-90°). As we expected from our assessment of cell angle, not only were cells isotropic after a single round of stretch, the shapes of cells were similar regardless of orientation (Fig. 2.7A and Fig. 7B). After a second regimen of stretch the next day however, differences arose and interesting patterns

46

resulted. We saw that cells that aligned parallel to the direction of stretch became much longer than cells in same orientation after one regimen of stretch (Fig. 2.7A: Parallel 1x 10% 16h vs. 2x 10% 16 h, p<0.05), and that these parallel aligned bMSCs were longer than the average cell length of the entire population (Fig. 2.7A: Parallel vs. All 2x 10% 16h, p<0.05). The perpendicular cells were no longer after a second regimen of stretch than they were after a single stretch regimen (Fig. 2.7A: Perpendicular 1x vs. 2x 10% for 16h). In contrast, after two stretch regimens they were shorter than the parallel and total cell population lengths (Fig. 2.7A: All vs. Perpendicular 2x 10% for 16h and Parallel vs. Perpendicular 2x 10% for 16h; p<0.05). Thus, the change in bMSC cell length in relation to stretch depended on initial bMSC orientation. At the same time, after two regimens of stretch repeated on consecutive days, parallel aligned bMSCs were less round compared to the entire population (Fig. 2.7B; p<0.05) while the perpendicularly aligned bMSCs were much rounder than the parallel bMSCs (Fig. 2.7B: Perpendicular 2x 10% 16h vs. Parallel 2x 10% 16h; p<0.05) and also much rounder than the entire population (Fig. 2.7B Perpendicular 2x 10% 16h vs. All 2x 10% 16h; p<0.05). Overall, this suggested that two regimens of stretch were necessary to induce changes in alignment and that the cell shapes changed throughout this alignment process. For parallel cells, an additional regimen increased cell length and decreased roundness while perpendicular cells became rounder as they elongated along the direction of stretch. Collectively, this suggested that bMSC morphology induced by cyclic stretch depended on cell orientation, and, in turn, that alignment played an instrumental function in generating bMSC morphology through cyclic stretch.
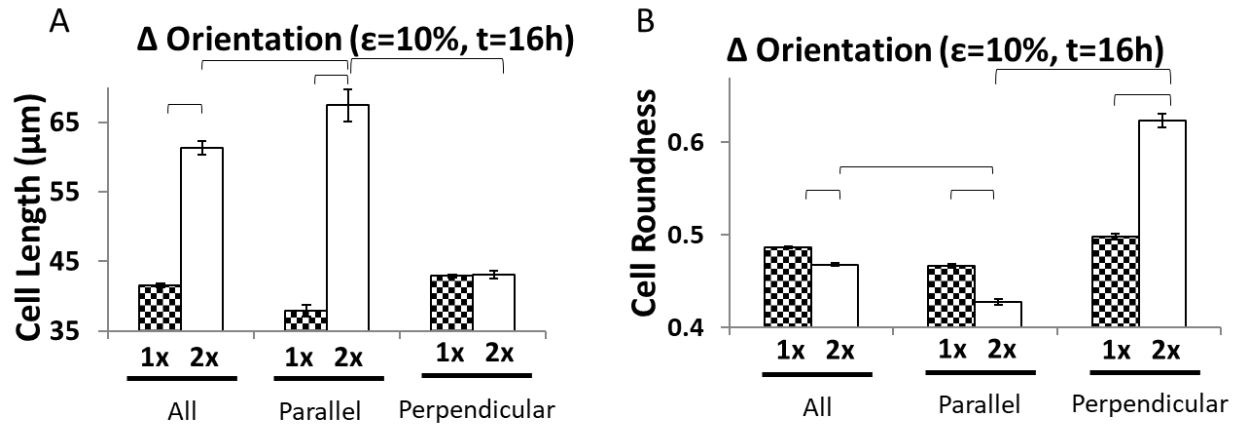
Figure 2.7: Influence of Orientation on Stretch Induced Changes in Morphology. When cells are stretched for a second regimen, the average cell length of the entire population would increase (A, $p<0.05$). By looking specifically at cells oriented in parallel with the direction of stretch, their change in length between the first and second cycle is even greater (A, $p<0.05$). When considering the cells oriented perpendicular to the direction of stretch, a second regimen does nothing to the cell length (A). Looking at cell roundness shows that a second regimen of 10% stretch produces cells that are less round than those only stretched for a single regimen (B, $p<0.05$). An exaggerated trend is seen in the cells solely oriented in parallel with the direction of stretch (B, $p<0.05$). When considering the cells oriented perpendicularly, the cells are rounder after a second regimen of stretch (B, $p<0.05$).

2.4 - Discussion

The application of cyclic stretch has actively been used for generating an elongated cell morphology [29] and also for inducing MSC differentiation into specific lineages [16, 24, 29, 30, 31, 32]. While this has made cyclic stretch an important and widely used tool in tissue engineering, we recently discovered that stretching a population of randomly aligned, initially isotropic, bMSCs generated a rounder phenotype and that this roundness was the result of a complex shape remodeling process that occurred during stretch and that continued afterward [21]. Here, we hypothesized that variations of parameters such as strain, stretch time and the repetition of stretch regimens would generate significantly different bMSC morphologies including elongated bMSCs, as this is commonly one of the major goals for applying cyclic stretch. Although variations of strain and time did indeed produce different morphologies, they were not the major determining factor. Instead, a second regimen of stretch repeated the next day was associated with more alignment and an elongated phenotype indicative of myogenic differentiation. Our results suggest

this second repetition is the minimum number of required regimens to induce alignment with the direction of stretch and initiate the morphological phenotype associated with differentiation and smooth muscle maturation. Thus, variations of strain and length of stretch regimen were modulators, which intensified or attenuated the effects of the respective stretch regimen. While we did not measure proliferation in this study, final cell counts per condition (or cell densities) in each condition were similar between conditions suggestions either similar rates of mitosis or an equilibrium state where cell loss is compensated by mitosis. Future studies could investigate the effect of additional stretch regimens by applying more than two consecutive runs. Collectively, these findings confirmed our general hypothesis that regimens of cyclic stretch can be used for engineering specific bMSC morphologies with distinct aspects of shape quantified by length, roundness, and circularity.

With the goal to produce a controlled range of contrasting bMSC morphologies, we asked which experimental conditions, including control culture conditions, would affect cell shape and orientation. The highest absolute length and lowest roundness values represented a long, thin morphology that has been typically associated with a smooth muscle phenotype [16, 17]. We confirmed this association and demonstrated that we can engineer a long, thin MSC morphology with two regimens of 10% stretch for 16h repeated on consecutive days. We also found that these conditions led to low circularity that indicated cell spreading. In complete contrast to long, thin MSCs, we also engineered a short, round morphology that fits with the traditional views of undifferentiated cells. Those were generated with applying stretch only briefly, as the smallest bMSC length was generated with 1 regimen of 10% stretch for 16h, and by not applying stretch, as highest roundness and lowest aspect ratio occurred in non-stretched controls over time. These data also highlighted the relationship between biomechanically engineered shape, biomaterial

choice, and select biochemical phenotypes. For this study, we used stiffness-optimized compressed collagen type I sheets with a concentration of 80 mg/ml because these sheets were associated with the most SMC-like phenotype among a range of (unstretched) biomaterials [21]. However, we confirmed that tuned stretch was even more effective in producing a long, thin morphology than the compressed collagen sheets alone. This is relevant for engineering environments to biomechanically induce specific lineages of differentiation for bMSCs. Next, we specifically demonstrated that the mRNA expression of ACTA and TAGLN correlated with the biomechanically generated cell length, and that the expression of analogous proteins, SMA and SM22, were significantly higher after the protocols producing the longest MSC morphology. While one interpretation of this data is that the upregulation of ACTA and SMA is a sign of cell shape change and alignment rather than maturation an indication of differentiation itself (ACTA and SMA are associated with cell cytoskeleton remodeling [33, 34]), the continuous elongation and decrease in roundness and circularity suggest increased expression beyond stages of cell reorientation. These data imply that additional stretch and a more elongated MSC would promote the upregulation of ACTA and TAGLN along with continued expression of SMA and SM22, leading to a more mature phenotype. Interestingly, CNN mRNA expression did not correlate with cell length and CNN protein expression was not statistically upregulated in stretched cells. In fact, we observed that shorter cells in the stretched population expressed more CNN than longer cells. Since calponin is an intermediate marker during differentiation and is involved in the development of contractile properties, it could mean that these bMSCs never were induced toward a more mature phenotype. This would imply that not all SMC markers necessarily correlate with cell length and that other morphological features, like roundness, may be better indicators of differentiation, as their relationship to stretch parameters (Fig. 2.2) and genes [21] is clearer. We have focused our

investigations on smooth muscle differentiation because elongated bMSC morphologies are firmly associated with an increased expression of SMC markers [16, 17], and because biomechanical forces increase bMSC differentiation towards a SMC phenotype [14, 15, 16]. However, the applications of engineering cell shape through biomechanical tensile forces extend beyond myogenic studies. Cell length is one of the few shape descriptors that has been actively quantified and associated with differentiation [17, 35, 36] and function of SMCs [37] but the control over additional shape factors introduced here are applicable in countless other studies pertaining to cell function and/or lineages of differentiation. Whether shape can potentially be engineered without simultaneously modulating bMSC differentiation is an interesting question and remains to be answered. We are currently designing a system to isolate these stimuli and determine if stretch and growth factor cocktails can induce differentiation despite restricting and controlling a cell's shape.

While this work has contributed to discerning the role of various stretch parameters on the change in bMSC morphology and phenotype, it also raises additional questions that need to be addressed in future studies. We kept the final timeline of regimens with different strains and durations consistent, which led to differences in relaxation time. Having constant endpoints meant we could not account for these differences in relaxation time. As the collagen substrates, and cells themselves, are viscoelastic in nature and relaxation times has effects on cell morphology [38], altering the relaxation time between regimens could prove interesting. This could be investigated by keeping constant stretch and relaxation times, which would result in differences in experimental length. However, in this investigation we were more concerned with comparing the effects of strain and duration of stretch and, thus, decided to keep the final endpoints consistent. We also kept the frequency during the stretch cycles consistent at 1 Hz, based on the literature, as previous studies applying cyclic stretch to MSCs have used a frequency of 1 Hz [14, 20, 39]. However, one study

compared different frequencies and demonstrated that 1 Hz vs. 2.75 Hz had no significant effect on MSC alignment but on the cell shape index, which is comparable to the here used roundness. Interestingly, 2.75 Hz at 1% strain exhibited the same trend as a frequency of 1 Hz at 5 % and 10% strain [16], as applied here. Nevertheless, it could very reasonably be conjectured that the strain rate impacts the phenotype of stretched cells as this is directly linked to the material and cell viscoelastic properties. We may have seen this phenomenon ourselves; to achieve 10% strain in the same amount of time as 5% strain, the average strain rate is effectively doubled. It could very well be that this difference drives the here reported responses to stretch and not the maximum strain itself. Future investigations could investigate this effect by decoupling maximum strain from strain rate. However, matching sinusoidal wave functions for change in rates could prove challenging. Answering this question may require adapting a sawtooth function for comparison across different frequency spaces. Another question that arises out of this work is how individual cells are affected by stretch. We have developed means to examine how the shape of individual cells is changed in response to biomechanical stimuli but our biochemical analyses of these cells has been on the population as a whole. It would be quite useful to examine how individual cells are responding to heterogeneity in binding to a non-homogenous material and how these disparities manifest in differences in the expression of differentiation markers on mRNA and protein levels. E. g. single cell PCR or even studying the development of single cell focal adhesions could help determine influences of heterogeneous strain on bMSCs.

Another important finding of the present study was the effect of cyclic stretch on bMSC alignment and corresponding shape. Alignment has been shown to be important for MSC differentiation [40] but when dissecting the pronounced effect of two consecutive stretch regimens into effects on parallel vs. perpendicularly aligned bMSCs, it became obvious that parallel aligned

bMSCs drastically increased in cell length but perpendicular aligned cells did not. To better understand these unexpected results, it is necessary to describe this stretch response in more detail as a function of the initial cell alignment prior to stretch. Cells that were coincidentally aligned parallel to the stretch direction elongated along the axis of stretch and contracted any protrusions perpendicular to the direction of stretch. Quantitatively, this resulted in cells being longer, less round, and less circular with additional stretch. The cells that coincidentally started oriented perpendicular to stretch contracted their perpendicular axis and started to elongate along the axis of stretch, resulting in a seemingly reoriented cell. Quantitatively, the first stretch regimen made the perpendicular MSCs shorter, rounder, and more circular, and this shape was similar to that of unstretched counterparts. Only a second stretch regimen increased the contraction along the perpendicular axis and the elongation along the axis of stretch, which made the bMSCs quantitatively longer and less circular and round, explaining how alignment can have differential effects on biomechanically engineered shape. Importantly, the majority of bMSCs were initially neither parallel nor perpendicular to the stretch axis. Because those cells initially contracted away from the perpendicular direction before elongating and reorienting along the axis of stretch, and because they made up the majority of the population, their behavior drove the average population values presented in our first results. Moreover, these data highlight that bMSC alignment can theoretically be explained by changes in overall bMSC morphology but not by length alone. Indeed, we found that isotropically plated bMSCs, when stretched and analyzed as a single population, would pass through a phase where their morphology was rounded, more circular and shorter. Typically, this phase occurred after a single regimen of stretch and only after a second regimen of stretch would the bMSCs begin to align with stretch and display the biomechanically engineered morphologies that are conventionally associated with the myogenic phenotype. To

better visualize these complex changes in bMSC morphology, it is helpful to consider 3 hypothetical MSCs with parallel, perpendicular and an oblique alignment (Fig. 2.8A). Because these data demonstrated collectively that engineering bMSC shape through applying cyclic stretch depends highly on bMSC alignment, and, in turn, that repeating the stretch regimen was necessary to control this alignment, one could consequently envision controlling cell alignment through biomaterial designs or other engineering controls to maximize the effects of stretch on bMSC morphology and differentiation.

In this view, our findings extend considerably to the importance of using the appropriate biomaterial for stretching and engineering the shape of adherent cells. Many previous studies have reported that MSCs and SMCs align under uniaxial stretch. Within 3D fibrin hydrogels, cells have been shown to align parallel to stretch [15] but on 2D protein-coated silicone, MSCs and vascular cells are reported to align perpendicular to the stretch axis [14, 16, 20, 25, 26]. It could be speculated that MSCs respond differently to forces when cultured in dissimilar dimensional conditions. We show here that when seeded on collagen, we can stimulate parallel MSC alignment on 2D substrates, a phenomenon previously seen with stem cells only in 3D. That being said, studies stretching osteosarcoma cells on 2D collagen substrates have also shown parallel alignment [27]. We briefly investigated this phenomenon and found corroborating results. When we plated bMSCs on the surface of collagen type I coated silicone and stretched, they aligned perpendicularly to the axis of stretch (Fig. 2.8B) as in [14, 16, 20, 25, 26]. When seeded on the surface of 2D collagen sheets and stretched, bMSCs aligned parallel to the axis of stretch (Fig. 2.8B), comparable to [27]. However, bMSCs seeded within a 3D collagen hydrogel aligned parallel to the direction of stretch (Fig. 2.8B), as they did in fibrin gels [15]. Based on these results it is clear that the substrate places a pivotal role in the resulting cellular alignment. In [15], the hypothesis is stated that this difference is

stiffness-driven and suggests that tests with the same material and different stiffnesses would be needed for confirmation. Here, we suggest an alternative explanation: that it is the *type* of substrate which determines alignment. It is plausible within our reported results and those of others, that non-fibrous substrates like silicone evoke perpendicular alignment while fibrous substrates are conducive if not inductive to parallel alignment in response to mechanical stress. We base this theory on the results seen in Fig. 2.8, along with the similar mechanical properties that the here used collagen sheets have [41], compared to thin silicone sheets. We did not calculate the differences in proliferation or compare cell densities between these conditions but our findings regarding alignment are consistent with the literature [27]. More experiments are needed to discern the exact cause, but regardless of the outcome, it is apparent by the data presented here that the substrate choice plays an instrumental role in the biomechanically achievable shape and differentiation potential of MSCs.
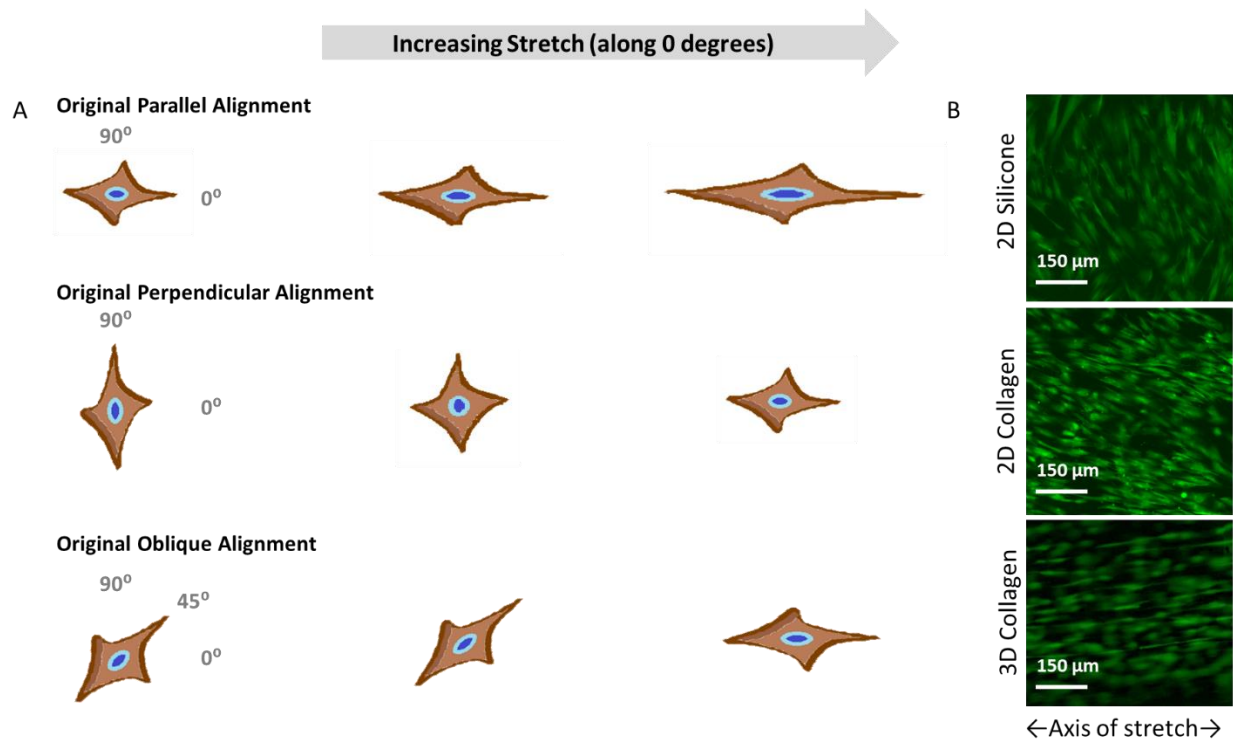
Figure 8: Change of bMSC Shape as a Function of Cell Orientation, Stretch Direction and Substrate. Here are three schematic representations of the changes that 3 hypothetical MSCs undergo as a result of stretch and initial orientation (A). Cell nuclei are in blue and cell outlines are in brown color and star-like to visualize the exaggerated changes in shape parallel and perpendicular to the direction of the applied stretch, which is left-to-right, horizontally. With parallel cell alignment (see the first row with the left most cell pointing to 0 degrees), a MSC becomes longer in the direction of stretch while simultaneously contracting perpendicular cell extensions. This change increases the length and decreases both circularity and roundness. With perpendicular cell alignment (see the second row with the left most cell pointing to 90 degrees), a single MSC first contracts in the perpendicular direction and extends along the direction of stretch, eventually looking like it simply reoriented. This change produces a rounder and more circular cell with a decreased length before additional stretch returns its shape to an elongated morphology. With an oblique cell alignment (see the third row with the left most cell pointing to 45 degrees), the elongated MSC is stretched and it contracts protrusions away from 90 degrees and elongates in the direction of stretch. Mathematically, this follows the perpendicular cell but to an exaggerated extent. Collectively, the morphological changes of these 3 hypothetical MSCs highlight how stretching differently aligned MSCs can change their resulting morphology. The next panels exhibit the differences in alignment and shape induced by seeding on different substrates (B). MSC seeded on collagen coated silicone aligned perpendicularly to the direction of stretch while MSC seeded at the same concentration on a collagen sheet aligned parallel to the direction of stretch. When the cells were embedded in a 3D hydrogel of collagen and stretched, the cells aligned parallel to the direction of stretch.

Another interesting extension to this work would be to study the development of focal adhesions and how cell binding influences shape, integrin signaling cascades, and differentiation. When examining the effects of ligand-cell affinity on smooth muscle differentiation, control of the surface area and cell aspect ratio were found to strongly influence this process [42]. Other groups have manipulated cell area [19] and cell spreading [18] to control subsequent stem cell differentiation

by changing the area available for focal adhesions. Previously, focal adhesion development has also been linked to substrate stiffness [43] and can also be stimulated by mechanical forces [44, 45]. These focal adhesions at integrin binding sites regulate the actin cytoskeleton and impact ERK/MAPK pathway [46], which has been shown to be instrumental in myogenic maturation and stem cell differentiation [47, 48, 49]. Additional ways that ECM interactions influence stem cell fate are reviewed in [50].

Finally, we have demonstrated in the present study that specific aspects of MSC shape change under cyclic stretch and can be captured by different shape descriptors. While a general emphasis on using cell length provides substantial insight into a changing phenotype [17, 35, 36, 37], focusing solely on this morphological feature may neglect multiple other shape aspects. Therefore, we advocate using a panel of shape descriptors such as those used in this study or introduced in our previous study [21] for quantitatively describing MSC shape.

In conclusion, altering the geometrical shape of bMSCs through applying cyclic stretch is possible and impact on differentiation makes it a promising field. Varying strain and duration of the stretch regimen were not the major determinants of engineering cellular shape; instead it was the repetition of the chosen stretch regimen, indicating that the engineered shape is a complex non-linear process that relies on sustained biomechanical stimulation. Additionally, substrate choice and initial cell alignment played roles in the cellular response to biomechanical forces. We envision the use of these effects to be used for the targeted design of clinically applicable force-transducing and shape-instructive biomaterials. Moving forward, as stem cells are continuously exposed *in vivo* to a dynamic biomechanical environment, these concepts will help us fine-tune the biomechanical engineering of cell shape and the associated phenotype, ultimately promoting better control of cells to be used in regenerative therapies.

2.5 - References

1.   Sanchez-Ramos J*, et al.* Adult bone marrow stromal cells differentiate into neural cells in vitro. *Experimental neurology* **164**, 247-256 (2000).

2.   Reyes M, Dudek A, Jahagirdar B, Koodie L, Marker PH, Verfaillie CM. Origin of endothelial progenitors in human postnatal bone marrow. *J Clin Invest* **109**, 337-346 (2002).

3.   Bianco P*, et al.* The meaning, the sense and the significance: translating the science of mesenchymal stem cells into medicine. *Nat Med* **19**, 35-42 (2013).

4.   Caplan AI. Adult mesenchymal stem cells for tissue engineering versus regenerative medicine. *J Cell Physiol* **213**, 341-347 (2007).

5.   Aicher WK, Buhring HJ, Hart M, Rolauffs B, Badke A, Klein G. Regeneration of cartilage and bone by defined subsets of mesenchymal stromal cells--potential and pitfalls. *Advanced drug delivery reviews* **63**, 342-351 (2011).

6.   Pilz GA*, et al.* Human term placenta-derived mesenchymal stromal cells are less prone to osteogenic differentiation than bone marrow-derived mesenchymal stromal cells. *Stem Cells Dev* **20**, 635-646 (2011).

7.   Brun J*, et al.* Smooth Muscle-Like Cells Generated from Human Mesenchymal Stromal Cells Display Marker Gene Expression and Electrophysiological Competence Comparable to Bladder Smooth Muscle Cells. *PloS one* **10**, e0145153 (2015).

8.   Bianco P. "Mesenchymal" stem cells. *Annual review of cell and developmental biology* **30**, 677-704 (2014).

9.   Klein G*, et al.* Mesenchymal stromal cells for sphincter regeneration. *Advanced drug delivery reviews* **82-83**, 123-136 (2015).

10.   Caplan AI, Mason C, Reeve B. The 3Rs of Cell Therapy. *Stem cells translational medicine*, (2016).

11.   Singhvi R*, et al.* Engineering cell shape and function. *Science* **264**, 696-698 (1994).

12.   Folkman J, Moscona A. Role of cell shape in growth control. *Nature* **273**, 345-349 (1978).

13.   Krause M, Gautreau A. Steering cell migration: lamellipodium dynamics and the regulation of directional persistence. *Nature reviews Molecular cell biology* **15**, 577-590 (2014).

14.   Hamilton DW, Maul TM, Vorp DA. Characterization of the response of bone marrow-derived progenitor cells to cyclic strain: implications for vascular tissue-engineering applications. *Tissue Eng* **10**, 361-369 (2004).

15.   Nieponice A, Maul TM, Cumer JM, Soletti L, Vorp DA. Mechanical stimulation induces morphological and phenotypic changes in bone marrow-derived progenitor cells within a three-dimensional fibrin matrix. *J Biomed Mater Res A* **81**, 523-530 (2007).

16.   Maul TM, Chew DW, Nieponice A, Vorp DA. Mechanical stimuli differentially control stem cell behavior: morphology, proliferation, and differentiation. *Biomech Model Mechanobiol* **10**, 939-953 (2011).

17.   Yang Y, Relan NK, Przywara DA, Schuger L. Embryonic mesenchymal cells share the potential for smooth muscle differentiation: myogenesis is controlled by the cell's shape. *Development* **126**, 3027-3033 (1999).

18.   Kilian KA, Bugarija B, Lahn BT, Mrksich M. Geometric cues for directing the differentiation of mesenchymal stem cells. *Proc Natl Acad Sci U S A* **107**, 4872-4877 (2010).

19.   McBeath R, Pirone DM, Nelson CM, Bhadriraju K, Chen CS. Cell shape, cytoskeletal tension, and RhoA regulate stem cell lineage commitment. *Developmental cell* **6**, 483-495 (2004).

20.   Park JS, Chu JS, Cheng C, Chen F, Chen D, Li S. Differential effects of equiaxial and uniaxial strain on mesenchymal stem cells. *Biotechnology and bioengineering* **88**, 359-368 (2004).

21.   Uynuk-Ool T*, et al.* The geometrical shape of mesenchymal stromal cells measured by quantitative shape descriptors is determined by the stiffness of the biomaterial and by cyclic tensile forces. *Journal of Tissue Engineering and Regenerative Medicine*, (2017, in press.).

22. Sun Y, Chen CS, Fu J. Forcing stem cells to behave: a biophysical perspective of the cellular microenvironment. *Annual review of biophysics* **41**, 519-542 (2012).

23. Engler AJ, Sen S, Sweeney HL, Discher DE. Matrix elasticity directs stem cell lineage specification. *Cell* **126**, 677-689 (2006).

24. Rothdiener M*, et al.* Stretching human mesenchymal stromal cells on stiffness-customized collagen type I generates a smooth muscle marker profile without growth factor addition. *Scientific reports* **6**, 35840 (2016).

25. Liu B*, et al.* Role of cyclic strain frequency in regulating the alignment of vascular smooth muscle cells in vitro. *Biophys J* **94**, 1497-1507 (2008).

26. Morita Y, Watanabe S, Ju Y, Xu B. Determination of optimal cyclic uniaxial stretches for stem cell-to-tenocyte differentiation under a wide range of mechanical stretch conditions by evaluating gene expression and protein synthesis levels. *Acta of bioengineering and biomechanics / Wroclaw University of Technology* **15**, 71-79 (2013).

27. Tondon A, Kaunas R. The direction of stretch-induced cell and stress fiber orientation depends on collagen matrix stress. *PloS one* **9**, e89592 (2014).

28. Beamish JA, He P, Kottke-Marchant K, Marchant RE. Molecular regulation of contractile smooth muscle cell phenotype: implications for vascular tissue engineering. *Tissue engineering Part B, Reviews* **16**, 467-491 (2010).

29. Wang W, Deng D, Li J, Liu W. Elongated cell morphology and uniaxial mechanical stretch contribute to physical attributes of niche environment for MSC tenogenic differentiation. *Cell biology international* **37**, 755-760 (2013).

30. Jagodzinski M*, et al.* Effects of cyclic longitudinal mechanical strain and dexamethasone on osteogenic differentiation of human bone marrow stromal cells. *European cells & materials* **7**, 35-41; discussion 41 (2004).

31. Driscoll TP, Nakasone RH, Szczesny SE, Elliott DM, Mauck RL. Biaxial mechanics and inter-lamellar shearing of stem-cell seeded electrospun angle-ply laminates for annulus fibrosus tissue engineering. *J Orthop Res* **31**, 864-870 (2013).

32.   McMahon LA, Reid AJ, Campbell VA, Prendergast PJ. Regulatory effects of mechanical strain on the chondrogenic differentiation of MSCs in a collagen-GAG scaffold: experimental and computational analysis. *Ann Biomed Eng* **36**, 185-194 (2008).

33.   Kim HR, Gallant C, Leavis PC, Gunst SJ, Morgan KG. Cytoskeletal remodeling in differentiated vascular smooth muscle is actin isoform dependent and stimulus dependent. *American journal of physiology Cell physiology* **295**, C768-778 (2008).

34.   Fultz ME, Li C, Geng W, Wright GL. Remodeling of the actin cytoskeleton in the contracting A7r5 smooth muscle cell. *Journal of muscle research and cell motility* **21**, 775-787 (2000).

35.   Gabella G. Hypertrophic smooth muscle. I. Size and shape of cells, occurrence of mitoses. *Cell Tissue Res* **201**, 63-78 (1979).

36.   Halayko AJ*, et al.* Divergent differentiation paths in airway smooth muscle culture: induction of functionally contractile myocytes. *The American journal of physiology* **276**, L197-206 (1999).

37.   Tolic-Norrelykke IM, Wang N. Traction in smooth muscle cells varies with cell spreading. *J Biomech* **38**, 1405-1412 (2005).

38.   Chaudhuri O*, et al.* Substrate stress relaxation regulates cell spreading. *Nature communications* **6**, 6364 (2015).

39.   Heo SJ*, et al.* Differentiation alters stem cell nuclear architecture, mechanics, and mechano-sensitivity. *eLife* **5**, (2016).

40.   Heo SJ, Nerurkar NL, Baker BM, Shin JW, Elliott DM, Mauck RL. Fiber stretch and reorientation modulates mesenchymal stem cell morphology and fibrous gene expression on oriented nanofibrous microenvironments. *Ann Biomed Eng* **39**, 2780-2790 (2011).

41.   Uynuk-Ool T*, et al.* The geometrical shape of mesenchymal stromal cells measured by quantitative shape descriptors is determined by the stiffness of the biomaterial and by cyclic tensile forces. *Journal of Tissue Engineering and Regenerative Medicine*, n/a-n/a (2017).

42.   Zhang D, Sun MB, Lee J, Abdeen AA, Kilian KA. Cell shape and the presentation of adhesion ligands guide smooth muscle myogenesis. *J Biomed Mater Res A* **104**, 1212-1220 (2016).

43.   Pelham RJ, Jr., Wang Y. Cell locomotion and focal adhesions are regulated by substrate flexibility. *Proc Natl Acad Sci U S A* **94**, 13661-13665 (1997).

44.   Galbraith CG, Yamada KM, Sheetz MP. The relationship between force and focal complex development. *J Cell Biol* **159**, 695-705 (2002).

45.   Grashoff C*, et al.* Measuring mechanical tension across vinculin reveals regulation of focal adhesion dynamics. *Nature* **466**, 263-266 (2010).

46.   Trappmann B*, et al.* Extracellular-matrix tethering regulates stem-cell fate. *Nature materials* **11**, 642-649 (2012).

47.   Gredinger E, Gerber AN, Tamir Y, Tapscott SJ, Bengal E. Mitogen-activated protein kinase pathway is involved in the differentiation of muscle cells. *J Biol Chem* **273**, 10436-10444 (1998).

48.   Roux PP, Blenis J. ERK and p38 MAPK-activated protein kinases: a family of protein kinases with diverse biological functions. *Microbiology and molecular biology reviews : MMBR* **68**, 320-344 (2004).

49.   Meyers VE, Zayzafoon M, Gonda SR, Gathings WE, McDonald JM. Modeled microgravity disrupts collagen I/integrin signaling during osteoblastic differentiation of human mesenchymal stem cells. *J Cell Biochem* **93**, 697-707 (2004).

50.   Guilak F, Cohen DM, Estes BT, Gimble JM, Liedtke W, Chen CS. Control of stem cell fate by physical interactions with the extracellular matrix. *Cell stem cell* **5**, 17-26 (2009).

51.   Brun J, Abruzzese T, Rolauffs B, Aicher WK, Hart ML. Choice of xenogenic-free expansion media significantly influences the myogenic differentiation potential of human bone marrow-derived mesenchymal stromal cells. *Cytotherapy* **18**, 344-359 (2016).

52.   Ulrich C*, et al.* Low osteogenic differentiation potential of placenta-derived mesenchymal stromal cells correlates with low expression of the transcription factors Runx2 and Twist2. *Stem Cells Dev* **22**, 2859-2872 (2013).

53.   Dominici M*, et al.* Minimal criteria for defining multipotent mesenchymal stromal cells. The International Society for Cellular Therapy position statement. *Cytotherapy* **8**, 315-317 (2006).

54.   Bustin SA, *et al.* The MIQE guidelines: minimum information for publication of quantitative real-time PCR experiments. *Clinical chemistry* **55**, 611-622 (2009).

55.   Paul AC, Rosenthal N. Different modes of hypertrophy in skeletal muscle fibers. *J Cell Biol* **156**, 751-760 (2002).

CHAPTER 3

Mesenchymal Stem Cell Phenotype as a Function of Mechanical Input Energy

3.1 - Introduction

Bone marrow derived mesenchymal stem cells (bMSC) are successfully being used in therapies like bone marrow transplants, wound healing, and cartilage repair. Their low immunogenic properties [1] and well-established techniques for harvesting make them prime candidates as a cell source for biologic therapies. In addition, the ability of bMSCs to differentiate into mesenchymal lineages including bone [2–6], cartilage [7,8], fat [3,9], and smooth muscle [7,10–13], as well as neurogenic potential [14] promises a variety of clinical applications. With this prospective, bMSCs are actively being researched for their potential use in regenerative medicine and tissue engineering applications [15,16].

Interestingly, bMSC differentiation is associated with extensive changes in cell morphology and quantitative measures have been developed, and recently emphasized, to assess cell shape. These techniques not only suggest objective means for ascertaining the stage of differentiation, but also offer a potential means of predicting future function and phenotype of the cells [17,18]. This association of bMSC shape with differentiation has been employed to control differentiation through engineering bMSC cell shape [3,19,20]. Given the many potential applications of differentiated stem cells in regenerative medicine, effectively controlling bMSC differentiation toward desired lineages is an active field of study. One of the most common techniques used for inducing bMSC differentiation is mechanical stimulation. Compression [8], shear [5] and particularly

tension [10,12,21–24] have been used, as bMSCs are highly sensitive to mechanical stimuli [25]. The phenotype of smooth muscle cells is well documented and their morphology and response to mechanical stimulation are well understood. By focusing on the transition of bMSCs toward an SMC-like phenotype, we could assess quantitative shape factors in response to stretch and associate their morphology with phenotypic markers associated with SMC differentiation. With is in mind, many studies have modulated the maximum strain, the duration of stimulation, frequency, the number of regimens, and the number of stretch axes [4,22,26], in order to understand their individual effects on bMSC differentiation, however, despite these valuable studies, there is still no unifying theory that considers the relationship between these parameters as means of controlling cell phenotype.

Previously, we established semi-automatic high-throughput techniques that measured changes in the geometric shape of cells and facilitated correlating cell shape with gene expression after exposure to different mechanical conditions. During that study we noticed a pair of conditions with different input parameters that would often induce comparable responses in cell phenotype. These relationships were found despite high variability between samples as every experimental sample represented data from a different primary cell line and a different patient. With this finding, we saw that one condition had a maximum strain twice that of a second condition but the duration was about four times less than the second condition. Hooke's Law states that doubling the strain on an elastic substrate increases the amount of input energy by a factor of four. This meant the conditions with comparable results also had similar amounts of input energy. For this study we asked how energy input specifically relates the phenotypic response of bMSCs to mechanical stimulation and if energy could be used to control cell shape. We knew the material properties of the constructs from previous work [12] and by integrating the cyclic strain over the stretch duration

and number of regimens (Equation 3.1 in methods) we established a range of input energies (Fig 3.1) that were applied to adhering MSCs through cyclic stretch.
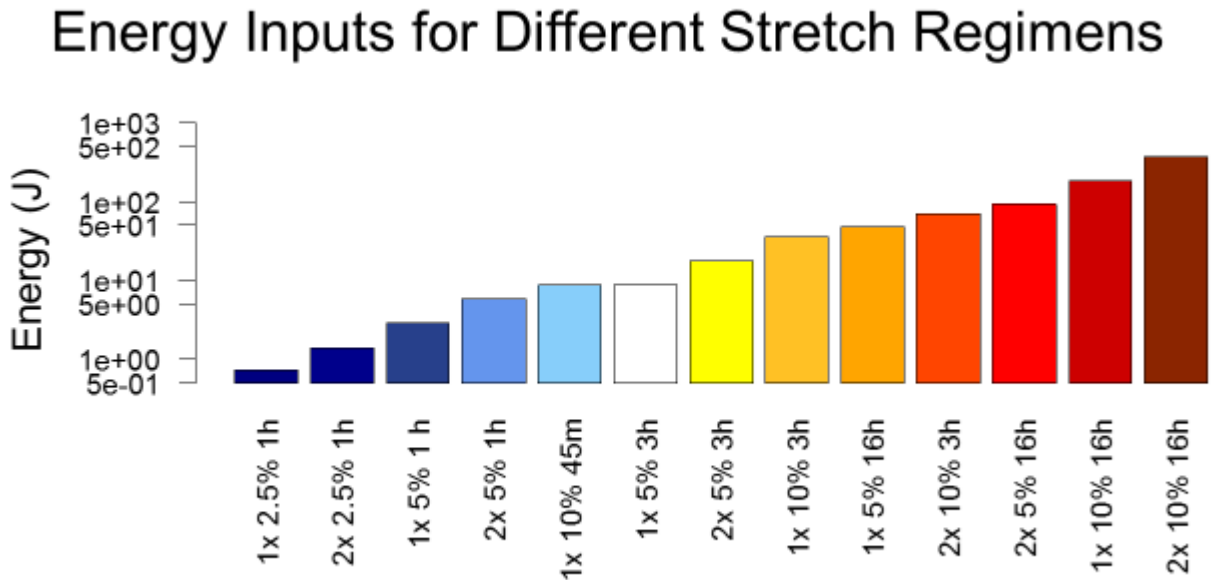
Figure 3.1: The corresponding energy inputs given different input parameters. Doubling the number of regimens (1x to 2x) but keeping the other parameters constant, doubled the amount of input energy. Doubling the strain (ex. 5% to 10%) but keeping the other parameters constant, quadrupled the amount of input energy. Increasing the time of stretch (ex. 1 hour to 3 hours) but keeping the other parameters constant, proportionally increased the amount of input energy. The lowest input energy came from the lowest strain for an hour and a single regimen (0.729 J). The highest input energy came from the highest strain stretched for 16 hours for two regimens (372 J).

In many fields of science, energy exists in a variety of forms, including mechanical energy, and an exchange of energy usually suggests a change in the system. In a biological context, cells utilize energy to undergo metabolic processes [27,28], to remodel their matrix and other environmental factors [27–30], and groups have examined how much energy is needed to produce intracellular forces and contract tissues [28,31,32]. Here we predicted that bMSC shape and differentiation initiated by cyclic stretch is controlled by the amount of the applied energy and not necessarily individual input parameters. To test our current hypothesis, we combined techniques

to quantitatively examine cell morphology and differentiation in response to defined amounts of energy. By calculating the mechanical energy that we applied to MSCs through specific stretch parameters, we set up a system to directly compare MSC shape and gene expression from samples stretched with different input parameters but with equal or different amounts of input energy. Following that, we assessed if these responses were consistent across a predetermined range of energy levels and if these changes could be statistically differentiated. Finally, to find the fundamental relationships between mechanical parameters, shape factors, and gene expression, we analyzed the data through partial least squared analysis, to account for multicollinearity among energy and energy-induced phenotypical parameters. The cells that we stimulated for were primary cells from patients that differed for every experiment making any relationship quite robust. In many non-biological mechanical and thermal processes, exchange of energy is a state function, meaning that the resulting condition is independent of the means used to deliver that energy. A biological response following this same principle would not only prove interesting but offer insight into how cells respond to mechanical forces.

Ultimately, in this manuscript, we asked if the cellular response to mechanical forces follows that of a state function and whether that response can account for multiple different stretch parameters through one, overarching measurement: energy. Unifying mechanical input parameters to control cell phenotype would not only provide a novel concept to the field of mechanobiology and enable connecting the findings of previous studies, it would also fundamentally improve the process of directed cell differentiation.

3.2 - Materials and Methods

bMSC isolation and expansion

Bone Marrow aspirates were obtained from the proximal femurs of osteoarthritic patients (n=29, age 50 to 86) who underwent total hip replacement in the Department of Trauma and Restorative Surgery, BG Trauma Clinic, University of Tuebingen. Aspirates were taken with approval of the local research ethics committee of the Medical Faculty of the University of Tuebingen (623/2013BO2) and with informed consent from the patients. All methods were carried out in accordance with the guidelines of the local research ethics committee of the medical faculty of the University of Tuebingen. Human bone marrow MSCs were isolated as described in [12,13]. Aspirates were washed with PBS, centrifuged at 150 g (10 minutes, room temperature), and the pellet was re-suspended in PBS, discarding the supernatant. The bMSCs were then separated using a Ficoll density gradient fractionation (density 1.077 g/mL, GE Healthcare Life Sciences, Uppsala, Sweden, 400 g, 30 min, room temp). The mononuclear cell layer was removed, washed in PBS and seeded in T75 flasks. The separated bMSCs were cultured and expanded at 37ºC and 5% CO_2 in good manufacturing practice (GMP)- compliant media made with DMEM low glucose (Sigma-Aldrich, Hamburg, Germany), 1000 IU heparin (Carl Roth, Karlsruhe, Germany), 25 mM hepes (Lonza, Basel, Switzerland), 5% human plasma (TCS Biosciences, Buckingham, UK), 5% human pooled platelet lysate (10^8 platelets/mL medium, ZKT Tuebingen, Germany), 2 mM L-glutamine (Lonza), and 1% penicillin-streptomycin solution (Life technologies, Darmstadt, Germany), according to [11]. 24h after seeding, GMP expansion media was replaced and then changed twice a week. At near confluence, after around 7 days, cells were removed with trypsin, counted, and re-plated (10^4 cells per flask) in GMP expansion media for further passaging.

Expression of cell surface antigens for bMSC identification and sorting

To distinguish and sort heterogenous populations from the marrow aspirates, the expression of CD90, CD14, CD11b (R&D Systems, Minneapolis, USA), CD105, CD73, CD45 and CD34 (BD Pharmingen, San Diego, USA) on bMSCs was analyzed by flow cytometry as we have shown previously [6,21]), and in accordance with [33]. bMSCs were detached gently using Accutase. Nonspecific binding of antibodies was blocked with Gamunex (Talecris Biotherapeutics, Frankfurt, Germany). The bMSCs were washed twice with PFEA buffer (PBS, 2% FCS, 2mM EDTA, 0.01% sodium azide) and incubated for 20 min at 4°C with phycoerythrin (PE)-conjugated or allophycocyanin (APC)-conjugated monoclonal antibodies (mAB, BD Pharmingen, Heidelberg, Germany). Unbound antibodies were washed away twice with PFEA buffer, and MSCs were analyzed by flow cytometry (BD LSRII, San Diego, USA). Data were evaluated using the software FlowJo (Tree Star, Inc., Ashland, Oregon, USA).

MSC seeding on compressed collagen sheets

Compressed rat collagen I sheets with a previously optimized collagen concentration of 80 mg/mL [12,13] were generated (Amedrix, Esslingen, Germany) and cut into 4x1 cm sheets. This fabrication method is well established and commercialized and while bovine collagen meets more clinical standards, collagen is highly conserved across species. After passaging in GMP expansion media (DMEM with pooled plasma and platelet lysate as described [12,13]), bMSCs (passages 3-5) were seeded at 15,000 bMSC/cm^2 at day 0 onto collagen sheets. Sheets were cultured in high glucose DMEM (4g/L, Life Technologies, Darmstadt, Germany), 10% FBS (Biochrom), 2% penicillin-streptomycin (Gibco/Life Technologies), and 1% fungicide (Biochrom) at 37°C and 5% CO_2 for 3 days before stretching on day 4.

<u>Sinusoidal cyclic stretch of collagen sheets and adhering bMSCs</u>

Collagen sheets seeded with bMSCs at passages 3-5 with 15,000 cells/cm^2 were cultured for 3 days and inserted on day 4 into the bioreactor chamber of an incubator-housed ElectroForce 5210 BioDynamic-Test-System (assembled by Bose, Minnesota, USA; now TA instruments). Identical bioreactor chambers filled with 200 mL of control media were used for applying cyclic stretch and for incubating unstretched control sheets. Uniaxial displacement-controlled cyclic stretch was applied at 1 Hz with either 2.5%, 5%, or 10% strain and for either 45 minutes, 1 hour, 3 hours or 16 hours before analysis. Sheets stretched for a single regimen and their unstretched control sheets cultured for the same duration were labeled "1x". Half of these sheets were analyzed, the remaining sheets were stretched for a second, identical regimen on day 5. These sheets and their respective controls were labeled "2x". These parameters were chosen based on common strain parameters in literature and previous findings in our lab. After cyclic stretch, the sheets were cut in two equally sized halves. One half was processed for qRT-PCR and one was prepared for fluorescence microscopy.

<u>Fluorescence microscopy for cell shape</u>

The bMSC-seeded sheets used for imaging were stained with Calcein and Hoechst Solution (Cell Viability Imaging Kit, Roche) based on the manufacturer's protocols and on our previous work [12,13]. bMSCs attached to the collagen sheets were imaged using a Zeiss LSM510 microscope with AxioVison4.8 and manual exposure correction. Calcein-stained bMSC morphology was visualized using the green filter and the nuclei were imaged using a blue filter. Using the MosaiX

module, a mosaic of 10x10 images (with a size of 12,633 x 9,429px corresponding to 8,211.45 x 6,128.85 µm using a 10x objective) were stitched together for analysis. Using the stitched mosaic images, the individual shapes of large quantities of bMSCs were counted and measured simultaneously with an ImageJ macro, according to [13]. The following six mathematical shape descriptors were quantified for each bMSC: length (major axis), area, circularity (4*π(area/perimeter^2), projection factor (perimeter^2/area), roundness (4*area/(π*major axis length^2)), and aspect ratio (major axis angle/minor axis). These measurements were averaged for each construct and the values for each construct were used to compare different regimens.

Quantitative RT-PCR

Compressed collagen sheets with cultured bMSCs were digested for 4 minutes at 55° C using Proteinase K (Fermentas/ThermoScientific). mRNA was isolated using the RNA-Extraction-RNeasy-Minikit (Qiagen, USA). cDNA was synthesized using the Advantage RT-for-PCR Kit (Clontech, USA). Quantitative RT-PCR was performed with the LightCycler 480 SybrGreen Master (catalog no. 04707516001, Roche) and LightCycler 480 Probes Master (no. 04707494001, Roche) using the LightCycler 480 system and Multiwell 96Plates (no. 04729692001, Roche). Gene expression levels of acta2 (ACTA), transgelin (TAGLN), calponin (CNN), desmin, (DES), peptidylproplyl isomerase A (PPIA), and human glyceraldehyde-3-phosphate-dehydrogenase (GAPDH) were determined according to MIQE guidelines [34]. PPIA and GAPDH were used as reference genes. As positive controls and calibrator samples human bladder derived smooth muscle cells (HBdSMC, Promocell, Heidelberg, Germany) were used, as described in [12]. The oligonucleotide primers used in qRT-PCR assays were TTGCCTGATGGGCAAGTGAT (forward

primer sequence) and TACATAGTGGTGCCCCCTGA (reverse primer sequence) for ACTA, AGATGGCATCATTCTTTGCGA and GCTGGTGCCAATTTTGGGTT for CNN, GGAGATTGCCACCTACCG and GGTCTGGATGGGGAGATTG for DES, CTCTGCTCCTCCTGTTCG and ACGACCAAATCCGTTGACTC for GAPDH, and TTCATCTGCACTGCCAAGAC and TCGAGTTGTCCACAGTCAGC for PPIA. For TAGLN, the Quiagen assay Hs_TAGLN_2_SG (QT01678516) was used. For TAGLN and PPIA, SybrGreen (Roche) was used. For ACTA, CNN, and GAPDH the Roche Universal Probe Library Probes N58 (ACTA2, catalog no. 04688554001), N71 (CNN1, no. 04688945001), and N60 (GAPDH, no. 04688589001) were used, as described in [12,13].

Energy Calculation

To compare the energy input for each stretch regimen, the force required to cyclically stretch the entire collagen sheet was measured over the course of multiple cycles [12]. Due to the nature of the strain profile, that force was integrated using Equation 1 where F=peak force measured, l=length of the collagen sheet, s=the maximum strain, h=the frequency of cycling, and t=the length of time, in hours, that the sheets were being stretched. The different regimens and their respective energy input are plotted in Figure 3.1. This equation assumes a perfectly elastic substrate and that the sheets do not plastically deform over the entire stretch regimen. Both of these assumptions are generally proven over the regimens used here according to [12].

$$E = \int_{0}^{2*l*s*h*3600*t} \frac{F}{\pi * \arccos(\cos\left(\frac{\pi x}{s * l}\right))}$$

Equation 1: The integral describing energy put into the system. "F" was the peak force exerted throughout the loading regimen, "l" was the length of the construct, "s" was the maximum strain in decimal form, "h" was the frequency, and "t" was the time in hours. Because the system never compressed the constructs, it simply cycled between 0 N and the peak F with a cosine function.

Statistical Analysis

Bar graphs comparing measurements with different energy levels were made using the average value from each construct/patient as a single sample (n=1). To compare, the values from constructs with the same calculated energy input were averaged together and these data are presented as mean ± standard error. All data for bar graphs was plotted and statistically analyzed in R. ANOVA and Dunn's Method was used for post-hoc analyses to compare individual groups. If no significant differences were noted, an asterisk and "ns" are noted in the top left corner. For regression analysis, the means of the average from each construct were plotted against input energy. Regression analysis was also done in R. Both R^2 and p values for fit were calculated and included.

Principle Component Analysis (PCA) and Partial Least Squares (PLS) Analysis

All PCA and PLS analysis was done in R using the mixOmics package. The data in each category were mean centered and normalized by the standard deviation. The PCA and PLS functions in the package were used to analyze the data. PCA was done without any gene expression included in the X block. The loadings for all PCA analyses were the same and color coding was implemented post analysis to distinguish data points based on author grouping. Normally this break was made between the biggest break in the rankings of expression for that gene. The numerical numbers correspond to different energy levels/conditions but have no bearings on the end results. PLS was done with all input parameters and shape factors as part of the X block and each gene as its own independent Y block. The finals loadings for each gene's X block are listed and color coding was implemented post analysis to distinguish data points based on author

grouping. Again, the color coding was done between the conditions with the biggest break when ranked according to expression for that gene and the numerical labels have no bearing on the final results.

3.3 - Results

<u>Comparing Cell Shape from Stretched Samples with Equal and Different Input Energies</u>

We first examined the resulting cell shape when the energy into the system was equal and compared them to the shape of cells stretched with higher input energy. For parameters that produced equal input energies, we stretched constructs to 10% for 45 minutes (Fig 3.2A) and 5% for 3 hours (Fig 3.2B) both having input energy of 8.75 J. The cells exposed to higher input energy were stretched at 10% for 16 hours for a total of 186 J (Fig 3.2E). Next, we directly compared the results of conditions that produced similar results in Chapter 2. They had different combinations of input parameters but they had a difference in energy input of around 25%: 10% for 3 hours (Fig 3.22C) and 5% for 16 hours (Fig 3.2D). These conditions had energy inputs of 35 and 46 J respectively. Both of these pairs were compared to samples stretched at 10% for 16 hours (Fig 2E) which had an input energy level of 186 J. Looking at the Calcein stained cells, cells stretched with the same amount of energy look similar despite their different input parameters (Fig 2A and 2B). Cells that have been stretched with 186 J look longer than those at 8.75 J and have finer protrusions. The pair of cells stretched with intermediate levels of energy (35 J and 46 J) seem to be intermediate in size as well and while there are differences between the cells of the two conditions, the differences are subtler. These observations are quantified using our shape factors in Figure 3.3-3.5.

A

1x 10% 45m: 8.75 J

B

1x 5% 3h: 8.75 J

E

1x 10% 16h: 186 J

C

1x 10% 3h: 35 J

D

1x 5% 16h: 46 J
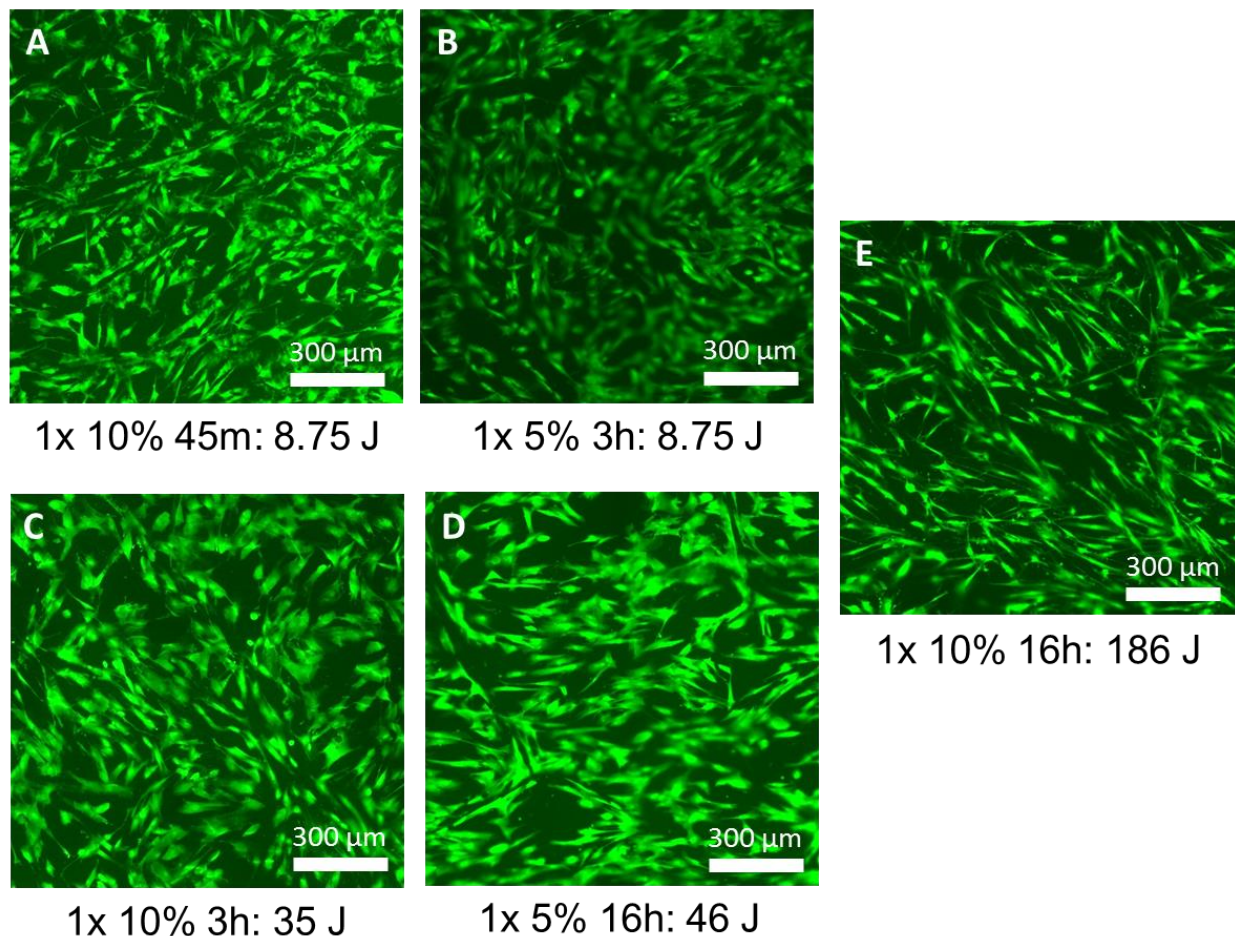
Figure 3.2: Morphology of Cells Stretched for One Regimen with Different Parameters and Different Energy Levels. All panels show the morphology of cells stretched with differing input parameters. The morphological results from these five conditions were used for morphological results in Figures 3.3-3.5. Panel A and B had the same input energy but different input parameters. A and B both had different input parameters and input energy than Panel E. Panel C and D had similar input energy but different input parameters from each other and much different inputs than Panel E. Cells with similar input energies had similar morphologies, especially when compared to cells stretch with vastly different input energies.

Cell Size Depended on Input Energy

The length of cells stretched with equal amounts of energy were statistically similar (Fig 3.3A) but a 25% difference in input energy at higher energy levels (35J and 46J), produced lengths that were different (Fig 3.3B, $p < 0.05$). Constructs stretched with much more energy (186 J compared to 8.75 J or 35 J) produced cells that were significantly longer than cells stretched with

lower input energy (Fig 3.3A and 3.3B, $p<0.05$). Cell area followed a similar trend. Cells whose constructs were stretched with equal input energies (both 8.75 J) produced cells of statistically similar areas (Fig 3.3C) and when cells were stretched with a 25% difference between them (35 J and 46 J), more energy with still produced cells of similar areas (Fig 3.3D). Only by increasing the input energy up to 186 J did we start seeing statistical differences in area (Fig 3.3C and 3.3D, $p<0.05$). In general cells from constructs with the same input energy had similar sizes, whereas a small difference in input energies produced small changes in cell size, and increasing the energy level increased the size of the cells significantly (Fig 3.3).

Figure 3.3: Cell Size with Similar Energy Input but Different Input Parameters. When the same amount of energy was input into the system (10% for 45 (n=4 patient cell samples averaged) minutes and 5% for 3 hours (n=6 patient cell samples averaged)) the resulting cell length and area (from these conditions but in A and C respectively) were statistically similar. Increasing the input energy (10% 16 for hours (n=13 patient cell samples averaged)) produced cells of different sizes (A and C, $p<0.05$). When different but similar amounts of energy were put into the system (10% for 3 hours (n=6 patient cell samples averaged) and 5% for 16 hours (n=12 patient cell samples averaged)) differences in length were significant (B, $p<0.05$) but not in area (D). Differences in area and length were still evident between cells stretched with much different energy (A-D, $p<0.05$).

Cell Polarization is Responsive to Input Energy

Here, we describe cell polarization as an increase in anisotropy as cells elongate in one direction preferentially to another. This behavior is described mathematically through changes in

roundness and aspect ratio. When comparing roundness of cells from samples stretched with the same amount of input energy, they were statistically indistinguishable from each other but cells stretched with the same low energy level (8.75 J) were also statistically similar in roundness to cells stretched with higher (186 J) energy (Fig 3.4A). When the input energy was increased and the differences were larger, significant differences in roundness were still not seen between categories of similar energies but there were differences in roundness between these and much larger input energies (Fig 3.4B, $p<0.05$). When comparing aspect ratio in regards to changes in energy levels, cells with the same input energy were statistically different from one another (Fig 3.4C, $p<0.05$) but cells from constructs with different input energies were statistically similar (Fig 3.4C and 3.4D). Thus, cell polarization was responsive to energy but the relationships were unlike that of cell size suggesting latent variables that were unaccounted by energy alone.
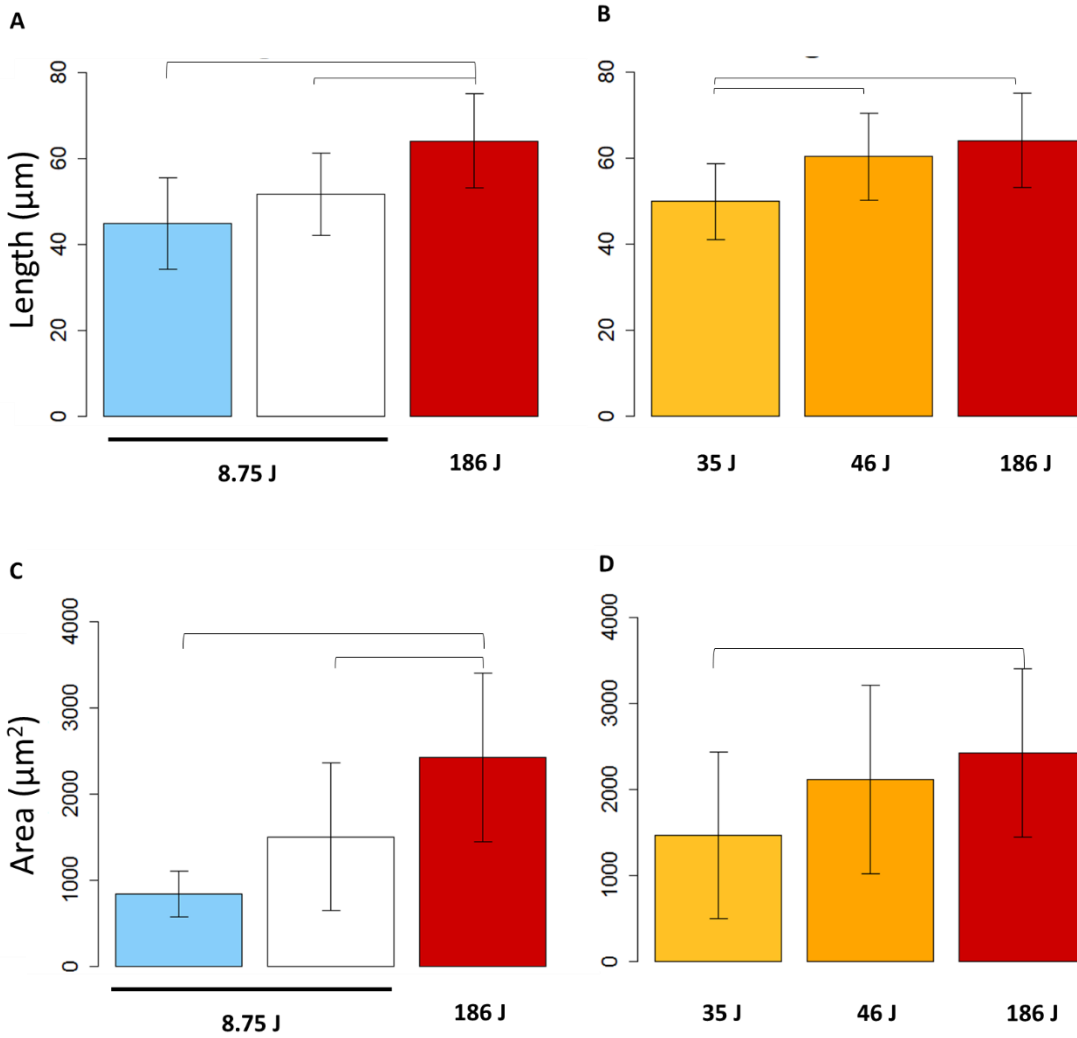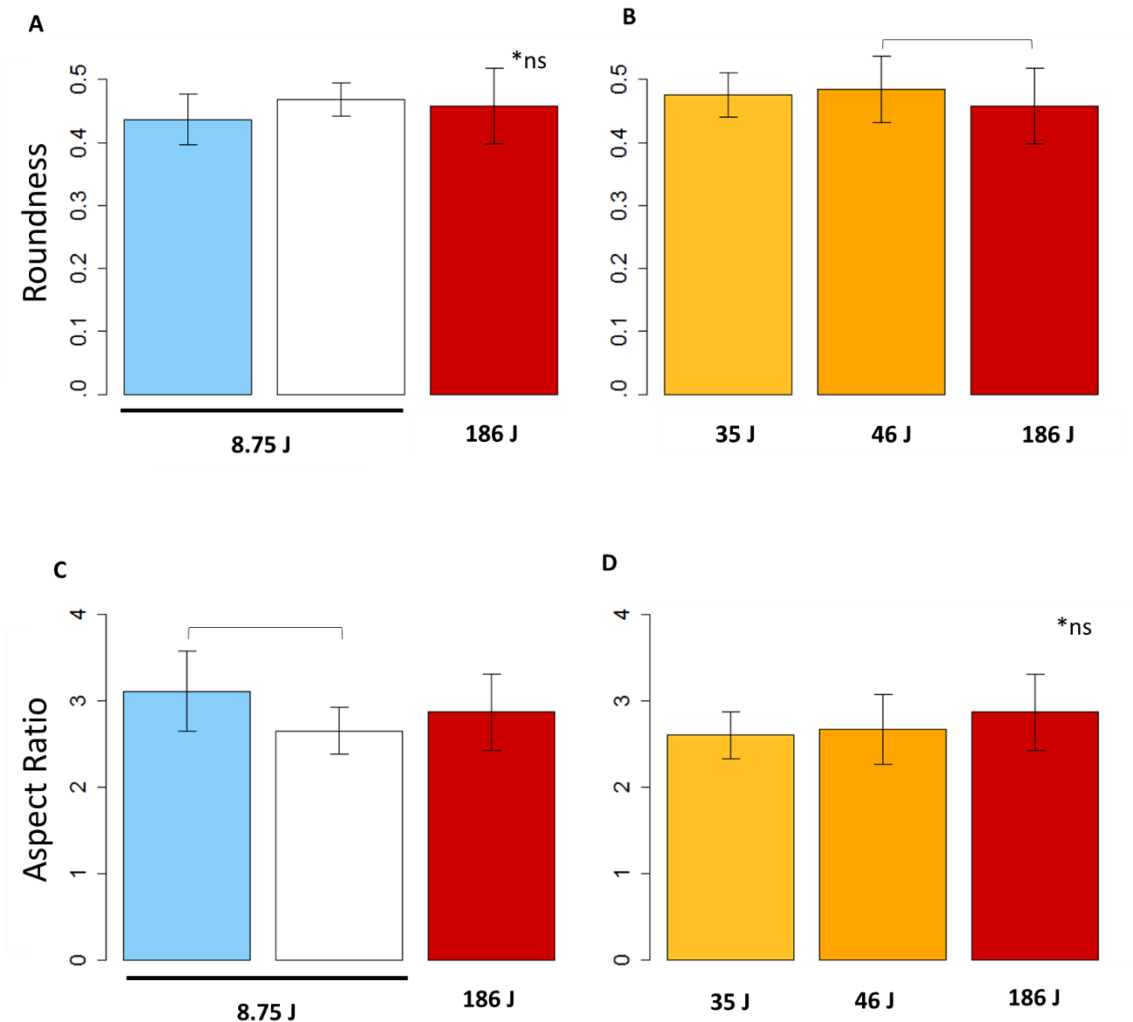
Figure 3.4: Cell Polarization with Similar Energy Input but Different Input Parameters. When the same amount of energy was input into the system (10% for 45 (n=4 patient cell samples averaged) minutes and 5% for 3 hours (n=6 patient cell samples averaged)) the resulting cell roundness (A) was statistically similar but aspect ratio was significantly different (C, p<0.05). Increasing the amount of energy (the 10% for 16 hours (n=13 patient cell samples averaged)) alone did not produce cells of different roundness or aspect ratio (A and C) and much higher energy input resulted in reduced roundness (B, p<0.05). When similar amounts of energy were put into the system (10% for 3 hours (n=6 patient cell samples averaged) and 5% for 16 hours (n=12 patient cell samples averaged)) the roundness and aspect ratio of the different conditions were statistically similar (B and D).

Cell Spreading Depends on Input Energy

In this manuscript we describe cells extending their membranes through filopodia and lamellipodia as "cell spreading". This can be described mathematically as a disproportional increase in perimeter relative to area. When the ratio of area to perimeter squared is normalized to

79

one, this is termed "circularity". We use this shape factor in other works and assess it here for consistency. Regardless of whether the input energy was the same, similar, or different, there were no statistical differences between the mean circularity of cells from different energy input levels (Fig 3.5A and 3.5B). When we considered the non-normalized inverse ratio, the perimeter squared to area, we get a different shape factor we define as the projection factor. When we analyzed the projection factor, cells whose constructs were stretched with equal input energies produced cells of statistically similar projection factor values (Fig 3.5C). Marginally increasing the energy difference still produced cells with similar projection factors (Fig 3.5D). By increasing the input energy up to 186 J we did see statistical differences in the average projection factor (Fig 3.5C and 3.5D, $p<0.05$). Thus, cell spreading was responsive to input energy, as cells from constructs with the same input energy spread similarly but by changing the energy input, cell spreading also changed.
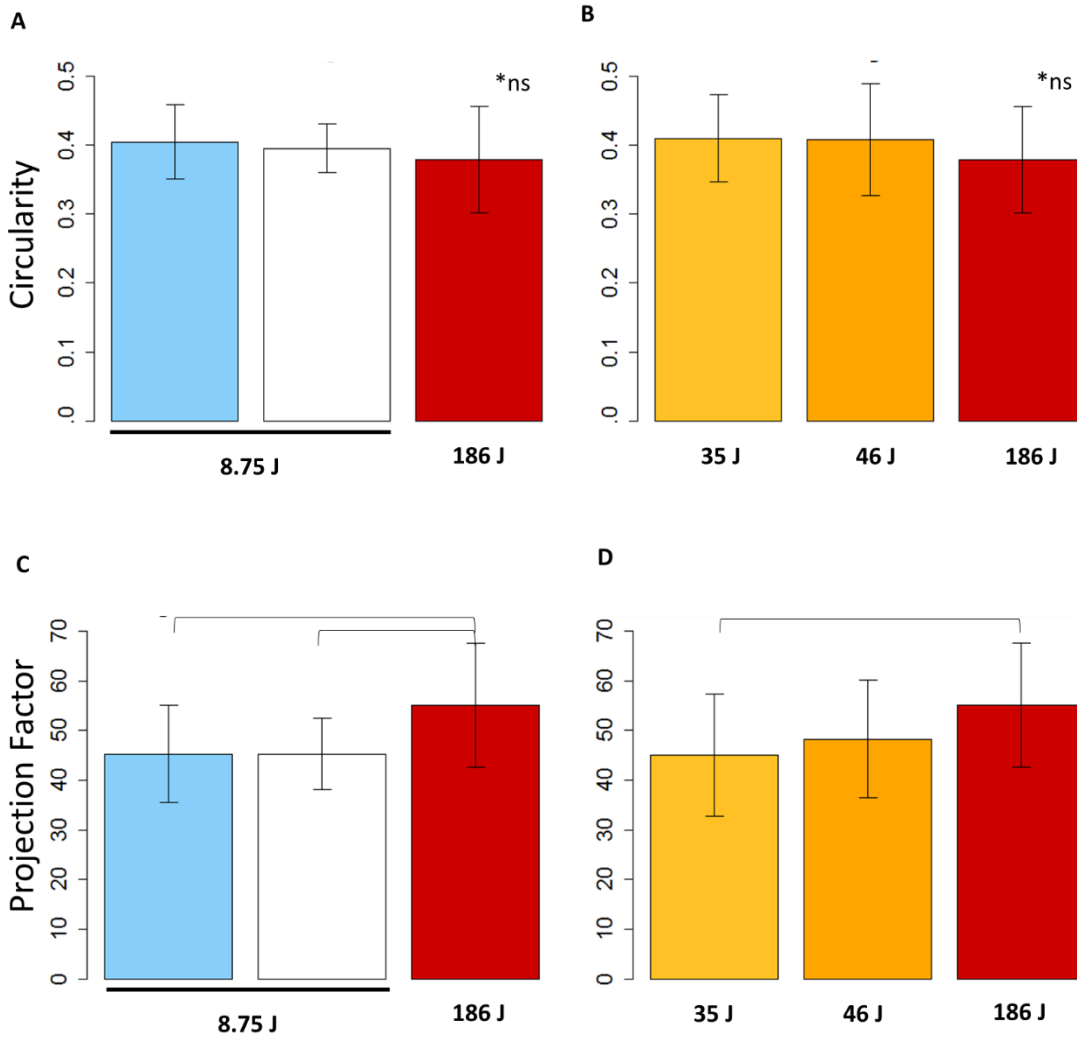
Figure 3.5: Cell Spreading with Similar Energy Input but Different Input Parameters. Regardless of the energy inputs, the average circularity values of the samples were statistically similar (A-B). When the same amount of energy was put into the system (10% for 45 minutes and 5% for 3 hours) the resulting cell projection factor was similar but when that energy was increased (10% for 16 hours), the projection factor increased significantly (C, $p<0.05$). When the energy input was similar but different (10% for 3 hours vs 5% for 16 hours), only the smallest energy input (10% for 3 hours) produced a projection factor that was significantly different from the larger energy input in the 10% for 16 hour condition (D, $p<0.05$).

Correlations Relating Energy Input to Cell Phenotype

After having established a relationship between cell shape measured with quantitative shape descriptors and energy inputs, we aimed to extend this relationship across multiple energy levels and examine cell phenotype as a function of energy input. Realizing it followed a

81

logarithmic relationship at higher energy levels, the shape descriptor was plotted against the log of the energy input and linear regression analysis was performed on this function as well.

Cell Shape as a Function of Energy Input

When we plotted cell length against the log of the energy input there was a strong positive correlation between the energy input and the average cell length (Fig 3.6A, $p<0.005$ and $R^2=0.63$). A similar strong positive correlation was seen between the log of the energy and the average area of cells stretched under those conditions (Fig 3.6B, $p<0.001$, $R^2=0.71$). Cell polarization also exhibited correlations with the energy input, as roundness was positively correlated with the log of the input energy (Fig 3.6D, $p<0.01$, $R^2=0.48$) and aspect ratio was negatively correlated with the log of the input energy (Fig 3.6C, $p<0.01$ and $R^2=0.50$). Although the change of aspect ratio in response to energy was initially difficult to understand when comparing individual energy levels with each other (Fig. 3.44), when we plotted aspect ratio against the input energy log we uncovered a near-stepwise, binary energy response, where the energy threshold was between identical energy levels, coded in this study with light blue and white. Comparison of cell spreading across all energy inputs also supported findings in Fig 3.5. Circularity had no significant relationship with input energy (Fig 3.6E) but the projection factor had a positive correlation to the log of the input energy (Fig 3.6F, $p<0.05$, $R^2=0.33$). Together these results demonstrated that cell morphology was not only dependent on the input energy but there was a linear correlation between the log of energy put into the system and the resulting cell shape.

A Length vs Energy

R² = 0.6271

B Area vs Energy

R² = 0.7065

C Aspect Ratio vs Energy

R² = 0.5039

D Roundness vs Energy

R² = 0.4762

E Circularity vs Energy *ns

R² = 0.0909

F Projection Factor vs Energy

R² = 0.3307
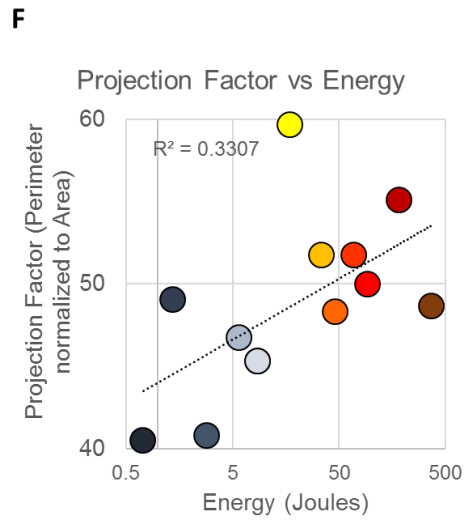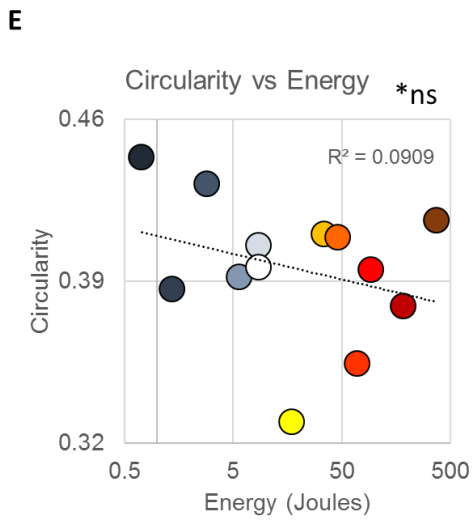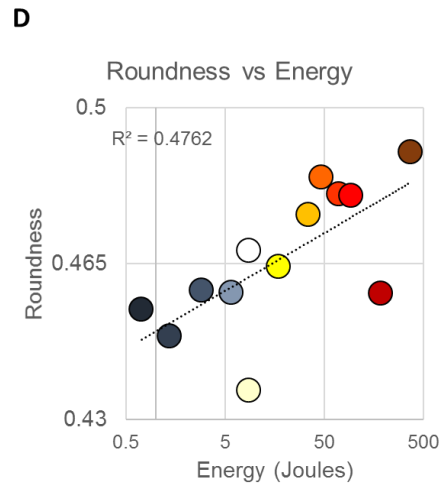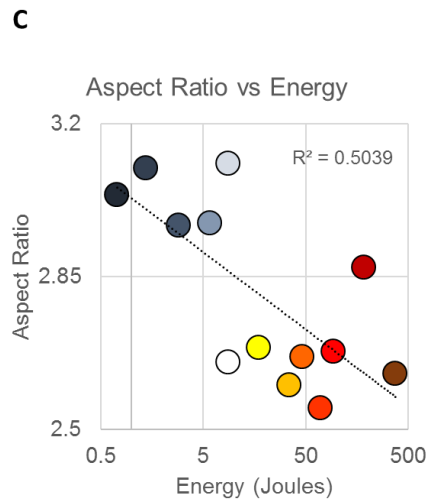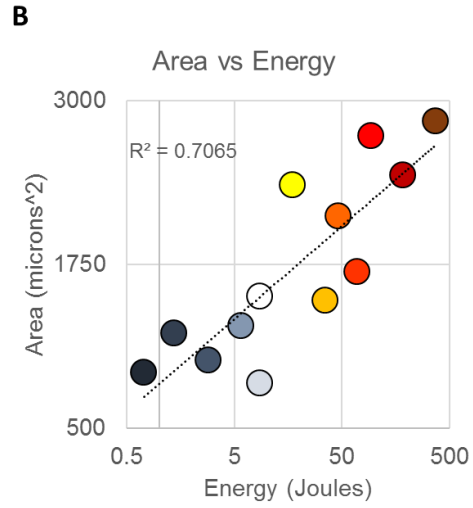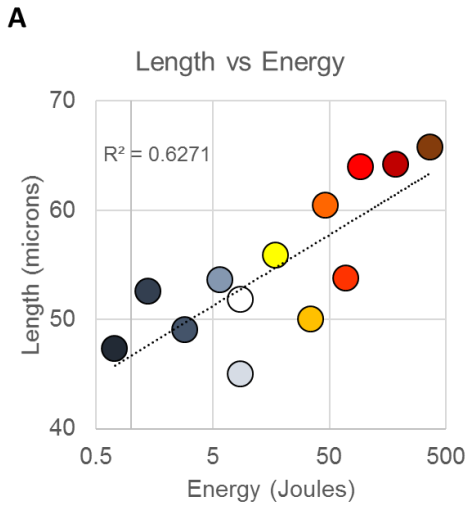
Figure 3.6: Relationship between Energy Input and Cell Shape Parameters. When comparing the average cell length to the log of the energy input, a positive linear relationship was observed (A, $p<0.005$). When comparing the average cell area to the log of the energy input, a positive linear relationship was also observed (B, $p<0.01$). When comparing cell polarization to the log of the energy input, cell aspect ratio exhibited a negative linear relationship (C, $p<0.001$) while cell roundness exhibited a positive linear relationship (D, $p<0.001$). When comparing the average cell circularity to the log of the energy input no relationship was observed (E). When comparing the average cell projection factor to the log of the energy input, a positive linear relationship was also observed (F, $p<0.05$)

Gene Expression as a Function of Energy Input

Next, we compared the expression of multiple genes to the log of the energy input. ACTA, an early marker for sensing and responding to mechanical stimulation, was negatively correlated the amount of input energy (Fig 3.7A, $p<0.01$ and $R^2=0.52$). None of the other genes that were expressed (TAGLN, CNN, or DES; Fig 3.7B, 3.7C, and 3.7D respectively) correlated with the amount of energy put into their system.
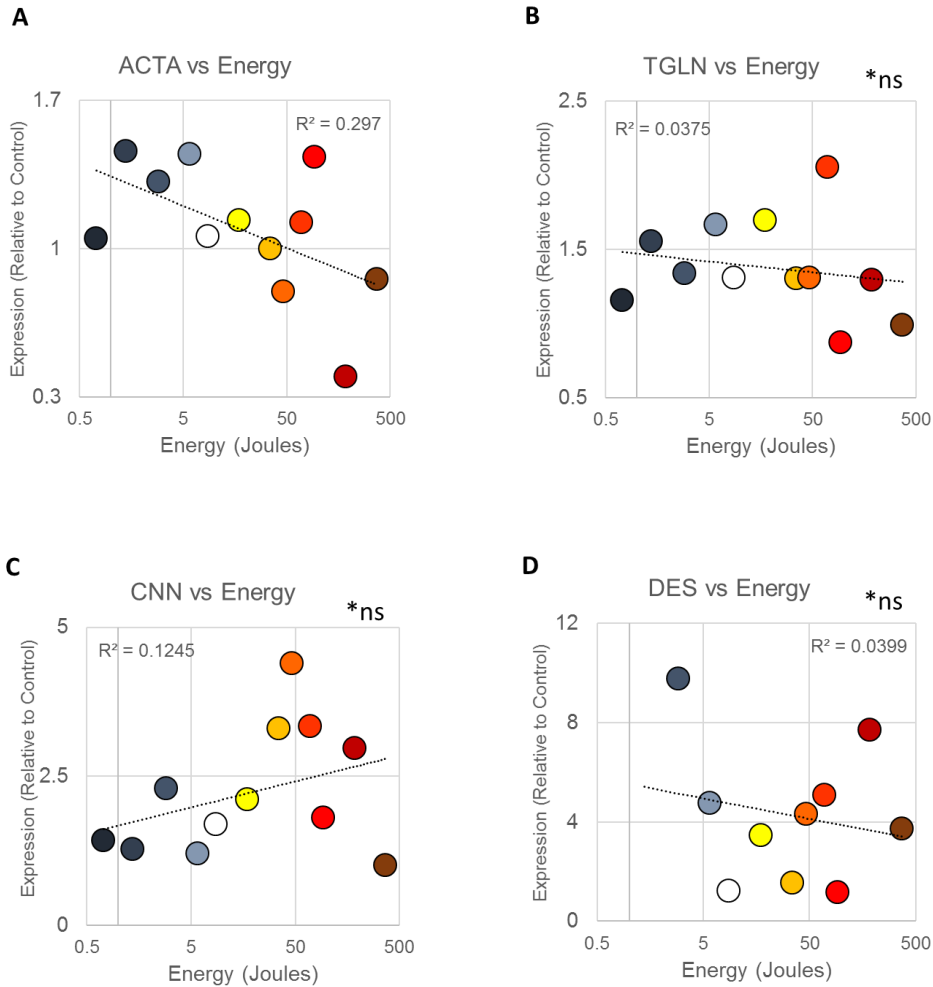
Figure 3.7: Relationship between Energy Input and Gene Expression. When comparing the expression of ACTA to the log of the energy input, a negative linear relationship was observed (A, $p<0.01$). When comparing the expression of TGLN, CNN, and DES to the log of the energy input, no statistical correlations were observed (B-D).

Determining Principle Relationships Between Genes and Input Parameters

While the there was a correlation between energy and shape, the relationship between energy and gene expression was less explicit. To determine which factors had the strongest relationships with expression of ACTA, TAGLN, CNN, and DES, we carried a partial least squares analysis in "R" using the mixOmics package. The first approach was visualizing how the different conditions were mathematically related and clustered. With biomechanical input parameters

(energy, strain, duration, etc.), the resulting shape descriptor values (length, projection factor, etc.), and gene expression (ACTA, CNN, etc.) all mean centered around 0, and normalized by their standard deviation, the individual conditions were organized into a hierarchy that related them by Euclidean distance from one another. When this was done, the biggest degree of separation occurred between constructs stretched for different durations of stretch (Fig 3.8), indicating that stretch duration played a large role in determining gene expression. The next level of separation was the number of stretch regimens the samples had undergone. Finally, the groups were separated by the amount of strain used during stimulation. Collectively, this indicated that the parameters used for varying stretch conditions displayed a hierarchy that clustered the conditions mathematically, and by which different durations of stretch were related to the largest variations in MSC phenotype.
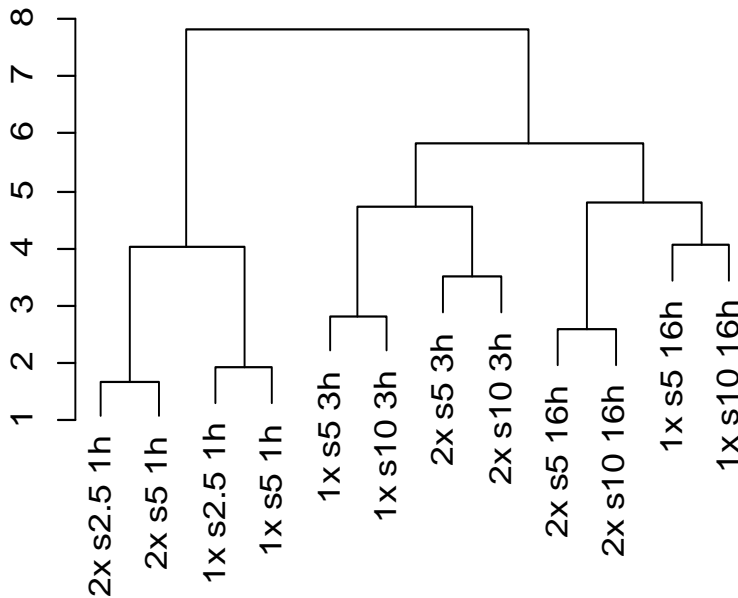
Figure 3.8: Quantitative Clustering of Conditions Based on Average Values. When the input values; Energy (logE), Strain, Number of Regimens (Day), and Duration, as well as output values; including all shape factors and gene expression were normalized and distinguished mathematically by their Euclidian distance from one another, the groups were categorized as described above. The groups were separated primarily by duration. After these initial breaks, the next level of bifurcation seemed to happen by separating the number of regimens the samples were stretched. Finally, within these groups, samples were separated by strain.

To examine this clustering further and compare the combinatorial effects of the input parameters on gene expression, partial least squares analysis (PLS) was carried out using the input parameters and cell shape as the X block and each gene as Y block data in its own analysis. For ACTA expression, PLS could account for up to 53% of the variability and two best fitting X variants positively correlated with ACTA expression (Fig 3.9A). As expected from the energy scatterplots, the log of the input energy was a primary latent variable meaning that, with all input parameters normalized, had a strong correlation with gene expression. Energy as well as area of the cell, duration of stretch, and the length of the cells all negatively correlated with ACTA expression (Fig 3.9B). For CNN, PLS accounted for 49% of the variability and both X variants generally correlated with its expression (Fig 3.9C). PLS ranked the aspect ratio and number of regimens (Day) negatively with expression and strain, roundness, and log of the energy positively with CNN expression (Fig 3.9D). The PLS components for TAGLN explained 28% and 45% of its variability and both generally correlated positively with TAGLN (Fig 3.10A). It weighted circularity, duration, length, and area as dominant factors, all of which negatively correlated with TAGLN expression (Fig 3.10B). PLS analysis explained 41% of variance of DES with its first two components, both of which generally correlated positively with DES expression (Fig 3.10C). It's first component had roundness, area, and aspect ratio as dominant factors, the first two of which negatively correlated with DES expression (Fig 3.10D). Together, these data explain that while energy correlates well with ACTA, cell shape was a better predictor for smooth muscle-specific genetic markers like CNN, TAGLN, and DES.
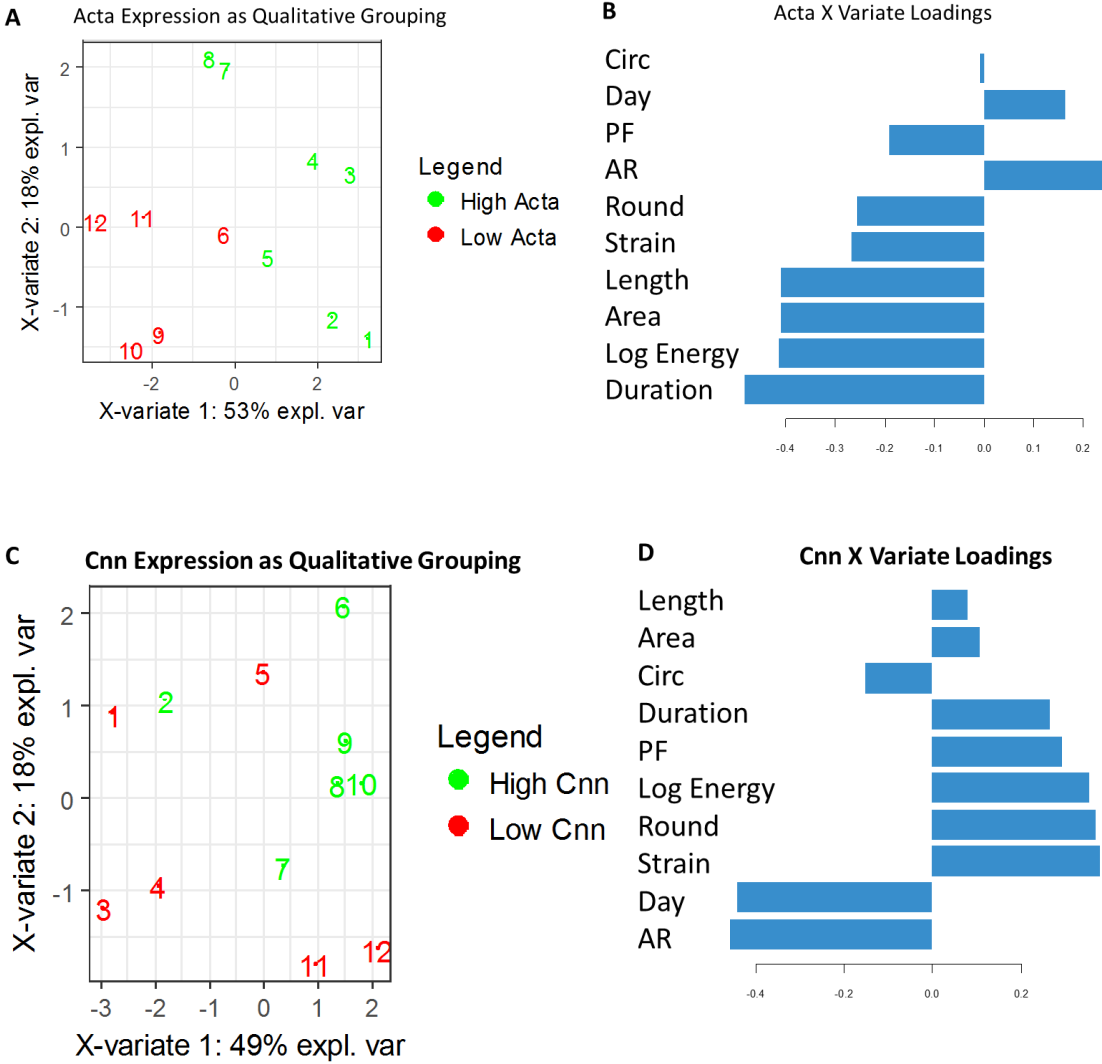
Figure 3.9: Partial Least Squares Regression (PLS) and Scores with Clusters Grouped by ACTA and CNN Expression with X Blocks. Partial Least Squares analysis with ACTA as the Y block yielded components explaining 53% and 18% of the variance. High ACTA expression was predicted by high scores in both component 1 and component 2 (A). Component 1 of the ACTA model weighted duration, LogE, area, and length as the dominant factors, all of which negatively correlated with acta expression (B). Partial Least Squares analysis incorporating CNN as the Y block yielded components explaining 49% and 18% of the variance. Generally, high scores in both components 1 and 2 predicted high CNN expression (C). The CNN model weighted aspect ratio and the number of regimens (Day) as the most dominant and negative latent variables with Roundness and Strain as less dominant but correlating positively with expression (D). The numbers correspond to specific conditions and have no impact on the interpretation of the data.
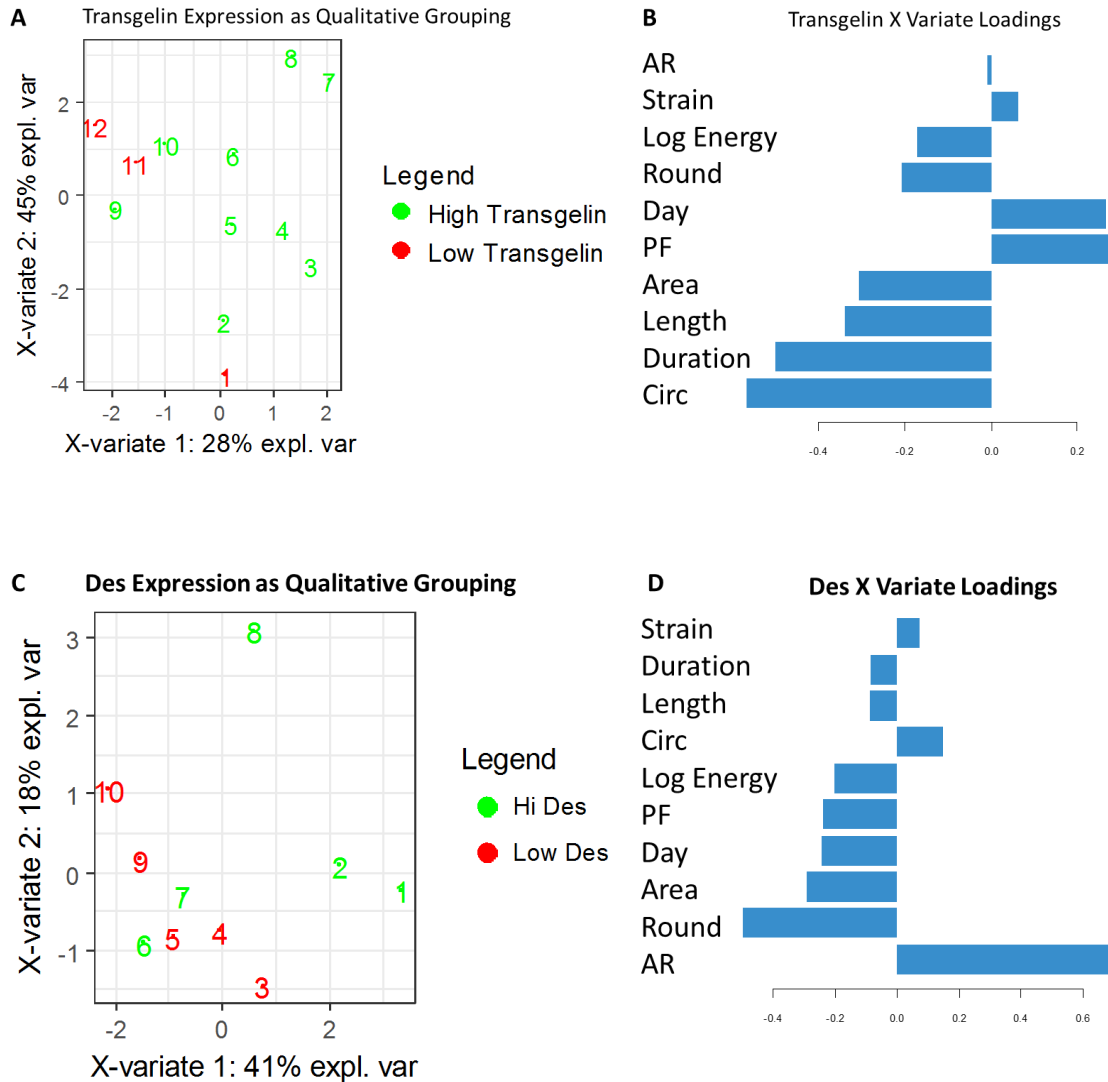
Figure 3.10: Partial Least Squares Regression (PLS) and Scores with Clusters Grouped by TAGLN and DES Expression with X Blocks. Partial Least Squares analysis with TAGLN as the Y block yielded principal components explaining 28% and 45% of the variance. High TAGLN expression was predicted by high scores in component 1 (A). The TAGLN model weighted circularity, duration, length, and area as the dominant factors, all of which negatively correlated with TAGLN expression (B). Partial Least Squares analysis incorporating DES as the Y block yielded components explaining 41% and 18% of the variance. High scores in both components 1 and 2 predicted high DES expression (C). It weighted roundness, area, and the aspect ratio, the first of which all of which positively correlated with DES while the latter two negatively correlated (D). The numbers correspond to specific conditions and have no impact on the interpretation of the data.

3.4 - Discussion

Asking if the phenotypic response of bMSCs to mechanical stimulation is a state function

of energy input, we first hypothesized that the effects of mechanically controlling bMSC shape

and differentiation through cyclic stretch are controlled by the amount of the applied energy. In

this manuscript, we demonstrated that multiple aspects of cell phenotype, particularly cell morphology, not only respond to different energy inputs, but they do so in a consistent correlation. Even though each data point used for analysis was an average from different patients and passages, cell shape demonstrated a marked coherence to a state function response to the amount of mechanical energy put into the system. Despite having different maximum strains and durations of stretch, when the same total amount of energy was used, the cells exhibited statistically similar lengths, areas, and projection factors. If this energy input was altered, even slightly, differences could be seen in the cell morphology, and if the difference in input energy was much larger, cell length, area, roundness, and projection factor all showed significantly different responses. One feature of cellular polarization (aspect ratio) did not follow this same linear trend with changes in the log of the energy but responded with a binary and threshold response. This implies a complex relationship between aspect ratio and energy, and might be related to the fact that aspect ratio was the only shape factor to weight strain as a principle loading factor during Partial Least Squares analysis. There is likely some underlying variable as why it has this binary response to energy when higher strains are used. That cell circularity showed no significant differences may have been due to subtle differences that our approach was not always sensitive enough to capture (i.e. the dynamic range of circularity, which is limited to values between 0 and 1, limits sensitivity to small changes). However, we uncovered that cell spreading indeed did follow the same trend, once we had introduced the "projection factor".

Next, we assessed if the association between the amount of applied energy with the resulting cell shape was consistent across many different energy levels and if these changes could be described mathematically. We demonstrated that the shape descriptors length, area, aspect ratio, roundness, and projection factor - but not circularity - exhibited a strong association with increased

90

amounts of energy input. By increasing the energy logarithmically, we uncovered a linear response for the five shape factors. Overall, our data suggest that cell shape is not only a result of the energy input of the system but a state function of the energy applied. Others have presented simulations, which predicted that this change in shape in due to increases in energy, particularly cell spreading and lengthening [32], but these authors do not specify the source of this energy and it may possibly be derived from mechanical stimuli like stretch. Jay Humphrey is an expert on the mechanical properties of blood vessels and has shown repeatedly that these structures develop and remodel anisotropically in response to forces/energy. Some of these principles are reviewed in [35]. It only follows that these effects could be reduced down to the cellular level. Our idea of controlling energy for engineering cell phenotype has numerous applications including serving as a critical process parameter within clinical production of regenerative cell therapies. While much work needs to be done to get to this stage, agencies like the United States' Food and Drug Administration (FDA) and the European Medicines Agency's (EMA) desire for critical quality attributes that sustain good manufacturing practices (GMP) during cell manipulation could be aided by novel means of producing more consistent cell phenotypes [36,37].

Cell morphology has been used for decades to qualify changes in phenotype and recently controlling shape and quantifying changes in morphology has been more recently shown to be related to differentiation. With recent advances in imaging and quantifying these morphological changes [13,17,18,38–42], new tools for assessing differentiation have never been more accessible. Stem cells have frequently been shown to elongate as they differentiate into certain lineages [43–48] and controlling stem cells' ability to elongate has been shown to hinder or augment differentiation [3,39,43,45,48–51]. We have demonstrated here that this lengthening process correlates with specific amounts of energy. This may be the very same process that has been partially understood during

varying cyclic loading differentiation protocols in other studies. The ability of a cell to increase in area has also been shown to determine differentiation trajectories [19,51–54]. While this has not been quantified in many differentiation processes, it's clear from the present study that energy can be an additional means of directing this progression. Controlling the area by controlling quantified amounts of input energy could offer new means of controlling and distinguishing stages of differentiation into multiple lineages. Similarly, lamellipodia and filipodia spreading and basic cell curvature can be quantified through terms like circularity and our here introduced "projection factor". Cell protrusions have previously been shown to vastly affect differentiation [3,13,53,54] and we have demonstrated here a way to increase and decrease this cell shape feature and that these changes may follow a linear correlation with the log of the energy used.

There are features of cell phenotype other than morphology, such as specific marker gene expression, that offer additional means of assessing the differentiation process. Accordingly, we tested four genes of interest, of which one, ACTA, is an early marker associated with cell motility, force production structure and integrity [55]. This is likely why it is so closely linked to changes in shape and the input energy. The other genes, TAGLN, CNN, and DES, are more intermediate markers more traditionally associated with the development of the contractile apparatus [55]. These were chosen in this study because elongated MSC shapes generated here through applying energy are associated with increased expression of smooth muscle markers [49,56]. Out of these four genes we tested, only one was as closely associated with energy as cell shape. The linear relationship to the log of the energy we saw in cell shape extended to expression of the ACTA gene. ACTA is an essential marker for differentiation and maintenance of the smooth muscle phenotype [10–13,26,57,58] but it is also present in myofibroblasts and some tumor lines as well [53]. Our results suggest that ACTA expression is an indication that cells are responding to mechanical forces and that they do

so in a predictably re-shaping of their morphology, likely in a logarithmic response to the energy being used to induce the changes. The other genes of interest in this study were mathematically more closely dependent on the shape of the cells and not the energy nor even the stretch parameters. This suggested that the expression of certain genes is closely related to energy but other genes require additional stimuli to upregulate their expression. Another independent study found supporting results when the authors demonstrated that cells spreading over larger areas acted as a primer to allow other morphological and biochemical changes but an additional stimulus (transforming growth factor beta) was necessary to induce a mature phenotype [7]. Thus, changing the area was necessary but insufficient to induce a mature phenotype. The current study found that input energy determines shape but it is ultimately the shape which best relates to phenotype. To follow this train of thought, we analyzed the data through partial least squared analysis with the goal to find the fundamental relationships between mechanical parameters, shape factors, and gene expression, as this analysis method accounts for multicollinearity among energy and energy-induced phenotypical parameters. This analysis uncovered that while energy was a predictor of cell shape, the expression of more mature genotypes is likely more closely related to the processes that occur after achieving a specific shape. Follow up studies with other genes outside the smooth muscle lineage would also serve as useful markers to establish the relationship between differentiation toward SMCs. Specifically, osteogenic markers like RUNX2 and ALP, adipogenic markers like leptin and PPARγ, and chondrogenic markers like Col II, would be particularly helpful to distinguish if the MSCs are moving toward an SMC lineage and away from other mesenchymal lineages.

In this study, we did not examine protein expression or cellular function (protein secretion, matrix deposition, and contraction in contractile lineages). This would be important for verifying

93

energy to be a distinguishing factor for differentiation but the present study undertook an important step into this direction by suggesting that cell phenotype in many ways acts like a state function of input energy. Future studies could incorporate other aspects of phenotype into their analyses as well as alternate modalities for biomechanical stimulation like bi-axial and radial tension, or possibly even compression and shear. It would also be interesting to use alternative cell lineages to examine their responses to different levels of energy. In this study we found that multiple aspects of cell phenotype responded similarly to equal amounts of energy even when applied via different combinations of input parameters. The response correlated to energy with defined patterns and even direct correlations were not directly associated with the input energy, they were indirectly achievable through association with cell shape. Being able to manipulate cell phenotype through general principles like energy input will not only improve our understanding of how to design or engineer cell-instructive constructs, it will contribute to our understanding of mechanobiology and how to resolve differences in studies that use combinations of different parameters for mechanical stimulation.

3.5 - References

1. Koç ON, Lazarus HM. Mesenchymal stem cells: Heading into the clinic. *Bone Marrow Transplant*. 2001;27(3):235-239. doi:10.1038/sj.bmt.1702791.

2. Shyu K-G. Cellular and molecular effects of mechanical stretch on vascular cells and cardiac myocytes. *Clin Sci*. 2009;116(5):377-389. doi:10.1042/CS20080163.

3. Kilian K a, Bugarija B, Lahn BT, Mrksich M. Geometric cues for directing the differentiation of mesenchymal stem cells. *Proc Natl Acad Sci U S A*. 2010;107:4872-4877. doi:10.1073/pnas.0903269107.

4. Dumas V, Ducharne B, Perrier A, et al. Extracellular matrix produced by osteoblasts cultured under low-magnitude, high-frequency stimulation is favourable to osteogenic differentiation of mesenchymal stem cells. *Calcif Tissue Int*. 2010;87(4):351-364. doi:10.1007/s00223-010-9394-8.

5.   Kavlock KD, Goldstein AS. Effect of Pulse Frequency on the Osteogenic Differentiation of Mesenchymal Stem Cells in a Pulsatile Perfusion Bioreactor. *J Biomech Eng*. 2011;133(9):091005. doi:10.1115/1.4004919.

6.   Pilz GA, Ulrich C, Ruh M, et al. Human Term Placenta-Derived Mesenchymal Stromal Cells Are Less Prone to Osteogenic Differentiation Than Bone Marrow-Derived Mesenchymal Stromal Cells. *Stem Cells Dev*. 2011;20(4).

7.   Gao L, Mcbeath R, Chen CS. Stem Cell Shape Regulates a Chondrogenic versus Myogenic Fate through Rac1 and N-cadherin. *Stem Cells*. 2010;28(3):564-572. doi:10.1002/stem.308.Stem.

8.   Jeong JY, Park SH, Shin JW, Kang YG, Han KH, Shin JW. Effects of intermittent hydrostatic pressure magnitude on the chondrogenesis of MSCs without biochemical agents under 3D co-culture. *J Mater Sci Mater Med*. 2012;23(11):2773-2781. doi:10.1007/s10856-012-4718-z.

9.   Khayat G, Rosenzweig DH, Quinn TM. Low frequency mechanical stimulation inhibits adipogenic differentiation of C3H10T1/2 mesenchymal stem cells. *Differentiation*. 2012;83(4):179-184. doi:10.1016/j.diff.2011.12.004.

10.   Ghazanfari S, Tafazzoli-Shadpour M, Shokrgozar MA. Effects of cyclic stretch on proliferation of mesenchymal stem cells and their differentiation to smooth muscle cells. *Biochem Biophys Res Commun*. 2009;388(3):601-605. doi:10.1016/j.bbrc.2009.08.072.

11.   Brun J, Lutz KA, Neumayer KMH, et al. Smooth Muscle-Like Cells Generated from Human Mesenchymal Stromal Cells Display Marker Gene Expression and Electrophysiological Competence Comparable to Bladder Smooth Muscle Cells. *PLoS One*. 2015:1-21. doi:10.1371/journal.pone.0145153.

12.   Rothdiener M, Hegemann M, Uynuk-Ool T, et al. Stretching human mesenchymal stromal cells on stiffness-customized collagen type I generates a smooth muscle marker profile without growth factor addition. *Sci Rep*. 2016;6(October):35840. doi:10.1038/srep35840.

13.   Uynuk-Ool T, Rothdiener M, Walters B, et al. The geometrical shape of mesenchymal stromal cells measured by quantitative shape descriptors is determined by the stiffness of the biomaterial and by cyclic tensile forces. *J Tissue Eng Regen Med*. 2017;11(12):3508-3522. doi:10.1002/term.2263.

14.   Song S, Song S, Zhang H, Cuevas J, Sanchez-Ramos J. Comparison of neuron-like cells derived from bone marrow stem cells to those differentiated from adult brain neural stem cells. *Stem Cells Dev*. 2007;16(5):747-756. doi:10.1089/scd.2007.0027.

15.   Caplan AI. Adult mesenchymal stem cells for tissue engineering versus regenerative medicine. *J Cell Physiol*. 2007;213(2):341-347. doi:10.1002/jcp.21200.

16.   Bianco P, Cao X, Frenette PS, et al. The meaning, the sense and the significance: Translating the science of mesenchymal stem cells into medicine. *Nat Med*. 2013;19(1):35-42. doi:10.1038/nm.3028.

17. Matsuoka F, Takeuchi I, Agata H, et al. Morphology-Based Prediction of Osteogenic Differentiation Potential of Human Mesenchymal Stem Cells. *PLoS One*. 2013;8(2). doi:10.1371/journal.pone.0055082.

18. Matsuoka F, Takeuchi I, Agata H, et al. Characterization of time-course morphological features for efficient prediction of osteogenic potential in human mesenchymal stem cells. *Biotechnol Bioeng*. 2014;111(7):1430-1439. doi:10.1002/bit.25189.

19. McBeath R, Pirone DM, Nelson CM, Bhadriraju K, Chen CS. Cell shape, cytoskeletal tension, and RhoA regulate stem cell lineage commitment. *Dev Cell*. 2004;6(4):483-495. http://www.ncbi.nlm.nih.gov/pubmed/15068789.

20. Fu J, Wang Y-K, Yang MT, et al. Mechanical regulation of cell function with geometrically modulated elastomeric substrates. *Nat Methods*. 2010;7(9):733-736. doi:10.1038/nmeth.1487.

21. Heo SJ, Nerurkar NL, Baker BM, Shin JW, Elliott DM, Mauck RL. Fiber stretch and reorientation modulates mesenchymal stem cell morphology and fibrous gene expression on oriented nanofibrous microenvironments. *Ann Biomed Eng*. 2011;39(11):2780-2790. doi:10.1007/s10439-011-0365-7.

22. Paxton JZ, Hagerty P, Andrick JJ, Baar K. Optimizing an Intermittent Stretch Paradigm Using ERK1/2 Phosphorylation Results in Increased Collagen Synthesis in Engineered Ligaments. *Tissue Eng Part A*. 2012;18(3-4):277-284. doi:10.1089/ten.tea.2011.0336.

23. Wu Y, Zhang X, Zhang P, Fang B, Jiang L. Intermittent traction stretch promotes the osteoblastic differentiation of bone mesenchymal stem cells by the ERK1/2-activated Cbfa1 pathway. *Connect Tissue Res*. 2012;53(6):451-459. doi:10.3109/03008207.2012.702815.

24. Morita Y, Watanabe S, Ju Y, Xu B. Determination of optimal cyclic uniaxial stretches for stem cell-to-tenocyte differentiation under a wide range of mechanical stretch conditions by evaluating gene expression and protein synthesis levels. *Acta Bioeng Biomech / Wrocław Univ Technol*. 2013;15(3):71-79. doi:10.5277/abb130309.

25. Friedl G, Schmidt H, Rehak I, Kostner G, Schauenstein K, Windhager R. Undifferentiated human mesenchymal stem cells (hMSCs) are highly sensitive to mechanical strain: transcriptionally controlled early osteo-chondrogenic response in vitro. *Osteoarthr Cartil*. 2007;15(11):1293-1300. doi:10.1016/j.joca.2007.04.002.

26. Park JS, Chu JSF, Cheng C, Chen F, Chen D, Li S. Differential effects of equiaxial and uniaxial strain on mesenchymal stem cells. *Biotechnol Bioeng*. 2004;88(3):359-368. doi:10.1002/bit.20250.

27. Joumaa V, Herzog W. Energy cost of force production is reduced after active stretch in skinned muscle fibres. *J Biomech*. 2013;46(6):1135-1139. doi:10.1016/j.jbiomech.2013.01.008.

28. Jiang L, Yang C, Zhao L, Zheng Q. Stress fiber response to mechanics: a free energy

dependent statistical model. *Soft Matter*. 2014;10(26):4603. doi:10.1039/c3sm52914b.

29. Nagel T, Kelly DJ. Remodelling of collagen fibre transition stretch and angular distribution in soft biological tissues and cell-seeded hydrogels. *Biomech Model Mechanobiol*. 2012;11(3-4):325-339. doi:10.1007/s10237-011-0313-3.

30. Kubow KE, Vukmirovic R, Zhe L, et al. Mechanical forces regulate the interactions of fibronectin and collagen i in extracellular matrix. *Nat Commun*. 2015;6:1-11. doi:10.1038/ncomms9026.

31. Stålhand J, Klarbring A, Holzapfel GA. A mechanochemical 3D continuum model for smooth muscle contraction under finite strains. *J Theor Biol*. 2011;268(1):120-130. doi:10.1016/j.jtbi.2010.10.008.

32. Brodland GW, Veldhuis JH. Assessing the mechanical energy costs of various tissue reshaping mechanisms. *Biomech Model Mechanobiol*. 2012;11(8):1137-1147. doi:10.1007/s10237-012-0411-x.

33. Zhang D, Sun MB, Lee J, Abdeen AA, Kilian KA. Cell shape and the presentation of adhesion ligands guide smooth muscle myogenesis. *J Biomed Mater Res - Part A*. 2016;104(5):1212-1220. doi:10.1002/jbm.a.35661.

34. Pelham R, Wang Y. Cell locomotion and focal adhesions are regulated by substrate flexibility. *Proc Natl Acad Sci*. 1997;94(December):13661-13665.

35. Humphrey JD. An Evaluation of Pseudoelastic Descriptors Used in Arterial Mechanics. *J Biomech Eng*. 1999;121(2):259. doi:10.1115/1.2835113.

36. Sheu J, Klassen H, Bauer G. Cellular manufacturing for clinical applications. *Cell-Based Ther Retin Degener Dis*. 2014;53:178-188. doi:10.1159/000357362.

37. Carpenter MK. *Regulatory Considerations for Pluripotent Stem Cell Therapies*. Vol 230. 1st ed. Elsevier B.V.; 2017. doi:10.1016/bs.pbr.2016.12.008.

38. Meijering E, Dzyubachyk O, Smal I, van Cappellen WA. Tracking in cell and developmental biology. *Semin Cell Dev Biol*. 2009;20(8):894-902. doi:10.1016/j.semcdb.2009.07.004.

39. Tay CY, Yu H, Pal M, et al. Micropatterned matrix directs differentiation of human mesenchymal stem cells towards myocardial lineage. *Exp Cell Res*. 2010;316(7):1159-1168. doi:10.1016/j.yexcr.2010.02.010.

40. Kato R, Matsumoto M, Sasaki H, et al. Parametric analysis of colony morphology of non-labelled live human pluripotent stem cells for cell quality control. *Sci Rep*. 2016;6(June 2015):1-12. doi:10.1038/srep34009.

41. Logan DJ, Shan J, Bhatia SN, Carpenter AE. Quantifying co-cultured cell phenotypes in high-throughput using pixel-based classification. *Methods*. 2016;96:6-11. doi:10.1016/j.ymeth.2015.12.002.

42. Grys BT, Lo DS, Sahin N, et al. Machine learning and computer vision approaches for phenotypic pro ling. 2016;216(1):65-72. doi:10.1083/jcb.201610026.

43. Halayko AJ, Camoretti-Mercado B, Forsythe SM, et al. Divergent differentiation paths in airway smooth muscle culture: induction of functionally contractile myocytes. *Am J Physiol*. 1999;276(1 Pt 1):L197-206. http://ajplung.physiology.org/content/276/1/L197.abstract.

44. Gillette BM, Jensen J a, Tang B, et al. In situ collagen assembly for integrating microfabricated three-dimensional cell-seeded matrices. *Nat Mater*. 2008;7(8):636-640. doi:10.1038/nmat2203.

45. Yin Z, Chen X, Chen JL, et al. The regulation of tendon stem cell differentiation by the alignment of nanofibers. *Biomaterials*. 2010;31(8):2163-2175. doi:10.1016/j.biomaterials.2009.11.083.

46. Li H, Wong YS, Wen F, et al. Human Mesenchymal Stem-Cell Behaviour On Direct Laser Micropatterned Electrospun Scaffolds with Hierarchical Structures. *Macromol Biosci*. 2013;13(3):299-310. doi:10.1002/mabi.201200318.

47. Thavandiran N, Dubois N, Mikryukov A, et al. Design and formulation of functional pluripotent stem cell-derived cardiac microtissues. *Proc Natl Acad Sci U S A*. 2013;110(49):E4698-707. doi:10.1073/pnas.1311120110.

48. Huethorst E, Hortigon M, Zamora-Rodriguez V, et al. Enhanced Human-Induced Pluripotent Stem Cell Derived Cardiomyocyte Maturation Using a Dual Microgradient Substrate. *ACS Biomater Sci Eng*. 2016;2(12):2231-2239. doi:10.1021/acsbiomaterials.6b00426.

49. Yang Y, Relan NK, Przywara D a, Schuger L. Embryonic mesenchymal cells share the potential for smooth muscle differentiation: myogenesis is controlled by the cell's shape. *Development*. 1999;126:3027-3033.

50. Li M, Li X, Meikle MC, Islam I, Cao T. Short Periods of Cyclic Mechanical Strain Enhance Triple-Supplement Directed Osteogenesis and Bone Nodule Formation by Human Embryonic Stem Cells *In Vitro*. *Tissue Eng Part A*. 2013;19(19-20):2130-2137. doi:10.1089/ten.tea.2012.0308.

51. Zhang D, Kilian KA. The effect of mesenchymal stem cell shape on the maintenance of multipotency. *Biomaterials*. 2013;34(16):3962-3969. doi:10.1016/j.biomaterials.2013.02.029.

52. Gao Y, Li W, Pappas D. Recent advances in microfluidic cell separations. *Analyst*. 2013;138(17):4714-4721. doi:10.1039/c3an00315a.

53. Lee J, Abdeen AA, Zhang D, Kilian KA. Directing stem cell fate on hydrogel substrates by controlling cell geometry, matrix mechanics and adhesion ligand composition. *Biomaterials*. 2013;34(33):8140-8148. doi:10.1016/j.biomaterials.2013.07.074.

54. Cameron AR, Frith JE, Gomez GA, Yap AS, Cooper-White JJ. The effect of time-

dependent deformation of viscoelastic hydrogels on myogenic induction and Rac1 activity in mesenchymal stem cells. *Biomaterials*. 2014;35(6):1857-1868. doi:10.1016/j.biomaterials.2013.11.023.

55. Beamish JA, He P, Kottke-Marchant K, Marchant RE. Molecular Regulation of Contractile Smooth Muscle Cell Phenotype: Implications for Vascular Tissue Engineering. *Tissue Eng Part B Rev*. 2010;16(5):467-491. doi:10.1089/ten.teb.2009.0630.

56. Maul TM, Chew DW, Nieponice A, Vorp D a. Mechanical stimuli differentially control stem cell behavior: morphology, proliferation, and differentiation. *Biomech Model Mechanobiol*. 2011;10(6):939-953. doi:10.1007/s10237-010-0285-8.

57. Orlic D, Kajstura J, Chimenti S, Bodine DM, Leri A, Anversa P. Transplanted adult bone marrow cells repair myocardial infarcts in mice. *Ann N Y Acad Sci*. 2001;938:221-230. http://www.ncbi.nlm.nih.gov/entrez/query.fcgi?cmd=Retrieve&db=PubMed&dopt=Citati on&list_uids=11458511.

58. Stegemann JP, Nerem RM. Phenotype modulation in vascular tissue engineering using biochemical and mechanical stimulation. *Ann Biomed Eng*. 2003;31(4):391-402. doi:10.1114/1.1558031.

CHAPTER 4

Adipose Derived Stem Cell Differentiation into Smooth Muscle Cells in Two- and Three-Dimensional Culture

4.1 – Introduction

Despite an ever-growing need for organs, the number of available donors remains relatively stagnant and alternative therapies or replacements are essential for alleviating this need [1]. One promising option is the development of artificial tissues through regenerative medicine. These artificial tissues could also serve as models for development and to test for human tissue's response to pharmaceutical and toxic agents. To produce these constructs, an adequate number of mature, functional cells are required are model or replace the physiological function of the tissue. One promising source of these cells has been mesenchymal stem cells. While bone marrow stem cells (bMSC) are the most well know source of these progenitors, adipose derived stem cells (ASCs) offer another potential supply, with possibly fewer complications. We chose to continue our studies with ASCs for multiple reasons. ASCs are easier to isolate and extraction techniques typically yield more regenerating cells [2]. This would promote more translatable therapies with faster recovery. In addition, mesenchymal stem cells MSCs[3,4] and ASCs [2,5–7] have been shown to both be immunoprivileged and multipotent. ASCs are already being capitalized on in over 120 clinical trials [7]. Their existence and role as adipogenic stem cells was first documented by Halverston et al [8]. In addition to being adipogenic [9–12], ASC are osteogenic [8,10–14], and chondrogenic [10,11,15–18]. Additional work has suggested their ability to differentiate into neurogenic

100

[10,19], skeletal muscle [20], and cardiomyocyte lineages [9]. Interest into their potential to differentiate into smooth muscle lineages [10,21–24] is also gaining traction because of their importance to the cardiovascular system as heart disease continues to be a leading cause of mortality [25].

Methods for inducing differentiation from stem cells are being actively studied and developed. Growth factor treatment [21,26], mechanical stimulation [21,27], and electrical stimulation [24] are all potential means of augmenting the differentiation process. A ubiquitous approach for differentiation into different lineages continues to be dimensionality i.e. culturing stem cells in a three-dimensional environment as opposed to the more traditional two-dimensional culturing conditions [13,28,29]. 3D culturing methods have been shown to enhance differentiation of cardiac myocytes [30–34], hepatocytes [35–37], neurons [38,39], osteocytes [18,40], adipocytes [18,41], and chondrocytes [42]. In vitro amniogenesis requires 3D culture to emulate the process [43]. This may due to the more analogous nature of a 3D in vitro environment to natural tissue [30,44]. 3D culture has been shown to improve the function of somatic cells suspended in 3D when compared to 2D culture [45–48]. Specifically, 3D culture better emulates the response of tumors to chemotherapy [44,49], facilitates cell organization [50,51], and affect cell spreading and morphology [30,46,52,53]. Additional comparisons of 2D and 3D interactions are reviewed in Doyle et al [54].

The 3D environment offers multiple different parameters to optimize for inducing a desired phenotype. Porosity, stiffness, substrate composition, and substrate concentration can all be altered to enhance cellular responses [54–58]. While isolating these parameters independently is possible, most often they work in concert to produce the cell's environment. This manuscript chose to focus on the effects matrix concentration on ASC differentiation. Increasing the matrix concentration typically increases stiffness and ligand density while decreasing porosity [54–56,58]. Subsequently, these factors affect cell migration and spreading [55,57,59] and differentiation [60,61]. Cell spreading and

morphology have been found to be tightly connected to differentiation [62], independently of matrix augmentation. Printing of cell substrate templates has introduced the idea that cell shape can be directly controlled by limiting cell spreading to certain sizes [10,63] or shapes [4,64]. Other studies have simply limited where and how the cells can adhere [65], elongate [66], contract [67] and how much volume they can fill [68]. Regardless of their approach, each study has shown the dependence of phenotype on the shape of the cell. Other groups have used these morphological features to predict future phenotypes and even function [69,70]. Our group has taken this knowledge and approached shape as not only a means of control but as an indication of progress toward a given lineage in response to a stimulus. We have shown that bone marrow derived MSC stretched on 2D collagen substrates undergo a dynamic transition in both morphology and expression as they differentiate toward a smooth muscle lineage [71].

Based on the inherent importance of cell morphology to phenotype, one goal of this study was to examine how ASC shape changes in response to 3D culture and matrix concentration and if our shape analysis could capture these differences. We followed up on this question by comparing how culture format impacts the expression of biochemical markers indicative of SMC differentiation. Collectively, we then asked if the trends described by these culture dimensions and protein concentration were corroborative of trends seen in other work. Based on the literature and our previous work, we expected 3D culture conditions and increased collagen concentration to enhance differentiation which we believed we could capture with our shape and biochemical analysis. Determining how shape changes throughout the differentiation of ASC toward SMC would offer new insight into the development of these cells, as well as open new avenues for regulating differentiation. In addition, distinguishing behavior of ASC cultured in 2D and 3D in

different concentrations would continue to advance the transition toward better physiological models while simultaneously offering new tools in regenerative medicine.

4.2 – Materials and Methods

ASC culture and expansion

Human adipose-derived mesenchymal stem cells (Rooster Bio, Frederick, MD) were expanded in T175 flasks in Alpha Modification Essential Medium (Alpha MEM, Fisher, Rockville, MD) supplemented with 10% qualified fetal bovine serum (FBS; Invitrogen, Carlsbad, CA) and 1% penicillin and streptomyocin (PS; Invitrogen). Cells were kept at 37ºC and 5% CO_2 and their media was changed every three days and passages 5-7 were used for experiments. On day 0, when ready to be used for construct production, cells were washed in PBS and incubated in 0.25% Trypsin (Fisher) at 37ºC for 3-4 minutes to lift cells from the flasks. After cells had lifted, they were counted, centrifuged, and resuspended in Dulbecco's Modified Essential Media (DMEM, Fisher) for use in collagen hydrogels. This DMEM was also supplemented with 10% qualified FBS (Invitrogen) and 1% PS (Invitrogen).

Tissue construct production and culture

Type I collagen (MP Biomedicals, Solon, Ohio) was dissolved in 0.02 N Acetic Acid (Sigma, St. Louis, MO) to a concentrations of 8 mg/mL 4 mg/mL, or 2 mg/mL. Collagen gels were made according to previous studies [56]. Briefly, to make 4 mg/mL, 2 mg/mL, or 1 mg/mL gels, 50% of the final gel volume of 8mg/mL, 4 mg/mL, or 2mg/mL were added respectively to different tubes. To each tube, a volume of 5X DMEM (Fisher) equal to 20% of the final gel, 0.01 N NaOH (Sigma) equal to 10% of the final volume, Fetal Bovine Serum (Fisher) equal to 10% of the final

103

volume, and 1x DMEM (Fisher) equal to 10% of the final volume were mixed together and allowed to set at 37ºC. For 2D gels, the mixture was incubated without cells in the mixture and, once solid, set gels were covered with cells suspended in media. For 3D gels, the media contained cells and was mixed homogenously into the gel mixture before setting. For 3D gels, a concentration of 500k cells/mL was used. Using this ratio, the volume of gel per cell was calculated (2e-6 cm^3) and subsequently the radius of the volume each cell was allotted (7.8e-3 cm). Using this radius, an area for each cell was calculated (1.8 cm^2) and converted into a ratio of cells/area (5400 cells/cm^2). For this study that seeding density was rounded to 5000 cells/cm^2. While this was a lower concentration than previous 2D studies, similar seeding densities have been used by other groups including our past studies. Higher 2D seeding densities would require higher 3D seeding densities as well and higher concentrations of ASCs in 3D gels caused gel compaction that reduced the ability to image cells. After setting, 1 mL of media was added to each gel (the 2D samples were seeded during this step) and the constructs were incubated at 37ºC until a media change (DMEM with supplements described earlier) on D3. On D4 samples were collected and analyzed. The remainder of the gels had their media changed again on D6 and were collected for analysis on D7.

Fluorescence microscopy for cell shape

The ASC-seeded constructs were collected and stained on either D4 or D7 using Calcein (1:1000, Lifetech/Fisher) and diamidino-2-phenylindole (DAPI, 1:1000, Lifetech, Fisher) based on our previous work (Rothdiener 2016, Uynuk-Ool 2017). ASCs embedded in or on top of collagen gels were imaged using an Olympus IX15 Microscope system (Olympus America, Center Valley, PA). Calcein-stained ASC morphology was detected using the green filter and the nuclei were imaged using a blue filter. The individual shapes of large quantities of ASCs were measured

simultaneously through 2D projections of fluorescence with an ImageJ macro (National Institute of Health, Bethesda, MD), according to [71]. The following six mathematical shape descriptors were quantified for each MSC: length (major axis), area, circularity (4*π(area/perimeter^2), projection factor (perimeter^2/area), roundness (4*area/(π*major axis length^2)), and aspect ratio (major axis angle/minor axis). These measurements from each cell were averaged and used to compare different culturing conditions.

Compaction of 3D Constructs

Before collection of samples for analysis on D4 and D7, images were taken of each gel using a bright field microscope (Olympus). In ImageJ (NIH) the long and short access of each sample were measured and approximated as an ellipse. The areas of the resulting ellipses were normalized to their initial area of the gels, essentially the area of the well. These areas were used to compare the functional compaction of the gels as cells began differentiating and generating forces.

Quantitative RT-PCR of cells in constructs

Constructs were collected on D4 and D7 and frozen at -80°C until processing. To process, Trizol (Fisher Scientific) was added to each sample and subsequently mechanically broken up using a S-250 Digital Sonifier (Branson Ultrasonics, Danbury, CT) set at 10% for 30 seconds. Samples were incubated at room temperature in chloroform (Sigma) for 3 minutes then centrifuged at 12000 x g and 4 °C for 15 minutes. The clear aqueous phase of each sample was mixed isopropanol (Sigma), incubated, and centrifuged for 10 minutes at 12000 x g and 4 °C. Pellets were resuspended in 75% ethanol and centrifuged again a 7,500 g for 5 minutes at 4°C. Supernatant was discarded and samples were air dried before being resuspended in RNase free water. Next, RNA

samples were incubated at 60ºC for 15 minutes and stored at -80ºC until use. cDNA was synthesized using 2 µL of RNA solution and Superscript III Synthesis System (Life Technology, Fisher) according to the manufacturer's protocol. A C100 Thermocycler (Bio-Rad, Hercules California) was to regulate temperature. Using SYBER GREEN PCR Mastermix (Life Technologies, Fisher) and an Applied Biosystems 7500 Fast PCR system, the cDNA was amplified. The cyclic threshold of peptidylproplyl isomerase A (PPIA), was used as a house keeping gene (Ct_{hk}) to calculate the relative expression of experimental samples' expression of target genes, smooth muscle actin (ACTA), transgelin (TGLN), smooth muscle myosin heavy chain (MHC), and caldesmin (CLDM). Melt curves were also examined to determine if dimerization contamination affected threshold values. If there were large degrees of dimer contamination according to the melt curve, these samples were excluded from analysis. Experimental thresholds were compared to negative controls, ASC expanded and cultured on plastic expansion flasks, using the $\Delta\Delta Ct$ method. Expression levels were calculated assuming expression followed $x=2^{-\Delta\Delta Ct}$ where $\Delta\Delta Ct = \Delta Ct_{exp} - \Delta Ct_{negative\ control}$ and $\Delta Ct = Ct_{target\ gene} - Ct_{hk}$. The forward and reverse primers were as follows; PPIA Forward Sequence: ACG TGG TAT AAA AGG GGC GG and Reverse Sequence: GTC TGC AAA CAG CTC AAA GGA G, ACTA Forward Sequence: TTG CCT GAT GGG CAA GTG AT and Reverse Sequence TAC ATA GTG CCC CCT GA, TGLN Forward Sequence: AAC AGC CTG TAC CCT GAT GG and Reverse Sequence: CGG TAG TGC CCA TCA TTC TT, MHC Forward Sequence: TGC TTT CGC TCG TCT TCC and Reverse Sequence: CGG CAA CTC GTG TCC AAC, and CLDM Forward Sequence: AGA TTG AAA GGC GAA GAG CA and Reverse Sequence: TTC AAG CCA GCA GTT TCC TT.

Immunocytochemistry and analysis of samples

Constructs were collected on D4 and D7, washed 2x with PBS, and fixed with Z-fix (Anatech, Battle Creek, MI) for 10 minutes at 4ºC. Samples were washed 2x with PBS and permeabilized with 0.5% Triton X-100 (Sigma) for 20 minutes at room temperature. All samples were washed 2x more in PBS and kept at 4ºC until staining. When staining, primary antibodies against smooth muscle actin (SMA, Millipore: ABT1487, Burlington, MA), transgelin protein (SM22, Santa Cruz: 50446, Dallas, TX), and smooth muscle myosin heavy chain (MHC, Millipore: MAB3568) we dissolved in 10 mg Bovine Serum Albumin (BSA). Samples were incubated at room temperature in primaries for 2 hours at 1:200, 1:50, and 1:50 for anti-SMA, anti-SM22, and anti-MHC respectively. Sample were washed 2x in PBS and incubated in secondary for 1 hour at room temperature. 488 Alex Fluor anti-rabbit (1:200, ThermoFisher, A-11070) or 488 Alexa Fluor anti-mouse (1:250, ThermoFisher, A-11001) were used for secondaries on SMA and SM22 or MHC respectively. DAPI (1:1000, Lifetech) was added to secondary stain as well. Secondaries and DAPI were washed off 2x with PBS in low light settings. Images were stored at 4ºC until imaging. Imaging was done on a Nikon A-1 Spectral Confocal Microscope (Melville, NY) maintaining exposure levels across all samples when imaging specific proteins. Analysis of images were carried out in ImageJ. Pixel intensities were summed across an image to obtain a "raw integrated intensity" value for each image. This value was normalized to the number of nuclei in the image to account for regional differences in the number of cells.

Statistical analysis

All data for bar graphs were plotted and statistically analyzed in R. ANOVA and Dunn's Method were used for post-hoc analyses to compare individual groups. If no significant differences were present, an asterisk and "NS" are noted in the top right corner. Differences between samples cultured at the same concentration but in different dimensions were compared as well as samples

cultured within the same dimension (ex. 2D) were also compared but statistics between samples that were cultured in different dimensions and at different concentrations are not indicated (2D at 1 mg may have been statistically different than 3D at 4 mg but it is not indicated). Statistical differences between samples at the same concentration but cultured in different dimensions are indicated by a colored letter above the bars (a blue 'a', a red 'b', and or a green 'c; indicate that there were differences between culturing dimensions in 1 mg/mL, 2 mg/mL, and 4 mg/mL respectively. Within the same dimensions of culturing, statistical differences between all concentrations within either 2D and 3D independently and indicated with a bar above the respective pair of concentrations. All error bars are plus/minus the standard error of the mean.

4.3 – Results

Cell Shape

ASCs were seeded either on-top-of or inside collagen hydrogels made of three different collagen concentrations (Fig 4.1). At times points of either 4 or 7 days, the samples were stained with Calcein, a dye that permeates the membrane of live cells, and fluoresces to illuminate the volume of the cell. 2D image projections of the stained cultures were used to visualize the shape of the cells (Fig 4.2). Differences in cell proliferation were not measured and cannot be extrapolated from image data. Differences in morphology between different concentrations and culture dimensions were subtle and aside from some general claims about length, needed the image analysis technique to describe differences between culturing conditions.
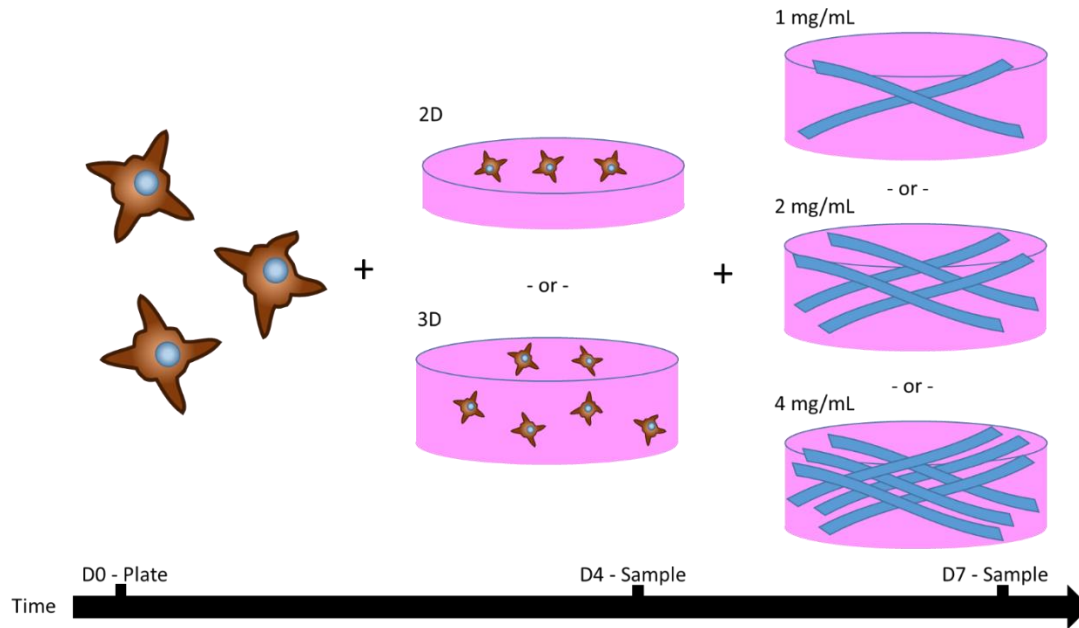
Figure 4.1: Methods. Adipose derived stem cells (ASC) were expanded and then seeded either inside or on-top-of collagen hydrogels. The hydrogels were made of type I collagen at concentrations of 1mg/mL, 2mg/mL, or 4mg/mL. The constructs were produced on day 0 and cultured for up to one week. Samples were collected and analyzed on either day 4 or day 7.
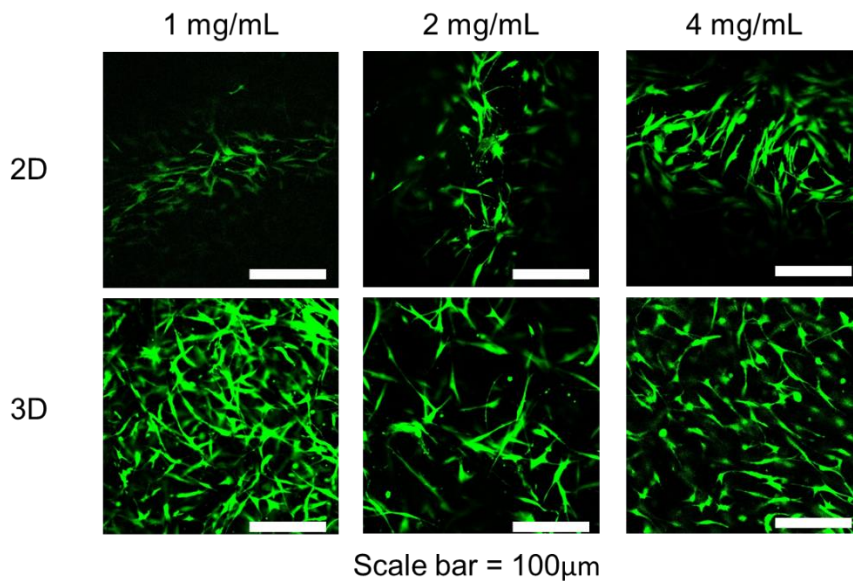
Figure 4.2: Morphology of ASC cultured either in or on top of different concentrations of collagen. ASC were cultured either on-top-of or inside collagen gels. Once collected, they were stained with Calcein and imaged with wide-field fluorescent microscopy to get projections of cell morphology. On D7 there appeared to be more cells in 3D that were shorter and broader. The cells in higher concentrations also appeared to have the most traditional shape commonly recognized as being smooth muscle-like. Scale bar represents 100 µm.

109

ASC Size in Different Dimensions and Concentrations of Collagen

Regardless of time point or concentration, cells cultured in 2D were significantly longer than their counterparts cultured in 3D (Fig 4.3A and 4.3B, $p<0.05$). In 2D, cell length increased with concentration and 4 mg/mL samples were significantly longer than those cultured in lower concentrations regardless of day (Fig 4.3A and 4.3B, $p<0.05$). In 3D, concentration seemed to have no impact on length except at D7 where cells cultured in 4mg/mL 3D gels were shorter than cells cultured in 1mg/mL (Fig 4.3B, $p<0.05$). Cells cultured in 2D also had larger areas than their 3D counterparts regardless of concentration or time points (Fig 4.3C and 4.3D, $p<0.05$). After 4 days, cells cultured on 4 mg/mL gels were larger in area than those cultured on 1 mg/mL but cells cultured on 2mg/mL gels had the smallest area of the three (Fig 4.3C, $p<0.05$). By D7, all gels in 2D had statistically similar areas (Fig 4.3D). In 3D on D4, collagen concentration initially had an inverse relationship with area, cells with higher protein concentrations were smaller in area (Fig 4.3C, $p<0.05$) but by D7, cells cultured in 2 mg/mL gels had the largest area of the 3D samples (Fig 4.3D, $p<0.05$). In general, 2D culture produced longer cells with larger area but while collagen concentration seemed to correlate with size in 2D, in 3D there is no effect at all.

A Length of Cells (D4)

B Length of Cells (D7)

C Area (D4)

D Area (D7)

E

Days of culture	4						7					
Dimensions of Culture	2D			3D			2D			3D		
Collagen Concentration (mg/mL)	1	2	4	1	2	4	1	2	4	1	2	4
Number of Biological Replicates	8						7					
Cells	1970	1325	2056	2128	1859	2323	2161	2698	2056	1983	2353	2159

Figure 4.3: The Size of Cells Cultured in Different Dimensions and Concentrations of Collagen. Cells cultured in 3D were significantly shorter than their counterparts cultured in 2D regardless of concentration or day (A and B, $p<0.05$). In 2D, cells cultured on 4 mg/mL were significantly longer than those cultured in lower concentrations, regardless of day (A and B, $p<0.05$). At D7, the cells cultured in 4mg/mL 3D gels were significantly shorter than cells cultured in 1mg/mL (B, $p<0.05$). Cells cultured in 2D also had larger areas than their 3D counterparts at every concentration and at both time points (C and D, $p<0.05$). After 4 days of culture, cells cultured on 4 mg/mL gels were larger in area than those cultured on 1 mg/mL and cells cultured on 2mg/mL gels were the smallest in area (C, $p<0.05$). At D7, all gels in 2D were statistically similar in area. In 3D, concentration initially (D4) had an inverse correlation with area and cells with progressively higher protein concentrations were smaller in area (C, $p<0.05$), By D7, cells cultured in 2 mg/mL gels had the largest area of the 3D samples (D, $p<0.05$). Blue bars represent gels with 1 mg/mL of collagen, red bars represent gels with 2 mg/mL of collagen, and green bars represent gels with 4 mg/mL of collagen. Lines ending above conditions indicate statistical differences between gels with different concentrations of collagen and colored letters above gels indicate significant differences between gels of the same concentrations but different culture dimensions ($p<0.05$). The number of biological replicates and cells analyzed from all replicates in each condition are displayed in panel E.

111

ASC Polarization in Different Dimensions and Concentrations of Collagen

All samples in 3D conditions were rounder than their 2D counterparts (Fig 4.4A and 4.4B, $p<0.05$), with the exception of samples in 1 mg/mL of collagen on D7. In 2D, roundness tended to decrease with increasing collagen concentration (Fig 4.4A and 4.4B, $p<0.05$). In 3D, cells in 1 mg/mL were statistically more round than other concentrations on D4 before becoming significantly less round than other conditions on D7 (Fig 4.4A and 4.4B, $p<0.05$). Samples in 2D had significantly larger aspect ratios than their 3D counterparts regardless of time point or concentration (Fig 4.4C and 4.4D, $p<0.05$). On D4, samples at 1mg/mL had significantly lower aspect ratios than the other two concentrations regardless of being in 2D or 3D (Fig 4.4C, $p<0.05$). On D4, 2 mg/mL in 2D also had lower aspect ratio than 4 mg/mL (Fig 4.4C, $p<0.05$). On D7, 4mg/mL samples had the largest aspect ratios in 2D and the smallest aspect ratios in 3D (Fig 4.4D, $p<0.05$). In 3D, cells in 1mg/mL had larger aspect ratios than cells from higher concentrations (Fig 4.4D, $p<0.05$). Together, 2D culture conditions tended to produce more polarized cells and higher concentrations increased this effect but in 3D, the lowest concentration had the highest aspect ratio by D7.

Figure 4.4: The Polarization of Cells Cultured in Different Dimensions and Concentrations of Collagen. Except for the 1 mg samples on D7, all other cells from 3D samples were statistically rounder than their 2D counterparts regardless of concentration (A and B, p<0.05). In 2D samples, samples on 4 mg/mL were always the least round and the cells on 2mg/mL were also less round than 1mg/mL at D4 (A and B, p<0.05). In 3D, cells in 1 mg/mL were statistically more round on D4 before becoming significantly less round on D7 (A and B, p<0.05). Samples in 2D had significantly larger aspect ratios than their 3D counterparts regardless of time point or concentration (C and D, p<0.05). On D4, samples at 1mg/mL had significantly lower aspect ratios than the other two concentrations regardless of being in 2D or 3D. In 2D, samples from 2 mg/mL also had lower aspect ratios than 4 mg/mL (C, p<0.05). On D7, 4mg/mL samples had the largest aspect ratios in 2D and the smallest aspect ratios in 3D. In 3D, cells in 1mg/mL had the largest aspect ratio (D, p<0.05). Blue bars represent gels with 1 mg/mL of collagen, red bars represent gels with 2 mg/mL of collagen, and green bars represent gels with 4 mg/mL of collagen. Lines ending above conditions indicate statistical differences between gels with different concentrations of collagen and colored letters above gels indicate significant differences between gels of the same concentrations but different culture dimensions (p<0.05). The number of biological replicates and cells analyzed from all replicates in each condition are displayed in panel E.

113

ASC Spreading in Different Dimensions and Concentrations of Collagen

Cells on 2D were generally more circular than their 3D counterparts (FIG 4.5A and 4.5B, $p<0.05$). When considering only 2D culture, cells were less circular with increasing concentration but in 3D, this was not the case and was inverted on D4 (FIG 4.5A and 4.5B, $p<0.05$). The projection factor of the cells in 3D were typically higher in 3D compared to 2D, except 4mg/mL where 2D produced higher projection factors (Fig 4.5C and 4.5D, $p<0.05$). In 2D, 1 mg/mL consistently has the lowest projection factor (Fig 4.5C and 4.5D, $p<0.05$). In 2D, at D4, 2 mg/mL had the highest projection factor but by D7, 4 mg/mL had surpassed it (Fig 4.5C and 4.5D, $p<0.05$). In 3D, 4 mg/mL consistently had the lowest projection factor (Fig 4.5C and 4.5D, $p<0.05$) but while 1 mg/mL and 2 mg/mL had similar projection factors on D4 in 3D, 2 mg/mL had significantly higher values on D7 (Fig 4.5C and 4.5D, $p<0.05$). Taken as a whole, 3D promoted more spreading but while higher concentrations increased spreading in 2D, it inhibited it in 3D.

Days of culture	4						7					
Dimensions of Culture	2D			3D			2D			3D		
Collagen Concentration (mg/mL)	1	2	4	1	2	4	1	2	4	1	2	4
Number of Biological Replicates	8						7					
Cells	1970	1325	2056	2128	1859	2323	2161	2698	2056	1983	2353	2159
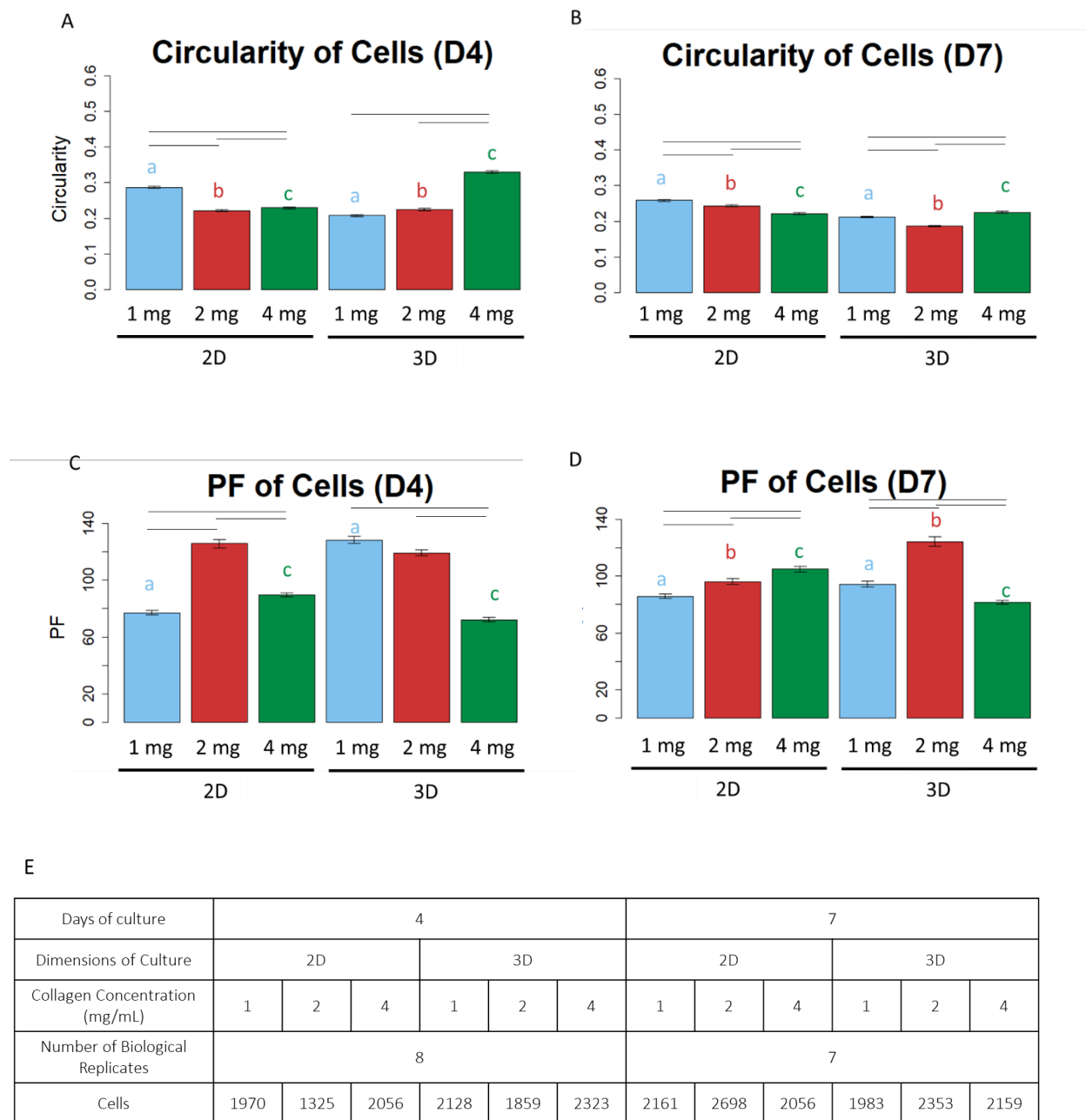
Figure 4.5: The Spreading of Cells Cultured in Different Dimensions and Concentrations of Collagen. Cells at 1 mg/mL and 2 mg/mL were significantly more circular than their 3D counterparts on D4 and D7 but cells at 4mg/mL exhibited the opposite trend (A and B, $p<0.05$). In 2D, cells were less circular with increasing concentration but in 3D cells at 4mg/mL were the most circular at D4 and D7 but cells in 1 mg/mL were more circular than at 2 mg/mL on D7 (A and B, $p<0.05$). The projection factor (PF), a ratio of the perimeter squared to the area of the cells, was significantly lower in 4 mg/mL of 3D gels compared to 2D and in 1 mg/mL they were significantly higher in 3D than in 2D on both days, while in 2 mg/mL they were significantly higher in 3D only after D7 (C and D, $p<0.05$). In 2D, 1 mg/mL consistently has the lowest projection factor (C and D, $p<0.05$). In 2D, at D4, 2 mg/mL had the highest projection factor but by D7, 4 mg/mL had surpassed it (C and D, $p<0.05$). In 3D, 4 mg/mL consistently had the lowest projection factor (C and D, $p<0.05$) and while 1 mg/mL initially had the highest on D4 (C, $p<0.05$), it was surpassed by 2 mg/mL on D7 (D, $p<0.05$). Blue bars represent gels with 1 mg/mL of collagen, red bars represent gels with 2 mg/mL of collagen, and green bars represent gels with 4 mg/mL of collagen. Lines ending above conditions indicate statistical differences between gels with different concentrations of collagen and colored letters above gels indicate significant differences between gels of the same concentrations but different culture dimensions ($p<0.05$). The number of biological replicates and cells analyzed from all replicates in each condition are displayed in panel E.

Construct Compaction

As cells become more mechanically active, they begin pulling on the surrounding matrix. This results in an overall decrease in volume of the hydrogels as the gels compact. 2D constructs did not exhibit this behavior but in 3D, on D4, the degree of compaction was inversely related to the concentration of collagen in the original hydrogels (FIG 5.6, $p<0.05$). By D7, they all had statitistically similar areas (Fig 5.6).

Days of culture	4		7	
Dimensions of Culture	2D	3D	2D	3D
Biological Replicates	9		6	
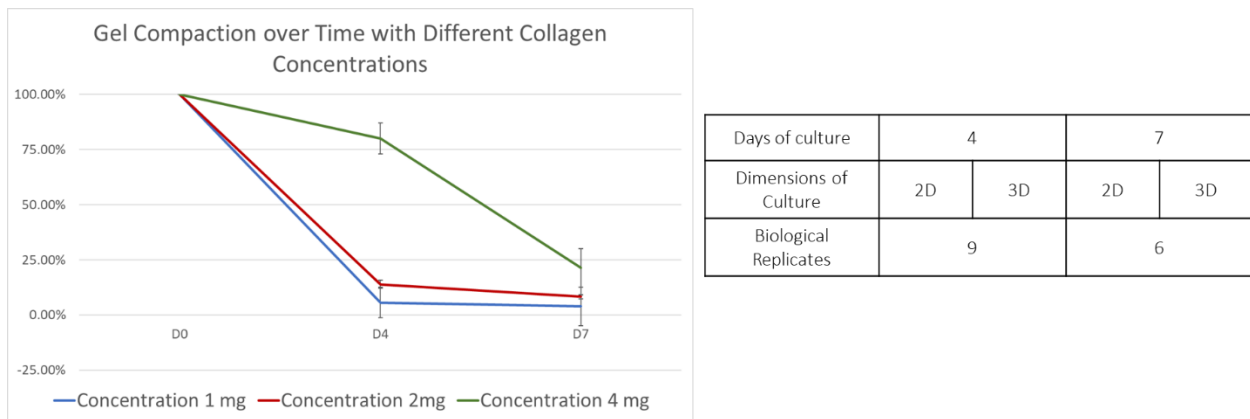
Figure 4.6: Compaction of Gels with Different Concentrations of Collagen. At D4, the amount of construct compaction was inversely related to collagen concentration. By D7, all gels had compacted similarly. The Blue line represents control gels with 1 mg/mL of collagen, the red line represents gels with 2 mg/mL of collagen, and the green line represents gels with 4 mg/mL of collagen. The table displays the number of samples measured from each condition at each time point.

Protein Expression

Samples were stained against three SMC proteins, SMA (Fig 4.7A), transgelin protein (SM22, Fig 4.7B), and smooth muscle myosin heavy chain (MHC, Fig 4.7C). These proteins were chosen as indicators of early, intermediate, and late differentiation, respectively. SMA and MHC are particularly inportant for force production while trangelin modulates the contractile aparatus. On D4, 3D gels with 2 mg/mL and 4 mg/mL had higher SMA expression than their 2D counterparts (Fig 4.8A, $p<0.05$) but by D7, only 2mg/mL 3D samples still had more SMA protein than their

respective 2D samples (Fig 4.8B, $p<0.05$). 3D samples of 2 mg/mL and 4 mg/mL in were higher than 1 mg/mL on D4 (Fig 4.8A, $p<0.05$) and, on the same day, 2 mg/mL in 2D also had more SMA than the 1 mg/mL condition (Fig 4.8A, $p<0.05$). There were no significant differences between transgelin protein of any conditions (Fig 4.8C and 4.8D). 3D samples of 2mg/mL had more MHC protein on D4 and D7 (Fig 4.8E and 4.8F, $p<0.05$) as did 4 mg/mL on D7 (Fig 4.8F, $p<0.05$). Samples on 2D, 1 mg/mL gels had significantly more MHC protein than its 3D counterpart on both days (Fig 4.8E and 4.8F, $p<0.05$). On D4 and D7, 3D samples of 2mg/mL and 4 mg/mL had more MHC protein expression than 1 mg/mL samples (Fig 4.8E and 4.8F, $p<0.05$). On D7 in 2D, 1 mg/mL samples had more MHC protein than both 2 mg/mL and 4 mg/mL (Fig 4.8F, $p<0.05$). As a whole, 3D samples had more protein than 2D samples and while collagen concentration didn't really affect 2D samples, 2 mg/mL and 4 mg/mL induced more expression in 3D.
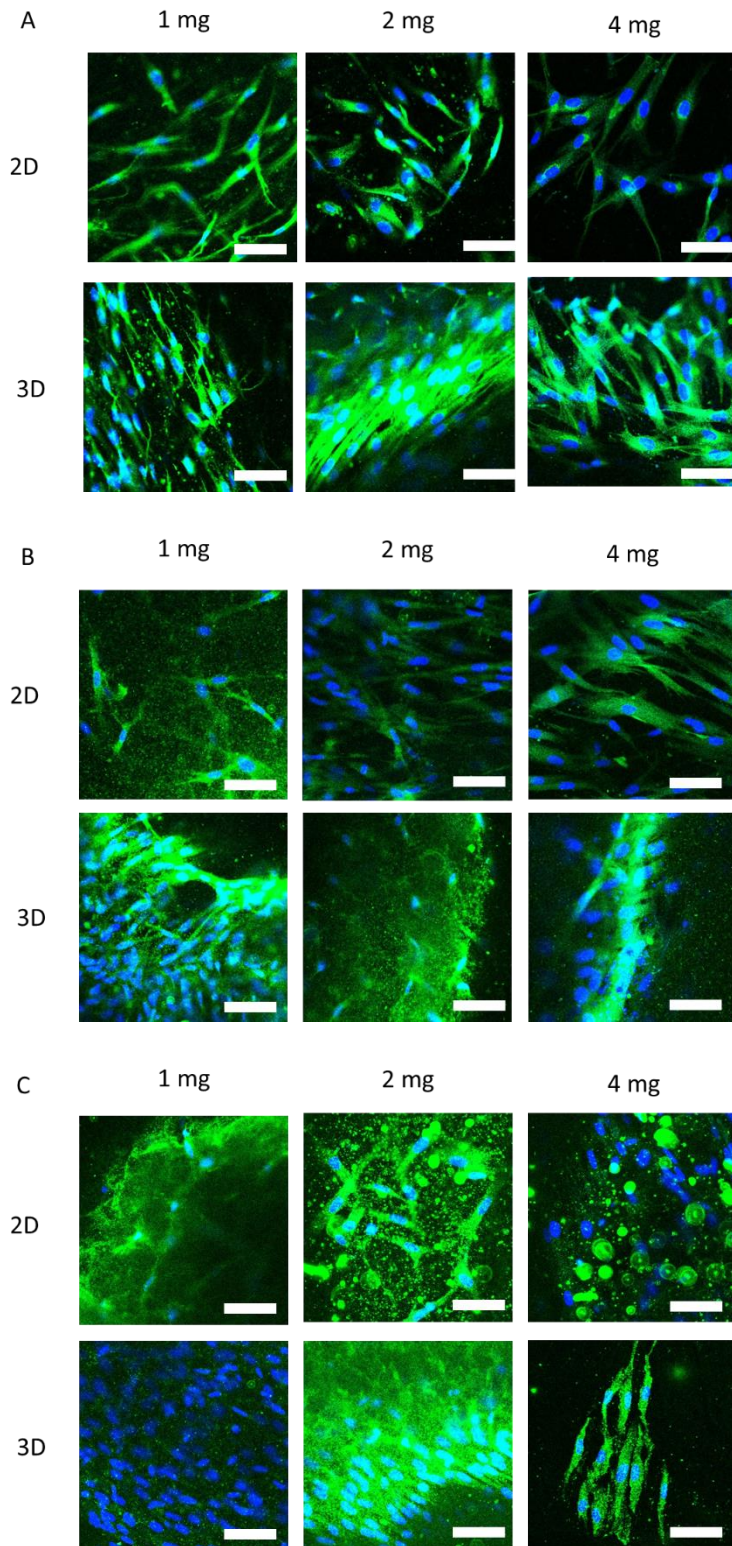
Figure 4.7: SMC Protein Expression of ASC from Gels Cultured in Different Dimensions and Concentrations of Collagen.
ASCs were cultured in either 2D or 3D collagen gels and stained on D7 for smooth muscle actin (SMA, A), transgelin protein (TGLN or SM22, B), or smooth muscle myosin heavy chain protein (MHC, C) (all green). Nuclei were stained with DAPI (blue). Scale bars represent 50 μm.
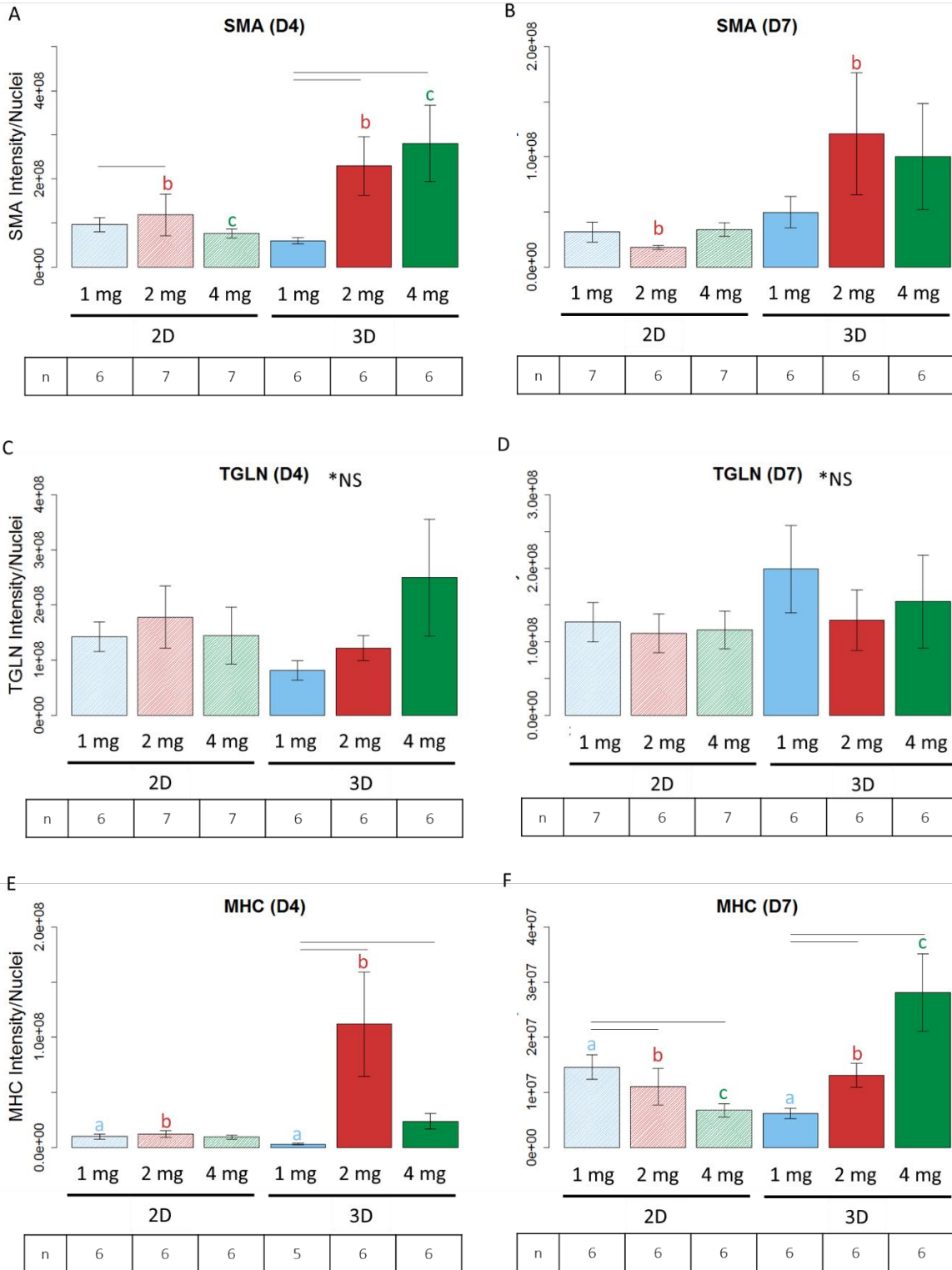
Figure 4.8: Protein Expression of ASC from Gels Cultured in Different Dimensions and Concentrations of Collagen. On D4, 3D gels with 2 mg/mL and 4 mg/mL had higher SMA expression than their 2D counterparts (A, p<0.05). 2 mg/mL in 2D was still higher than 1 mg/mL on D4 (A, p<0.05). 2 mg/mL in 3D continued to have more SMA than its 2D analog into D7 (B, p<0.05). There were no significant differences between TGLN protein (SM22) in of any conditions (C and D). On D4, 3D samples of 2mg/mL had more MHC protein expression than its 2D counterpart while 2D samples of 1 mg/mL had more MHC

protein expression than its 3D samples (E, p<0.05). On D4 in 3D, both 2 mg/mL and 4 mg/mL had more MHC protein expression than 1 mg/mL (E, p<0.05). On D7, 3D samples of 2 mg/mL and 4 mg/mL had more MHC protein expression than their 2D counterparts but for 1 mg/mL, 2D culture resulted in more MHC protein (F, p<0.05). At this time point in 2D, 1 mg/mL MHC protein expression was larger than higher concentrations, but in 3D, 1 mg/mL MHC protein was actually lower than that of samples at higher concentrations (F, p<0.05). Blue bars represent gels with 1 mg/mL of collagen, red bars represent gels with 2 mg/mL of collagen, and green bars represent gels with 4 mg/mL of collagen. Lighter bars with striated pattern represent 2D samples and solid bars with darker tones represent 3D samples. Lines ending above conditions indicate statistical differences between gels with different concentrations of collagen and colored letters above gels indicate significant differences between gels of the same concentrations but different culture dimensions (p<0.05). The number of biological replicates and cells analyzed from all replicates in each condition are displayed below each panel.

Theoretical Shape

Recognizing that differences between 2D and 3D suggested increased SMC protein in 3D, limitations in our shape analysis were further considered. While cultured in 2D, cells will generally be in the plane of the image. In 3D, this is not always the case. Our results would indicate that cells are oriented isotropically in the plane (data not shown) and we would expect that random orientation to extend into the Z direction (out of the image plane) in 3D. This would imply that our projected images are underrepresenting the length of cells. To accommodate that, we artificially scaled the panel of shape factors to consider the effects of this limitation.

To account for underestimation in length, we multiplied the values of the 3D values by the square root of 2. Assuming all cells are oriented isotropically, the average cell would have an orientation of 45° in all planes. That would mean to correct it, the value would need to be divided by the cos(45°) or multiplied by the √2. When these values are adjusted, on both days, the length of ASCs in 3D are longer than those in 2D (Fig 4.9A and 4.9B, p<0.05). To compensate for area, this correction could be done in both dimensions and the values should be multiplied by 2. Doing so results in 3D areas being larger than 2D areas in every concentration on both days (Fig 4.9C and 4.9D, p<0.05).

Figure 4.9: The Theoretical Size of ASCs Cultured in Different Dimensions and Concentrations of Collagen. Considering the likely underestimation of length by 2D projections, ASCs cultured in 3D were significantly longer than their counterparts cultured in 2D regardless of concentration or day (A and B, $p < 0.05$). When theoretical orientation was taken into account, ASCs in 3D also had larger areas than their 2D counterparts at every concentration and at both time points (C and D, $p < 0.05$). Differences in area and length between ASCs in selected concentration were the same as indicated earlier in Fig 4.3. Blue bars represent gels with 1 mg/mL of collagen, red bars represent gels with 2 mg/mL of collagen, and green bars represent gels with 4 mg/mL of collagen. Lines ending above conditions indicate statistical differences between gels with different concentrations of collagen and colored letters above gels indicate significant differences between gels of the same concentrations but different culture dimensions ($p < 0.05$). The number of biological replicates and cells analyzed from all replicates in each condition are displayed in panel E.

Considering the theroretical correction for roundness, cell length is in the denomintaor of the formula, so 3D values were divided by the √2. Doing so resulted in all 3D roundness values being lower than their 2D analogs regardless of concentration or days in culture (Fig 4.10A and 4.10B, p<0.05). The opposite is true for aspect ratio. Length is in the numerator for this shape factor so all values would be multiplied by √2. This results in 3D samples having higher aspect ratios than all 2D counterparts (Fig 4.10C and 4.10D, p<0.05).

E

	Days of culture											
Days of culture	4						7					
Dimensions of Culture	2D			3D			2D			3D		
Collagen Concentration (mg/mL)	1	2	4	1	2	4	1	2	4	1	2	4
Number of Biological Replicates	8						7					
Cells	1970	1325	2056	2128	1859	2323	2161	2698	2056	1983	2353	2159

Figure 4.10: The Theoretical Polarization of ASCs Cultured in Different Dimensions and Concentrations of Collagen. When the likely underestimation of length by 2D projections is considered, cells from 2D samples were statistically rounder than their 2D counterparts regardless of concentration (A and B, $p<0.05$). Taking orientation into account, samples in 3D had significantly larger aspect ratios than their 2D counterparts regardless of time point or concentration (C and D, $p<0.05$). Differences in roundness and aspect ratio between ASCs in selected concentration were the same as indicated earlier in Fig 4.4. Blue bars represent gels with 1 mg/mL of collagen, red bars represent gels with 2 mg/mL of collagen, and green bars represent gels with 4 mg/mL of collagen. Lines ending above conditions indicate statistical differences between gels with different concentrations of collagen and colored letters above gels indicate significant differences between gels of the same concentrations but different culture dimensions ($p<0.05$). The number of biological replicates and cells analyzed from all replicates in each condition are displayed in panel E.

The effects of this underestimation would affect measurements of cell spreading particularly. Circularity is a normalized ratio of the area to the perimeter squared and our projection factor value is the opposite ratio. To calculate the perimeter, we must at least double the scaling factor to length. This is conservative if the width is higher. Both shape factors square this scaling factor making it a factor of 8 higher in the theroretical calculations. While area is doubled, it still results in circularity being reduced by a factor of 4 and projection factor being increased by the same amount. This results in 3D ASCs being much more spread than their 2D counterparts considering both cicrularity (Fig 4.11A and 4.11B, $p<0.05$) and projection factor (Fig 4.11C and 4.11D, $p<0.05$).
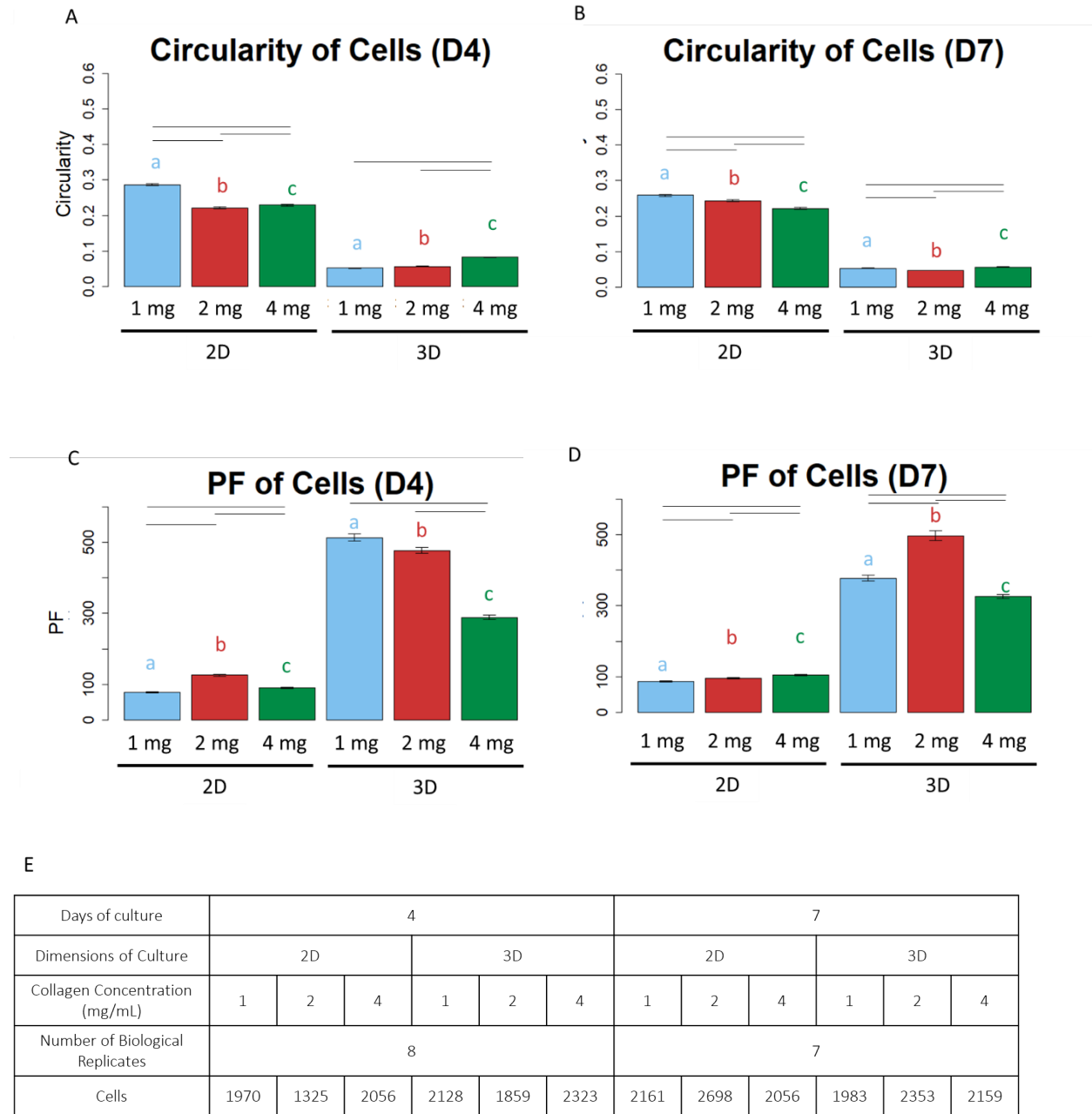
Figure 4.11: The Theoretical Size of ASCs Cultured in Different Dimensions and Concentrations of Collagen. By taking into account the likely underestimation of length by 2D projections, ASCs cultured in 2D were significantly more circular than their counterparts cultured in 3D regardless of concentration or day (A and B, $p<0.05$). When the orientation is accounted for artificially, ASCs in 3D also had larger projection factors than their 2D counterparts at every concentration and at both time points (C and D, $p<0.05$). Differences in area and length between ASCs in selected concentration were the same as indicated earlier in Fig 4.5. Blue bars represent gels with 1 mg/mL of collagen, red bars represent gels with 2 mg/mL of collagen, and green bars represent gels with 4 mg/mL of collagen. Lines ending above conditions indicate statistical differences between gels with different concentrations of collagen and colored letters above gels indicate significant differences between gels of the same concentrations but different culture dimensions ($p<0.05$). The number of biological replicates and cells analyzed from all replicates in each condition are displayed in panel E.

Together these estimates would suggest that cells in 3D are actually becoming larger, more polarized, and more spread than their counterparts in 2D.

4.4 – Discussion

In this study we asked whether 3D collagen culture facilitated a more mature SMC morphology than cells cultured on 2D collagen of the same concentration. The traditional morphology of SMC cells are long spindle shaped cells but this characterization is almost exclusively taken from 2D histology. The ASC in our 3D system were smaller (Fig 4.3) and less polarized (Fig 4.4) than their 2D counterparts. Previous research has found that that fibroblasts, another type of stromal cell, are also smaller [53,72] and more rounded in 3D [72]. While very different from SMCs, chondrocytes also remained more rounded up in 3D culture, which promoted their phenotype and function [52]. This contradicted what we initially expected. The traditional view from literature would imply that if the ASCs in 3D are smaller and less oblong, they are less SMC-like as well, but we have indicated that comparing 2D and 3D morphology is a more complex process that our current approach can fully describe (Fig 4.9-4.11). This discrepancy would demonstrate the current limitations of our shape analysis for directly comparing morphology from 2D culture to 3D culture. With that in mind, these results also validate the use of these shape descriptors within the same dimension of culture as well. The scaling factors used to estimate corrected cell shape in 3D would be used ubiquitously across all conditions in 3D canceling any effect they would have on distinguishing differences between conditions. Regardless, these results do suggest a large need for new technology and algorithms that account for this error and could validate these findings.

In order to better optimize culture conditions, this project also assessed the effects of collagen concentration on the resulting morphological phenotype. Interestingly, we found opposite

effects for results in 2D and 3D. In 2D, concentration generally correlated with an SMC phenotype and cells were larger and more polarized with higher concentrations. In 3D, the opposite trend was seen and higher concentrations seemed to inhibit spreading. It's known that as matrix concentration increases, matrix stiffness increases as well [56–58]. This higher stiffness slows degradation [58] and slowed degradation inhibits spreading in 3D [73]. This disparity is also likely related to trends seen in cell migration. In 2D, cells spread more on stiff substrates leading to faster migration [74]. In 3D, stiffer matrices inhibit spreading and slow migration [54,55]. This could be the result of complex interplay between the forces cells apply and the resistance they encounter from the ECM. For example, in addition to stiffness, changes in concentration influence ligand presentation [54] and pore size [54,57]. Fewer ligands in lower concentrations in 2D may be present fewer potential points to attach and spread. In 3D, higher concentrations in protein decreases pore size and may physically prohibit spreading [57]. The effects of ligand density and the spreading have been demonstrated to alter differentiation of MSC [10,75]. Future work should control for these factors individually to determine how differences in stiffness, ligand density, or pore size affect morphology and differentiation in 3D.

In addition to morphology, we examined how dimensionality influenced expression of smooth muscle genes and proteins. There were not many significant differences in gene expression between 2D samples and their counterparts in 3D (Appendix B). In the few cases where there were differences, 2D samples expressed higher amounts of expression. Literature would support this as cells in 2D tend to express more SMC genes than cells in 3D [76,77]. At the same time our protein data and theoretically corrected morphology data would support the conjecture of 3D culture being superior as stem cells that are allowed to enlarge and elongate move away from an adipogenic lineage [4,10,75] or chondrogenic lineage [10] and toward myogenic [66] or even a smooth muscle lineage

[10]. Nevertheless, SMC genes are shown to be highly variable in ASC with smooth muscle myosin heavy chain having particularly large amounts of variation [23]. In general, expression of SMC genes was highly variable while protein data would suggest superior SMC differentiation in 3D of higher concentrations of matrix.

These results have several implications for the field of stem cell biology, cell morphometrics, and regenerative medicine. They suggest that when assessed separately, a panel of shape factors describing the morphology of cells based on a projection can be used to quantify morphology in 2D and 3D. They cannot be compared across culture dimensions without taking in to account limitations to the method. When these limitations are considered, it would suggest that 3D enhances an SMC-like morphology and the expression of SMA and MHC protein supporting the idea of 3D enhancing differentiation of ASCs toward and smooth muscle lineage.

4.5 – References

1. Sheehy E, Conrad SL, Brigham LE, et al. Estimating the Number of Potential Organ Donors in the United States. *N Engl J Med*. 2003;349(7):667-674. doi:10.1056/NEJMsa021271.

2. Lindroos B, Suuronen R, Miettinen S. The Potential of Adipose Stem Cells in Regenerative Medicine. *Stem Cell Rev Reports*. 2011;7(2):269-291. doi:10.1007/s12015-010-9193-7.

3. Koç ON, Lazarus HM. Mesenchymal stem cells: Heading into the clinic. *Bone Marrow Transplant*. 2001;27(3):235-239. doi:10.1038/sj.bmt.1702791.

4. Kilian K a, Bugarija B, Lahn BT, Mrksich M. Geometric cues for directing the differentiation of mesenchymal stem cells. *Proc Natl Acad Sci U S A*. 2010;107:4872-4877. doi:10.1073/pnas.0903269107.

5. Fang B, Song Y, Liao L, Zhang Y, Zhao RC. Favorable Response to Human Adipose Tissue-Derived Mesenchymal Stem Cells in Steroid-Refractory Acute Graft-Versus-Host Disease. *Transplant Proc*. 2007;39(10):3358-3362. doi:10.1016/j.transproceed.2007.08.103.

6. Cawthorn WP, Scheller EL, MacDougald OA. Adipose tissue stem cells: The great WAT

hope. *Trends Endocrinol Metab*. 2012;23(6):270-277. doi:10.1016/j.tem.2012.01.003.

7.   Dai R, Wang Z, Samanipour R, Koo K, Kim K. Adipose-Derived Stem Cells for Tissue Engineering and Regenerative Medicine Applications. *Stem Cells Int*. 2016;2016:1-19. doi:10.1155/2016/6737345.

8.   Halvorsen YDC, Bond A, Sen A, et al. Thiazolidinediones and glucocorticoids synergistically induce differentiation of human adipose tissue stromal cells: Biochemical, cellular, and molecular analysis. *Metabolism*. 2001;50(4):407-413. doi:10.1053/meta.2001.21690.

9.   Choi YS, Matsuda K, Dusting GJ, Morrison WA, Dilley RJ. Engineering cardiac tissue in vivo from human adipose-derived stem cells. *Biomaterials*. 2010;31(8):2236-2242. doi:10.1016/j.biomaterials.2009.11.097.

10.   Gao L, Mcbeath R, Chen CS. Stem Cell Shape Regulates a Chondrogenic versus Myogenic Fate through Rac1 and N-cadherin. *Stem Cells*. 2010;28(3):564-572. doi:10.1002/stem.308.Stem.

11.   Iyyanki T, Hubenak J, Liu J, Chang EI, Beahm EK, Zhang Q. Harvesting technique affects adipose-derived stem cell yield. *Aesthetic Surg J*. 2015;35(4):467-476. doi:10.1093/asj/sju055.

12.   Furuhata Y, Yoshitomi T, Kikuchi Y, Sakao M, Yoshimoto K. Osteogenic Lineage Commitment of Adipose-Derived Stem Cells Is Predetermined by Three-Dimensional Cell Accumulation on Micropatterned Surface. *ACS Appl Mater Interfaces*. 2017;9(11):9339-9347. doi:10.1021/acsami.6b15688.

13.   Helder MN, Knippenberg M, Klein-Nulend J, Wuisman PIJM. Stem Cells from Adipose Tissue Allow Challenging New Concepts for Regenerative Medicine. *Tissue Eng*. 2007;13(8):1799-1808. doi:10.1089/ten.2006.0165.

14.   Lim S, Cho H, Lee E, et al. Osteogenic stimulation of human adipose-derived stem cells by pre-treatment with fibroblast growth factor 2. *Cell Tissue Res*. 2016;364(1):137-147. doi:10.1007/s00441-015-2311-8.

15.   Estes BT, Wu AW, Guilak F. Potent induction of chondrocytic differentiation of human adipose-derived adult stem cells by bone morphogenetic protein 6. *Arthritis Rheum*. 2006;54(4):1222-1232. doi:10.1002/art.21779.

16.   Kabiri A, Esfandiari E, Hashemibeni B, Kazemi M, Mardani M, Esmaeili A. Effects of FGF-2 on human adipose tissue derived adult stem cells morphology and chondrogenesis enhancement in Transwell culture. *Biochem Biophys Res Commun*. 2012;424(2):234-238. doi:10.1016/j.bbrc.2012.06.082.

17.   Gomez D, Swiatlowska P, Owens GK. Epigenetic Control of Smooth Muscle Cell Identity and Lineage Memory. *Arterioscler Thromb Vasc Biol*. 2015;35(12):2508-2516. doi:10.1161/ATVBAHA.115.305044.

18.   Lin CY, Huang CH, Wu YK, Cheng NC, Yu J. Maintenance of human adipose derived stem

cell (hASC) differentiation capabilities using a 3D culture. *Biotechnol Lett*. 2014;36(7):1529-1537. doi:10.1007/s10529-014-1500-y.

19.   Choi SA, Lee JY, Wang KC, et al. Human adipose tissue-derived mesenchymal stem cells: Characteristics and therapeutic potential as cellular vehicles for prodrug gene therapy against brainstem gliomas. *Eur J Cancer*. 2012;48(1):129-137. doi:10.1016/j.ejca.2011.04.033.

20.   Desiderio V, De Francesco F, Schiraldi C, et al. Human Ng2+ adipose stem cells loaded in vivo on a new crosslinked hyaluronic acid-lys scaffold fabricate a skeletal muscle tissue. *J Cell Physiol*. 2013;228(8):1762-1773. doi:10.1002/jcp.24336.

21.   Lee W-CC, Maul TM, Vorp DA, Rubin JP, Marra KG. Effects of uniaxial cyclic strain on adipose-derived stem cell morphology, proliferation, and differentiation. *Biomech Model Mechanobiol*. 2007;6(4):265-273. doi:10.1007/s10237-006-0053-y.

22.   Heydarkhan-Hagvall S, Schenke-Layland K, Yang JQ, et al. Human adipose stem cells: A potential cell source for cardiovascular tissue engineering. *Cells Tissues Organs*. 2008;187(4):263-274. doi:10.1159/000113407.

23.   Harris LJ, Abdollahi H, Zhang P, McIlhenny S, Tulenko TN, DiMuzio PJ. Differentiation of adult stem cells into smooth muscle for vascular tissue engineering. *J Surg Res*. 2011;168(2):306-314. doi:10.1016/j.jss.2009.08.001.

24.   Bjorninen M, Gilmore K, Pelto J, et al. Electrically Stimulated Adipose Stem Cells on Polypyrrole-Coated Scaffolds for Smooth Muscle Tissue Engineering. *Ann Biomed Eng*. 2016;45(4):1-12. doi:10.1007/s10439-016-1755-7.

25.   Arias E, Heron M, Tejada-Vera B. United States life tables eliminating certain causes of death , 1999-2001 . PubMed Commons. *Natl Vital Stat*. 2014;61(9):1-128.

26.   Brun J, Lutz KA, Neumayer KMH, et al. Smooth Muscle-Like Cells Generated from Human Mesenchymal Stromal Cells Display Marker Gene Expression and Electrophysiological Competence Comparable to Bladder Smooth Muscle Cells. *PLoS One*. 2015:1-21. doi:10.1371/journal.pone.0145153.

27.   Rothdiener M, Hegemann M, Uynuk-Ool T, et al. Stretching human mesenchymal stromal cells on stiffness-customized collagen type I generates a smooth muscle marker profile without growth factor addition. *Sci Rep*. 2016;6(October):35840. doi:10.1038/srep35840.

28.   Mason C, Dunnill P. A brief definition of regenerative medicine. *Regen Med*. 2008;1:1-4.

29.   Pampaloni F, Reynaud EG, Stelzer EHK. The third dimension bridges the gap between cell culture and live tissue. *Nat Rev Mol Cell Biol*. 2007;8(10):839-845. doi:10.1038/nrm2236.

30.   Edelman DB, Keefer EW. A cultural renaissance: In vitro cell biology embraces three-dimensional context. *Exp Neurol*. 2005;192(1):1-6. doi:10.1016/j.expneurol.2004.10.005.

31.   Zhang D, Shadrin IY, Lam J, Xian H-Q, Snodgrass HR, Bursac N. Tissue-engineered cardiac patch for advanced functional maturation of human ESC-derived cardiomyocytes.

Biomaterials. 2013;34(23):5813-5820. doi:10.1016/j.biomaterials.2013.04.026.

32. Fong AH, Romero-López M, Heylman CM, et al. Three-Dimensional Adult Cardiac Extracellular Matrix Promotes Maturation of Human Induced Pluripotent Stem Cell-Derived Cardiomyocytes. *Tissue Eng Part A*. 2016;22(15-16):1016-1025. doi:10.1089/ten.tea.2016.0027.

33. Lo H-Y, Huang A-L, Lee P-C, Chung T-W, Wang S-S. Morphological transformation of hBMSC from 2D monolayer to 3D microtissue on low-crystallinity SF-PCL patch with promotion of cardiomyogenesis. *J Tissue Eng Regen Med*. 2017;(April):1-13. doi:10.1002/term.2616.

34. Correia C, Koshkin A, Duarte P, et al. 3D aggregate culture improves metabolic maturation of human pluripotent stem cell derived cardiomyocytes. *Biotechnol Bioeng*. 2018;115(3):630-644. doi:10.1002/bit.26504.

35. Talaei-Khozani T, Khodabandeh Z, Jaberipour M, Hosseini A, Bahmanpour S, Vojdani Z. Comparison of hepatic nuclear factor-4 expression in two and three-dimensional culture of Wharton's jelly-derived cells exposed to hepatogenic medium. *Rom J Morphol Embryol*. 2015;56(4):1365-1370.

36. Meier F, Freyer N, Brzeszczynska J, et al. Hepatic differentiation of human iPSCs in different 3D models: A comparative study. *Int J Mol Med*. 2017;40(6):1759-1771. doi:10.3892/ijmm.2017.3190.

37. Wu Q, Tang J, Li Y, et al. Hepatic differentiation of mouse bone marrow-derived mesenchymal stem cells using a novel 3D culture system. *Mol Med Rep*. 2017;16(6):9473-9479. doi:10.3892/mmr.2017.7818.

38. Ma W, Fitzgerald W, Liu QY, et al. CNS stem and progenitor cell differentiation into functional neuronal circuits in three-dimensional collagen gels. *Exp Neurol*. 2004;190(2):276-288. doi:10.1016/j.expneurol.2003.10.016.

39. Chandrasekaran A, Avci HX, Ochalek A, et al. Comparison of 2D and 3D neural induction methods for the generation of neural progenitor cells from human induced pluripotent stem cells. *Stem Cell Res*. 2017;25:139-151. doi:10.1016/j.scr.2017.10.010.

40. Yamamoto M, Kawashima N, Takashino N, et al. Three-dimensional spheroid culture promotes odonto/osteoblastic differentiation of dental pulp cells. *Arch Oral Biol*. 2014;59(3):310-317. doi:10.1016/j.archoralbio.2013.12.006.

41. Bae Y-J, Kwon Y-R, Kim HJ, Lee S, Kim Y-J. Enhanced differentiation of mesenchymal stromal cells by three-dimensional culture and azacitidine. *Blood Res*. 2017;52(1):18-24. doi:10.5045/br.2017.52.1.18.

42. Xu Y, Balooch G, Chiou M, Bekerman E, Ritchie RO, Longaker MT. Analysis of the material properties of early chondrogenic differentiated adipose-derived stromal cells (ASC) using an in vitro three-dimensional micromass culture system. *Biochem Biophys Res Commun*. 2007;359(2):311-316. doi:10.1016/j.bbrc.2007.05.098.

43. Shao Y, Taniguchi K, Gurdziel K, et al. Self-organized amniogenesis by human pluripotent stem cells in a biomimetic implantation-like niche. *Nat Mater*. 2016;16(4):419-425. doi:10.1038/nmat4829.

44. Herrmann D, Conway JRW, Vennin C, et al. Three-dimensional cancer models mimic cell-matrix interactions in the tumour microenvironment. *Carcinogenesis*. 2014;35(8):1671-1679. doi:10.1093/carcin/bgu108.

45. Selden C, Shariat A, Mccloskey P, Ryder T, Roberts E, Hodgson H. Three-dimensional in Vitro Cell Culture Leads to a Marked Upregulation of Cell Function in Human Hepatocyte Cell Lines-an Important Tool for the Development of a Bioartifcial Liver Machine. *Ann N Y Acad Sci*. 2006;875(1):1-9.

46. O'Connor SM, Andreadis JD, Shaffer KM, Ma W, Pancrazio JJ, Stenger DA. Immobilization of neural cells in three-dimensional matrices for biosensor applications. *Biosens Bioelectron*. 2000;14(10-11):871-881. doi:10.1016/S0956-5663(99)00055-X.

47. Ferrera D, Poggi S, Biassoni C, et al. Three-dimensional cultures of normal human osteoblasts: Proliferation and differentiation potential in vitro and upon ectopic implantation in nude mice. *Bone*. 2002;30(5):718-725. doi:10.1016/S8756-3282(02)00691-9.

48. Sasaki T, Takagi M, Soma T, Yoshida T. 3D culture of murine hematopoietic cells with spatial development of stromal cells in nonwoven fabrics. *Cytotherapy*. 2002;4(3):285-291. doi:10.1080/146532402320219808.

49. Fong ELS, Lamhamedi-Cherradi S-E, Burdett E, et al. Modeling Ewing sarcoma tumors in vitro with 3D scaffolds. *Proc Natl Acad Sci U S A*. 2013;110(16):6500-6505. doi:10.1073/pnas.1221403110.

50. Akins RE, Boyce RA, Madonna ML, et al. Cardiac Organogenesis in Vitro: Reestablishment of Three-Dimensional Tissue Architecture by Dissociated Neonatal Rat Ventricular Cells. *Tissue Eng*. 1999;5(2):103-118. doi:10.1089/ten.1999.5.103.

51. Evans HJ, Sweet JK, Price RL, Yost M, Goodwin RL. Novel 3D culture system for study of cardiac myocyte development. *Am J Physiol Hear Circ Physiol*. 2003;285(2):H570-H578. doi:10.1152/ajpheart.01027.2002.

52. Kisiday J, Jin M, Kurz B, et al. Self-assembling peptide hydrogel fosters chondrocyte extracellular matrix production and cell division: Implications for cartilage tissue repair. *Proc Natl Acad Sci*. 2002;99(15):9996-10001. doi:10.1073/pnas.142309999.

53. Hakkinen KM, Harunaga JS, Doyle AD, Yamada KM. Direct comparisons of the morphology, migration, cell adhesions, and actin cytoskeleton of fibroblasts in four different three-dimensional extracellular matrices. *Tissue Eng Part A*. 2011;17(5-6):713-724. doi:10.1089/ten.tea.2010.0273.

54. Doyle AD, Yamada KM. Mechanosensing via cell-matrix adhesions in 3D microenvironments. *Exp Cell Res*. 2015:1-7. doi:10.1016/j.yexcr.2015.10.033.

55. Zaman MH, Trapani LM, Sieminski AL, et al. Migration of tumor cells in 3D matrices is

governed by matrix stiffness along with cell-matrix adhesion and proteolysis. *Proc Natl Acad Sci U S A*. 2006;103(29):10889-10894. doi:10.1073/pnas.0604460103.

56. Rao RR, Peterson AW, Ceccarelli J, Putnam AJ, Stegemann JP. Matrix composition regulates three-dimensional network formation by endothelial cells and mesenchymal stem cells in collagen/fibrin materials. *Angiogenesis*. 2012;15(2):253-264. doi:10.1007/s10456-012-9257-1.

57. Wolf K, te Lindert M, Krause M, et al. Physical limits of cell migration: Control by ECM space and nuclear deformation and tuning by proteolysis and traction force. *J Cell Biol*. 2013;201(7):1069-1084. doi:10.1083/jcb.201210152.

58. Blum KM, Novak T, Watkins L, et al. Acellular and cellular high-density, collagen-fibril constructs with suprafibrillar organization. *Biomater Sci*. 2016;4(4):711-723. doi:10.1039/C5BM00443H.

59. Lan F, Lee AS, Liang P, et al. Abnormal calcium handling properties underlie familial hypertrophic cardiomyopathy pathology in patient-specific induced pluripotent stem cells. *Cell Stem Cell*. 2013;12(1):101-113. doi:10.1016/j.stem.2012.10.010.

60. Huebsch N, Arany PR, Mao AS, et al. Harnessing traction-mediated manipulation of the cell/matrix interface to control stem-cell fate. *Nat Mater*. 2010;9(6):518-526. doi:10.1038/nmat2732.

61. Murphy CM, Matsiko A, Haugh MG, Gleeson JP, O'Brien FJ. Mesenchymal stem cell fate is regulated by the composition and mechanical properties of collagen-glycosaminoglycan scaffolds. *J Mech Behav Biomed Mater*. 2012;11:53-62. doi:10.1016/j.jmbbm.2011.11.009.

62. Hart M, Lauer J, Selig M, Hanak M, Walters B, Rolauffs B. Shaping the Cell and the Future: Recent Advancements in Biophysical Aspects Relevant to Regenerative Medicine. *J Funct Morphol Kinesiol*. 2017;3(1):2. doi:10.3390/jfmk3010002.

63. McBeath R, Pirone DM, Nelson CM, Bhadriraju K, Chen CS. Cell shape, cytoskeletal tension, and RhoA regulate stem cell lineage commitment. *Dev Cell*. 2004;6(4):483-495. http://www.ncbi.nlm.nih.gov/pubmed/15068789.

64. Zhang D, Sun MB, Lee J, Abdeen AA, Kilian KA. Cell shape and the presentation of adhesion ligands guide smooth muscle myogenesis. *J Biomed Mater Res - Part A*. 2016;104(5):1212-1220. doi:10.1002/jbm.a.35661.

65. Eng G, Lee BW, Parsa H, et al. Assembly of complex cell microenvironments using geometrically docked hydrogel shapes. *Proc Natl Acad Sci*. 2013;110(12):4551-4556. doi:10.1073/pnas.1300569110.

66. Tay CY, Yu H, Pal M, et al. Micropatterned matrix directs differentiation of human mesenchymal stem cells towards myocardial lineage. *Exp Cell Res*. 2010;316(7):1159-1168. doi:10.1016/j.yexcr.2010.02.010.

67. Fu J, Wang Y-K, Yang MT, et al. Mechanical regulation of cell function with geometrically modulated elastomeric substrates. *Nat Methods*. 2010;7(9):733-736.

doi:10.1038/nmeth.1487.

68. Bao M, Xie J, Piruska A, Huck WTS. 3D microniches reveal the importance of cell size and shape. *Nat Commun*. 2017;8(1):1-12. doi:10.1038/s41467-017-02163-2.

69. Matsuoka F, Takeuchi I, Agata H, et al. Morphology-Based Prediction of Osteogenic Differentiation Potential of Human Mesenchymal Stem Cells. *PLoS One*. 2013;8(2). doi:10.1371/journal.pone.0055082.

70. Matsuoka F, Takeuchi I, Agata H, et al. Characterization of time-course morphological features for efficient prediction of osteogenic potential in human mesenchymal stem cells. *Biotechnol Bioeng*. 2014;111(7):1430-1439. doi:10.1002/bit.25189.

71. Uynuk-Ool T, Rothdiener M, Walters B, et al. The geometrical shape of mesenchymal stromal cells measured by quantitative shape descriptors is determined by the stiffness of the biomaterial and by cyclic tensile forces. *J Tissue Eng Regen Med*. 2017;11(12):3508-3522. doi:10.1002/term.2263.

72. Chen X, Thibeault SL. Response of Fibroblasts to Transforming Growth Factor-β1 on Two-Dimensional and in Three-Dimensional Hyaluronan Hydrogels. *Tissue Eng Part A*. 2012;18(23-24):2528-2538. doi:10.1089/ten.tea.2012.0094.

73. Khetan S, Guvendiren M, Legant WR, Cohen DM, Christopher S, Burdick JA. Degradation-mediated cellular traction directs stem cell fate in covalently crosslinked three-dimensional hydrogels. *Nat Mater*. 2013;12(5):458-465. doi:10.1038/nmat3586.Degradation-mediated.

74. C. M. Lo, H. B. Wang, M. Dembo and YLW. Cell movement is guided by the rigidity of the substrate, vol. 79, no. 1, pp. 144–152, 2000. *Biophys J*. 2000;79(1):144-152.

75. Lee J, Abdeen AA, Zhang D, Kilian KA. Directing stem cell fate on hydrogel substrates by controlling cell geometry, matrix mechanics and adhesion ligand composition. *Biomaterials*. 2013;34(33):8140-8148. doi:10.1016/j.biomaterials.2013.07.074.

76. Li S. Genomic analysis of smooth muscle cells in three-dimensional collagen matrix. *FASEB J*. 2002;17(1):97-99. doi:10.1096/fj.02-0256fje.

77. O'Cearbhaill ED, Murphy M, Barry F, McHugh PE, Barron V. Behavior of human mesenchymal stem cells in fibrin-based vascular tissue engineering constructs. *Ann Biomed Eng*. 2010;38(3):649-657. doi:10.1007/s10439-010-9912-x.

CHAPTER 5

The Influence of Growth Factor Delivery and Stretch on Adipose Derived Stem Cell

Differentiation into Smooth Muscle Cells

5.1 – Introduction

As the population ages, higher numbers of patients will need to be treated for cardiovascular disease [1] and urinary incontinence [2]. While technology offers many palliative options and changes in life style can slow progression, tissue engineered therapies offer one of the few potential options to reverse the degeneration of tissues due to aging. In order to produce constructs to treat all three of these devastating areas of disease, a reliable and well characterized source of smooth muscle cells must be established. Mesenchymal stem cells offer the most readily available source for these cells and adipose derived stem cells (ASCs) in particular are being considered for their higher yield during extraction, ease of access, and less donor co-morbidity [3–6]. ASCs were first recognized for their adipogenic properties [7–12] but have since been demonstrated to be ASCs are osteogenic [7–10,12,13], chondrogenic [9,10,14,15], neurogenic [9,16], and myogenic [17,18]. More recently their potential as a source for smooth muscle cells (SMCs) has garnered a lot of interest [9,19–21] but substantial work still needs to be done to understand their differentiation into an SMC lineage and how best to induce this process at large scales and to the degree needed for functional cells that could be used in therapeutic treatments.

The extracellular environment of smooth muscle cells and their progenitors contains a range of stimuli that induce and maintain their phenotype. Growth factors have been actively used

to recapitulate some of these signals and induce a SMC phenotype from other cell lineages. The transforming growth factor beta (TGFβ) superfamily of cytokines were first discovered in cancer lines and were noted for their ability to fundamentally change the phenotype of fibroblasts (reviewed in [22]). Since their discovery, TGFβ1 in particular has been noted for its ability to induce both chondrogenesis [23,24] and differentiation into smooth muscle cells [25–29]. Other growth factors being utilized for smooth muscle differentiation are Platelet Derived Growth Factor (PDGF) [27,28,30], Transforming Growth Factor β3 (TGFβ3) [31], Sphingosylphosphorylcholine [31], and Bone Morphogenic Factor 4 (BMP4) [32–34]. These growth factors have been shown to, at least transiently, upregulate the expression of SMC genes and protein [25–29,31,32,34]. These growth factors are typically delivered to in vitro cultures by dissolving them in culture media but replenishing the growth factor in vivo becomes more difficult, especially when bolus injections can be diluted into the surrounding tissue and certain tissues may impede diffusion [35]. To compensate for this idea, groups have developed methods to load growth factors into the cell substrate [36] or into modular delivery devices [37,38] in effort to promote local and sustained delivery [23,38]. These have been used to deliver Bone Morphogenic Protein 2 (BMP2) [24,37,38], Vasculogenic Endothelial Growth Factor (VEGF, [38]), Fibroblast Growth Factor (FGF, [39]), and TGFβ1 [23,24,35]. Because of their size and general shape, these carriers have been called microspheres (μspheres) and they hold potential to augment growth factor delivery for clinical uses.

Another commonly used method for inducing a smooth muscle-like phenotype in stem cells is mechanical stimulation. Cyclic strain has been used to induce MSCs [40–44] as well as ASCs [29,45] into an SMC-like phenotype. This stimulation and has been shown to upregulate SMC genes and protein [29,41,42,45]. It has also been shown to induce alignment of cells although the direction of alignment appears to be dependent on the substrate as seeding on 2D silicone or non-fibrous

substrates induces perpendicular alignment [19,46–48] while collagen and other fiber based scaffolds induce parallel alignment regardless of dimensionality [49]. Often stretch and growth factors are used in combination to maximize effects [19,29] and whether stretched in 2D or 3D, with growth factors or without, stem cells seem to enlarge after mechanical stimulation [19,40,48–50], which is an important indication of differentiation.

The change in cell morphology induced by different stimuli has been closely linked to differentiation, especially in mesodermal lineages. Fabrication methods that allow the printing of specific shapes and areas of cell contact have been extremely informative into how cells regulate differentiation and offer approaches to direct the process [9,51,52]. Controlling where cells can spread by controlling ligands [53] and limiting elongation [54,55] offer yet another means of regulating differentiation. Shape has proven a valuable tool for predicting future phenotype [56,57] and many groups use it as a qualitative measure of phenotype. It has also been found that growth factors and stretch affect the size [19,25,32,33,48,49] and polarization [19,25,45,48,58] of cells as they differentiate.

Our group has used the relationship between cell shape and phenotype on 2D substrates to quantify changes in morphology throughout the process of smooth muscle differentiation [59]. Here we apply these principles in 3D with ASCs. Other groups have found that 3D culture impedes SMC differentiation compared to analogous 2D systems. We asked whether delivery of growth factors, particularly through μsphere-mediated release could improve the differentiation of ASCs. We also asked if cyclic strain alone or in combination with growth factors could augment this process. Collectively, we aimed to induce differentiation of ASCs into smooth muscle cells and to characterize these changes through quantitative analysis of shape factors and SMC gene and protein expression. By improving differentiation of ASCs into SMCs we could gain better understanding of how smooth muscle naturally develops and harness a new source of cellular

materials for tissue engineering. By objectively quantifying these changes through cell shape, we might develop new insight into relationships between morphology and differentiation. Together these principles could develop new standards for cardiovascular care and enhance regenerative medicine as whole.

5.2 – Materials and Methods

ASCs culture and expansion

Human adipose-derived mesenchymal stem cells (Rooster Bio, Frederick, MD) were expanded in T175 flasks in Alpha Modification Essential Medium (Alpha MEM, Fisher, Rockville, MD) supplemented with 10% qualified fetal bovine serum (FBS; Invitrogen, Carlsbad, CA) and 1% penicillin and streptomyocin (PS; Invitrogen). Cells were kept at 37ºC and 5% CO_2 and their media was changed every three days and passages 5-7 were used for experiments. On day 0, when ready to be used for construct production, cells were washed in PBS and incubated in 0.25% Trypsin (Fisher) at 37ºC for 3-4 minutes to lift cells from the flasks. After cells had lifted, they were counted, centrifuged, and resuspended in Dulbecco's Modified Essential Media (DMEM, Fisher) for use in collagen hydrogels. This DMEM was also supplemented with 10% qualified FBS (Invitrogen) and 1% penicillin and streptomyocin (Invitrogen).

Production of μSpheres

Made 2.5% v/v NaOH diluent by adding 1N NaOH (Sigma, St. Louis MO) to water. Made 10% by weight gelatin A stock solution by dissolving gelatin A (Sigma G6144) in water and vortexing vigorously. Incubated at 37˚C until completely dissolved. Made 6% working solution by diluting stock gelatin with water. Made 1% genipin crosslinker by dissolving genipin (Wako

078-3021, Fisher) in PBS. Heated and mixed until dissolved and yellow. Kept genipin at 4˚C until use. Made 0.01% PBS+L101 oil washing solution by adding Pluronic L101 (BASF, Ludwigshafen, Germany) to PBS dissolving at 4˚C and storing at room temperature until use. Added 100 CS silicone oil (Clearco, Willow Grove, PA) to a beaker and warmed it and working 6% gelatin solution to 37˚C. Set beaker with oil just below impeller of Servodyne mixer (Cole Palmer, Vernon Hills, IL). Immersed impeller and verified that speeds of 2300 RPM did not splash. Slowly added desired volume of 6% gelatin to beaker allowing gelatin to emulsify for 5 min. Ran rotor on 66% duty cycle every 1.5 minutes for 3 minutes. Placed the silicone and emulsified gelatin on ice and ran mixer for another 30 minutes. Added 25 mL of gelatin oil mixture to 50 mL tubes and diluted 1:2 with PBS+L101 solution. Mixed for 5 minutes by constantly inverting the tubes on a Rotoflex tube rotator (Argos, Vernon Hills, IL). Centrifuged tubes at 300g for 5 minutes and removed top oil phase. Transferred bottom phase to new tubes and repeated the wash step bringing each tube's volume to 50 mL again with PBS+L101. Centrifuged again and removed oil phase. Repeated washes until remaining gelatin and PBS phase was about 10-15 mL. Vortexed and added 1% genipin. Mixed tubes overnight (18-24 hours) on Rotoflex tube rotator allowing genipin to crosslink. The next day, centrifuged at 200g for 5 minutes. Removed liquid phase and brought volume to 50 mL with ethanol (200 proof, 459844 Sigma). Inverted on Rotoflex for 1 hour, centrifuged at 200g for 5 minutes. Repeated wash twice more with ethanol and then three times with water. Sonified gelatin sphere using 50% duty cycle every minute for 3 minutes with Digital 250 Sonifier (Branson, Danbury, CT). Gelatin spheres were freeze dried until use.

Loading growth factor into μspheres

Lyophilized spheres were massed into three sterile centrifuged tubes. The first contained 0.11 mg of gelatin spheres/mL of hydrogel to contain loaded spheres. The second contained 0.27

mg of spheres/mL of hydrogel to contain loaded spheres. The third contained 0.38 mg of spheres/mL of hydrogel to contain unloaded spheres. Tubes were centrifuged to collect spheres at bottom. Added TGFβ (20 µg/mL PBS, Peprotech, Rocky Hill, NJ), PDGF-AB (20 µg/mL (100-00AB-10UG, Peprotech, Rocky Hill, NJ), or PBS, to first second and third tubes respectively at 10 µL/mg of spheres. Centrifuged each tube to collect growth factor and spheres at the bottom. Incubated over night at 37°C. Resuspended spheres in each tube with FBS (Invitrogen) to final concentration of 10 mg spheres/mL. Incubated in FBS at room temperature for one hour. Homogenized sphere solutions with Digital Sonifier (Branson) at 10% amplitude for 2 minutes with 50% duty cycle every 20 seconds.

<u>Tissue construct production and culture</u>

Type I collagen (MP Biomedicals, Solon, Ohio) was dissolved in 0.02 M Acetic Acid (Sigma) to a concentration of 4 mg/mL. Collagen gels were made according to previous studies (Rao 2012). Briefly, to make 2 mg/mL gels, 4 mg/mL collagen, composing 50% of the final gel volume, of was added to different tubes, one for each type of growth factor loading. To each tube, a volume of 5X DMEM (Fisher) equal to 20% of the final gel volume and 0.01 M NaOH (Sigma) equal to 10% of the final volume was mixed with the collagen to neutralize acid and to make the solution isotonic. Fetal Bovine Serum (Fisher) equal to 10% of the final volume was added with the respective amounts of µspheres to each tube. For controls gels (Con), no spheres were added to the FBS. For gels with unloaded spheres and growth in the media (GF), 38% of the FBS contained control spheres (10 mg of spheres/mL FBS). For gels with growth factor loaded into the spheres (LS), 11% of the FBS contained spheres loaded with TGFβ and 27% of the FBS contained spheres loaded with PDGF (Both at 10 mg spheres/mL FBS). ASCs, which were suspended at 5e6 cells/mL in 1x DMEM (Fisher) were mixed in two equal to 10% of the final gel volume. The

139

hydrogel mixtures were dispersed to wells for static culture or bioreactor chambers for mechanical stimulation. 0.5 mL of hydrogel solution was dispersed to wells of a 24 well TC treated plate (Corning, Fisher) and 4 mL was dispensed to each bioreactor chamber custom made for stretching (TGT LigaGenTM, Minnetonka, MN). All plates and chambers were incubated and allowed to set at 37ºC. After setting, 0.5 mL of respective media was added to each static gel and 4 mL of respective media was added to each construct in the bioreactor chambers. Control gels (Con) received 1X DMEM with 10% FBS (Fisher), gels with unloaded spheres (GF US) received 1X DMEM with 10% FBS, 5 ng/mL PDGF (Peprotech), 5ng/mL TGF (Peprotech), and 30 μM ascorbic acid, and gels containing loaded spheres received 1X DMEM with 10% FBS and 30 μM ascorbic acid. Constructs were incubated at 37ºC until each gel's respective media was changed on D3. Gels in bioreactor chambers were released from their molds and suspended from anchor points before replacing media. On D4 samples were collected and analyzed while all remaining gels continued to be cultured. The gels in bioreactor chambers were stretched starting on D4 (described below). Media was changed again on D6 and the final samples were collected for analysis on D7.

<u>Determining Growth Factor Release</u>

PDGF μspheres and TGFβ μspheres (Loaded) were incubated in 5U/mL Collagenase I (MP Biomedical) for 24 hours. Empty spheres in collagenase served as negative controls (Control) and growth factor, equal to the amount loaded into the spheres, was dissolved in PBS to serve as a positive control (GF in PBS). Samples from the PDGF μspheres and controls were collected at 0, 1, 2, 3, 4, 7, 9, 11, 14, and 24 hours. Samples from the TGFβ μspheres and controls were collected at 0, 4, 7, 9, 11, 14, and 24 hours. Samples were analyzed using a PDGF-AB Quantikine ELISA Kit (DHD00C, R&D Systems) and Human TGFβ 1 Quantikine ELISA Kit (DB100B, R&D

Systems). Samples were analyzed on a Synergy H1 microplate reader (BioTek, Winooski, VT), accounting for the removed volume at each time point. The time point that growth factor release plateaued was recorded. Control spheres were kept in 4 U/mL and 5U/mL Collagenase I (MP Biomedical) and samples were collected every 15 minutes until the spheres were fully dissolved (~12 hours). Exploiting the autofluorescence of the genipin-crosslinked gelatin, a Synergy H1 microplate reader (BioTek) was used to measure the amount of gelatin dissolved in each sample. This was calculated by normalizing the fluorescence by that of fully dissolved μspheres and, again, accounting for the volume removed during each sampling. The percentage of μsphere degradation that occurred when growth factor release plateaued was recorded. ASCs in collagen hydrogels with control spheres as described above were cultured for two weeks collecting media samples every two days. Using the autofluorescence of the solubilized genipin-crosslinked gelatin, the amount of degradation was calculated accounting for volume removed from each sample. The time it would take ASCs to degrade the μspheres and facilitate the highest amount of release was calculated using the degree of degradation known to correspond to full release in collagenase. To examine the effects of growth factor delivery method on the degradation of the spheres, ASCs were cultured with loaded spheres (LS as described above), with unloaded spheres and growth factor in the media (GF as described above), and control conditions (Con as described above) for one week changing respective media on D3 and D6. Removed media was analyzed for solubilized gelatin with the Synergy H1 microplate reader.

Stretching Gels

As described above, 4 mL hydrogels from each growth factor delivery condition (LS, GF, and Con) were cast into custom molds inside bioreactor chambers designed to facilitate cyclic uniaxial stretch (TGT LigaGenTM). On D3, during the standard media change, the molds for

setting the hydrogels were removed and constructs were suspended in fresh media between two anchoring points. On D4 the chambers with hydrogels were inserted in a bioreactor (TGT LigaGenTM) and proprietary software was used to apply cyclic uniaxial stretch at 10% strain and 1 Hz for 6 hours a day for 3 consecutive days (D4, D5, D6). On D6 after stretch, media from each chamber was replaced with the media for that respective condition in parallel with the respective control gels. On D7, samples from each chamber were collected and analyzed for shape, gene expression, and protein expression.

<u>Fluorescence Microscopy for Cell Shape</u>

The ASCs-seeded constructs were collected and stained on D7 using Calcein (1:1000, Lifetech/Fisher) and diamidino-2-phenylindole (DAPI, 1:1000, Lifetech, Fisher) based on our previous work (Rothdiener 2016, Uynuk-Ool 2017). ASCs embedded in or on top of collagen gels were imaged using an Olympus IX15 Microscope system (Olympus America, Center Valley, PA). Calcein-stained ASC morphology was detected using the green filter and the nuclei were imaged using a blue filter. The individual shapes of large quantities of ASCs were measured simultaneously through 2D projections of fluorescence with an ImageJ macro (National Institute of Health, Bethesda, MD), according to (Uynuk-Ool 2017*)*. The following six mathematical shape descriptors were quantified for each MSC: length (major axis), area, circularity ($4*\pi(area/perimeter^2)$), projection factor ($perimeter^2/area$), roundness ($4*area/(\pi*major\ axis\ length^2)$), and aspect ratio (major axis angle/minor axis). These measurements from each cell were averaged and used to compare different culturing conditions.

<u>Compaction of Static Constructs</u>

Every day and before collection of samples for analysis, images were taken of each gel using a bright field microscope (Olympus). In ImageJ (NIH), the long and short access of each sample were measured and approximated as an ellipse. The areas of the resulting ellipses were normalized to their initial area of the gels, effectively, the area of the well.

Quantitative RT-PCR of Cells in Constructs

Constructs were collected on D4 and D7 and frozen at -80ºC until processing. To process, Trizol (Fisher Scientific) was added to each sample and subsequently mechanically broken up using a S-250 Digital Sonifier (Branson Ultrasonics, Danbury, CT) set at 10% for 30 seconds. Samples were incubated at room temperature in chloroform (Sigma) for 3 minutes then centrifuged at 12000 x g and 4 ºC for 15 minutes. The clear aqueous phase of each sample was mixed isopropanol (Sigma), incubated, and centrifuged for 10 minutes at 12000 x g and 4 ºC. Pellets were resuspended in 75% ethanol and centrifuged again a 7,500 g for 5 minutes at 4ºC. Supernatant was discarded and samples were air dried before being resuspended in RNase free water. Next, RNA samples were incubated at 60ºC for 15 minutes and stored at -80ºC until use. cDNA was synthesized using 2 µL of RNA solution and Superscript III Synthesis System (Life Technology, Fisher) according to the manufacturer's protocol. A C100 Thermocycler (Bio-Rad, Hercules California) was to regulate temperature. Using SYBER GREEN PCR Mastermix (Life Technologies, Fisher) and an Applied Biosystems 7500 Fast PCR system, the cDNA was amplified. The cyclic threshold of peptidylproplyl isomerase A (PPIA), was used as a house keeping gene (Ct_{hk}) to calculate the relative expression of experimental samples' expression of target genes, smooth muscle actin (ACTA), transgelin (TGLN), smooth muscle myosin heavy chain (MHC), and caldesmin (CLDM). Melt curves were also examined to determine if dimerization contamination affected threshold values. If there were large degrees of dimer

contamination according to the melt curve, these samples were excluded from analysis. Experimental thresholds were compared to negative controls, ASCs expanded and cultured on plastic expansion flasks, using the ΔΔCt method. Expression levels were calculated assuming expression followed $x=2^{-\Delta\Delta Ct}$ where $\Delta\Delta Ct = \Delta Ct_{exp} - \Delta Ct_{negative\ control}$ and $\Delta Ct = Ct_{target\ gene} - Ct_{hk}$ (Wu, 2017). The forward and reverse primers were as follows; PPIA Forward Sequence: ACG TGG TAT AAA AGG GGC GG and Reverse Sequence: GTC TGC AAA CAG CTC AAA GGA G, ACTA Forward Sequence: TTG CCT GAT GGG CAA GTG AT and Reverse Sequence TAC ATA GTG GTG CCC CCT GA, TGLN Forward Sequence: AAC AGC CTG TAC CCT GAT GG and Reverse Sequence: CGG TAG TGC CCA TCA TTC TT, MHC Forward Sequence: TGC TTT CGC TCG TCT TCC and Reverse Sequence: CGG CAA CTC GTG TCC AAC, and CLDM Forward Sequence: AGA TTG AAA GGC GAA GAG CA and Reverse Sequence: TTC AAG CCA GCA GTT TCC TT.

Immunocytochemistry and analysis of samples

Constructs were collected on D7, washed 2x with PBS, and fixed with Z-fix (Anatech, Battle Creek, MI) for 10 minutes at 4ºC. Samples were washed 2x with PBS and permeabilized with 0.5% Triton X-100 (Sigma) for 20 minutes at room temperature. All samples were washed 2x more in PBS and kept at 4ºC until staining. When staining, primary antibodies against smooth muscle actin (SMA, Millipore: ABT1487, Burlington, MA), transgelin protein (SM22, Santa Cruz: 50446, Dallas, TX), and smooth muscle myosin heavy chain (MHC, Millipore: MAB3568) we dissolved in 10 mg BSA. Samples were incubated at room temperature in primaries for 2 hours at 1:200, 1:50, and 1:50 for anti-SMA, anti-SM22, and anti-MHC respectively. Sample were washed 2x in PBS and incubated in secondary for 1 hour at room temperature. 488 Alex Fluor anti-rabbit (1:200, ThermoFisher, A-11070) or 488 Alexa Fluor anti-mouse (1:250, ThermoFisher, A-11001)

were used for secondaries on SMA and SM22 or MHC respectively. DAPI (1:1000, Lifetech) was added to secondary stain as well. Secondaries and DAPI were washed off 2x with PBS in low light settings. Images were stored at 4ºC until imaging. Imaging was done on a Nikon A-1 Spectral Confocal Microscope (Melville, NY) maintaining exposure levels across all samples when imaging specific proteins. Analysis of images were carried out in ImageJ. Pixel intensities were summed across an image to obtain a "raw integrated intensity" value for each image. This value was normalized to the number of nuclei in the image to account for regional differences in the number of cells.

Statistical analysis

All data for bar graphs were plotted and statistically analyzed in R. ANOVA and Dunn's Method were used for post-hoc analyses to compare individual groups. If no significant differences were present, an asterisk and "NS" were noted in the top right corner. For bar graphs comparing different GF treatments on shape or gene expression, only significant differences between conditions at the same time point were indicated using a bar above the two conditions. Differences between growth factor treatments from different days were not indicated, regardless of significance. For bar graphs comparing the effects of stretch on shape or gene expression, only statistical differences between stretched and static controls were indicated (blue 'a' for Con, red 'b' for GF, and a green 'c' for LS). When comparing differences in proteins expression between different growth factor delivery treatments or comparing the effects of stretch, a letter was used to comparing static and stretched conditions (blue 'a' for Con, red 'b' for GF, and a green 'c' for LS) and a bar above conditions indicates statistical difference between growth factor treatment within the same mechanical loading treatment. Differences in gene expression or protein expression between growth factor delivery methods within either static or stretched conditions are indicated

145

by lines above significantly different methods. Again, static conditions with one growth factor delivery treatment were not compared to stretched samples with a different growth factor delivery treatment. All error bars are plus/minus the standard error of the mean.

5.3 – Results

Cell Shape

ASCs were seeded collagen hydrogels along with either no μspheres (Con), unloaded μspheres with growth factors in the media (GF), or with μspheres that had been loaded with growth factors (LS). At times points D4 or D7, the subset of the samples were stained collected for analysis including staining with Calcein to visualize the morphology of the cells, staining for protein, or collection for PCR. A portion of the remaining constructs were stretched for the next three days as described in the methods. On D7 the remainder of the constructs were collected for analysis. This process is outlined in Figure 5.1.
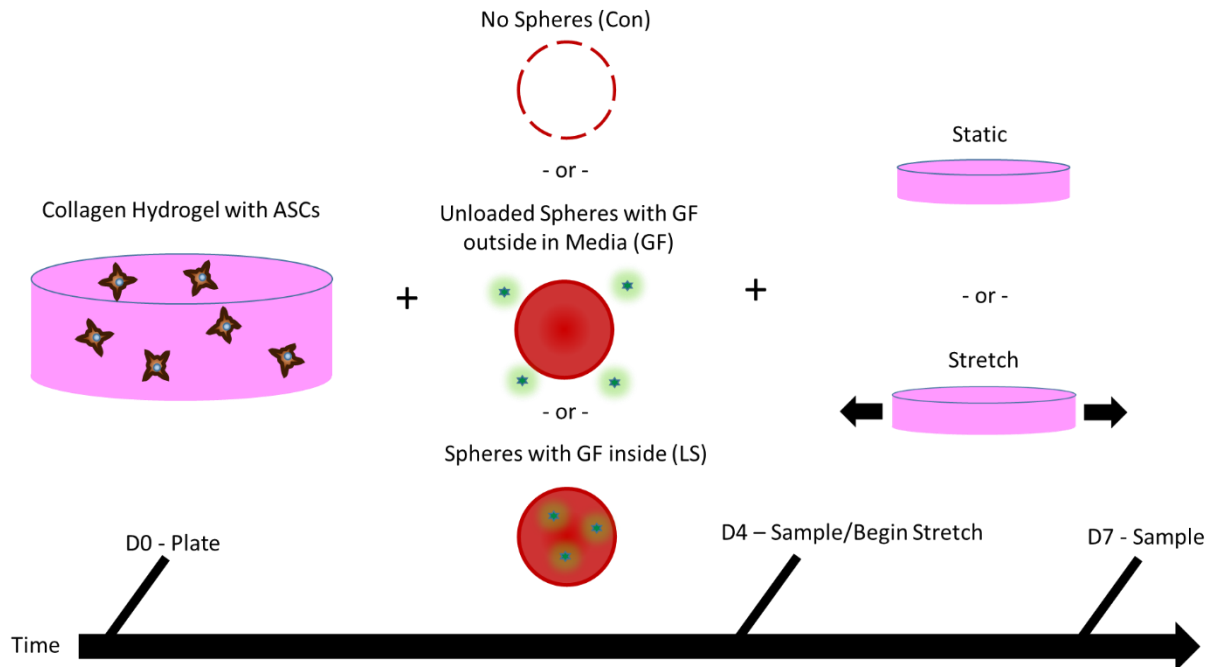
Figure 5.1: Methods for ASC Construct Production, Culture, and Sampling. Adipose derived stem cells (ASCs) were expanded and then seeded collagen hydrogels. The hydrogels were contained either no spheres (Con), unloaded control spheres (GF), or spheres loaded with growth factors (LS). For four days, the gels were cultured either in media containing no additional growth factor (Con), media containing growth factors and ascorbic acid (GF US, 5 ng/mL PDGF, 5 ng/mL TGFB, and 30 μM ascorbic acid), or media containing just ascorbic acid (LS, 30 μM ascorbic acid). On day 4 (D4) samples were collected and a subset of hydrogels fit in a bioreactor were stretched once a day for three days. On day 7 (D7) all remaining samples were collected for analysis.

Growth Factor Release from Genipin Crosslinked Gelatin μSpheres

Both 4U/mL and 5 U/mL of collagenase concentrations facilitated a semi-linear degradation of gelatin μspheres with 5 U/mL degrading about 7% of the mass per hour and 4 U/mL degrading about 5% of the mass an hour (Fig 5.2A). Loaded μspheres containing PDGF were degraded using 5 U/mL and release was gradual before plateauing around 4 hours (Fig 5.2B). When the release of PDGF from spheres was compared to control levels, PDGF release was similar to the negative controls (empty spheres) at D0 and reached around 50% of the positive control (growth factor in media) release by 4 hours (Fig 5.2C). Based on the degradation curve (Fig 5.2A), we could expect that the maximum amount of PDGF would be released after 30% of the loaded

spheres had been degraded. Comparing the release of TGFβ from loaded µspheres to controls, we see that immediate release of TGFβ from loaded spheres is comparable to negative controls but by 4 hours in collagenase, the release of TGFβ has also plateaued (Fig 5.2D). Like PDGF, it appears that by the time 30% of the spheres had been degraded, all TGFβ will have been released into solution. When ASCs were cultured with control spheres, degradation was linear and they degraded about 3% of the sphere mass per day (Fig 5.2E). This would imply that by D10, ASCs should degrade spheres enough to facilitate the maximum release of growth factors. To test if the growth factors would affect degradation, ASCs were cultured with the spheres and the mass of spheres degraded over time was measured. Regardless of how the cells were cultured with the growth factors, they accelerated degradation to around 6% of the mas per day (Fig 5.2F).
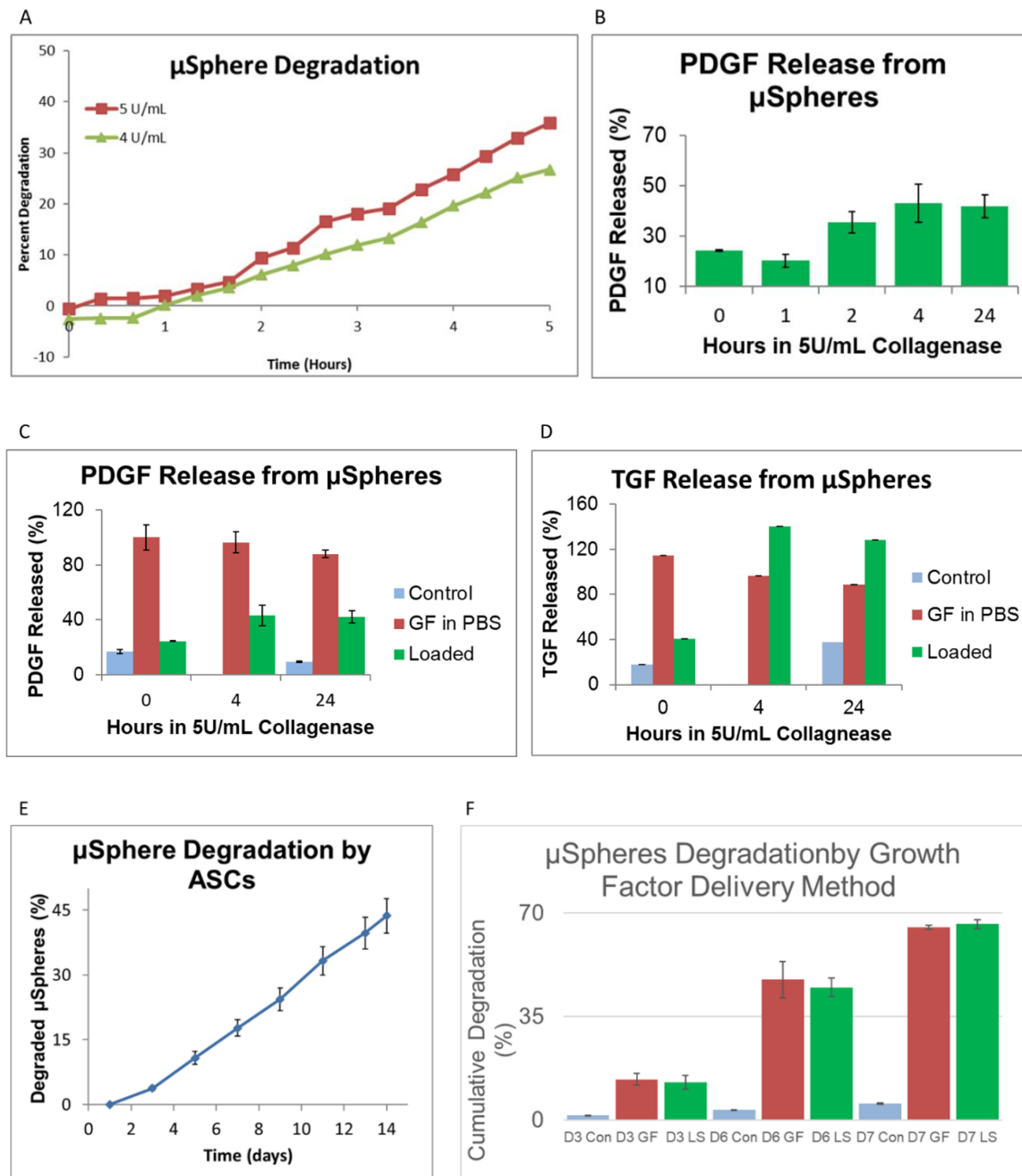
Figure 5.2: Growth Factor Release from µSpheres. When control spheres were kept in collagenase I they degraded at a linear rate dependent on enzyme concentration (A, n=5 for each time point) ELISAs were used to compare the release of PDGF (B and C, n=3 for each time point and concentration) or TGF (D, n=3 for each time point and concentration) from loaded µspheres (Loaded) being degraded in Collagenase. µSpheres with PDGF (Loaded) showed gradual release from µspheres through 4 hours where it plateaued having a similar amount released up through 24 hours (B). We compared this release against controls where PBS containing the same absolute amount of protein in the µspheres and same concentration of collagenase served as a positive control (GF in PBS) and empty control µspheres in the same concentration of collagenase served as a negative control (Control). The positive controls (Growth Factors in PBS) remained relatively constant, around 100%, throughout all time points and the negative control (Control) remained at baseline levels from the beginning to the end of the time course (C and D). µSpheres with PDGF (C) and TGFβ (D) initially showed baseline level concentrations of growth factor comparable to negative controls (Control) but by 4 hours, the highest amount of each had been released and this level was maintained throughout 24 hours of collagenase incubation (C and D). For PDGF this was about 45% of the amount loaded into the spheres (C) while TGFβ levels were higher than positive controls (D). When control spheres were cultured with ASCs in hydrogels (n=4 for time point), degradation was linear and it took

about 10 days to degrade 30% of the spheres (E). When growth factors were present either within the spheres (LS) or in the surrounding media (GF) ACS degraded over 35% by D6 but there were not differences in the levels of degradation of spheres between the two growth factor delivery methods (F, n= 5 for each condition and time point).

The Morphology of ASCs Differentiated Using Growth Factor Treatments and Mechanical Stretch

ASCs were cultured one of three growth factor treatments and after four days, a portion of these hydrogels were cyclically stretched once a day for 3 days. On D7, ASCs cultured in static conditions with growth factors, especially with the loaded µspheres, appear more spindle shaped than control cells. In particular, cells immediately adjacent to growth factor loaded spheres appear particularly SMC-like. When stretched, regardless of the growth factor treatment, all cells align with the axis of stretch (the horizontal plane in images, Fig 5.3). Stretched cells have fewer lateral projections and elongate along the axis of stretch. Differences between the different growth factor treatments of stretched cells are less obvious. These observations are quantified in the next section.
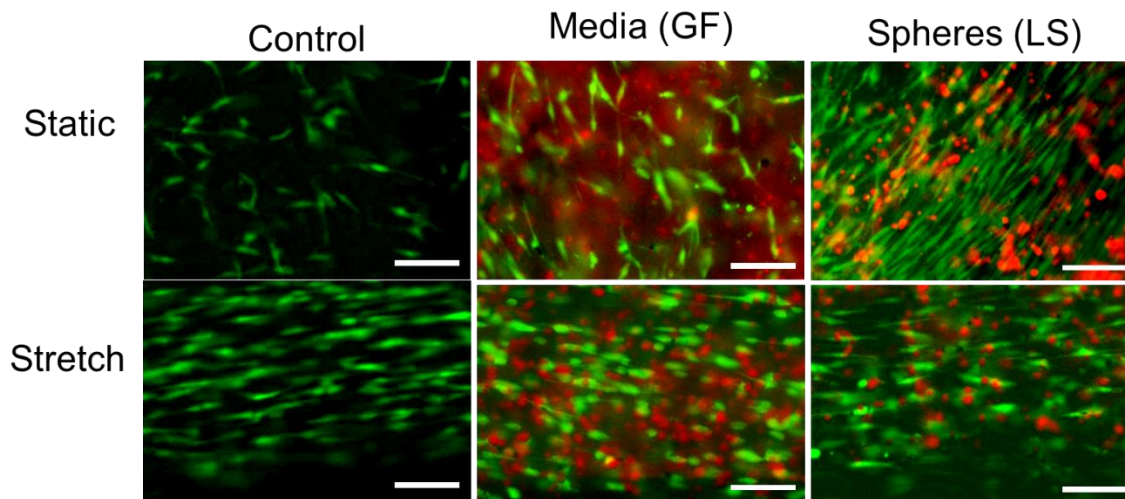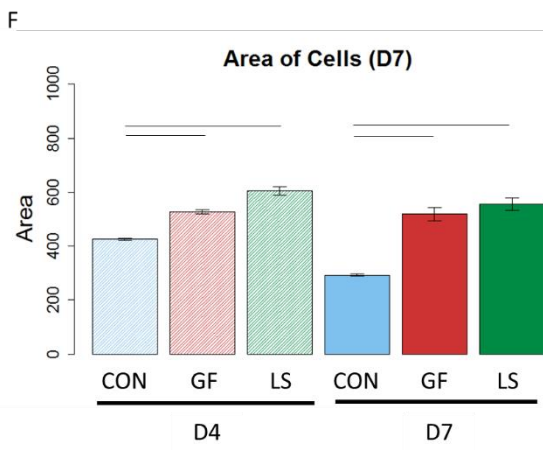

Figure 5.3: Morphology of ASCs Cultured with Different Mechanisms of Growth Factor Delivery in Either Static or Mechanically Stretched Culture (D7). ASCs were cultured with either no spheres (Control), with unloaded spheres and growth factor in the media (GF), or with spheres preloaded with PDGF and TGFβ (LS). A subset of these hydrogels were cyclically strained for 6 hours a day for 3 days starting on D4. When ASCs are cultured in static conditions, on D7, cells with growth factors appear more spindle and rod shaped than control cells with cells next spheres being particularly SMC-like. All cells appear more spindle like under stretched conditions but differences between growth factor treatments are more difficult to distinguish. Green indicates live ASC stained with Calcein, Red indicates µspheres (unloaded and loaded). Scale bar represents 50 µm.

150

The Shape of ASCs Differentiated Using Growth Factor Treatments

ASCs with growth factor loaded µspheres (LS) were the most round on D4 followed by ASCs with unloaded µspheres and growth factors in the media (GF) and Con ASCs being the least round. By D7, the Con ASCs were the most round and LS ASCs were the least round (Fig 5.4A, $p<0.05$). The aspect ratio gave a similar description of morphology as the trends of its values were reversed. Con ASCs had the highest aspect ratios followed by GF ASCs and then LS ASCs on D4 but by D7, the ranking was completely reversed and LS ASCs had the highest aspect ratio (Fig 5.4B, $p<0.05$). On D4, GF ASCs had the lowest circularity followed by LS ASCs and then Con ASCs but by D7, ASCs from the LS condition the lowest circularity (Fig 5.4C, $p<0.05$). LS ASCs had the highest projection factor values followed by GF ASCs and then Con ASCs on both D4 and D7 (Fig 5.4D, $p<0.05$). Initially on D4, GF ASCs had the highest length and LS ASCs were the shortest but by D7, LS ASCs were significantly longer than Con ASCs and GF ASCs (Fig 5.4E, $p<0.05$). GF ASCs and LS ASCs had larger areas than Con ASCs at both time points (Fig 5.4, $p<0.05$). In summary, on D7, delivery of growth factors, and especially through the µspheres, prduced the most SMC-like morphology. At D4 these trends were less consistent, as cells in growth factors were more spread and larger but were less polarized.

A — Roundness of Cells (D7)

B — AR of Cells (D7)

C — Circularity of Cells (D7)

D — PF of Cells (D7)

E — Length of Cells (D7)

F — Area of Cells (D7)
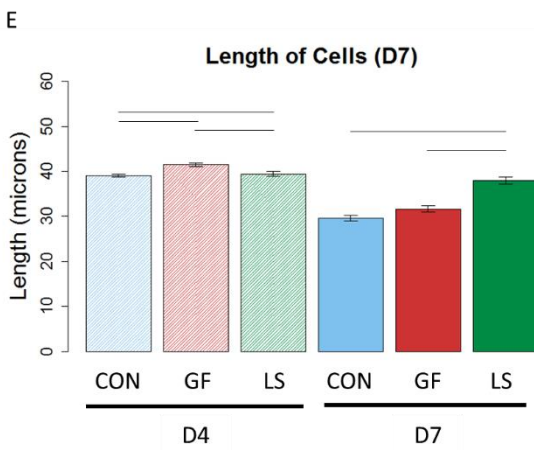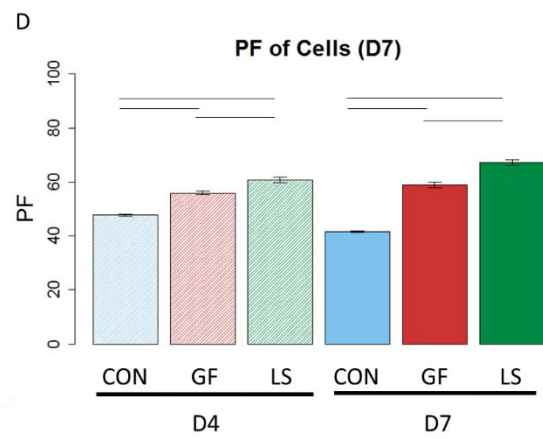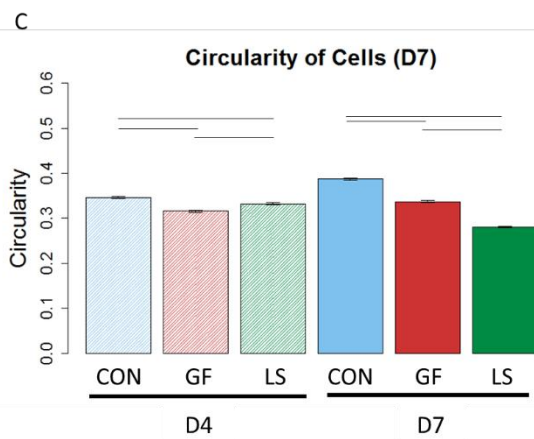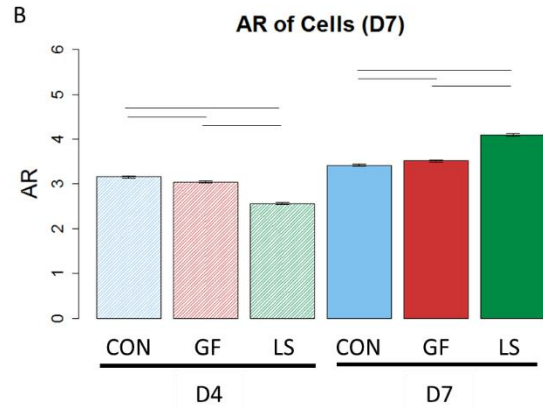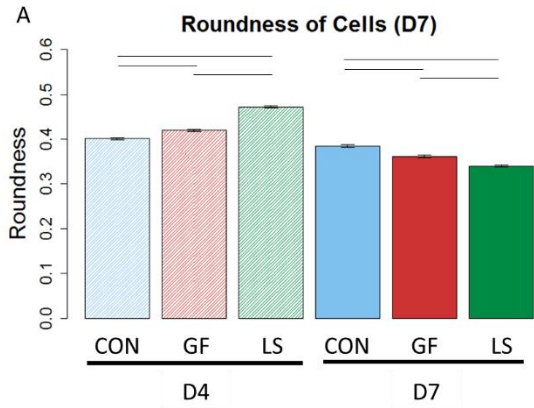
G

n for each condition by day	D4		D7	
	n	cells	n	cells
Con	7	1786	8	2674
GF	8	2998	7	3913
LS	9	3075	9	3244

152

Figure 5.4: The Shape of ASCs Differentiated with Different Growth Factor Delivery Methods. On D4, ASCs with loaded µsphere (LS) were the most round followed by ASCs with growth factor in the media (GF) and then ASCs with no growth factor (Con) but by D7, these rankings were the complete reversed (A, p<0.05). Con ASCs had the highest aspect ratios on D4, followed by GF ASCs and then LS ASCs but by D7, the order had completely reversed (B, p<0.05). On D4, Con ASCs had the highest circularity followed by LS ASCs and then GF ASCs but after 7 days, LS ASCs had lower circularity than GF ASCs (C, p<0.05). LS ASCs had the highest projection factor followed by GF ASCs and then Con ASCs on both D4 and D7 (D, p<0.05). GF ASCs were the longest and LS ASCs were the shortest on D4, but by D7, LS ASCs were significantly longer than Con ASCs and GF ASCs (E, p<0.05). GF ASCs and LS ASCs were larger in area than Con ASCs on D4 and D7 (F, p<0.05). Blue bars represent control gels with no growth factors, red bars represent gels with unloaded µspheres and growth factor in the media, and green bars represent gels with growth factors in loaded µspheres. Lighter bars with striated pattern represent samples from D4 and solid bars with darker tones represent samples from D7. Lines ending above conditions indicate statistical differences between growth factor conditions (p<0.05). Panel G indicates the number of biological replicates and the numbers of cells from each condition.

The Compaction of Constructs Cultured with Different Growth Factor Treatments

All contructs started compacting after a single day in culture. Constructs with growth factor loaded spheres (LS) had already compacted to about 10% of their original area while constructs with growth factor in the media (GF) had compacted to less than 40% of their original volume and control constructs with no growth factor had compacted down to less than 75% (Fig 5.5). Starting on D2 both gels delivery methods of growth factor induced statistically similar compaction but were both more compacted than the Con gels (Fig 5.5). The Con gel contnued to compact until it was statistically similar to the growth factors gels on D5 (Fig 5.5). By D6, all contructs had compacted to about 10% of their original area.

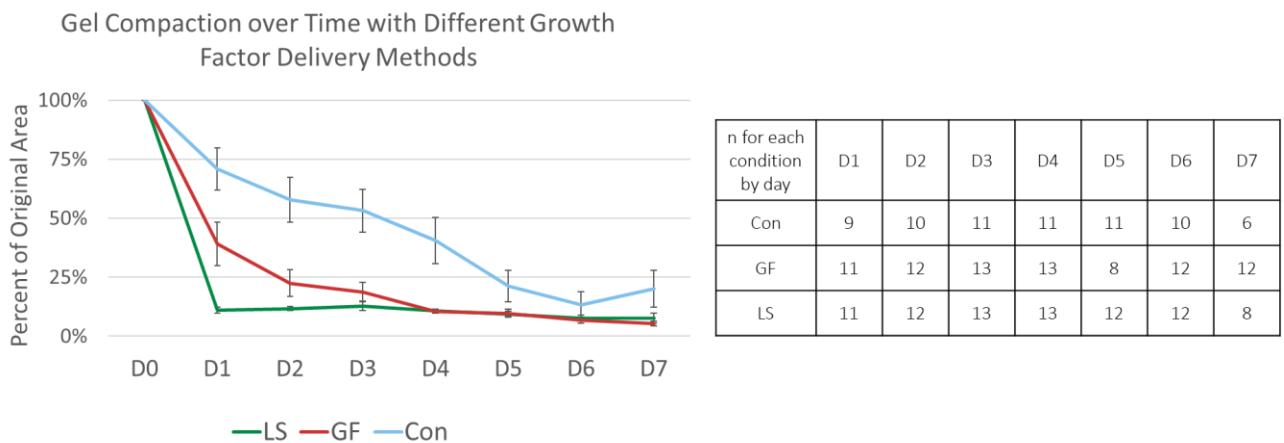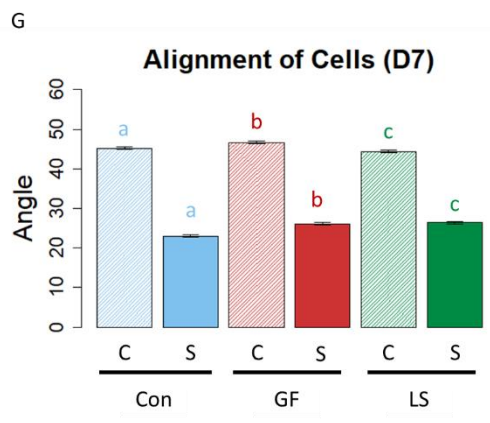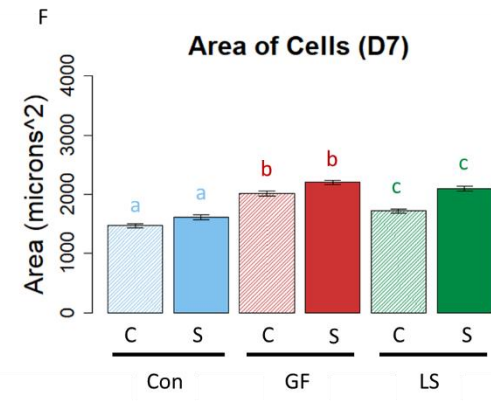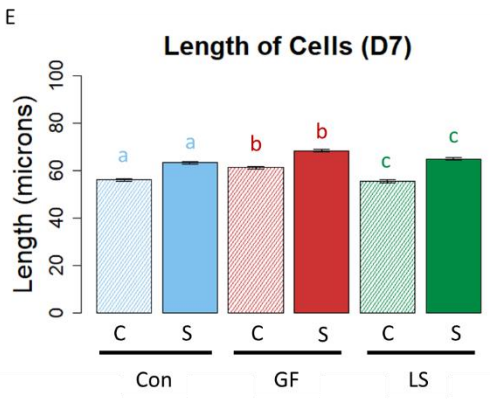

n for each condition by day	D1	D2	D3	D4	D5	D6	D7
Con	9	10	11	11	11	10	6
GF	11	12	13	13	8	12	12
LS	11	12	13	13	12	12	8

Figure 5.5: Compaction of Gels with Different Growth Factor Delivery Treatments. By D1, constructs with growth factors loaded into the µspheres (LS) were more compacted than constructs with growth factor in the media (GF) which were more compacted than gels without any treatment (Con) (p<0.05). By D2 LS and GF were statistically similar but they were both still statistically more compacted than the Con until D5. The blue line represents control gels with no growth factors, the red line represents gels with unloaded µspheres and growth factor in the media, and green line represents gels with growth factors in loaded µspheres. The table displays the number of samples measured from each condition at each time point.

The Shape of ASCs Cultured with Growth Factor Treatments and Mechanical Stretch

In corroboration of the cell morphologies seen in Fig 5.3, ASCs from stretched contructs were less round than their statically cultured counterparts regardless of growth factor delivery treatment (Fig 5.6A, p<0.05). Stretched cells also had higher aspect ratios than static ASCs with every growth factor treatment (Fig 5.6B, p<0.05). Stretched Con ASCs and LS ASCs had higher projection factors than those in static culture, however with GF constructs, static cells had higher projection factors than stretched cells (Fig 5.6C, p<0.05). ASC circularity from cells in stretched conditions was significantly lower than that of static conditions for all growth factor conditions (Fig 5.6D, p<0.05) and both the length (Fig 5.6E) and area (Fig 5.6F) of cells in stretched samples were higher than their statically cultured counterparts (p<0.05). ASCs from all growth factor treatments were more aligned when their constructs were stretched (Fig 5.6G, p<0.05).

A — Roundness of Cells (D7)
B — Aspect Ratio of Cells (D7)
C — PF of Cells (D7)
D — Circularity of Cells (D7)
E — Length of Cells (D7)
F — Area of Cells (D7)
G — Alignment of Cells (D7)
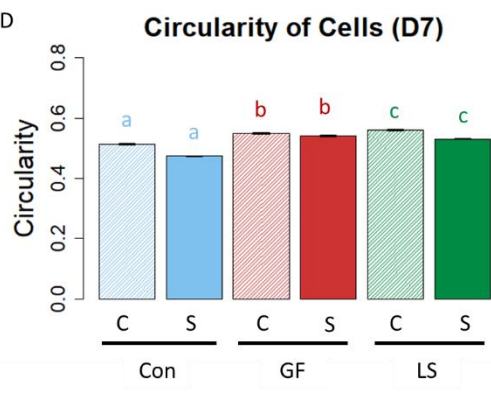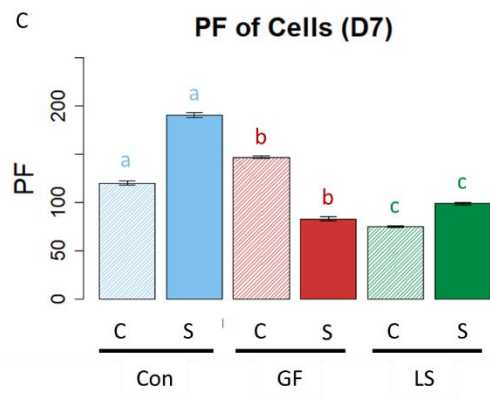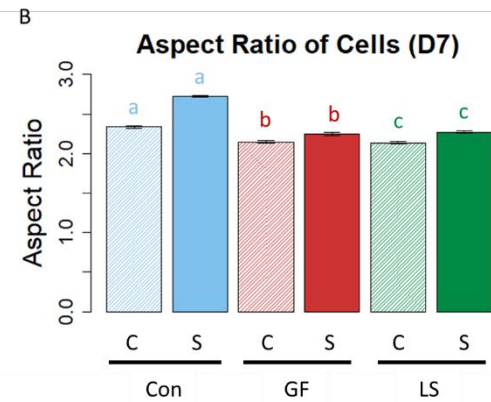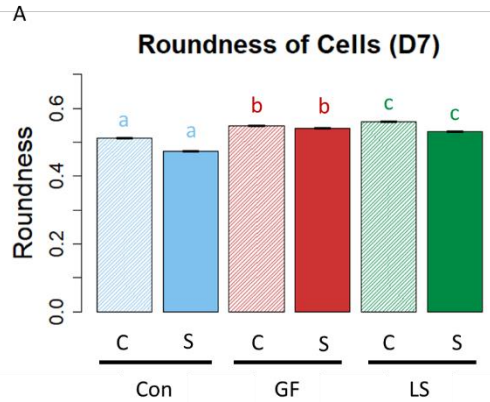
H

Growth Factor	Control		GF		LS	
Stretch or Static	C	S	C	S	C	S
n	10	6	9	6	10	11
Cells	6583	3377	4096	3158	4802	5480

155

Figure 5.6: The Shape of ASCs in Mechanically Stretched Constructs Compared to Statically Cultured Constructs. Regardless of growth factor delivery treatment, ASCs from stretched constructs were less round than their statically cultured counterparts (A, p<0.05). Stretched ASCs also had higher aspect ratios than static ASCs regardless of treatment (B, p<0.05). Stretched ASCs in control conditions (Con) and with loaded spheres (LS) had higher projection factors than their static counterparts but with constructs with growth factor in the media, static cells had higher projection factors than stretched cells (C, p<0.05). The circularity of cells from stretched conditions was significantly lower than those of static conditions regardless of growth factor treatment (D, p<0.05) and the length (E) and area (F) of ASCs from stretched samples were also higher than those from static cultures (p<0.05). For all growth factor treatments, ASCs from stretched constructs were more aligned than their static counterparts (G, p<0.05). Blue bars represent control gels with no growth factors, red bars represent gels with unloaded μspheres and growth factor in the media, and green bars represent gels with growth factors in loaded μspheres. Lighter bars with striated pattern represent unstretched controls and solid bars with darker tones represent stretched samples. Letters above bars indicate significant differences between static and stretched gels with the same growth factor delivery (p<0.05). Panel H indicates the number of biological replicates and the numbers of cells from each condition.

The Expression of Smooth Muscle-Associated Proteins by ASCs Cultured with Growth Factor Treatments and Mechanical Stretch

Constructs were stained for SMA, TGLN protein (SM22), and MHC (Fig 5.7). These proteins were chosen as indicators of early, intermediate, and late differentiation, respectively. SMA and MHC are particularly inportant for force production while TGLN modulates the contractile aparatus. Constructs that were cultured with growth factors (GF and LS) had increased SMA expression in statically cultured gels compared to Con gels (Fig 5.8A, p<0.05). After stretch, constructs with GF expressed less SMA than Con or LS samples (Fig 5.8A, p<0.05). Control samples that were stretched increased SMA expression over static controls but stretched GF constructs had less SMA expression than static GF cultures (Fig 5.8A, p<0.05). Without stretch, LS constructs expressed lower TGLN protein than Con samples but after LS consucts were stretched they expressed more TGLN protein than static LS samples and more TGLN protein than stretched Con samples (Fig 5.8B, p<0.05). MHC protein expression was higher in LS samples than controls whether or not they were stretched (Fig 5.8C, p<0.05). Stretched LS samples and stretched Con samples had higher MHC protein expression than the static counterparts receiving the same growth factor delivery (Fig 5.8C, p<0.05).

A

	Con	Growth Factor	Spheres
Static			
Stretch			

B

	Con	Growth Factor	Spheres
Static			
Stretch			

157
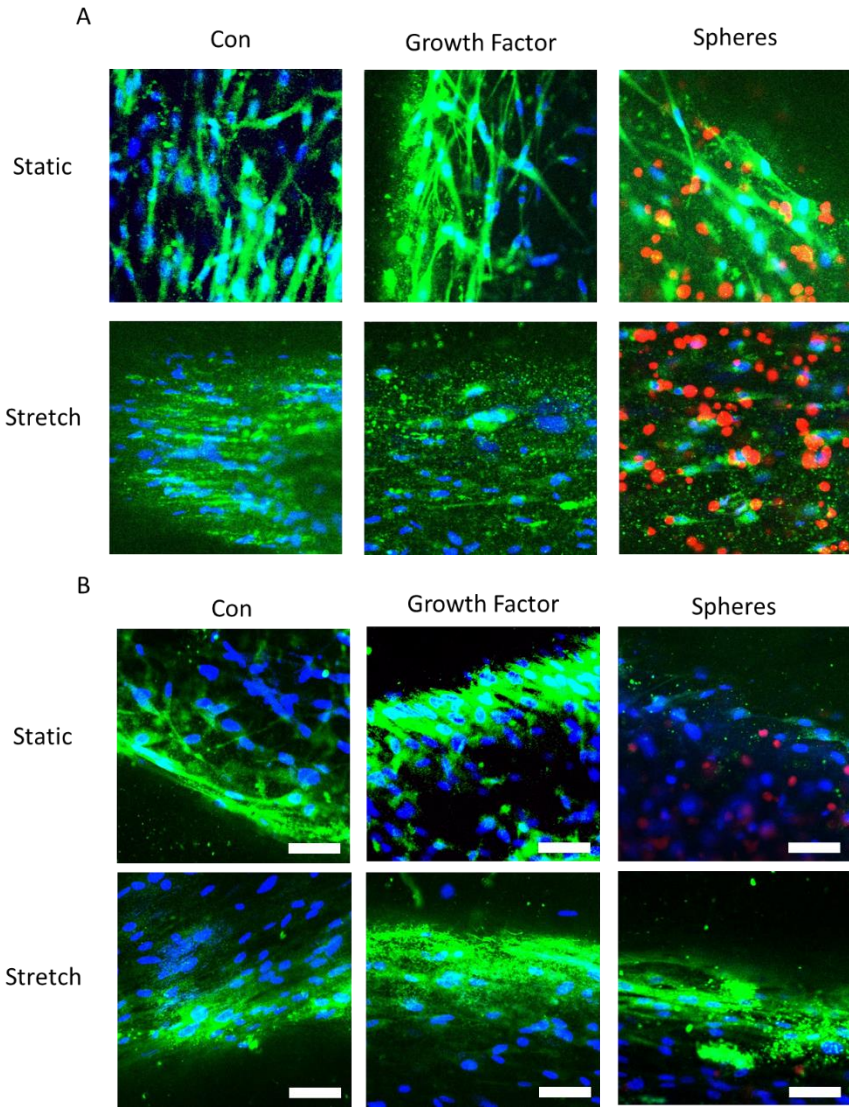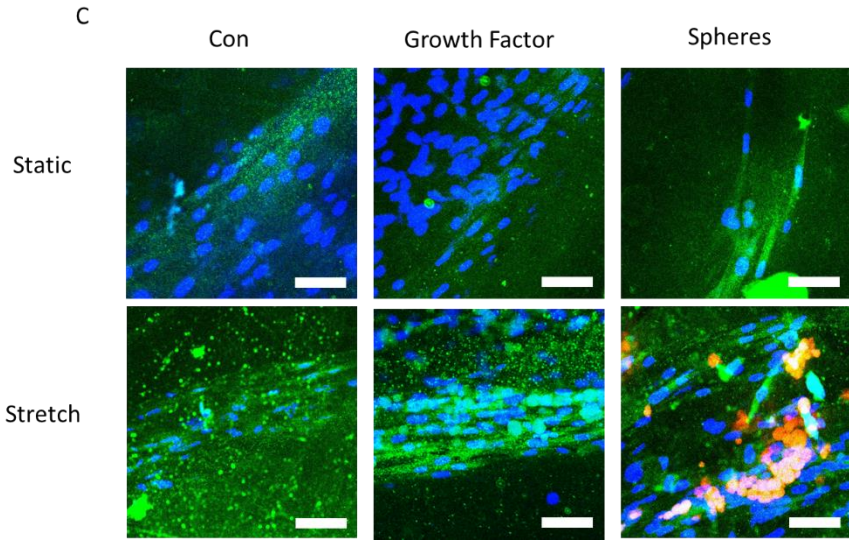
Figure 5.7: SMC Protein Expression of ASC from Gels Cultured in Different Dimensions and Concentrations of Collagen. ASCs were cultured without growth factor, with growth factor in the media, or with µspheres to deliver growth factor. A subset were stretched for three consecutive days and all gels were stained on D7 for SMA (A), TGLN protein (SM22, B), or MHC protein (C) (all green). Nuclei were stained with DAPI (blue). Loaded spheres (red can be seen in some images. Scale bars represent 50 µm.
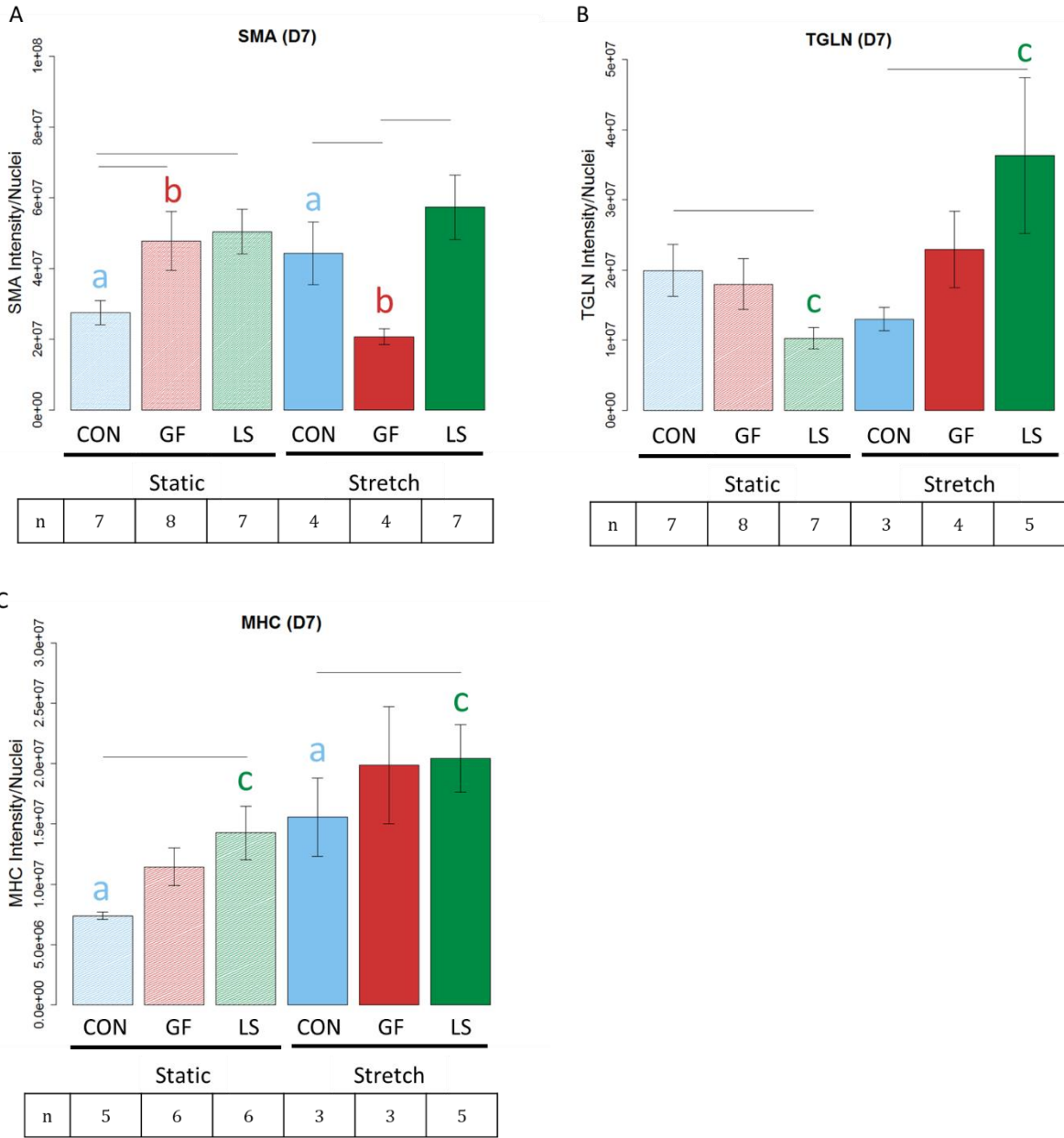
Figure 5.8: Expression of Smooth Muscle Protein from ASCs in Mechanically Stretched Constructs Compared to Statically Cultured Constructs and Differentiated with Different Growth Factor Delivery Methods. (D7). Treatment with growth factors (GF and LS) increased SMA expression in statically cultured gels (A, $p<0.05$). When constructs were stretched, constructs with GF expressed less SMA than Con or LS (A, $p<0.05$). Stretching the constructs increased SMA expression in Con treatments but decreased it GF treatments (A, $p<0.05$). In static conditions LS samples expressed lower TGLN protein than Con samples but stretched LS samples expressed more TGLN protein than static LS samples and more TGLN protein than stretched Con samples (B, $p<0.05$). LS samples expressed more MHC protein than controls whether they were both cultured in static conditions or both stretched (C, $p<0.05$). Stretched LS samples and stretched Con samples expressed more MHC protein than their respective static counterparts (C, $p<0.05$). Blue bars represent control gels with no growth factors, red bars represent gels with unloaded μspheres and growth factor in the media, and green bars represent gels with growth factors in loaded μspheres. Lighter bars with striated pattern represent unstretched controls and solid bars with darker tones represent stretched samples. Lines ending above conditions indicate statistical differences between growth factor conditions and colored letters above bars indicate significant differences between static and stretched gels with the same growth factor delivery ($p<0.05$).

159

5.4 – Discussion

Our goals in this study were to elucidate the effects of growth factors and their delivery methods on ASC differentiation toward SMCs, examine how mechanical stimulation worked in tandem with growth factors, and if the changes in ASC shape throughout this process could be quantified and used to validate the transition.

Since we intended to compare delivery of growth factors from μspheres to standard delivery through media, our first task in this study was to examine the release of growth factors from the μspheres as they degrade. We found that both collagenase concentrations produced linear degradation rates providing a model system to correlate degradation with growth factor release. This was similar to earlier work in our group where we developed μspheres for other applications [38]. When loading the μspheres with PDGF and degrading them in collagenase, we found PDGF released slowly and the total amount recovered plateaued at around 45% of the loaded growth factor. When μspheres were loaded with TGFβ and degraded with collagenase, growth factor was released more quickly and to a higher degree. In fact, we measured more TGFβ than we loaded into the spheres, a practical impossibility. Some of this excess signal may be background caused by the gelatin degrading. It could also be that the collagenase or another enzymatic process degraded the growth factor and multiplied the epitopes producing signal during the assay. While worth questioning, the absolute amount we recovered was irrelevant: Based on the negative and positive controls, the μspheres would release TGFβ as they degraded and the maximum level of release would occur by 4 hours in collagenase.

We next measured the degradation of the μspheres directly in collagenase and found that by 4 hours, 30% of the μspheres' mass had been degraded. This implied that if and when cells degraded 30% of the μsphere mass, the maximum amount of growth factor would be released from

the spheres. This release profile of PDGF is similar to that of VEGF from this µsphere system (60% recovery of the growth factor after 40% of the mass had been degraded) and was much faster release than BMP2 (80% recovered after 100% of the mass had dissolved) [38]. Based on the degradation of the µspheres by cells, this release may be too slow or too fast. This kinetics could be altered through using gelatin B [38] or by changing the extent of crosslinking [37]. We found that 30% of empty spheres would be degraded ASCs after 9 days in culture but by exposing them to growth factor (either through the media or in the spheres themselves) 35% of the mass would be degraded by D6. This meant that when we induced differentiation, the maximum release from the spheres would occur around D6. This increased rate of degradation is likely due to growth factor mediated upregulation of matrix metalloproteinases [60]. ELISAs to confirm release by cell mediated degradation were not run based on the fact the cells secrete and absorb growth factors which would confound the results. By running these experiments, we confirmed that we could load µspheres with exogenous growth factor and after 6 days with ASCs the spheres would be degraded enough to release the maximum amount of growth factor.

Next, we asked whether growth factor delivery and, more specifically, the method of delivery, enhanced the differentiation of these ASCs toward a SMC morphology. By D7, growth factor treatments induced an SMC-like morphology as quantified by our shape factors. This is consistent with previous findings as growth factors have been qualitatively observed to increase the size [32,33,61–63] and polarization [25,32,62,63] of cells. Our data also suggest that the localized and sustained delivery of growth factors are more effective at producing this phenotype than delivery through media, a trend consistent with induction of other lineages from µsphere studies [64]. The delayed polarization from the conditions with loaded or control spheres may have been due cells'

161

natural attraction to the spheres [37] and the cells may have needed to partially degrade the spheres before taking on an elongated and polarized morphology.

After examining the effects of growth factors on shape, we asked how these new methods impacted the expression of four smooth muscle genes. We discuss the results in Appendix C but ultimately our findings were inconclusive. According to literature, growth factors and differentiation media increase expression of smooth muscle genes [27,28,32,33,61,63,65]. There are two explanations that might reconcile this discrepancy with our work. It is possible that our growth factors are inducing a synthetic SMC phenotype. Other groups have shown that overexposure of TGFβ causes downregulation in smooth muscle genes and an increase in collagen gene expression [30,66]. However, this would also result in a less contractile cell population with lower SMC protein as well. The ASCs exposed to growth factors in this study were functional (they compacted the hydrogels) and they expressed more SMC protein than control samples. These biochemical markers and functional activity in combination with the morphometric data suggest that we are inducing a more SMC-like phenotype. To confirm this theory in future studies, collagen expression could also be measured. Alternatively, a second conjecture, is that our time points for testing expression failed to capture the temporal upregulation of SMC genes. Our group has shown that this combination of growth factors induces peak expression of ACTA, TGLN, and CNN genes on D14 before dropping at later time points [27]. This was shown on bone marrow MSCs cultured with 2D substrates. MHC gene expression peaked even earlier, by D7 [27]. If our protocol accelerates this timeline, we may have missed the phase of upregulation. Some protocols induce peak expression as early as D1 [31] and Xu et al found that mesenchymal stem cells from teeth treated with TGFβ peaked with their expression of SMC genes at D5 before dropping at D7 [67]. Based on higher protein expression in 3D of control gels compared to cells on 2D gels in earlier studies, it is possible that

ASCs in 3D exposed to growth factors expressed more SMC genes at earlier time point that we did not sample before being downregulated.

If the cells exposed to growth factors were differentiating earlier and to a greater degree than controls, that should be reflected in their protein expression and function of the constructs. Multiple groups have demonstrated increased compaction in gels with cells exposed to growth factors [26,32]. Our study showed that growth factors increased compaction after a single day in culture. To promote this activity, the contractile apparatus of the SMC-like ASCs would already need to be established and the protein would need to have already been expressed. Other groups have seen increased SMA, CNN, SM22, CDLM, and MHC protein in response to growth factors [25–28,31–34,36,61,63,67,68]. We saw increased protein expression of SMA and MHC in constructs with growth factor despite having lower gene expression. This would imply that at some point, these genes were upregulated and these constructs already passed through early stages of differentiation.

Our final objective in this study was to examine how cyclic strain influenced the differentiation of ASCs into SMCs, especially when applied in combination with growth factors. Stretch has also been documented to reduce the synthetic SMC phenotype and induce a contractile phenotype [49]. Like with growth factors delivery, we first examined cell shape. We found that stretch enhanced the size, polarity, spreading, and alignment of ASCs into a more SMC-like morphology regardless of which growth factor treatment they received. Although rarely quantified, other groups have also found that stretch increased cell length [40,47–49,69], area [40,69], polarization [19,45,48] and alignment [19,40,45–49]. We also examined SMC genes after 3 days of stretch and found that ACTA, TGLN, and MHC, were all lower in the stretched constructs compared to their static controls with the same growth factor treatment. Contradictory to these findings, other groups have shown that stretch increased SMC genes [42,45] and combinations of growth factor and stretch

maximized SMC differentiation [19]. The lack of SMC gene expression after stretch is likely the same reason for otherwise more SMC-like cells in static conditions. It could be that stretch induced a synthetic SMC phenotype or it could be that our sampling simply failed to catch the earlier upregulation and subsequent downregulation of the process. The latter theory was again support by our protein data where stretched samples generally had higher protein signals than their static counterparts.

While shape and protein data supported the beneficial effects of growth factors and stretch (especially through localized delivery in μspheres), the influence of these two stimuli on SMC gene expression is less clear. As protein production and compaction are "functional" endpoints of differentiation, these results suggest that ASC differentiation into SMCs can be augmented by administration of growth factors and stretch, and that the morphological changes throughout this process can be quantified and are strong indications as to the extent of differentiation. In the future, further research is needed to better understand ASC differentiation, its timeline through the process, and their potential uses in development of SMC therapies and regeneration.

5.5 – References

1. Arias E, Heron M, Tejada-Vera B. United States life tables eliminating certain causes of death , 1999-2001 . PubMed Commons. *Natl Vital Stat*. 2014;61(9):1-128.

2. Hart ML, Neumayer KMH, Vaegler M, et al. Cell-based therapy for the deficient urinary sphincter. *Curr Urol Rep*. 2013;14(5):476-487. doi:10.1007/s11934-013-0352-7.

3. Lindroos B, Suuronen R, Miettinen S. The Potential of Adipose Stem Cells in Regenerative Medicine. *Stem Cell Rev Reports*. 2011;7(2):269-291. doi:10.1007/s12015-010-9193-7.

4. Fang B, Song Y, Liao L, Zhang Y, Zhao RC. Favorable Response to Human Adipose Tissue-Derived Mesenchymal Stem Cells in Steroid-Refractory Acute Graft-Versus-Host Disease. *Transplant Proc*. 2007;39(10):3358-3362. doi:10.1016/j.transproceed.2007.08.103.

5. Cawthorn WP, Scheller EL, MacDougald OA. Adipose tissue stem cells: The great WAT hope. *Trends Endocrinol Metab*. 2012;23(6):270-277. doi:10.1016/j.tem.2012.01.003.

6.   Dai R, Wang Z, Samanipour R, Koo K, Kim K. Adipose-Derived Stem Cells for Tissue Engineering and Regenerative Medicine Applications. *Stem Cells Int*. 2016;2016:1-19. doi:10.1155/2016/6737345.

7.   Halvorsen YDC, Bond A, Sen A, et al. Thiazolidinediones and glucocorticoids synergistically induce differentiation of human adipose tissue stromal cells: Biochemical, cellular, and molecular analysis. *Metabolism*. 2001;50(4):407-413. doi:10.1053/meta.2001.21690.

8.   Helder MN, Knippenberg M, Klein-Nulend J, Wuisman PIJM. Stem Cells from Adipose Tissue Allow Challenging New Concepts for Regenerative Medicine. *Tissue Eng*. 2007;13(8):1799-1808. doi:10.1089/ten.2006.0165.

9.   Gao L, Mcbeath R, Chen CS. Stem Cell Shape Regulates a Chondrogenic versus Myogenic Fate through Rac1 and N-cadherin. *Stem Cells*. 2010;28(3):564-572. doi:10.1002/stem.308.Stem.

10.   Iyyanki T, Hubenak J, Liu J, Chang EI, Beahm EK, Zhang Q. Harvesting technique affects adipose-derived stem cell yield. *Aesthetic Surg J*. 2015;35(4):467-476. doi:10.1093/asj/sju055.

11.   Li R, Liang L, Dou Y, et al. Mechanical stretch inhibits mesenchymal stem cell adipogenic differentiation through TGFβ1/Smad2 signaling. *J Biomech*. 2015;48(13):3665-3671. doi:10.1016/j.jbiomech.2015.08.013.

12.   Furuhata Y, Yoshitomi T, Kikuchi Y, Sakao M, Yoshimoto K. Osteogenic Lineage Commitment of Adipose-Derived Stem Cells Is Predetermined by Three-Dimensional Cell Accumulation on Micropatterned Surface. *ACS Appl Mater Interfaces*. 2017;9(11):9339-9347. doi:10.1021/acsami.6b15688.

13.   Lim S, Cho H, Lee E, et al. Osteogenic stimulation of human adipose-derived stem cells by pre-treatment with fibroblast growth factor 2. *Cell Tissue Res*. 2016;364(1):137-147. doi:10.1007/s00441-015-2311-8.

14.   Estes BT, Wu AW, Guilak F. Potent induction of chondrocytic differentiation of human adipose-derived adult stem cells by bone morphogenetic protein 6. *Arthritis Rheum*. 2006;54(4):1222-1232. doi:10.1002/art.21779.

15.   Kabiri A, Esfandiari E, Hashemibeni B, Kazemi M, Mardani M, Esmaeili A. Effects of FGF-2 on human adipose tissue derived adult stem cells morphology and chondrogenesis enhancement in Transwell culture. *Biochem Biophys Res Commun*. 2012;424(2):234-238. doi:10.1016/j.bbrc.2012.06.082.

16.   Choi SA, Lee JY, Wang KC, et al. Human adipose tissue-derived mesenchymal stem cells: Characteristics and therapeutic potential as cellular vehicles for prodrug gene therapy against brainstem gliomas. *Eur J Cancer*. 2012;48(1):129-137. doi:10.1016/j.ejca.2011.04.033.

17.   Choi YS, Matsuda K, Dusting GJ, Morrison WA, Dilley RJ. Engineering cardiac tissue in

vivo from human adipose-derived stem cells. *Biomaterials*. 2010;31(8):2236-2242. doi:10.1016/j.biomaterials.2009.11.097.

18. Desiderio V, De Francesco F, Schiraldi C, et al. Human Ng2+ adipose stem cells loaded in vivo on a new crosslinked hyaluronic acid-lys scaffold fabricate a skeletal muscle tissue. *J Cell Physiol*. 2013;228(8):1762-1773. doi:10.1002/jcp.24336.

19. Lee W-CC, Maul TM, Vorp DA, Rubin JP, Marra KG. Effects of uniaxial cyclic strain on adipose-derived stem cell morphology, proliferation, and differentiation. *Biomech Model Mechanobiol*. 2007;6(4):265-273. doi:10.1007/s10237-006-0053-y.

20. Heydarkhan-Hagvall S, Schenke-Layland K, Yang JQ, et al. Human adipose stem cells: A potential cell source for cardiovascular tissue engineering. *Cells Tissues Organs*. 2008;187(4):263-274. doi:10.1159/000113407.

21. Harris LJ, Abdollahi H, Zhang P, McIlhenny S, Tulenko TN, DiMuzio PJ. Differentiation of adult stem cells into smooth muscle for vascular tissue engineering. *J Surg Res*. 2011;168(2):306-314. doi:10.1016/j.jss.2009.08.001.

22. Moses HL, Roberts AB, Derynck R. The Discovery and Early Days of TGF-β: A Historical Perspective. *Cold Spring Harb Perspect Biol*. 2016;8(7):a021865. doi:10.1101/cshperspect.a021865.

23. Solorio LD, Dhami CD, Dang PN, Vieregge EL, Alsberg E. Spatiotemporal regulation of chondrogenic differentiation with controlled delivery of transforming growth factor-β1 from gelatin microspheres in mesenchymal stem cell aggregates. *Stem Cells Transl Med*. 2012;1(8):632-639. doi:10.5966/sctm.2012-0039.

24. Solorio LD, Phillips LM, Mcmillan A, et al. Spatially Organized Differentiation of Mesenchymal Stem Cells within Biphasic Microparticle-Incorporated High Cell Density Osteochondral Tissues. *Adv Healthc Mater*. 2015;4(15):2306-2313. doi:10.1002/adhm.201500598.

25. Williams C, Xie AW, Emani S, et al. A Comparison of Human Smooth Muscle and Mesenchymal Stem Cells as Potential Cell Sources for Tissue-Engineered Vascular Patches. *Tissue Eng Part A*. 2012;18(9-10):986-998. doi:10.1089/ten.tea.2011.0172.

26. Park WS, Heo SC, Jeon ES, et al. Functional expression of smooth muscle-specific ion channels in TGF- 1-treated human adipose-derived mesenchymal stem cells. *AJP Cell Physiol*. 2013;305(4):C377-C391. doi:10.1152/ajpcell.00404.2012.

27. Brun J, Lutz KA, Neumayer KMH, et al. Smooth Muscle-Like Cells Generated from Human Mesenchymal Stromal Cells Display Marker Gene Expression and Electrophysiological Competence Comparable to Bladder Smooth Muscle Cells. *PLoS One*. 2015:1-21. doi:10.1371/journal.pone.0145153.

28. Brun J, Abruzzese T, Rolauffs B, Aicher WK, Hart ML. Choice of xenogenic-free expansion media significantly influences the myogenic differentiation potential of human bone marrow-derived mesenchymal stromal cells. *Cytotherapy*. 2016;18(3):344-359.

doi:10.1016/j.jcyt.2015.11.019.

29. Parvizi M, Bolhuis-Versteeg LAM, Poot AA, Harmsen MC. Efficient generation of smooth muscle cells from adipose-derived stromal cells by 3D mechanical stimulation can substitute the use of growth factors in vascular tissue engineering. *Biotechnol J*. 2016;11(7):932-944. doi:10.1002/biot.201500519.

30. Yang L, Geng Z, Nickel T, et al. Differentiation of human induced-pluripotent stem cells into smooth-muscle cells: Two novel protocols. *PLoS One*. 2016;11(1):1-11. doi:10.1371/journal.pone.0147155.

31. Jeon ES, Moon HJ, Lee MJ, et al. Sphingosylphosphorylcholine induces differentiation of human mesenchymal stem cells into smooth-muscle-like cells through a TGF- -dependent mechanism. *J Cell Sci*. 2006;119(23):4994-5005. doi:10.1242/jcs.03281.

32. Wang C, Yin S, Cen L, et al. Differentiation of Adipose-Derived Stem Cells into Contractile Smooth Muscle Cells Induced by Transforming Growth Factor-β1 and Bone Morphogenetic Protein-4. *Tissue Eng Part A*. 2010;16(4):1201-1213. doi:10.1089/ten.tea.2009.0303.

33. Aji K, Maimaijiang M, Aimaiti A, et al. Differentiation of Human Adipose Derived Stem Cells into Smooth Muscle Cells Is Modulated by CaMKIIGamma. *Stem Cells Int*. 2016;2016. doi:10.1155/2016/1267480.

34. Elçin AE, Parmaksiz M, Dogan A, et al. Differential gene expression profiling of human adipose stem cells differentiating into smooth muscle-like cells by TGFβ1/BMP4. *Exp Cell Res*. 2017;352(2):207-217. doi:10.1016/j.yexcr.2017.02.006.

35. Strobel HA, Dikina AD, Levi K, Solorio LD, Alsberg E, Rolle MW. Cellular Self-Assembly with Microsphere Incorporation for Growth Factor Delivery Within Engineered Vascular Tissue Rings. *Tissue Eng Part A*. 2017;23(3-4):143-155. doi:10.1089/ten.tea.2016.0260.

36. Moghadasi Boroujeni S, Mashayekhan S, Vakilian S, Ardeshirylajimi A, Soleimani M. The synergistic effect of surface topography and sustained release of TGF-β1 on myogenic differentiation of human mesenchymal stem cells. *J Biomed Mater Res - Part A*. 2016;104(7):1610-1621. doi:10.1002/jbm.a.35686.

37. Solorio L, Zwolinski C, Lund A, Farrell M, Stegemann J. Gelatin microspheres crosslinked with genipin for local delivery of growth factors. *J Tissue Eng Regen Med*. 2010;4(7):514-523. doi:10.1002/term.

38. Turner PA, Thiele JS, Stegemann JP. Growth factor sequestration and enzyme-mediated release from genipin-crosslinked gelatin microspheres. *J Biomater Sci Polym Ed*. 2017;28(16):1826-1846. doi:10.1080/09205063.2017.1354672.

39. Kawai K, Suzuki S, Tabata Y, Ikada Y. Accelerated tissue regeneration through incorporation of basic Fibroblast growth factor-impregnated gelatin microspheres into artificial dermis. *Biomaterials*. 2000;21:489-499.

40. Zhang L, Kahn CJF, Chen H-Q, Tran N, Wang X. Effect of uniaxial stretching on rat bone mesenchymal stem cell: orientation and expressions of collagen types I and III and tenascin-

C. *Cell Biol Int*. 2008;32(3):344-352. doi:10.1016/j.cellbi.2007.12.018.

41. Ghazanfari S, Tafazzoli-Shadpour M, Shokrgozar MA. Effects of cyclic stretch on proliferation of mesenchymal stem cells and their differentiation to smooth muscle cells. *Biochem Biophys Res Commun*. 2009;388(3):601-605. doi:10.1016/j.bbrc.2009.08.072.

42. Maul TM, Chew DW, Nieponice A, Vorp D a. Mechanical stimuli differentially control stem cell behavior: morphology, proliferation, and differentiation. *Biomech Model Mechanobiol*. 2011;10(6):939-953. doi:10.1007/s10237-010-0285-8.

43. Kim T, Sun J, Lu S, Qi Y, Wang Y. Prolonged Mechanical Stretch Initiates Intracellular Calcium Oscillations in Human Mesenchymal Stem Cells. 2014;9(10):1-9. doi:10.1371/journal.pone.0109378.

44. Rothdiener M, Hegemann M, Uynuk-Ool T, et al. Stretching human mesenchymal stromal cells on stiffness-customized collagen type I generates a smooth muscle marker profile without growth factor addition. *Sci Rep*. 2016;6(October):35840. doi:10.1038/srep35840.

45. Rabbani M, Tafazzoli-Shadpour M, Shokrgozar MA, Janmaleki M, Teymoori M. Cyclic Stretch Effects on Adipose-Derived Stem Cell Stiffness, Morphology and Smooth Muscle Cell Gene Expression. *Tissue Eng Regen Med*. 2017;14(3):279-286. doi:10.1007/s13770-017-0033-6.

46. Kanda K, Matsuda T, Oka T. Two-dimensional Orientational Response of Smooth Muscle Cells to Cyclic Stretching. *ASAIO*. 1992;14:382-385.

47. Liu B, Qu M-J, Qin K-R, et al. Role of cyclic strain frequency in regulating the alignment of vascular smooth muscle cells in vitro. *Biophys J*. 2008;94(4):1497-1507. doi:10.1529/biophysj.106.098574.

48. Wanjare M, Agarwal N, Gerecht S. Biomechanical strain induces elastin and collagen production in human pluripotent stem cell-derived vascular smooth muscle cells. *Am J Physiol - Cell Physiol*. 2015;309(4):C271-C281. doi:10.1152/ajpcell.00366.2014.

49. Kurpinski K, Park J, Thakar RG, Li S. Regulation of vascular smooth muscle cells and mesenchymal stem cells by mechanical strain. *Mol Cell Biomech*. 2006;3(1):21-34.

50. Liu CZ, Xia ZD, Han ZW, Hulley P a, Triffitt JT, Czernuszka JT. Novel 3D collagen scaffolds fabricated by indirect printing technique for tissue engineering. *J Biomed Mater Res B Appl Biomater*. 2008;85(2):519-528. doi:10.1002/jbm.b.30975.

51. Kilian K a, Bugarija B, Lahn BT, Mrksich M. Geometric cues for directing the differentiation of mesenchymal stem cells. *Proc Natl Acad Sci U S A*. 2010;107:4872-4877. doi:10.1073/pnas.0903269107.

52. Zhang D, Sun MB, Lee J, Abdeen AA, Kilian KA. Cell shape and the presentation of adhesion ligands guide smooth muscle myogenesis. *J Biomed Mater Res - Part A*. 2016;104(5):1212-1220. doi:10.1002/jbm.a.35661.

53. Lee J, Abdeen AA, Zhang D, Kilian KA. Directing stem cell fate on hydrogel substrates by

controlling cell geometry, matrix mechanics and adhesion ligand composition. *Biomaterials*. 2013;34(33):8140-8148. doi:10.1016/j.biomaterials.2013.07.074.

54. Yang Y, Relan NK, Przywara D a, Schuger L. Embryonic mesenchymal cells share the potential for smooth muscle differentiation: myogenesis is controlled by the cell's shape. *Development*. 1999;126:3027-3033.

55. Tay CY, Yu H, Pal M, et al. Micropatterned matrix directs differentiation of human mesenchymal stem cells towards myocardial lineage. *Exp Cell Res*. 2010;316(7):1159-1168. doi:10.1016/j.yexcr.2010.02.010.

56. Matsuoka F, Takeuchi I, Agata H, et al. Morphology-Based Prediction of Osteogenic Differentiation Potential of Human Mesenchymal Stem Cells. *PLoS One*. 2013;8(2). doi:10.1371/journal.pone.0055082.

57. Matsuoka F, Takeuchi I, Agata H, et al. Characterization of time-course morphological features for efficient prediction of osteogenic potential in human mesenchymal stem cells. *Biotechnol Bioeng*. 2014;111(7):1430-1439. doi:10.1002/bit.25189.

58. Chen ZG, Wang PW, Wei B, Mo XM, Cui FZ. Electrospun collagen-chitosan nanofiber: a biomimetic extracellular matrix for endothelial cell and smooth muscle cell. *Acta Biomater*. 2010;6(2):372-382. doi:10.1016/j.actbio.2009.07.024.

59. Uynuk-Ool T, Rothdiener M, Walters B, et al. The geometrical shape of mesenchymal stromal cells measured by quantitative shape descriptors is determined by the stiffness of the biomaterial and by cyclic tensile forces. *J Tissue Eng Regen Med*. 2017;11(12):3508-3522. doi:10.1002/term.2263.

60. Gomes LR, Terra LF, Wailemann RAM, Labriola L, Sogayar MC. TGF-β1 modulates the homeostasis between MMPs and MMP inhibitors through p38 MAPK and ERK1/2 in highly invasive breast cancer cells. *BMC Cancer*. 2012;12:1-15. doi:10.1186/1471-2407-12-26.

61. Feng C, Hu J, Liu C, et al. Association of 17-β estradiol with adipose-derived stem cells: New strategy to produce functional myogenic differentiated cells with a nano-scaffold for tissue engineering. *PLoS One*. 2016;11(10):1-18. doi:10.1371/journal.pone.0164918.

62. Floren M, Bonani W, Dharmarajan A, Motta A, Migliaresi C, Tan W. Human mesenchymal stem cells cultured on silk hydrogels with variable stiffness and growth factor differentiate into mature smooth muscle cell phenotype. *Acta Biomater*. 2016;31:156-166. doi:10.1016/j.actbio.2015.11.051.

63. Song B, Jiang W, Alraies A, et al. Bladder Smooth Muscle Cells Differentiation from Dental Pulp Stem Cells: Future Potential for Bladder Tissue Engineering. *Stem Cells Int*. 2016;2016. doi:10.1155/2016/6979368.

64. Solorio LD, Fu AS, Hernández-Irizarry R, Alsberg E. Chondrogenic differentiation of human mesenchymal stem cell aggregates via controlled release of TGF-β1 from incorporated polymer microspheres. *J Biomed Mater Res - Part A*. 2010;92(3):1139-1144.

doi:10.1002/jbm.a.32440.

65. Zhao Z, Yu H, Fan C, Kong Q, Liu D, Meng L. Differentiate into urothelium and smooth muscle cells from adipose tissue-derived stem cells for ureter reconstruction in a rabbit model. 2016;8(9):3757-3768.

66. Rajangam T, Park MH, Kim S-H. 3D Human Adipose-Derived Stem Cell Clusters as a Model for In Vitro Fibrosis. *Tissue Eng Part C Methods*. 2016;22(7):679-690. doi:10.1089/ten.TEC.2016.0037.

67. Xu JG, Zhu SY, Heng BC, Dissanayaka WL, Zhang CF. TGF-β1-induced differentiation of SHED into functional smooth muscle cells. *Stem Cell Res Ther*. 2017;8(1):1-10. doi:10.1186/s13287-016-0459-0.

68. Liu X, Wang J, Dong F, Li H, Hou Y. Induced differentiation of human gingival fibroblasts into VSMC-like cells. *Differentiation*. 2017;95(January):1-9. doi:10.1016/j.diff.2017.01.001.

69. Girão-Silva T, Bassaneze V, Campos LCG, et al. Short-term mechanical stretch fails to differentiate human adipose-derived stem cells into cardiovascular cell phenotypes. *Biomed Eng Online*. 2014;13(1):1-15. doi:10.1186/1475-925X-13-54.

CHAPTER 6

Discussion, Conclusions, and Future Directions

6.1 – Summary of Thesis

The first Aim of this dissertation (Chapter 3) quantified and compared the morphological changes that bMSCs exhibit after stretch. These changes were examined for relationships between shape and both gene and protein expression associated with a phenotype shift toward an SMC lineage. bMSCs are recognized for their multipotency [1–3] and mechanical stimulation is frequently used to induce bMSCs toward an SMC lineage [4–7]. The cells changed morphologically after being stretched and the degree of change was dependent on the strain, the number of stretch regimens, and the duration of stretch. Repetition of stretch regimens was found to be a highly significant factor in controlling phenotype. Cells initially aligned perpendicular or oblique to the axis of stretch would initially pull protrusions in and away from that axis after one regimen of stretch. After being stretched again, for a second regimen, they would elongate as observed in previous studies [8–10]. Cells that were already aligned with the direction of stretch would begin elongating after a single regimen. This elongation process correlated with other markers indicative of a shift toward an SMC phenotype [11–13] including increased expression of both genes and proteins. Cell alignment was also demonstrated to be important as shape change was dependent on the cell's initial orientation. This finding also suggested the importance of substrate choice when trying to direct phenotype of progenitor cells. While many studies have used silicone sheets to apply cyclic loading, these results suggest that the perpendicular alignment induced by silicone may hamper

the final phenotype of the cells. On collagen sheets and in collagen gels, parallel alignment was seen and this facilitated more elongation.

The second Aim of this dissertation (Chapter 4) focused on achieving a better understanding of how to control bMSC shape, by establishing relationships between the input energy of specific stretch regimens and the resulting shape of the cells. Chemical potential energy is used in multiple metabolic processes [14,15] and cells convert this energy into mechanical forces when they contract and migrate. It has been theorized that changes in cell shape require a portion of this energy from the cell or its surroundings [16]. Our results show that combinations of stretch parameters producing the same amount of mechanical input energy also induced a similar shape from bMSCs. Increasing the input energy, even while maintaining two of the three experimental parameters, resulted in distinct bMSC shapes. Not only was cellular shape responsive to different amounts of input energy, but this response correlated to the log of the input energy, exhibiting a relationship similar to that of a state function. Expression of ACTA was also found to be correlated to the log of the input energy, suggesting that multiple aspects of cell phenotype are directly related to energy input. We established a clear relationship between energy input, the shape of cells, and the expression of ACTA. While other SMC genes did not directly correlate with the energy input, Partial Least Squares (PLS) analysis revealed that these genes were still related to shape factors. This emphasizes the importance of shape and its role in establishing cell phenotype.

Aim 3 (Chapter 4) examined the translation of shape factor analysis to three-dimensional culture systems with ASCs. In a first series of studies, ASCs were seeded in collagen hydrogels for 3D culture as well as on top of collagen hydrogels for 2D controls. 3D culture is more emulative of the *in vivo* environment, recapitulating more aspects of cell interactions with the matrix and with other cells [17–22]. In many progenitor systems, these effects increase the propensity of stem

cells to differentiate toward mature lineages [23–29]. In addition to the number of culture dimensions, the concentration of the collagen matrix was varied to assess associated changes. When our analysis was translated directly into 3D and these cells were compared to those in 2D, ASCs in 2D were larger, more polarized, and more spread out than their 3D counterparts While these data would suggest that culture in 3D decreased their differentiation toward SMCs, the cells in 3D actually had higher expression of SMA and MHC protein. This indicated that analysis comparing shape of cells in 2D and 3D would require more complex methods. This is likely because cells in 3D are partially oriented along the axis perpendicular to image projections. Within 3D culture, relationships between culture conditions and morphology were still evident and by mathematically compensating for cell orientation, the relationship between morphology and biochemical expression was reestablished. As these corrections apply ubiquitously across samples in the same dimension, this also means the corrections are unnecessary when comparing cells in the same culture dimension and that this method can be used for 3D culture where it still produces robust and accurate data describing morphology. Together, these results suggest that 3D culture enhanced differentiation of ASCs toward the SMC phenotype.

A second series of studies in Aim 3 (Chapter 5) applied shape factors to characterize morphology of ASC differentiation in 3D matrices in response to growth factors and mechanical stretch. The use of growth factors has been actively employed to induce SMC differentiation from MSCs [30–34] and using microcarriers to deliver the growth factor to the cells has been shown to enhance this process [35,36]. Analysis of ASCs in our study showed that the combination of PDGF and TGFβ induced an SMC-like morphology, particularly when delivered through μspheres. Stretching MSCs has been shown to induce differentiation into SMCs as well [4,9,10,37]. The panel of shape factors suggested that the ASCs exposed to stretch were larger, more polarized, and had

higher degrees of alignment, all indicative of a SMC-like morphology. Expression of SMA and MHC protein supported the shape analysis, suggesting that growth factor delivery improved differentiation and that stretching the gels also enhanced the extent of differentiation. In summary, growth factors and stretch can be used to induce differentiation of ASCs into SMC-like cells and this process can be confirmed both through protein expression and a robust set of shape parameters that describe multiple aspects of morphology.

6.2 – Discussion

This work has emphasized the connection between cell shape and associated biochemical phenotype, which has relevance in the fields of tissue engineering, stem cell biology, mechanobiology, and regenerative medicine. In order to develop mature, lineage-specific cells from progenitors, we must have objective means of characterizing their phenotype and how they respond to environmental stimuli. This will insure that cell differentiation can be reproducibly achieved and validated. This work offers an advanced, imaging- and computational-based technique for characterizing these morphological changes in stem cells as they undergo differentiation.

In previous work, shape factors were introduced as a means of characterizing bMSC shape exposed to different environments [38]. In the first Aim of this work we implemented an extended panel of shape factors that could be automatically measured in images to characterize changes in morphology. Altering stretch parameters has been used before to induce different behaviors from cells [6,39,40] but the morphological response to these stimuli had yet to be quantified or used to characterize these behaviors [8,9,13,41–44]. Our morphological analysis not only provided quantitative evidence supporting previous claims, it gave additional insight into the changes that cells undergo

as they align with stretch and emphasized the importance of the type of substrate when trying to align, elongate, and differentiate cells.

In order to reproducibly differentiate functional tissue-specific cells from progenitors, methods must be established to efficiently and consistently produce cells with similar phenotypes. This would make cell manufacturing, regulation, and oversight more standardized [45,46], thereby accelerating the application of stem cell therapies in the clinic. Some groups have addressed this issue by fabricating specific patterns for cells to adhere on otherwise non-adherent substrates [1–3]. This area of research has shown great promise for regulating phenotype but at a scale that is not commercially or clinically pragmatic. In Aim 2 we also address this need but on a larger scale without the need for complex fabrication to control individual cell shape. We show that by applying the same input energy with different combinations of stretch parameters, we can achieve statistically identical cell shapes. These results are based on data from primary cells from different donors. Despite the patient variability, this relationship between input energy and morphology establishes a means of inducing consistent cell phenotypes in bMSCs. The relationship extends to expression of ACTA, which further supports the use of energy as a process parameter to control phenotype. While three genes tested did not correlate with input energy specifically, they did correlate with other shape factors, further substantiating the importance of cell shape in controlling phenotype. Application of this concept may extend into multiple other systems and not only offers additional means of controlling cell shape but give substantial insight into cell biomechanics.

Both *in vitro* and *in vivo* studies are increasingly using 3D matrices [20,21,47], and therefore understanding cellular phenotype in 3D will continue to become more important. While biochemical assays are well established and functional assays reflect the end goal of tissue engineered constructs, morphometric strategies have the potential to add a non-destructive,

objective, and quantitative means of assessing cell phenotype. While our method has limitations when comparing cell morphology between 2D and 3D culture systems, it retains its utility to reliably measure and compare cell shape in 3D culture systems. Our studies validated previous work showing that stretch and growth factors increase the differentiation of MSCs into SMCs.

Multiple studies have used growth factors [30–34] and stretch [4,9,10,12,34,44] to induce differentiation of MSCs into SMCs. Many of these studies have made qualitative observations about corresponding changes in morphology after exposure to external stimuli, but our techniques objectively and quantitatively validate their findings [8,9,13,41,43]. Shape factor analysis confirmed these stimuli's effects on progenitors, and furthermore demonstrated differences more consistently than biochemical results. Considering the same number of samples were used for morphometric and protein analysis, this suggests that shape is more sensitive than biochemical expression. Furthermore, this process is being applied in a complex and difficult model system. MSCs are predisposed to differentiate into osteogenic, chondrogenic, or adipogenic lineages. Differentiation of MSCs into SMCs is less robust, and therefore promoting myogenic differentiation substantiates this work, and the additional insights provided by morphometric analysis further increases the utility of these methods.

There is an important need for cell-based therapies and MSCs have great potential for filling that need. There are many potential sources of these cells, a variety of methods used to differentiate them, and the relationship between cell shape and its role in cell phenotype is recognized as important. The objective of this study was to advance our understanding of this relationship, using an objective panel of shape factors to characterize differentiation and to relate the effects of commonly used stimuli to shape and the corresponding biochemical phenotype. We showed that we could induce differentiation using mechanical stimulation and describe this change

176

in phenotype using quantitative measures of morphology. Other groups in the future can use this algorithm or similar means to assess cell morphology and use it to characterize their cells. Next, we showed that shape could be directed through the application of defined amounts of input energy. Furthermore, markers of SMC phenotype correlated with either energy input and/or cell shape. This principle could be exploited by other groups to mechanically simultaneously direct the fate of many cells and energy may be used as a process parameter in future studies. We continued to apply these techniques in 3D and showed they generate rich data that can be used to describe phenotype. Finally, we used shape factors to characterize changes in morphology as cells in 3D responded to stimuli and differentiated in 3D culture systems exposed to growth factors and mechanical stretch. In the future, large-scale morphometric analysis of cell shape may serve as a robust method of assessing phenotype and describing differentiation. These techniques and findings can be used to promote differentiation and the insights they provide will improve our understanding of, and control over, cells and may be used to improve cell therapies in the near future.

6.3 – Conclusion

Aim 1: Quantify MSC Morphology After Stretch Using a Panel of Shape Factors

- bMSCs changed their phenotype in response to the application of specific stretch parameters

- Cellular responses corresponded to changes in morphology which could be quantified and related to other measures of phenotype

- The use of shape factors provided a rich data set for describing differentiation and also providing insight into other cell behaviors such as alignment and spreading

Aim 2: Apply Shape Factors to Determine the Effects of Energy Input and Assess Potential of Mechanical Stimulation as a Means of Controlling Cell Shape

- Different combinations of stretch parameters with the same effective energy input elicited the same morphological phenotype from cells

- The change in shape induced by different amounts of energy was linear with the log of energy input suggesting cell morphology may be a state function of energy

- A key genetic marker for SMC differentiation also correlated with energy and genes were associated with shape factors, bolstering the utility of cell shape in determining phenotype.

Aim 3: Translate Shape Analysis from 2D into 3D Constructs and Use Shape to Compare Effects of Culture Conditions on ASC Differentiation into SMC

- Shape factors derived from 2D and 3D culture systems could not be directly compared because of the additional axis of potential orientation in 3D.

- The effect of an additional dimension in 3D culture could be corrected mathematically, and suggested that 3D culture produced a more SMC-like phenotype in ASCs.

- Morphological analysis was valid when comparing between 3D culture systems, and captured the effects of differentiation induced by growth factors and stretch.

- Biochemical analysis of phenotype also showed SMC differentiation was improved by growth factors and stretch

6.4 – Future Directions

Better segmentation methods are being developed which could improve the efficiency of distinguishing cells and further increase the accuracy and effectiveness of these shape factors. One advance that may be particularly helpful is to develop a "rolling threshold" to improve image processing. The current algorithm performs a rolling mean filter which reduces artificial gradients of pixel intensity in images. Essentially, a background intensity is subtracted from a pixel based on the average of the pixels surrounding it in a predetermined radius. This normalizes the cells across the entire image and was used as the principle means or normalizing images for shape analysis. This process still leaves some cells washed out while diminishing the footprint of other cells before the image is thresholded for segmentation. With more advanced programming, it might be possible to identify cells and threshold them each individually. This would increase the accuracy of the shape factors and is likely possible based on the increasing knowledge of segmentation [48]–[50].

The use of shape to assess phenotype would also benefit from better 3D shape analysis. There are software packages that can process 3D renderings [51]–[53] but they are incompatible with our methods in ImageJ, often require proprietary software, and are very computationally demanding. With current functions of ImageJ, cells could be located and examined from multiple planes. Confocal microscopy can make Z-stacks or sequences of images from consecutive planes which could be extrapolated and filled into volumes. This would allow for more complete analysis of cells in 3D but would also require rigorous algorithms and substantial computational processing power. Such 3D techniques would also provide additional factors to be examined (volume, surface area, etc.), and it could eliminate the complications that currently prevent accurate and direct comparison between cells in 2D and 3D.

To improve our knowledge of differentiation using the current system, additional controls should be investigated. Gels with unloaded control μspheres and no growth factors present one interesting possibility. We analyzed a small number of gels with this composition and found interesting results, which are described more full in Appendix D. Running one round of static biological replicates (n=3), we found that adding spheres without any growth factor produced cells which were longer (Fig. D.1A, $p<0.05$) and larger in area (Fig. D.1B, $p<0.05$) than cells in control gels or even in gels with growth factor. Delivery of control μspheres in this small number of replicates also induced as much SMA protein expression as growth factor conditions (Fig D.1C) and more expression of MHC protein (Fig D.1D, $p<0.05$). This preliminary finding suggests that the μspheres alone are myogenically inductive.

Optimization of the type of matrix used for cell culture may also prove beneficial to fully realizing SMC differentiation from MSC precursors. Other types of protein and synthetic matrices are being used to culture cells [54]–[63] and these may be beneficial to control for aspects of the microenvironment that we were unable to recapitulate. As described more fully in Appendix D, preliminary studies with bMSCs and fibrin, a common natural protein used in our lab, suggests that adding fibrin into our 3D hydrogels can change the length (Fig. D.2A) and aspect ratio (Fig. D.2B) of cells. In addition, the addition of fibrin might upregulate SMC genes like calponin (Fig. D.2C) and desmin (Fig. D.2D).

The temporal relationship between shape and SMC gene expression in 3D collagen needs to be further elucidated. Expression of SMC genes was assessed on D4 and D7, the same time points as the protein assays, but the results did not correlate well with protein expression and shape factor findings. To reconcile out these discrepancies, additional genes should be analyzed to verify a synthetic SMC phenotype is not being induced and that the cells are not becoming fibroblasts.

Assessment at earlier time points would also be beneficial. Given that the compaction of gels with growth factors occurred much earlier than control gels, as early as D1, it is possible that the upregulation of differentiation genes occurs before the time points we tested. Several groups have reported different timelines for the upregulation and down regulation of SMC genes during differentiation [32], [64], [65].

Other features of phenotype should also be assessed to fully understand how shape influences cell behavior. In this study we assessed compaction of gels when possible but Western blots and other protein assays could also be used to correlate shape with cell phenotype. Other functions like protein secretion, matrix production, or electrophysiology would also serve as markers for differentiation. These characteristics could be assessed in relation to cell shape, for example, and some studies have already suggested that larger cells are more contractile [66].

Applications of this technology outside our model system also offer substantial and exciting possibilities. Cell shape is relevant in other lineages of cells [2], [3], [67] and should be explored to characterize their development and differentiation as well. This would demand similar parallel studies where morphology is characterized and correlated with other phenotypic features. In addition, cyclic strain is only one of many forces that cells experience *in vivo* so application of other forms of stimulation would also greatly enhance the robustness and implications of our findings. Compression and shear in particular have been shown to influence cell phenotype [34], [68], [69] and should be explored as alternative means for controlling cell shape/phenotype. This would not only increase the usefulness and claim that energy is a means of controlling differentiation, it could expand our understanding of how cells respond to biomechanical forces in general.

6.5 – References

1.	McBeath R, Pirone DM, Nelson CM, Bhadriraju K, Chen CS. Cell shape, cytoskeletal tension, and RhoA regulate stem cell lineage commitment. *Dev Cell*. 2004;6(4):483-495. http://www.ncbi.nlm.nih.gov/pubmed/15068789.

2.	Kilian K a, Bugarija B, Lahn BT, Mrksich M. Geometric cues for directing the differentiation of mesenchymal stem cells. *Proc Natl Acad Sci U S A*. 2010;107:4872-4877. doi:10.1073/pnas.0903269107.

3.	Gao L, Mcbeath R, Chen CS. Stem Cell Shape Regulates a Chondrogenic versus Myogenic Fate through Rac1 and N-cadherin. *Stem Cells*. 2010;28(3):564-572. doi:10.1002/stem.308.Stem.

4.	Ghazanfari S, Tafazzoli-Shadpour M, Shokrgozar MA. Effects of cyclic stretch on proliferation of mesenchymal stem cells and their differentiation to smooth muscle cells. *Biochem Biophys Res Commun*. 2009;388(3):601-605. doi:10.1016/j.bbrc.2009.08.072.

5.	Heo SJ, Nerurkar NL, Baker BM, Shin JW, Elliott DM, Mauck RL. Fiber stretch and reorientation modulates mesenchymal stem cell morphology and fibrous gene expression on oriented nanofibrous microenvironments. *Ann Biomed Eng*. 2011;39(11):2780-2790. doi:10.1007/s10439-011-0365-7.

6.	Paxton JZ, Hagerty P, Andrick JJ, Baar K. Optimizing an Intermittent Stretch Paradigm Using ERK1/2 Phosphorylation Results in Increased Collagen Synthesis in Engineered Ligaments. *Tissue Eng Part A*. 2012;18(3-4):277-284. doi:10.1089/ten.tea.2011.0336.

7.	Wu Y, Zhang X, Zhang P, Fang B, Jiang L. Intermittent traction stretch promotes the osteoblastic differentiation of bone mesenchymal stem cells by the ERK1/2-activated Cbfa1 pathway. *Connect Tissue Res*. 2012;53(6):451-459. doi:10.3109/03008207.2012.702815.

8.	Liu B, Qu M-J, Qin K-R, et al. Role of cyclic strain frequency in regulating the alignment of vascular smooth muscle cells in vitro. *Biophys J*. 2008;94(4):1497-1507. doi:10.1529/biophysj.106.098574.

9.	Zhang L, Kahn CJF, Chen H-Q, Tran N, Wang X. Effect of uniaxial stretching on rat bone mesenchymal stem cell: orientation and expressions of collagen types I and III and tenascin-C. *Cell Biol Int*. 2008;32(3):344-352. doi:10.1016/j.cellbi.2007.12.018.

10.	Maul TM, Chew DW, Nieponice A, Vorp D a. Mechanical stimuli differentially control stem cell behavior: morphology, proliferation, and differentiation. *Biomech Model Mechanobiol*. 2011;10(6):939-953. doi:10.1007/s10237-010-0285-8.

11.	Yang Y, Relan NK, Przywara D a, Schuger L. Embryonic mesenchymal cells share the potential for smooth muscle differentiation: myogenesis is controlled by the cell's shape. *Development*. 1999;126:3027-3033.

12.	Kim T, Sun J, Lu S, Qi Y, Wang Y. Prolonged Mechanical Stretch Initiates Intracellular

Calcium Oscillations in Human Mesenchymal Stem Cells. 2014;9(10):1-9. doi:10.1371/journal.pone.0109378.

13.   Wanjare M, Agarwal N, Gerecht S. Biomechanical strain induces elastin and collagen production in human pluripotent stem cell-derived vascular smooth muscle cells. *Am J Physiol - Cell Physiol*. 2015;309(4):C271-C281. doi:10.1152/ajpcell.00366.2014.

14.   Joumaa V, Herzog W. Energy cost of force production is reduced after active stretch in skinned muscle fibres. *J Biomech*. 2013;46(6):1135-1139. doi:10.1016/j.jbiomech.2013.01.008.

15.   Jiang L, Yang C, Zhao L, Zheng Q. Stress fiber response to mechanics: a free energy dependent statistical model. *Soft Matter*. 2014;10(26):4603. doi:10.1039/c3sm52914b.

16.   Brodland GW, Veldhuis JH. Assessing the mechanical energy costs of various tissue reshaping mechanisms. *Biomech Model Mechanobiol*. 2012;11(8):1137-1147. doi:10.1007/s10237-012-0411-x.

17.   O'Connor SM, Andreadis JD, Shaffer KM, Ma W, Pancrazio JJ, Stenger DA. Immobilization of neural cells in three-dimensional matrices for biosensor applications. *Biosens Bioelectron*. 2000;14(10-11):871-881. doi:10.1016/S0956-5663(99)00055-X.

18.   Sasaki T, Takagi M, Soma T, Yoshida T. 3D culture of murine hematopoietic cells with spatial development of stromal cells in nonwoven fabrics. *Cytotherapy*. 2002;4(3):285-291. doi:10.1080/146532402320219808.

19.   Edelman DB, Keefer EW. A cultural renaissance: In vitro cell biology embraces three-dimensional context. *Exp Neurol*. 2005;192(1):1-6. doi:10.1016/j.expneurol.2004.10.005.

20.   Helder MN, Knippenberg M, Klein-Nulend J, Wuisman PIJM. Stem Cells from Adipose Tissue Allow Challenging New Concepts for Regenerative Medicine. *Tissue Eng*. 2007;13(8):1799-1808. doi:10.1089/ten.2006.0165.

21.   Mason C, Dunnill P. A brief definition of regenerative medicine. *Regen Med*. 2008;1:1-4.

22.   Dai R, Wang Z, Samanipour R, Koo K, Kim K. Adipose-Derived Stem Cells for Tissue Engineering and Regenerative Medicine Applications. *Stem Cells Int*. 2016;2016:1-19. doi:10.1155/2016/6737345.

23.   Pineda ET, Nerem RM, Ahsan T. Differentiation Patterns of Embryonic Stem Cells in Two- versus Three-Dimensional Culture. *Cells Tissues Organs*. 2013;197(5):399-410. doi:10.1159/000346166.

24.   Zhang D, Kilian KA. The effect of mesenchymal stem cell shape on the maintenance of multipotency. *Biomaterials*. 2013;34(16):3962-3969. doi:10.1016/j.biomaterials.2013.02.029.

25.   Lin CY, Huang CH, Wu YK, Cheng NC, Yu J. Maintenance of human adipose derived stem cell (hASC) differentiation capabilities using a 3D culture. *Biotechnol Lett*. 2014;36(7):1529-1537. doi:10.1007/s10529-014-1500-y.

26. Yamamoto M, Kawashima N, Takashino N, et al. Three-dimensional spheroid culture promotes odonto/osteoblastic differentiation of dental pulp cells. *Arch Oral Biol*. 2014;59(3):310-317. doi:10.1016/j.archoralbio.2013.12.006.

27. Talaei-Khozani T, Khodabandeh Z, Jaberipour M, Hosseini A, Bahmanpour S, Vojdani Z. Comparison of hepatic nuclear factor-4 expression in two and three-dimensional culture of Wharton's jelly-derived cells exposed to hepatogenic medium. *Rom J Morphol Embryol*. 2015;56(4):1365-1370.

28. Meier F, Freyer N, Brzeszczynska J, et al. Hepatic differentiation of human iPSCs in different 3D models: A comparative study. *Int J Mol Med*. 2017;40(6):1759-1771. doi:10.3892/ijmm.2017.3190.

29. Wu Q, Tang J, Li Y, et al. Hepatic differentiation of mouse bone marrow-derived mesenchymal stem cells using a novel 3D culture system. *Mol Med Rep*. 2017;16(6):9473-9479. doi:10.3892/mmr.2017.7818.

30. Williams C, Xie AW, Emani S, et al. A Comparison of Human Smooth Muscle and Mesenchymal Stem Cells as Potential Cell Sources for Tissue-Engineered Vascular Patches. *Tissue Eng Part A*. 2012;18(9-10):986-998. doi:10.1089/ten.tea.2011.0172.

31. Park WS, Heo SC, Jeon ES, et al. Functional expression of smooth muscle-specific ion channels in TGF- 1-treated human adipose-derived mesenchymal stem cells. *AJP Cell Physiol*. 2013;305(4):C377-C391. doi:10.1152/ajpcell.00404.2012.

32. Brun J, Lutz KA, Neumayer KMH, et al. Smooth Muscle-Like Cells Generated from Human Mesenchymal Stromal Cells Display Marker Gene Expression and Electrophysiological Competence Comparable to Bladder Smooth Muscle Cells. *PLoS One*. 2015:1-21. doi:10.1371/journal.pone.0145153.

33. Brun J, Abruzzese T, Rolauffs B, Aicher WK, Hart ML. Choice of xenogenic-free expansion media significantly influences the myogenic differentiation potential of human bone marrow-derived mesenchymal stromal cells. *Cytotherapy*. 2016;18(3):344-359. doi:10.1016/j.jcyt.2015.11.019.

34. Parvizi M, Bolhuis-Versteeg LAM, Poot AA, Harmsen MC. Efficient generation of smooth muscle cells from adipose-derived stromal cells by 3D mechanical stimulation can substitute the use of growth factors in vascular tissue engineering. *Biotechnol J*. 2016;11(7):932-944. doi:10.1002/biot.201500519.

35. Solorio L, Zwolinski C, Lund A, Farrell M, Stegemann J. Gelatin microspheres crosslinked with genipin for local delivery of growth factors. *J Tissue Eng Regen Med*. 2010;4(7):514-523. doi:10.1002/term.

36. Solorio LD, Dhami CD, Dang PN, Vieregge EL, Alsberg E. Spatiotemporal regulation of chondrogenic differentiation with controlled delivery of transforming growth factor-β1 from gelatin microspheres in mesenchymal stem cell aggregates. *Stem Cells Transl Med*. 2012;1(8):632-639. doi:10.5966/sctm.2012-0039.

37. Benders KEM, van Weeren PR, Badylak SF, Saris DBF, Dhert WJ a, Malda J. Extracellular matrix scaffolds for cartilage and bone regeneration. *Trends Biotechnol*. 2013;31(3):169-176. doi:10.1016/j.tibtech.2012.12.004.

38. Uynuk-Ool T, Rothdiener M, Walters B, et al. The geometrical shape of mesenchymal stromal cells measured by quantitative shape descriptors is determined by the stiffness of the biomaterial and by cyclic tensile forces. *J Tissue Eng Regen Med*. 2017;11(12):3508-3522. doi:10.1002/term.2263.

39. Park JS, Chu JSF, Cheng C, Chen F, Chen D, Li S. Differential effects of equiaxial and uniaxial strain on mesenchymal stem cells. *Biotechnol Bioeng*. 2004;88(3):359-368. doi:10.1002/bit.20250.

40. Dumas V, Ducharne B, Perrier A, et al. Extracellular matrix produced by osteoblasts cultured under low-magnitude, high-frequency stimulation is favourable to osteogenic differentiation of mesenchymal stem cells. *Calcif Tissue Int*. 2010;87(4):351-364. doi:10.1007/s00223-010-9394-8.

41. Kurpinski K, Park J, Thakar RG, Li S. Regulation of vascular smooth muscle cells and mesenchymal stem cells by mechanical strain. *Mol Cell Biomech*. 2006;3(1):21-34.

42. Lee W-CC, Maul TM, Vorp DA, Rubin JP, Marra KG. Effects of uniaxial cyclic strain on adipose-derived stem cell morphology, proliferation, and differentiation. *Biomech Model Mechanobiol*. 2007;6(4):265-273. doi:10.1007/s10237-006-0053-y.

43. Girão-Silva T, Bassaneze V, Campos LCG, et al. Short-term mechanical stretch fails to differentiate human adipose-derived stem cells into cardiovascular cell phenotypes. *Biomed Eng Online*. 2014;13(1):1-15. doi:10.1186/1475-925X-13-54.

44. Rabbani M, Tafazzoli-Shadpour M, Shokrgozar MA, Janmaleki M, Teymoori M. Cyclic Stretch Effects on Adipose-Derived Stem Cell Stiffness, Morphology and Smooth Muscle Cell Gene Expression. *Tissue Eng Regen Med*. 2017;14(3):279-286. doi:10.1007/s13770-017-0033-6.

45. Sheu J, Klassen H, Bauer G. Cellular manufacturing for clinical applications. *Cell-Based Ther Retin Degener Dis*. 2014;53:178-188. doi:10.1159/000357362.

46. Carpenter MK. *Regulatory Considerations for Pluripotent Stem Cell Therapies*. Vol 230. 1st ed. Elsevier B.V.; 2017. doi:10.1016/bs.pbr.2016.12.008.

47. Pampaloni F, Pampaloni F, Stelzer EHK, Masotti A. Three-Dimensional Tissue Models for Drug Discovery and Toxicology Three-Dimensional Tissue Models for Drug Discovery and Toxicology. *Recent Pat Biotechnol*. 2009;3:103-117. doi:10.2174/187220809788700201.

APPENDICES

<u>Appendix A - Selected Protocols</u>

<u>A.1 Fabrication of 2D/3D Gels</u>

Materials
FBS
Collagen (8 mg/mL in 0.02 N Acetic Acid)
0.02 N Acetic Acid
NaOH (0.1 N)
5x DEMEM
Cells (suspended at 1E6/100 μL in 1x DMEM)
1x DMEM with 10% FBS and 1% Pen/Strep

Make Collagen Solutions
1. Add 2.5 mL of 8 mg/mL to a 15 mL tube
2. Add 1.25 mL of 8 mg/mL to a new 15 mL tube
3. Add 1.25 mL of 0.02 N Acetic Acid to the same tube
4. Add 0.675 mL of 8 mg/mL to a new 15 mL tube
5. Add 1.875 mL of 0.02 N Acetic Acid to the same tube

2D 4 mg/mL Gels
1. Take 1 mL from 8 mg/mL tube and add it to a new 15 mL tube
2. Add 0.36 mL of 5x DMEM
3. Mix in 0.18 mL of 0.1 N NaOH
4. Add 0.18 mL of FBS
5. Add 0.18 mL of 1x DMEM
6. Distribute 0.250 mL to 6 wells of a 24 well plate
7. Incubate for 30 minutes at 37 °C

2D 2 mg/mL Gels
1. Take 1 mL from 4 mg/mL tube and add it to a new 15 mL tube
2. Add 0.36 mL of 5x DMEM
3. Mix in 0.18 mL of 0.1 N NaOH
4. Add 0.18 mL of FBS
5. Add 0.18 mL of 1x DMEM
6. Distribute 0.250 mL to 6 wells of a 24 well plate
7. Incubate for 30 minutes at 37 °C

2D 1 mg/mL Gels
1. Take 1 mL from 1 mg/mL tube and add it to a new 15 mL tube
2. Add 0.36 mL of 5x DMEM
3. Mix in 0.18 mL of 0.1 N NaOH
4. Add 0.18 mL of FBS
5. Add 0.18 mL of 1x DMEM
6. Distribute 0.250 mL to 6 wells of a 24 well plate
7. Incubate for 30 minutes at 37 °C

3D 4 mg/mL Gels
1. Add 0.6 mL 5x DEME to remaining 4 mg/mL collagen (should be 1.5 mL left in the tube)
2. Mix in 0.3 mL of 0.1 N NaOH
3. Add 0.3 mL of FBS
4. Add 0.3 mL of cells suspended in 1x DMEM (1E6/100 μL)
5. Distribute 0.480 mL to 6 wells of a 24 well plate
6. Incubate for 1 hour at 37 °C

3D 2 mg/mL Gels
1. Add 0.6 mL 5x DEME to remaining 2 mg/mL collagen (should be 1.5 mL left in the tube)
2. Mix in 0.3 mL of 0.1 N NaOH
3. Add 0.3 mL of FBS
4. Add 0.3 mL of cells suspended in 1x DMEM (1E6/100 μL)
5. Distribute 0.480 mL to 6 wells of a 24 well plate
6. Incubate for 1 hour at 37 °C

3D 1 mg/mL Gels
1. Add 0.6 mL 5x DEME to remaining 2 mg/mL collagen (should be 1.5 mL left in the tube)
2. Mix in 0.3 mL of 0.1 N NaOH
3. Add 0.3 mL of FBS
4. Add 0.3 mL of cells suspended in 1x DMEM (1E6/100 μL)
5. Distribute 0.480 mL to 6 wells of a 24 well plate
6. Incubate for 1 hour at 37 °C

Add Cells to 2D Gels
1. Dilute 27 μL of cell suspension in 18 mL of media
2. Add 1 mL of cell suspension to each 2D well (every concentration)
3. Add 1 mL of control DMEM to each 3D well.

Culture Gels
1. On d3 remove media on all gels
2. Collecting appropriate gels for requirements
3. Replace 1 mL of 1x DMEM on remaining 2D and 3D Gels

4. On d6 replace 1 mL of 1x DMEM on remaining 2D and 3D Gels
5. On d7 collect the remaining gels for processing

	2D 4 mg	2D 2 mg	2D 1 mg	3D 4 mg	3D 2 mg	3D 1 mg
Collagen	0.9 mL	0.9 mL	0.9 mL	1.5 mL	1.5 mL	1.5 mL
5X DMEM	0.36 mL	0.36 mL	0.36 mL	0.6 mL	0.6 mL	0.6 mL
NaOH	0.18 mL	0.18 mL	0.18 mL	0.3 mL	0.3 mL	0.3 mL
FBS	0.18 mL	0.18 mL	0.18 mL	0.3 mL	0.3 mL	0.3 mL
Media/Cells	0.18 mL	0.18 mL	0.18 mL	0.3 mL	0.3 mL	0.3 mL

A2. Fabrication of Gelatin Microspheres

Based on Protocol by Paul Turner

Preparing Solutions

Make Diluent (2.5% v/v NaOH)

1. Add 750 µL 1N NaOH in distilled water, make total volume to 30 ml
2. Store at 4˚C

Make 10% Gel A (Sigma G6144-100G 175 bloom porcine) or Gel B (G9382-100G 225 bloom bovine)

1. Dissolve 4 g gelatin gradually in 40 ml distilled water, vortexing vigorously
2. Leave in 37 ˚C water bath for 30 min-1 hr,
3. Set on rotate plate at 37 ˚C overnight if not dissolved
4. Store in 4˚C

Make 6% Gelatin A or Gelatin B (working solution)

1. Mix 30 ml 10% Gelatin A or B with 20 ml Diluent
2. Store at 4˚C

Make 1% Genipin (cross-linker, Wako 078-03021)

1. In a 50ml tube, dissolve 200 mg genipin in 20 ml PBS
2. Heat to 37˚C in water bath and vortex vigorously
3. Solution should be light yellow. Store at 4 ˚C (may precipitate over time at 4 ˚C)

   * Add to microspheres at 4°C to prevent dissolution!

   *When crosslinking, add genipin to gelatin spheres in a 3-to-1 volume ratio, i.e. if 6 ml 6% gelatin was made into spheres, add 18 ml 1% genipin for crosslinking

Make PBS+L101 (oil washing solution)

1. Add 100 µL L101 into 1L PBS
2. Dissolve at 4°C

3. Agitate to mix, store in room temperature

Prepare Silicone oil (emulsification solution, Clearco 100CST)

*Smaller spheres can be made with higher viscosity (200,350, and 500 CS)

Prepare Ethanol (dehydration solution, Sigma 459844-4L ACS reagent >99.5% 200 proof)

Synthesis Procedure

1. Add 60-70 ml 100 CS Silicone oil into a 100 ml beaker, and warm up the silicone oil and 6% gelatin to 37 ˚C for at least 15 min on a hotplate.

2. Have some ice ready on the side and tighten the impeller onto the spinner.

3. After everything is warmed up, place the oil beaker on the beaker clamp. Place a container (in which ice will be added into) on the extendable stand. Adjust the position of the beaker such that the impeller is in the center of the beaker and ~half inch above the bottom of the beaker.

4. First set the spinner speed to 1000 rpm to test if it splashes. If not, increase speed to 2300rpm.

5. Use 1 ml pipette to add desired amount of 6% gelatin solution (usually 6-7mL) into the oil. It's better to immerse the tip of the pipette into oil near the side of the beaker and add gelatin into oil continuously and slowly. Let emulsification run for 5 minutes at 37°C.

6. Leave the rotator on for ~1 min, then stop for ~30 s, then spin for another 1 min, stop for 30s again.

7. Set the rotator time to 30 – 40 min, pack the container with ice, and start the spinner again.

8. After 30-40 min, stop the rotator, bring down the beaker on the stand, remove the impeller and try to get oil on the impeller into the beaker.

9. Get two 50 ml tubes, split oil/gelatin spheres evenly into two tubes. Add PBS/L101 into the tube until volume gets to 50 ml. Mix PDMS/gelatin and PBS/L101 together for at least 5 minutes on tumbler.

10. Centrifuge tubes for 5 min at 300g (for Gel A) or 200g (for Gel B). Note: lower centrifuge deceleration rate helps keep gelatin spheres pelleted after spin.

11. After centrifuging check to see if phases separated, if not, repeat step 10 at higher speed, if they did separate, remove the oil phase on top (and some PBS if you don't lose spheres), transfer the aggregated gelatin to a clean 50ml tube. Add PBS/L101 until the total volume reaches 50 mL. Centrifuge at 300g (for Gel A) or 200g (for Gel B) for another 5 min.

12. Remove the remaining oil and extra PBS until the remaining sphere/PBS volume is ~10-15ml.

13. Perform two additional washes (repeat steps 10-12 twice) to remove residual oil droplets.

14. Vortex / mix gelatin well prior to crosslinking reaction to disperse spheres. Add (cold, 4°C!) 1% genipin depending on the initial gelatin volume (18 ml 10% genipin for 6 ml 6% gelatin). Leave on tube tumbler for desired reaction period; usually 18-24 hrs for Gel A to reach "completion" (60-70% amines reacted) or 96-120 hrs for Gel B to reach 70-80% amines reacted. As the genipin polymerizes and reacts with gelatin over several hours, the

mixture will turn yellow, brown, and finally dark blue. Note: tumbler/shaker is recommended versus stirring plate with stir bar as the later has been found to damage and deform microspheres during mixing.

Ethanol Wash

1. After the reaction is complete, centrifuge at 200g for 5 min.

2. Prepare two 25 ml pipettes, one for removing waste, and the other for adding ethanol. Get the ethanol ready.

3. After centrifuging, remove liquid from the tube, try to save as many spheres as possible. (At this stage, some spheres may be still floating in the PBS, consider centrifuging again if necessary).

4. Add ethanol into spheres until total volume reaches 50 ml.

5. Place tube on a rotator or tumbler for 1 hr. Centrifuge at 200g for 5 min, discard supernatant, and wash with ethanol two more times for an hour each.

6. After 3 ethanol washes, rehydrate spheres in DI water. Wash at least twice more with DI water using the same techniques as ethanol.

Sonification / Deflocculation

1. Gelatin spheres tend to clump together in solution and may become crosslinked into aggregates. A probe sonifier may be used to break up the aggregates and disperse the spheres into a suspension. With 5-10 mL microspheres, sonify the crosslinked spheres at 10% power for 3 minutes using 30 second on/off cycles using a Branson digital 250 sonifier. Higher power settings may destroy the spheres. The sample should be placed in a small ice bath to prevent overheating during sonification. Microspheres may be observed by phase contrast or brightfield microscopy to verify sphere dispersion and homogeneity.

Freeze Drying

1. After washing and sonification, gelatin spheres may be freeze-dried for storage and later application or characterization. Usually, ~10 mL crosslinked gelatin is suspended in DI water and transferred to a 15 mL centrifuge tube.

A3. Loading μspheres with Growth Factors

Materials
Dissolved TGFβ1 60 μg/mL (100-21-10UG, Peprotech, Rocky Hill, NJ)
Dissolved PDGF-AB 20 μg/mL (100-00AB-10UG, Peprotech, Rocky Hill, NJ)
FBS
μspheres

1. Measure out μspheres to be loaded in microcentrifuge tubes
a.   For 1 mL of gel measure out >0.11 mg for TGF and >0.27 mg for PDGF
b.   For 10 mL of gel measure out >1.12 mg for TGF and >2.69 mg for PDGF
2. Spin down μspheres in centrifuge tubes

3. Add the volume of dissolved growth factor to achieve initial concentrations of 600 ng/mg for TGF and 200 ng/mg for PDGF
    a. For 20 μg/mL dissolved PDGF and 60 μg/mL dissolved TGF, add 10 μL dissolved growth factor for every 1 mg of spheres
        1. For 1.12 mg of spheres add 11.2 μL of dissolved growth factor
        2. For 2.69 mg of spheres add 26.9 μL of dissolved growth factor
4. Spin down the μspheres in centrifuge tubes with growth factor
5. Incubate at 37°C overnight in shaker
6. The following day dilute μspheres in FBS at 10 mg/mL
    a. For 1.12 mg of spheres add 11.2 μL of FBS
    b. For 2.69 mg of spheres add 26.9 μL of FBS
7. Also dilute control μspheres in FBS at 10 mg/mL
    a. For 1 mL of gel, dilute 0.381 mg of spheres in 3.8 μL of FBS
    b. For 10 mL of gel, dilute 3.81 mg of spheres in 38 μL of FBS
3. Allow to incubate at room temperature for 1 hour
4. Sonify each tube of beads for 1 minute with 10 second duty cycles

**Note: Bioreactor gels require 12 mL of media. If the growth factor is at 5 ng/mL and the media is changed three times, 180 ng of growth factor is required. With working concentrations of 400 ng/mg of TGF and 166 ng/mg of PDGF from the procedure above

A4. Fabrication of Gels with Loaded μspheres and Growth Factors

Materials
Dissolved TGF μspheres (600 ng/mg, functionally 400 ng/mg, spheres suspended at 10 mg/mL)
Dissolved PDGF μspheres (200 ng/mg, functionally 166 ng/mg, spheres suspended at 10 mg/mL)
Control μspheres (Suspended at 10 mg/mL)
FBS
Collagen (4 mg/mL in 0.02 N Acetic Acid)
NaOH (0.1 N)
5x DEMEM
Cells (suspended at 500k/100 μL in 1x DMEM without phenol red)

Control Gel
1. Add enough collagen to compose 50% of gel volume. Because of viscosity, measured to receptacle not the amount in pipette
    a. For 1 mL of gel add 0.5 mL of collagen
    b. For 6 mL of gel add 3.0 mL of collagen
2. Add 5x DMEM to compose 20% of gel volume.
    a. For 1 mL of gel add 0.2 mL of 5x DMEM
    b. For 6 mL of gel add 1.2 mL of 5x DMEM
5. Add NaOH to compose 10% of gel volume and mix thoroughly
    a. For 1 mL of gel add 0.1 mL of NaOH
    b. For 6 mL of gel add 0.6 mL of NaOH
6. Add FBS to compose 10% of gel volume

     a. For 1 mL of gel add 0.1 mL of FBS
     b. For 6 mL of gel add 0.6 mL of FBS
7. Add cell suspension to compose 10% of gel volume
     a. For 1 mL of gel add 0.1 mL of cell suspension
     b. For 6 mL of gel add 0.6 mL of cell suspension
8. Add 0.5 mL to each static well
9. Add 3.5 mL to each dynamic chamber
10. Carefully incubate at 37°C for 45 minutes to an hour
11. Add 0.5 mL of control DMEM media without phenol red to each static well
12. Add 3.5 mL of control DMEM media without phenol red to each dynamic chamber
13. On Day 3 change media and remove molds from dynamic chambers
14. Replace 1.5 mL of control DMEM media without phenol red to each static well and 12 mL to each dynamic well
15. On Day 6 replace 1.5 mL of control DMEM media without phenol red to each static well and 12 mL to each dynamic well

Growth Factor Media Gels
1. Add enough collagen to compose 50% of gel volume. Because of viscosity, measured to receptacle not the amount in pipette
     a. For 1 mL of gel add 0.5 mL of collagen
     b. For 6 mL of gel add 3.0 mL of collagen
2. Add 5x DMEM to compose 20% of gel volume.
     a. For 1 mL of gel add 0.2 mL of 5x DMEM
     b. For 6 mL of gel add 1.2 mL of 5x DMEM
3. Add NaOH to compose 10% of gel volume and mix thoroughly
     a. For 1 mL of gel add 0.1 mL of NaOH
     b. For 6 mL of gel add 0.6 mL of NaOH
4. Add control sphere suspension to match concentration of loaded microspheres
     a. For 1 mL of gel add 38 μL of control μspheres in FBS
     b. For 6 mL of gel add 230 μL of control μspheres in FBS
5. Add FBS to round up control microspheres such that both compose 10% of gel volume
     a. For 1 mL of gel add 62 μL of FBS
     b. For 10 mL of gel add 370 μL of FBS
6. Add cell suspension to compose 10% of gel volume
     a. For 1 mL of gel add 0.1 mL of cell suspension
     b. For 6 mL of gel add 0.6 mL of cell suspension
7. Add 0.5 mL to each static well
8. Add 3.5 mL to each dynamic chamber
9. Carefully incubate at 37°C for 45 minutes to an hour
10. Add 0.5 mL of control DMEM media without phenol red but with 5 ng/mL PDGF, 5 ng/mL TGF, and 30 μM ascorbic acid, to each static well
11. Add 3.5 mL of control DMEM media without phenol red but with 5 ng/mL PDGF, 5 ng/mL TGF, and 30 μM ascorbic acid, to each dynamic chamber
12. On Day 3 change media and remove molds from dynamic chambers

13. Replace 1.5 mL of control DMEM media without phenol red but with 5 ng/mL PDGF, 5 ng/mL TGF, and 30 μM ascorbic acid, to each static well and 12 mL to each dynamic well
14. On Day 6 replace 1.5 mL of control DMEM media without phenol red but with 5 ng/mL PDGF, 5 ng/mL TGF, and 30 μM ascorbic acid, to each static well and 12 mL to each dynamic well

Growth Factor Loaded μspheres Gels
1. Add enough collagen to compose 50% of gel volume. Because of viscosity, measured to receptacle not the amount in pipette
   a. For 1 mL of gel add 0.5 mL of collagen
   b. For 10 mL of gel add 5.0 mL of collagen
2. Add 5x DMEM to compose 20% of gel volume.
   a. For 1 mL of gel add 0.2 mL of 5x DMEM
   b. For 10 mL of gel add 2.0 mL of 5x DMEM
3. Add NaOH to compose 10% of gel volume and mix thoroughly
   a. For 1 mL of gel add 0.1 mL of NaOH
   b. For 10 mL of gel add 1.0 mL of NaOH
5. Add growth factor loaded spheres to achieve appropriate delivery of microspheres (see **Note below)
   a. For 1 mL of gel add 11.2 μL of TGF sphere solution and 26.9 μL of PDGF sphere solution
   b. For 10 mL of gel add 112 μL of TGF sphere solution and 269 μL of PDGF sphere solution
4. Add FBS to round up loaded microspheres such that both compose 10% of gel volume
   a. For 1 mL of gel add 61.9 μL of FBS
   b. For 10 mL of gel add 0.619 mL of FBS
5. Add cell suspension to compose 10% of gel volume
   a. For 1 mL of gel add 0.1 mL of cell suspension
   b. For 10 mL of gel add 1 mL of cell suspension
6. Add 0.5 mL to each static well
7. Add 3.5 mL to each dynamic chamber
8. Carefully incubate at 37°C for 45 minutes to an hour
9. Add 0.5 mL of control DMEM media without phenol red but with 30 μM ascorbic acid, to each static well
10. Add 3.5 mL of control DMEM media without phenol red but with 30 μM ascorbic acid, to each dynamic chamber
11. On Day 3 change media and remove molds from dynamic chambers
12. Replace 1.5 mL of control DMEM media without phenol red but with 30 μM ascorbic acid, to each static well and 12 mL to each dynamic well
13. On Day 6 replace 1.5 mL of control DMEM media without phenol red but with 30 μM ascorbic acid, to each static well and 12 mL to each dynamic well

Appendix B – Chapter 4 Supplemental Results and Discussion

ASC Expression of Early Smooth Muscle Genes in Different Dimensions and Concentrations of Collagen

Despite orders of magnitude difference between means of 2D and 3D samples, due to high variance, there were no statistical differences between expression of ACTA from 2D samples when compared to their 3D counterparts (Fig B.1A and B.1B). There were also no statistical differences beween ACTA expression of any concentrations except on D4 where the 1 mg/mL 3D sample of had significantly higher expression than the 4mg/mL sample (Fig B.1A, $p<0.05$). 2D samples of 2 mg/mL had significantly more TGLN expression than their respective 3D samples on D4, as did 2D samples of 1 mg/mL on D7 (Fig B.1C and B.1D, $p<0.05$). 2D samples of 4 mg/mL higher TGLN expression than their 3D counterparts on D4 and D7. Like ACTA, the only sample where different concentrations had significant differences in TGLN was on D4 where 2 mg/mL had less TGLN than the 1 mg/mL sample (Fig B.1C, $p<0.05$).
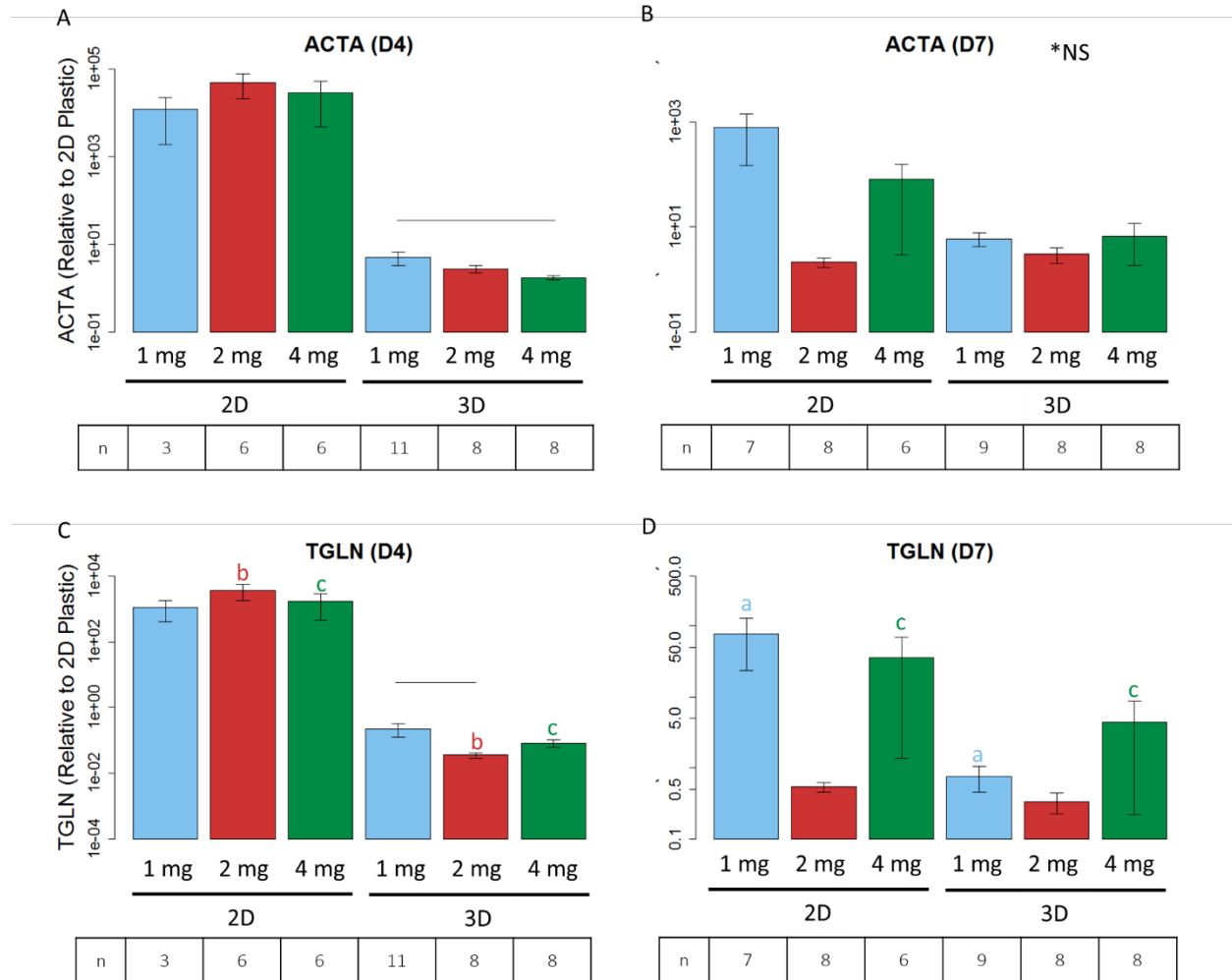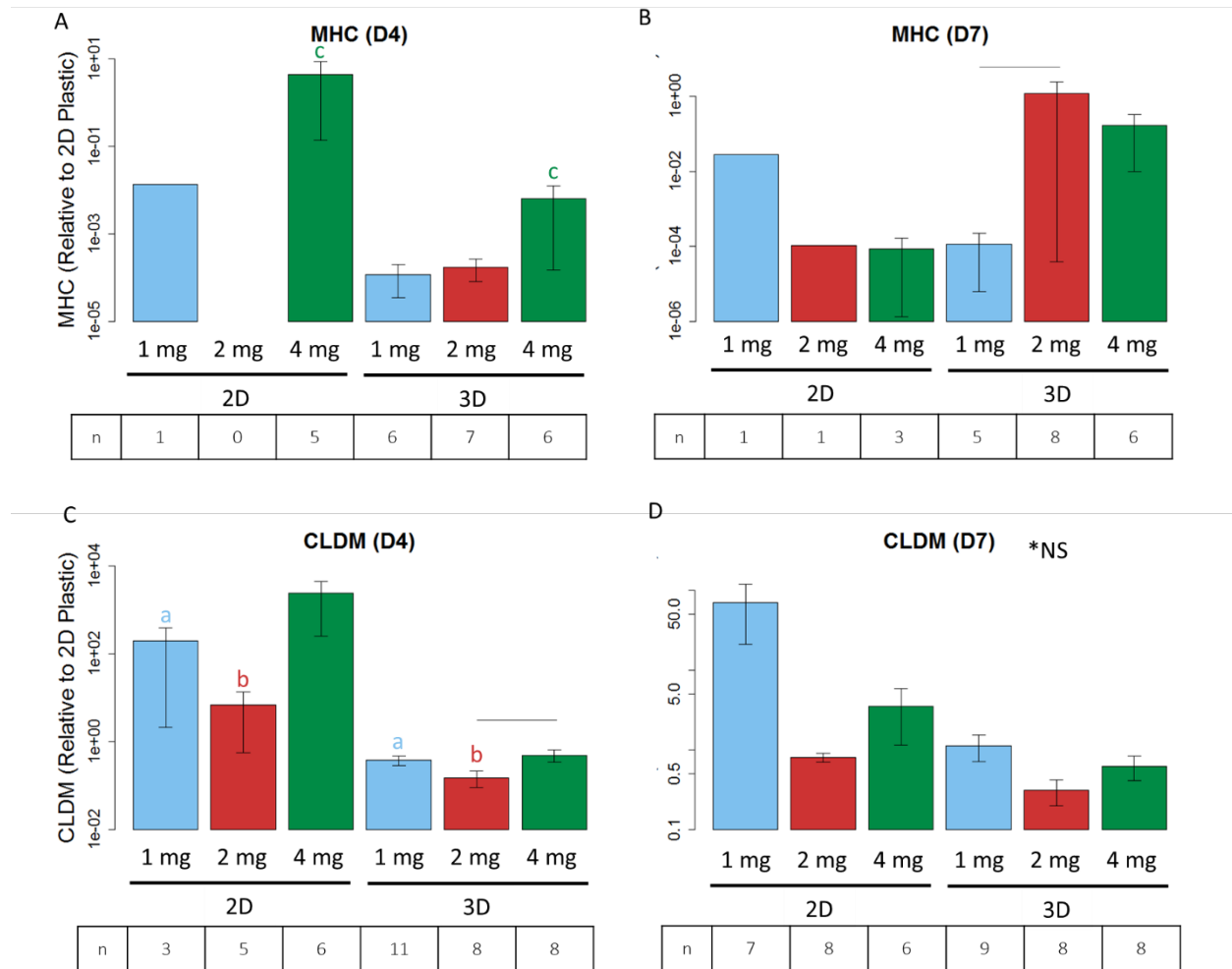
Supplemental Figure B.1: Early Smooth Marker Genes of ASC from Gels Cultured in Different Dimensions and Concentrations of Collagen. There were no statistical differences between expression of ACTA between 2D samples and their respective 3D counterparts (A and B). There were no statistical differences between concentrations in any system except on D4 when the 3D sample of 1 mg/ml was significantly higher than the 4mg/mL sample (A and B, $p<0.05$). With TGLN, on D4, 2mg/mL and 4 mg/mL samples had higher expression than their 3D counterparts. On D7, 1 mg/mL and 4 mg/mL were higher than the samples with the same concentration in 3D (C and D, $p<0.05$). Like ACTA, the only sample, from different concentrations, that was significantly different, was on D4 where 2 mg/mL had less TGLN than the 1 mg/mL sample (C, $p<0.05$). Blue bars represent gels with 1 mg/mL of collagen, red bars represent gels with 2 mg/mL of collagen, and green bars represent gels with 1 mg/mL of collagen. Lines ending above conditions indicate statistical differences between concentrations and colored letters above bars indicate significant differences between gels of different culture dimensions but the same concentrations.

ASC Expression of Mature Smooth Muscle Genes in Different Dimensions and Concentrations of Collagen

Only 2D gels of 4mg/mL had significantly higher MHC expression than their 3D counterparts, and only on D4 (Fig B.2A, $p<0.05$). Considering concentration, on D7, 2 mg/mL samples in 3D had significantly more MHC expression than 1 mg/mL samples (Fig B.2B, $p<0.05$). On D4, 1 mg/mL and 2 mg/mL gels in 2D had significantly higher expression of CLDM than their

3D counterparts (Fig B.2C, p<0.05). Also on D4, 4 mg/mL 3D gels expressed more CLDM than

2mg/mL gels (Fig B.2C, p<0.05). There were no significant differences between any condition on

D7 (Fig B.2D).

Supplemental Figure B.2: Late Marker Genes of ASC from Gels Cultured in Different Dimensions and Concentrations of Collagen. Only 4mg/mL samples on 2D gels had significantly higher MHC expression than their 3D counterparts, and only on D4 (A, p<0.05). When comparing concentrations, D7, 2 mg/mL samples in 3D had significantly more MHC expression than 1 mg/mL samples (B, p<0.05). On D4, 1 mg/mL and 2 mg/mL gels in 2D had significantly higher CLDM than their 3D counterparts (C, p<0.05). Also on D4, 4 mg/mL 3D gels had more CLDM than 2mg/mL gels (C, p<0.05). There were no significant differences between any condition on D7 (D). Blue bars represent gels with 1 mg/mL of collagen, red bars represent gels with 2 mg/mL of collagen, and green bars represent gels with 1 mg/mL of collagen. Lines ending above conditions indicate statistical differences between concentrations and colored letters above bars indicate significant differences between gels of different culture dimensions but the same concentrations.

<u>**Appendix C – Chapter 5 Supplemental Results**</u>

<u>The Expression of Smooth Muscle Genes by ASCs Differentiated Using Growth Factor Treatments</u>

ASCs exposed to growth factors either by media or in loaded spheres expressed more ACTA than Con ASCs on D4, but after seven days LS ASCs expressed less ACTA than both Con ASCs and GF ASCs (FIG 5A, $p<0.05$). Like ACTA, LS ASCs and GF ASCs expressed more TGLN on D4 than Con ASCs but by the ed of the week all conditions expressed statistically similar levels of TGLN (FIG 5B, $p<0.05$). There were no statistical differences in expression MHC on D4, but by D7 Con ASCs had significnatly more expression of MHC than either of the growth factor treatments (FIG 5C, $p<0.05$). On D4, both constructs with growth factors expressed more CLDM than control constructs but by D7, Con ASCs had significnatly more expression of CLDM than either LS ASCs or GF ASCs (FIG 5D, $p<0.05$).
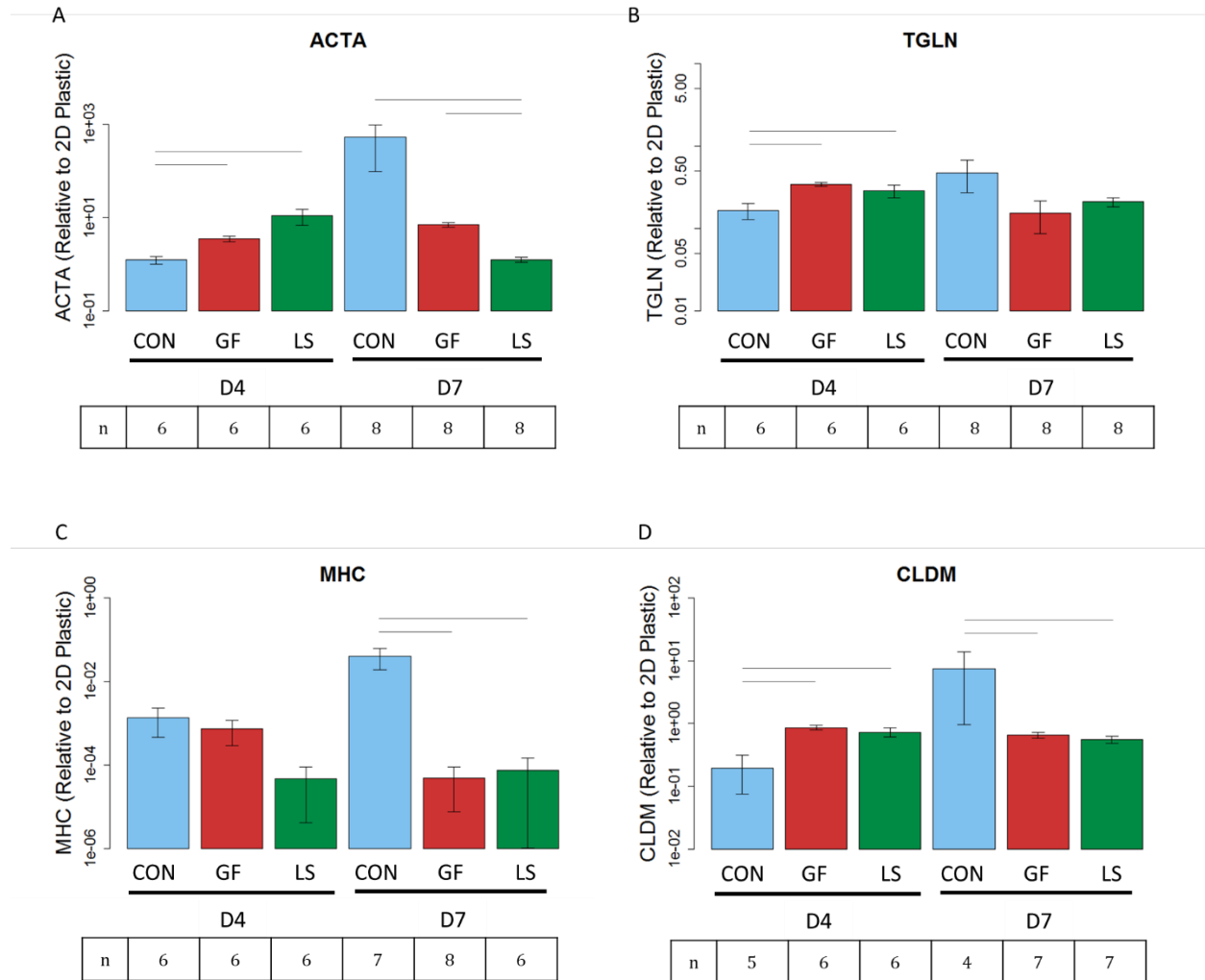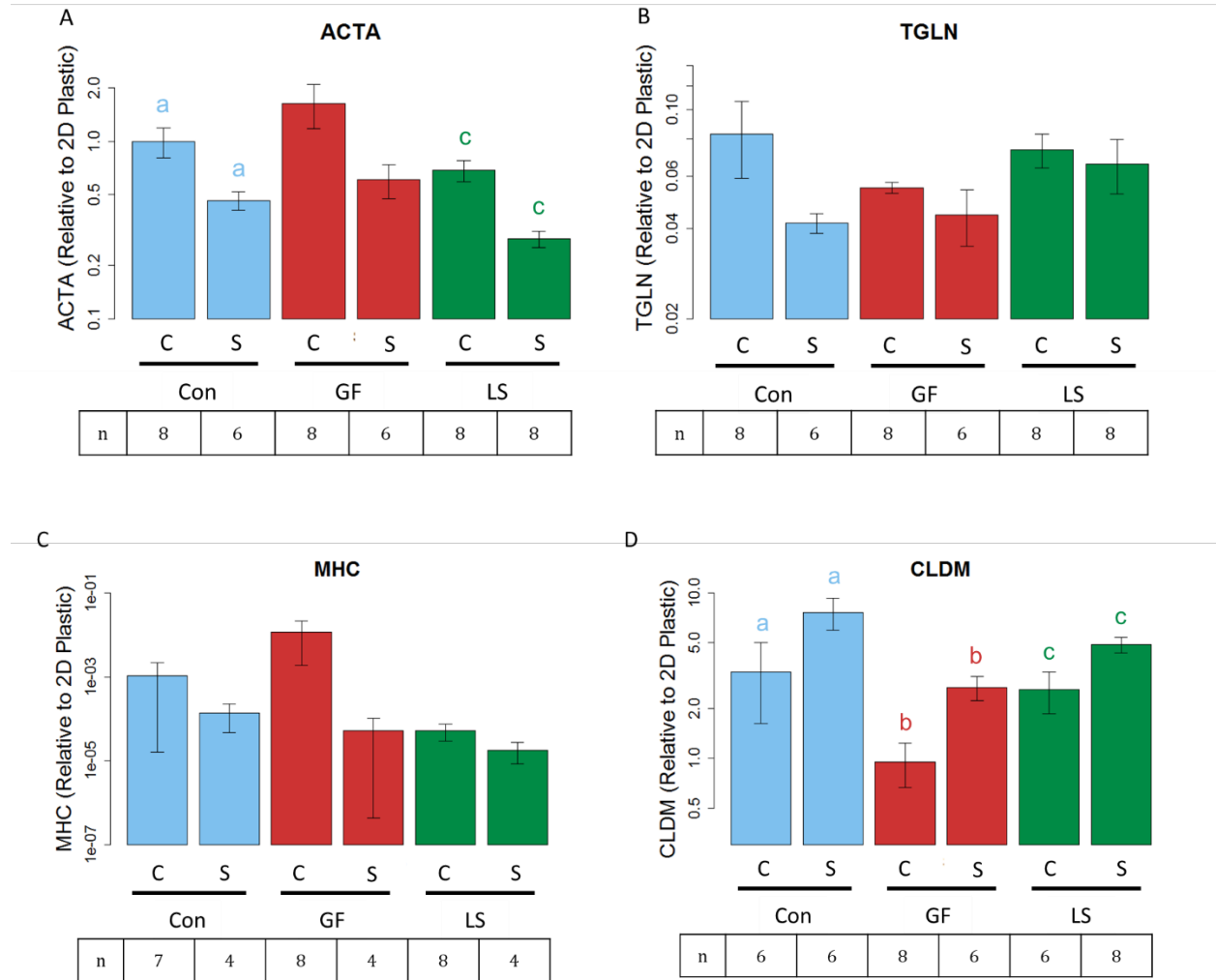
Supplemental Figure C.1: Expression of Smooth Muscle Genes from ASCs Differentiated with Different Growth Factor Delivery Methods. On D4, LS ASCs and GF ASCs expressed the more ACTA than Con ASCs but by D7, LS ASCs expressed less ACTA than Con ASCs or GF ASCs (A, p<0.05). On D4, LS ASCs and GF ASCs also expressed more TGLN than Con ASCs but by D7, there were no significant differences in expresses ion of TGLN (B, p<0.05). There were no statistical differences in expression MHC on D4, but Con ASCs had significantly more expression of MHC than either of the growth factor treatments on D7 (C, p<0.05). On D4, LS ASCs and GF ASCs expressed the more CLDM than Con ASCs but on D7, Con ASCs had significantly more expression of CLDM than either of the growth factor treatments (D, p<0.05). Blue bars represent control conditions without growth factor, red bars represent static gels with growth factor in the media and unloaded spheres, and green bars represent gels embedded with μspheres loaded with growth factor. The row of numbers below each graph indicates the number of biological samples used to calculate each value. Lines ending above conditions indicate statistical differences with p<0.05.

The Expression of Smooth Muscle Genes by ASCs Cultured with Growth Factor Treatments and

Mechanical Stretch

    Constructs from the Control and the LS growth factor treatment had siginificantly less

ACTA expression when the contructs were stretched (Fig C2.A, p<0.05). Expresion of TGLN and

MHC were not statistically different between any static and stretech condition (Fig 2C.B and 2C.C). Stretched samples from every growth factor treatment expressed more CLDM than the same growth factor treatment in static culture (Fig C2.D, p<0.05).
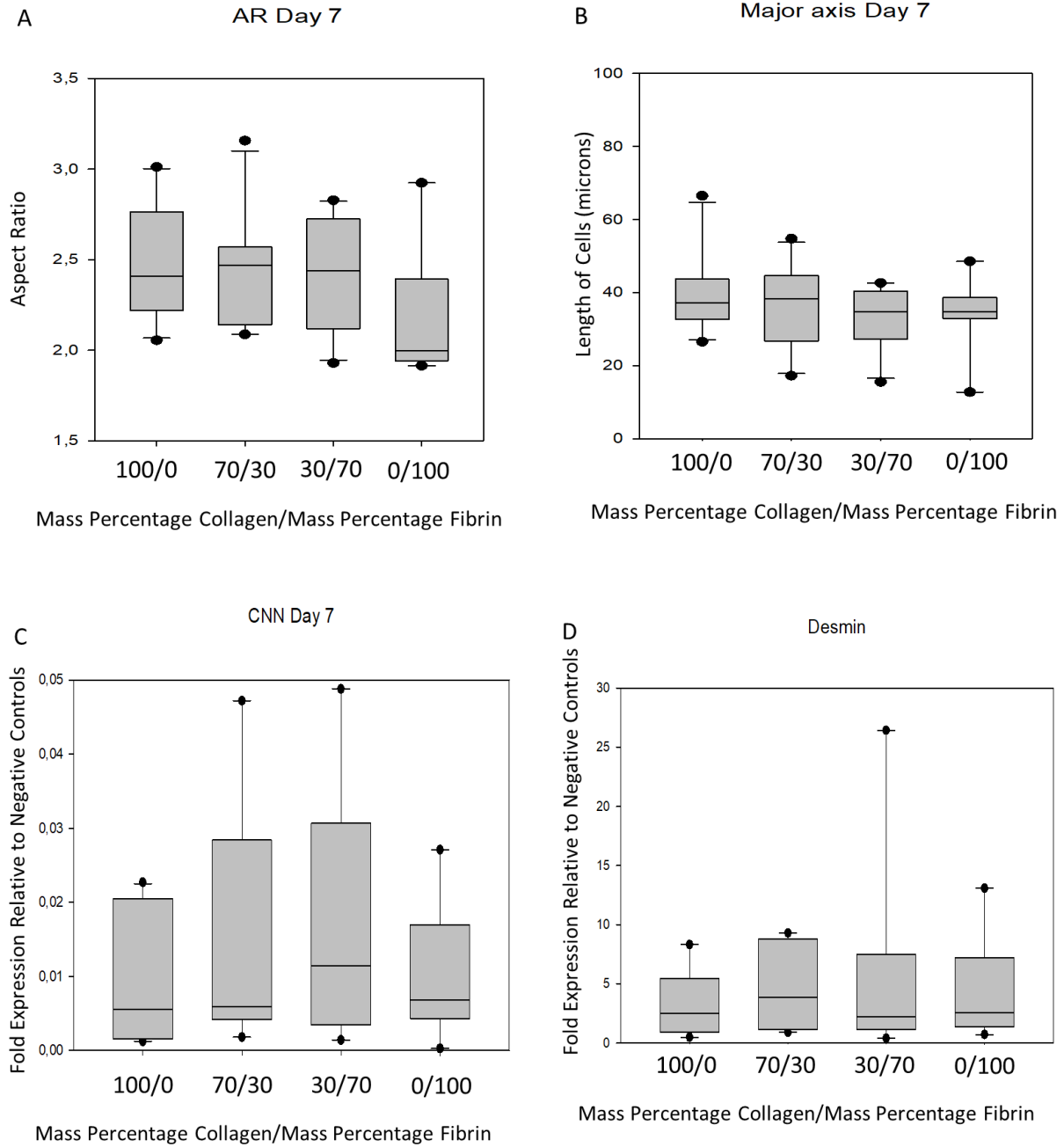

Supplemental Figure C.2: Expression of Smooth Muscle Genes from ASCs in Mechanically Stretched Constructs Compared to Statically Cultured Constructs (D7). Constructs with Con treatment and the LS treatment expressed significantly less ACTA when the constructs were stretched (A, p<0.05). There were no significant differences between of expression of TGLN (B) or MHC (C) between stretched and static conditions regardless of growth factor treatment. Stretched samples expressed significantly more CLDM than their static counterparts regardless of growth factor treatment (D, p<0.05). "C" indicates static control conditions and "S" indicates stretched condition. Blue bars represent control conditions without growth factor, red bars represent static gels with growth factor in the media and unloaded spheres, and green bars represent gels embedded with μspheres loaded with growth factor. The row of numbers below each graph indicates the number of biological samples used to calculate each value. Colored letters above the bars indicate significant differences between static "C and stretched "S" conditions with p<0.05. Differences between different growth factors were not compared in this figure.
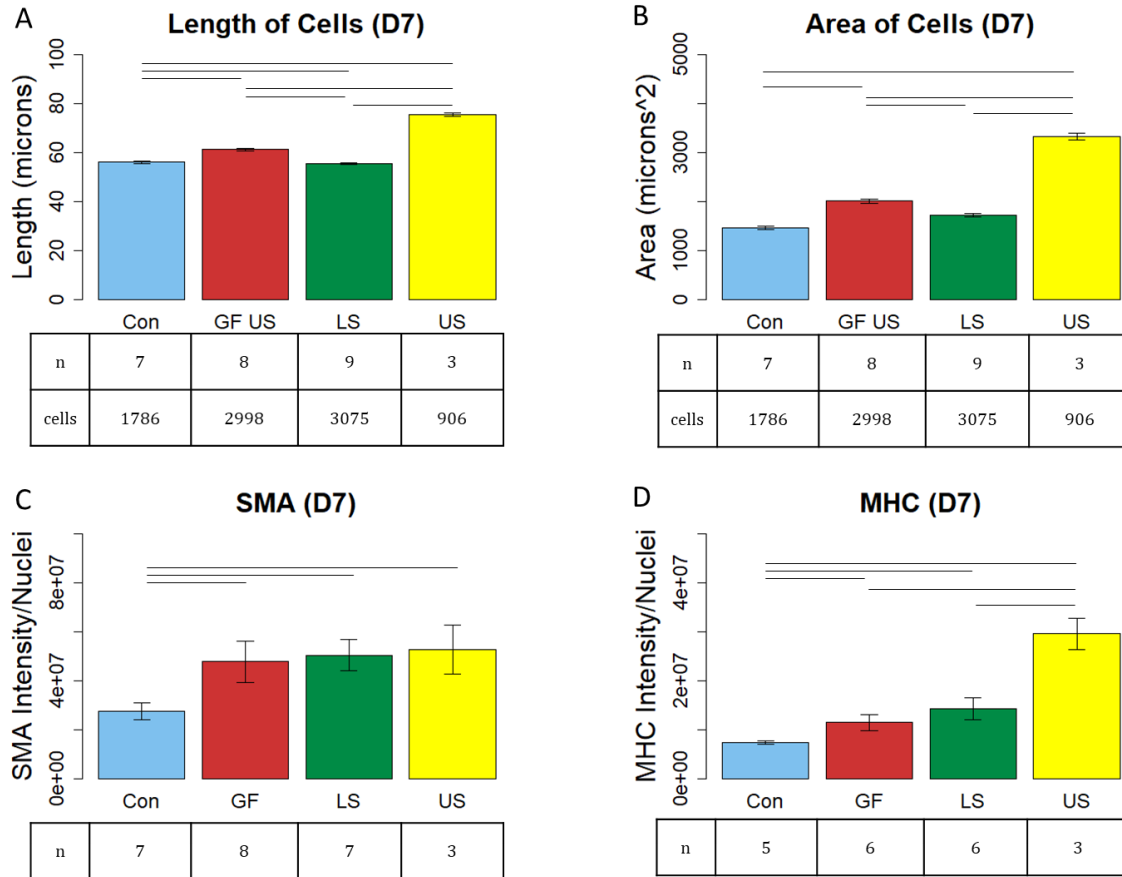
Supplemental Figure D.1: The Shape of ASCs and the Expression of Smooth Muscle Protein Differentiated with Different Growth Factor Delivery Methods. ASCs with empty spheres and no growth factors (US) were longer (A, $p<0.05$) and had larger area (B, $p<0.05$) than cells with growth factors (GF and LS) or control cells (Con). They also expressed as much SMA protein as other samples with growth factor being delivered (C) and expressed more MHC protein (D, $p<0.05$). Blue bars represent static controls, red bars represent static gels with growth factor in the media and unloaded spheres, green bars represent gels embedded with μspheres loaded with growth factor, and yellow bars represent gels with unloaded spheres and no growth factors. The row of numbers below each graph indicates the number of cells and biological samples used to calculate each value. Lines ending above conditions indicate statistical differences with $p<0.05$.

Supplemental Figure D.2: The Shape of bMSCs and the Expression of Smooth Muscle Genes with Different ratios of Collagen and Fibrin in the Matrix. bMSCs cultured in composites of fibrin and collagen have different aspect ratios (A, $p<0.05$) and lengths (B, $p<0.05$) than in pure gels of either protein. Composites also induce higher expression of SMC genes Calponin (C, $p<0.05$) and Desmin (D, $p<0.05$).